

University of Southampton

Department of Mechanical Engineering

THE COMPOUNDING METHOD OF DETERMINING STRESS INTENSITY FACTORS  
FOR CRACKS IN ENGINEERING STRUCTURES

by

D. P. Rooke

Materials Department  
Royal Aircraft Establishment  
Farnborough  
Hants

*Thesis submitted for the degree of Doctor of Philosophy*

September 1982

ACKNOWLEDGEMENTS

The author wishes to express his gratitude for the assistance given by members of both the Royal Aircraft Establishment and Southampton University during the course of this research. In particular he would like to thank his supervisors Dr D.J. Cartwright (Southampton), and Mr W.T. Kirkby (RAE) for their unfailing help, advice and criticism. Special thanks are due to Mrs C. Carney for help in preparing the manuscript and to all those involved in the production of the thesis.

The research was conducted with the permission and support of RAE management and the results are published by permission of the Controller, HMSO.

CONTENTS

	<u>Page</u>
Abstract	(v)
1 INTRODUCTION	1
2 ERRORS IN STRESS ANALYSIS AND THEIR EFFECTS	11
2.1 Development of asymptotic stress analysis	14
2.1.1 Loading remote from the hole	16
2.1.2 Loading on the perimeter of the hole	16
2.1.3 Residual strength and fatigue crack growth calculations	18
2.2 Applications of asymptotic stress analysis	20
2.2.1 One crack from a circular hole - remote loading	21
2.2.2 Two cracks from a circular hole - remote loading	23
2.2.3 Two cracks from an elliptical hole - remote loading	24
2.2.4 One crack from a circular hole - local loading	26
2.2.5 Cracks at the bore of a rotating annular disc	28
2.3 Discussion	30
2.4 Conclusions	33
3 CRACKS NEAR BOUNDARIES	35
3.1 The compounding method	35
3.2 Application to plane sheets	38
3.2.1 Test solutions	38
3.2.2 A solution for two different boundaries	41
3.3 Discussion and conclusions	42
4 CRACK(S) AT AN UNLOADED HOLE	43
4.1 Equivalent crack concept	44
4.1.1 One crack at the edge of a circular hole	44
4.1.2 Two equal-length cracks at the edge of a circular hole	48
4.1.3 Two unequal-length cracks at the edge of a circular hole	49
4.2 Boundary-boundary interactions	50
4.3 Test configuration: cracks at a central hole in a strip	54
4.4 Other configurations	57
4.4.1 Crack at an off-centre hole in a strip	57
4.4.2 Crack at a hole near another hole	58
4.5 Discussion and conclusions	60
5 CRACKS AT UNLOADED HOLES IN AN ARRAY OF HOLES	62
5.1 Crack(s) at one of the holes in a row of holes	62
5.2 Cracks at every hole in a row of holes	64
5.2.1 General configuration of holes with cracks	65
5.2.2 Periodic configuration of holes with cracks	68
5.3 Fatigue crack growth	70
5.4 Discussion and conclusions	71

CONTENTS (concluded)

	<u>Page</u>	
6	CRACKS AT LOADED HOLES	73
	6.1 Equivalent loading on crack	73
	6.1.1 Self-equilibrated loads on the perimeter of the hole	74
	6.1.2 Resultant load on the perimeter: zero stress on sheet boundary	76
	6.1.3 Resultant load on the perimeter: finite stress on sheet boundary	77
	6.2 Cracks at pressurized holes	80
	6.3 Loaded holes near a boundary	84
	6.4 Discussion and conclusions	91
7	A CRACK IN A STIFFENED SHEET	93
	7.1 Theory of compounding applied to stiffened sheets	93
	7.2 Application to periodically stiffened sheets	95
	7.2.1 Test solutions	95
	7.2.2 New solution	99
	7.3 Discussion and conclusions	99
8	MANY CRACKS IN A STIFFENED SHEET	101
	8.1 Development of theory	101
	8.2 Periodically stiffened sheets	105
	8.3 Conclusions	107
9	DESIGN STUDY - CRACKS AT A DOUBLE ROW OF HOLES	108
	9.1 Evaluation of the stress intensity factor	108
	9.2 Growth of fatigue cracks	112
	9.2.1 Rates of crack growth	112
	9.2.2 Fatigue lifetimes	113
	9.3 Discussion	115
	9.4 Conclusions	118
10	CONCLUDING REMARKS	119
Appendix A	Evaluation of growth-time integrals for a circular hole	120
Appendix B	Evaluation of growth-time integrals for an elliptical hole	122
Appendix C	Evaluation of growth-time integrals for a loaded circular hole	123
Appendix D	Evaluation of boundary-boundary interactions	125
References		127
Illustrations - Figures	1.1 to 1.19; 2.1 to 2.22; 3.1 to 3.8; 4.1 to 4.14; 5.1 to 5.13; 6.1 to 6.10; 7.1 to 7.5; 8.1 to 8.7; 9.1 to 9.8	132-215

UNIVERSITY OF SOUTHAMPTON

ABSTRACT

FACULTY OF ENGINEERING AND APPLIED SCIENCE

MECHANICAL ENGINEERING

Doctor of Philosophy

THE COMPOUNDING METHOD OF DETERMINING STRESS INTENSITY FACTORS  
FOR CRACKS IN ENGINEERING STRUCTURES

by David Percy Rooke

In this thesis the compounding method for determining stress intensity factors is developed and presented. The method enables stress intensity factors to be evaluated for complex geometrical cracked configurations with many boundaries from the factors for several simpler configurations with one boundary only. It is based on an alternating technique in which only the important interactions between boundaries are taken into account. The method is applied to a wide range of structural configurations which include cracks near other boundaries (*eg* edges, holes or other cracks) cracks at the edges of loaded or unloaded holes, and cracks near stiffeners.

The method is assessed by comparing 'compounded solutions' with known solutions for several configurations. It is shown that the errors resulting from the approximations in the compounding method are a function of the number and type of boundaries near the crack. It is further shown that these errors in stress intensity factors lead to uncertainties in residual strengths and fatigue lifetime which are within engineering tolerances.

CHAPTER 1INTRODUCTION

Materials used in engineering structures often contain flaws or crack-like defects. These may exist at either the manufacturing or the fabricating stage or they may be initiated during service use. For example flaws which do originate during the manufacturing processes are often associated with impurities or second phase particles. Fabrication processes such as drilling and welding can result in crack-like flaws, for example at the edge of a drilled hole or at the edge of a weld. The initial dimensions of these defects are usually small, perhaps even microscopic. Under service conditions they may grow to macroscopic dimensions and their presence may lead to a reduction in the static strength of the structure. The growth may be caused by variable service loads (fatigue), environmental attack (corrosion), or both. These two factors may also cause new cracks to be initiated in the material. If the static strength of the cracked structure (residual strength) falls too low then failure can result under normal operating conditions.

Despite precautions failures do sometimes occur and some examples of in-service and on-test failures have been collected by Kirkby<sup>1</sup> and are shown in Figs 1.1 to 1.18. A noticeable feature of the failures shown is that many of the cracks originate from regions of stress concentration such as holes, cut-outs, changes of section, etc. This feature is common to many crack problems and will be considered in detail in subsequent chapters.

Cracks which have grown from holes are illustrated in Figs 1.1 to 1.5, 1.11, 1.14 to 1.18. In the components manufactured from thin-section material, Figs 1.1 to 1.3, 1.14 and 1.15, the crack penetrates through the thickness for most of the life and so, in practice, surface observations would give an accurate estimate of crack-length. This is not necessarily so for cracks in thick components such as shown in Figs 1.4, 1.5, 1.11, 1.16 to 1.18. Many of these cracks start in a small area, often a region that has been subjected to fretting damage, and do not grow through the thickness until the final failure of the component occurs. Figs 1.1 and 1.2 illustrate how extensive damage due to crack growth can occur in regions of multiple stress concentrations, *eg* a row of holes. Sometimes several cracks develop from multiple origins, *eg* from both sides of a hole as in Figs 1.4, 1.14 and 1.17, from several holes in a row of holes as in Fig 1.1, from various positions round a uniform stress concentration as in Fig 1.13. Despite the

reinforcement around the cut-out shown in Fig 1.15, a crack occurred at the maximum stress concentration at the corner of the cut-out.

Cracks which have started from regions of stress concentration associated with changes in section thickness or re-entrant corners are shown in Figs 1.6 to 1.9 and 1.13. In Figs 1.7 and 1.8 the crack occurred at an abrupt change in thickness which involved a corner with a small radius of curvature. Fig 1.9 shows a crack starting from the root of a circumferential groove and Fig 1.13 shows many cracks growing from an area where there is a change in section thickness, a corner and multiple grooves (ie screw threads).

Figs 1.10 and 1.12 show crack growth from pre-existing flaws. In Fig 1.10 a flaw in the original extrusion developed into a crack which grew through the thickness and caused a failure. In Fig 1.12 a weld defect grew into a crack around the weld line leading to failure.

Various design philosophies have been developed for dealing with the problem of loss of structural strength due to the initiation and subsequent growth of cracks by fatigue. Chronologically the first was the 'safe-life' design philosophy; this was developed in the years 1945-55. Safe-life design is based on the concept that significant fatigue damage will not develop during the service life of the component or structure: if a crack is initiated, or is already present, it will not grow enough to produce a significant reduction in strength. The life for which this is true, for any given component, is calculated and then checked by a suitable test programme; an appropriate safety factor on the test-life is chosen; the factored life is known as the safe-life. When the service life equals the safe-life the component is taken out of service whether crack damage is evident or not. This philosophy can lead to the inefficient replacement of components which are still safe and would remain so for a long time.

In the early 1960s a more efficient philosophy known as 'fail-safe' design was developed. With this philosophy a structure is designed to have an adequate life free from significant fatigue damage, but continued operation is permitted beyond the life at which such damage may develop. Safety is incorporated into the fail-safe approach by the proviso that any fatigue cracks that develop will be detected by routine inspection procedures before they result in a dangerous reduction of the static strength of the structure. Two requirements are necessary for this approach to be successful: they are to be able to define a minimum crack size which will not go undetected at a routine

inspection and to be able to predict the growth of such a crack during the time until the next inspection. The lengths of cracks detected by straightforward inspection procedures will usually be measured in centimetres rather than millimetres. Safety factors are introduced to allow for variability in parameters, such as loading and material properties, which affect the rate at which cracks grow.

In the early 1970s a third design philosophy was proposed, the object of which was to design a 'damage-tolerant' structure. This philosophy is similar to the fail-safe approach but goes further in that consideration is given to crack growth from flaws which are assumed to be present in the structure as manufactured. Such flaws may arise from metallurgical imperfections in the material, or from manufacturing faults. Examples of such imperfections have already been seen in Figs 1.10 and 1.12. The size of flaws which are assumed to exist in certain specified critical areas have dimensions between 0.1 mm and 1.5 mm. The implementation of the 'damage-tolerant' approach to a given component depends on whether the component is classed as 'inspectable' in the course of routine service inspections or 'non-inspectable'. For instance the component in Fig 1.12 would be classed as inspectable and that in Fig 1.10 as non-inspectable. For components that are inspectable the procedures closely follow those used in fail-safe design. However, in the case of non-inspectable parts it must be demonstrated that the time for the crack to grow to failure, from the prescribed initial flaw, is greater than the desired service life. Since, under service loading conditions, most of the life of a cracked component is spent while the crack is short it is necessary to be able to predict accurately the rate of growth of these short cracks.

Thus it is clear that quantitative methods of assessing crack growth and its effect on structural strength are needed in order to ensure that optimum use is made of engineering structures, and that reliability and safety are guaranteed under service conditions. Such assessments are needed at all stages in the life of a component or structure. They are needed:

- (1) to assist in design;
- (2) to assist in material selection;
- (3) to devise inspection schedules;
- (4) to plan maintenance procedures;
- (5) to decide on repair or replacement.

Fracture mechanics, which depends on the assumption that 'crack-behaviour' is governed by the stress-field at the tip, provides a basis for quantifying both crack-growth and strength-reduction which may lead to structural failure. The important parameter in fracture mechanics is the stress intensity factor  $K$  since it is a measure of the magnitude of the stress occurring in the highly stressed region at the tip of a crack in an elastic solid.

The linear elastic solution for the stress-field around a crack shows that the stress components  $\sigma_{ij}$  are always of the same form; they are, in terms of the polar coordinates  $r, \theta$  from the tip (see Fig 1.19),

$$\sigma_{ij}(r, \theta) = \frac{K}{\sqrt{2\pi r}} f_{ij}(\theta) + \text{'other terms'}. \quad (1.1)$$

If the point  $(r, \theta)$  is sufficiently close to the tip, ie  $r \ll$  crack length, the 'other terms' in the above equation are negligible compared to the first term. The elastic solution predicts infinite stresses at the crack tip ( $r = 0$ ) which cannot occur in practice since there is plastic flow in the highly stressed region near the tip. However, if the region of plastic flow is small compared to the region over which the  $r^{-\frac{1}{2}}$  term dominates the stress-field, it may be assumed that the behaviour of the crack is determined by the elastic stress intensity factor. This assumption forms the basis of linear elastic fracture mechanics.

The constant  $K$ , the stress intensity factor, is a function of the loading on the cracked configuration and of the size and shape of the crack and other geometrical boundaries; it has the dimensions of stress  $\times \sqrt{\text{length}}$ . There are three distinct types of cracking modes which are characterized by different symbols for the stress intensity factor, these are illustrated in Fig 1.19. Mode I, characterized by  $K_I$  and known as the opening mode, is the most common mode found in practical situations. Mode II, characterized by  $K_{II}$  is known as the sliding mode and mode III, characterized by  $K_{III}$ , is known as the tearing mode. The stress intensity factor for each mode can be formally defined, as  $r$  tends to zero along  $\theta = 0$ , in terms of the stress components shown in Fig 1.19, as follows:

$$\left. \begin{aligned}
 K_I &= \lim_{r \rightarrow 0} \left\{ \sqrt{2\pi r} \sigma_{22}(r, 0) \right\} ; \\
 K_{II} &= \lim_{r \rightarrow 0} \left\{ \sqrt{2\pi r} \sigma_{21}(r, 0) \right\} ; \\
 K_{III} &= \lim_{r \rightarrow 0} \left\{ \sqrt{2\pi r} \sigma_{23}(r, 0) \right\} .
 \end{aligned} \right\} \quad (1.2)$$

For most two-dimensional representations of straight-fronted cracks the coordinate system  $(x_1, x_2, x_3)$  in Fig 1.19 is a Cartesian system  $(x, y, z)$  with the origin of coordinates translated to the crack centre and the crack lies in the  $y = 0$  plane with the front parallel to the  $z$  axis. In some three-dimensional configurations with planar cracks which have a curved crack-front the stress intensity factors vary with position on the crack-front. In contrast to two-dimensional configurations the crack usually lies in the  $z = 0$  plane of a Cartesian system but the stress intensity factors must now be defined in terms of a local coordinate system at the point under consideration;  $x_1$  becomes the outward normal to the crack-front,  $x_2$  the normal to the plane of the crack and  $x_3$  the tangent to the crack-front.

Fracture mechanics is widely used to describe many aspects of crack behaviour, *eg* the onset of crack growth due to corrosion or fatigue, the rate of growth due to corrosion or fatigue and the occurrence of final failure. Material constants such as  $K_{Isc}$ , the value of  $K$  at which stress corrosion cracking starts, and  $K_{Ic}$ , the value of  $K$  at which plane strain failure occurs under a continuously increasing load, have been measured for many materials. Crack growth laws have been suggested to explain the strong dependence of the rate of growth of a fatigue crack on the range  $\Delta K$  over which the stress intensity factor fluctuates. In order to apply these concepts and laws to a practical situation it is necessary to know the stress intensity factor for the particular configuration. Solutions for many configurations are now available; many of them are recorded in the collections by Rooke and Cartwright<sup>2</sup>, Tada, Paris and Irwin<sup>3</sup>, and Sih<sup>4</sup>. Most of the solutions are applicable to linear, elastic, isotropic and homogeneous materials containing stationary cracks although some solutions are for anisotropic and bi-materials. The majority of the solutions are for two-dimensional structures, as three-dimensional problems are much more difficult to solve.

In addition to the collected solutions<sup>2-4</sup> many others are available, for instance, in the series of Special Technical Publications (STP) published by the American Society for Testing Materials (ASTM), in the series entitled 'Fracture' edited by H. Liebowitz<sup>5</sup> and in the series entitled 'Mechanics of Fracture' edited by G.C. Sih<sup>6</sup>. The methods, both theoretical and experimental, of obtaining these solutions have been reviewed by Cartwright and Rooke<sup>7</sup>, Liebowitz (Vol II of Ref 5), Sih (Vol I of Ref 6), and Kobayashi<sup>8</sup>. Numerical methods have also been reported recently<sup>9</sup>.

In practical problems, structural geometries and loadings are often so complex (see Figs 1.1 to 1.18) that the available stress intensity factor solutions are inadequate. Evaluation of the stress intensity factor for the actual problem using standard methods may be prohibitively expensive in both time and money. Thus there is a need to develop simpler methods which will be cheap and easy-to-use even if less accurate than most standard methods. Many simple methods have been suggested; the more important ones have been reviewed and their relative merits discussed by Rooke, Baratta and Cartwright<sup>10</sup>.

Devising a simple method for solving a given problem depends first on recognising what are the essential features of the problem and then ensuring that the method takes due account of these features. Other aspects of lesser importance can be dealt with in a more approximate manner. However the approximate nature of these simple methods must be recognised and the likely sources of error identified. Errors are estimated by comparison with known solutions and the practical consequences of using these approximations investigated.

As mentioned earlier, examination of many crack configurations (see for example Figs 1.1 to 1.18) suggests that the two most important features are stress concentrations at holes and notches, and other boundaries such as edges. Cracks frequently start at or near stress concentrations which dominate crack behaviour while the crack is short that is during the majority of the fatigue lifetime. Stress concentrations are usually characterized by a parameter called the stress *concentration* factor, denoted by  $K_t$ . As the crack grows longer the effect of the stress concentration on the crack-tip stress field diminishes and the stress intensity factor approaches that for an isolated crack, provided the crack tip does not approach any other boundaries. These two limiting cases, short cracks and long cracks,

provide the asymptotes for a simple interpolation model used by Rooke<sup>11</sup> and described in detail in Chapter 2.

Because the results of the interpolation model are simple analytical functions, they are very suitable for investigating the consequences of using approximate stress analysis in fracture mechanics calculations of residual strength and fatigue lifetimes. The results of these calculations contain uncertainties which arise as a consequence of errors in the stress intensity factor; these uncertainties are examined in Chapter 2 where it is shown that they are no greater than and often less than the uncertainties in crack sizes, service loads and material properties. Although the simple interpolation model was used in the study of the errors and their consequences the conclusions reached are not restricted to that model. Any model which results in errors of a similar magnitude in the stress intensity factor will lead to uncertainties in the residual strength and the fatigue lifetime similar to those calculated in Chapter 2.

In many real components, the above long crack limit may not be appropriate because of the presence of other boundaries near the tip of the crack. Where multiple boundaries are present, even short cracks at one boundary may be affected by the presence of all the other boundaries. It is therefore necessary to develop a method to evaluate the effects of all the boundaries on the crack. Such a method known as the 'compounding method' has been developed<sup>12</sup>. Its further development and use to evaluate stress intensity factors for various crack configurations forms the main topic of this thesis (Chapters 3 to 9). Only opening-mode stress intensity factors are considered here, as they are the most important in engineering structures, but the same principles could be applied to the other modes.

In the compounding method the effect on the crack of each boundary is considered separately, and these effects are then combined in a simple manner. Thus complex geometric configurations can be built up from relatively simple ones. Combining the effects of each boundary depends on the principle of superposition with the addition of interaction effects between the separate boundaries. The compounding method is developed using the iterative procedures of the Schwarz alternating technique: the major terms in the iteration represent interactions between the crack and the boundaries and the minor terms represent boundary-boundary interactions. These latter interactions may or may not be important; certain types of crack configurations for which they

are important are identified and methods of evaluating the effects investigated. The compounding method is presented in terms of normalized stress intensity factors in order to make use of the many simple solutions available in the Compendium of Stress Intensity Factors<sup>2</sup>.

In Chapter 3 the theoretical development is described and the method is applied to plane problems with a crack near boundaries of different curvatures. Results for the stress intensity factors are compared with those obtained by other more accurate methods for some test configurations; it is shown that the differences arising from ignoring boundary-boundary interactions are small (within normal engineering tolerances) and that they are a function of the curvature of the boundaries and the number of the boundaries. A formal procedure is described for evaluating the boundary-boundary interactions by using the Schwarz alternating technique.

In Chapter 4 compounding is applied to one or two cracks growing from a hole near to other boundaries, which may be the edges of a sheet or other holes. The hole with the crack is considered to be unloaded, *ie* no normal or shear forces acting on the perimeter of the hole. In this configuration a boundary, namely the edge of the hole, crosses the crack and it is necessary to introduce the concept of an 'equivalent crack'. This crack replaces the original crack plus the hole; the boundaries other than the hole are then considered to interact with the equivalent crack and these effects are compounded. It is found that the boundary-boundary interactions, *ie* between the hole and other boundaries, are often important and must be taken into account when evaluating the stress intensity factor. Since the stress *concentration* factor is the dominant parameter at short crack lengths (see Chapter 2), this factor is used as a basis for determining the magnitude of the boundary-boundary effect.

Structural components frequently contain many holes, or cutouts, and the holes are often arranged in periodic arrays, for instance a row of fastener holes. The stress intensity factor for a crack at one of the holes is increased by the presence of the other holes. Since similar stress fields exist around each hole, it is likely that other cracks will be initiated at other holes at about the same time during the service life. Interactions with these other cracks will result in further increases in the stress intensity factor of the original crack. It is shown in Chapter 5 how the compounding method can be used to study the effects of many cracks at the edges of the holes in a row of unloaded holes.

In some structural components, loads are applied to the edges of holes, *eg* pin-loaded lugs and lap joints, and some fastener holes are loaded. In Chapter 6 the problem is considered of many cracks at the edges of the holes in a row of loaded holes near a boundary. For these types of configuration, a further development of the compounding theory is required. This development which introduces the concept of the 'equivalent load' is described in Chapter 6.

Many structural components are made from large panels which are reinforced at intervals with stiffeners. The stress intensity factor for cracks in these panels, which often start at the rivets attaching the stiffeners to the panel can also be obtained using the compounding method if the stiffeners are treated as boundaries. In Chapter 7 it is shown how the stress intensity factor of a crack at one of the stiffeners, broken or unbroken, in a stiffened sheet may be obtained. If the stiffener actually crosses the crack, it is necessary to use the concept of the 'equivalent crack' which was developed for cracks at holes.

Because of the periodic nature of stiffened sheet construction, *ie* stiffeners are regularly spaced, cracks are likely to be initiated at more than one stiffener as the stress fields will be similar at similar locations. The stress intensity factor for any given crack will be increased by the presence of other cracks, and since this will lead to a reduction in the fatigue life of the structure, it must be considered in the original design and in the determination of inspection and maintenance schedules. In Chapter 8 it is shown how compounding can be used to obtain stress intensity factors when there are many cracks in a periodically stiffened panel.

Since the importance of boundaries and their effects on cracks is an essential part of the compounding method, and since it is quick and cheap to use, it is an ideal tool for design studies. Chapter 9 contains a design study in which it is shown that by arranging fastener holes in two rows instead of one, significant improvements can be obtained in the fatigue life-time of a cracked component. Such studies are necessary to design optimum structures subject to the requirements of damage-tolerant specifications. Recently Brussat, Chiu, Rudd and Creager<sup>13</sup> have performed a reliability assessment of the use of the compounding method in the damage tolerance analysis of reinforced structural panels. They demonstrated that this simple analytical approach produces predictions of fatigue lifetimes which agree with test

results to an accuracy sufficient to justify its use in damage tolerant design analysis.

In this thesis we identify the important structural features, namely stress concentrations and boundaries, which affect the magnitude of the stress intensity factor when the structure is cracked, and develop approximate stress analysis methods which quantify the effects of these features. It is shown that the uncertainties in calculated values of residual static strength and fatigue lifetimes, due to the approximate analysis, are acceptable in most engineering applications. The methods can be used to plan reliable and safe inspection and maintenance procedures in existing aerospace structures, and they can be used to design damage-tolerant components. The compounding method is particularly useful in design since it isolates the effect of each boundary in turn and therefore enables the important ones to be identified. While some emphasis has been placed on airframe components, the methods are not limited to these applications.

CHAPTER 2ERRORS IN STRESS ANALYSIS AND THEIR EFFECTS<sup>11</sup>

Calculated values of stress intensity factors will contain errors if approximate stress analysis techniques are used. The magnitude of the errors can often be estimated, but their importance will depend on the practical application. The commonest fracture mechanics applications are the determination of residual strengths and fatigue lifetimes for cracked structures. Errors in the stress intensity factors will cause uncertainties in these two important quantities. In this chapter uncertainties that arise from using an approximate method of stress analysis are evaluated and compared with those arising from other sources. A particularly simple method of stress analysis was chosen in order to facilitate the calculations of residual strength and fatigue lifetime, but the conclusions are applicable to any method of stress analysis that leads to similar errors in the stress intensity factors.

The successful application of the principles of fracture mechanics to a practical problem requires a knowledge of the following:

- (1) the crack size (length, shape, etc);
- (2) the stresses due to service loads;
- (3) the stress intensity factor, at the tip of the crack;
- (4) material properties (*eg*  $K_{Ic}$ ,  $K_c$ ,  $d\ell/dN$ , etc).

These four items are known imperfectly. The uncertainties in items 1, 2 and 4 are usually presented to the fracture mechanics analyst who must then decide on what degree of accuracy is required in the evaluation of the stress intensity factor. This section investigates the possibility of using very simple and cheap approximations for the stress intensity factor for cracks initiated at stress concentrations such as holes and compares the possible errors introduced into a fracture mechanics calculation with those due to the other uncertainties.

The measurement of crack length in practice is often difficult and can result in inaccuracies which may be significant, particularly if the crack is short. Access to the cracked component may be difficult; the ends of the crack may be obscured by other parts of the structure or by protective coatings; the crack length within the thickness of a component may be different from that observed on the surface. It is not possible to specify the likely inaccuracies in a general way, since they will depend on the actual configuration.

The stresses in the uncracked structure may not be known accurately, because the external loads are not known accurately, or because the structural configuration is so complex that an accurate stress analysis is not possible, or because residual stresses of unknown magnitude may be locked in it as a result of overstraining during fabrication. The uncertainties in external loads often arise because the loads themselves are of a variable nature, *eg* gust loading on aircraft wings, or wave loading. It is not possible to assess accurately what the uncertainties in the stresses are, but it is likely that they will be at least 10% over much of the structure and probably more in some cases. Differences as large as 5:1 between the fatigue life established by full-scale testing under anticipated service loads and the actual service life have been measured (see, for example, Ref 14). Although these results will include scatter in crack initiation they suggest that actual service stresses may differ by more than 10% from the design stresses. (The dependence of fatigue life or crack growth rate on the stress intensity factor, which is proportional to the applied stress, is discussed later.)

Although many stress intensity factors are now known<sup>2-4</sup> the one appropriate to a given complex structural configuration is often not known. The calculation of the necessary stress intensity factor by standard techniques may be very costly and time-consuming and may still not be very accurate. There is thus a need for simple and cheap, even if approximate, methods to obtain stress intensity factors which could be used in parametric studies in preliminary design (parts of the final design may require a more detailed analysis), and in the determination of maintenance schedules for structures which may contain cracks.

Materials data books, for example Ref 15, show that, for what is nominally the same material, the scatter in  $K_{Ic}$  and  $K_c$  values may be 10% or more; fatigue crack growth-rates, usually expressed in terms of the increment in crack-length per stress-cycle  $dl/dN$ , may vary by a factor of 2 or more for the same nominal test conditions. Further uncertainties may arise because  $K_c$ , the thin-section toughness parameter, depends not only on the material but also on the sheet thickness; in fact it also depends on the crack-length, the specimen geometry and the type of loading.

Most applications of fracture mechanics involve calculations of the residual static strength, *ie* the strength of a component which contains a crack, and also calculations of the rate of growth of fatigue cracks.

Simple methods of doing such calculations are discussed in this section. Estimates of the errors due to using simplified expressions for the stress intensity factors, are obtained by comparing the 'simplified results' with accurate numerical results for some representative configurations of cracks at the edges of holes. These errors are then compared with those due to uncertainties in material properties and structural stresses.

The simple expressions for stress intensity factors, derived in section 2.1, consist of a combination of the two limiting cases, that for the short crack and that for the long crack. Cracks are considered 'short' when the length is small compared to the hole-size and 'long' when the length is large compared to the hole-size. The need to distinguish between 'short' cracks and 'long' cracks has been demonstrated by Novak and Barsom<sup>16</sup> for notched specimens used in fracture toughness testing. The important parameter when the crack is short is the stress concentration factor  $K_t$  (the ratio of the maximum stress to the applied stress). The shape, size and position of the initial stress-concentrator (hole, notch, etc) loses significance when the crack is long; the total crack-length, including the hole, is now the controlling parameter.

The geometric configurations studied represent some common practical problems concerned with cracks growing in the vicinity of stress concentrations. Circular holes in large sheets are considered first, with either one crack (section 2.2.1) or two cracks (section 2.2.2) at the edge of the hole; in both cases the sheet is loaded by uniform tensile stresses remote from the hole. In section 2.2.3 two cracks at the edges of elliptical holes of various eccentricities are considered subject to similar loading conditions. Since a common site for cracking is the edge of pin-loaded holes and bolt-holes the effect of localized loading at the edge of a cracked circular hole on the calculations of residual strength and the growth times of fatigue cracks is studied in section 2.2.4. A solution for cracks at the bore of a rotating disc is obtained in section 2.2.5.

It is shown that errors resulting from the use of these simple limits for stress intensity factors are of the same order as, or less than, errors due to other uncertainties in a fracture mechanics calculation. Improvements in the prediction of residual strength and fatigue growth-times can be made by considering the stress field in the uncracked structure along the crack-site (specifically the stress at the tip or the

mean stress over the crack-site). These improvements however require a knowledge of the stress fields which are not as readily available as the stress *concentration* factors<sup>17</sup> and are more difficult to obtain.

Thus these simple methods are often the only methods available for use in a reasonable time and at a reasonable cost, although their use will introduce additional errors into any fracture mechanics calculations. A knowledge of the magnitude of these additional errors, evaluated in this chapter and a comparison with the other sources of error will enable engineers and designers to decide whether the use of these simplifications is acceptable in any given case.

## 2.1 Development of asymptotic stress analysis

A common site for cracks in engineering structures is the edge of a filled hole (rivet hole or bolt hole, window, inspection hatch, etc) where there is usually a high stress concentration<sup>1</sup>. The most likely site for a crack is at the edge of the hole where the maximum stress  $\sigma_{\max}$  occurs; the crack will usually extend in a direction perpendicular to the applied tensile stress. The behaviour of a crack is controlled by the opening mode stress intensity factor  $K_I$  which can be written in the following general form\*:

$$K = Ys\sqrt{\pi\ell} \quad (2.1)$$

where  $Y$ , called the geometry factor, is a variable which is a function of the specific cracked geometry,  $s$  is an applied stress, the form of which will depend on the loading and  $\ell$  is the crack-length measured from the edge of the hole. Some general limiting values of  $Y$  can be obtained from physical considerations, and these form the basis of an approximate method of determining  $K$ .

It is usual to express the maximum stress  $\sigma_{\max}$  at the edge of the hole in terms of an applied stress  $s$  and a stress *concentration* factor  $K_t$ , thus

$$\sigma_{\max} = K_t s \quad (2.2)$$

The stress  $s$  takes different forms depending on the type of loading. Cracks will initiate at the edge of a hole where the maximum stress occurs. If the relevant dimension of the hole is  $D$ , *ie* the 'diameter'

---

\* The subscript I on  $K_I$  is omitted in the rest of this thesis as only the opening mode is considered.

of the hole parallel to the crack (see Fig 2.1), then a crack of length  $\ell$  is considered short if  $\ell \ll D$ . In the limit as  $\ell/D \rightarrow 0$ , very short cracks will experience a stress field similar to that experienced by a similar crack at the edge of a sheet subjected to a uniform stress of the same magnitude and direction as the maximum stress at the hole. The stress intensity factor will therefore tend to that for an edge crack (Case 1.1.20 of Ref 2), *ie*

$$\lim_{\ell/D \rightarrow 0} \{K\} = 1.12 \sigma_{\max} \sqrt{\pi \ell} . \quad (2.3)$$

From equations (2.1) to (2.3) it follows that the limiting value of  $Y$  is given by

$$\lim_{\ell/D \rightarrow 0} \{Y\} = 1.12 K_t . \quad (2.4)$$

The tip of a very long crack ( $\ell/D \rightarrow \infty$ ) will be in a stress field similar to that for an isolated crack whose length is equal to the original length plus the width of the hole. If the length of the equivalent isolated crack is  $2a$ , then for a single crack of length  $\ell$  at the edge of a hole

$$2a = \ell + D , \quad (2.5)$$

and for two collinear cracks of lengths  $\ell_1$  and  $\ell_2$  on opposite sides of the hole

$$2a = \ell_1 + D + \ell_2 . \quad (2.6)$$

The limiting value of  $K$ , when  $\ell/D$  is infinite, will depend on the type of loading.

A simple approximation for the stress intensity factor can be obtained using just these two limits. It is suggested that for 'short' cracks the geometry factor  $Y$  is replaced by its limiting ( $\ell/D = 0$ ) value, and for 'long' cracks  $Y$  is replaced by its limiting ( $\ell/D = \infty$ ) value. The crack length at which the transition between 'short' and 'long' cracks occurs depends on the configuration; it will normally be chosen so as to minimise the errors in the stress intensity factor over the whole range of crack lengths. The transition crack length will be a function of the local radius of curvature of the hole at the root of the crack.

### 2.1.1 Loading remote from the hole

If the hole and the crack are in a large sheet which is loaded remote from the hole with a uniform uniaxial tensile stress  $\sigma$ , acting in a direction perpendicular to the crack, then in equations (2.1) and (2.2)

$$s = \sigma \quad (2.7)$$

and equation (2.4) for the short-crack limit is unchanged. For this loading, the limit of the stress intensity factor at very long crack-lengths is that of an isolated crack of length  $2a$  in a sheet uniformly stressed at infinity, and is given by

$$\lim_{\ell/D \rightarrow \infty} \{K\} = \sigma \sqrt{\pi a} \quad , \quad (2.8)$$

where  $a$  is given by equations (2.5) or (2.6). The limit for the geometry factor  $Y$  is given by

$$\lim_{\ell/D \rightarrow \infty} \{Y\} = \sqrt{\frac{a}{\ell}} \quad . \quad (2.9)$$

Simple expressions for the stress intensity factor can be obtained by using equations (2.4) and (2.9) in equation (2.1);  $Y$  is given by

$$\text{and } \left. \begin{aligned} Y &= 1.12 K_t \quad \text{for 'short' cracks} \\ Y &= \sqrt{\frac{a}{\ell}} \quad \text{for 'long' cracks.} \end{aligned} \right\} \quad (2.10)$$

### 2.1.2 Loading on the perimeter of the hole

If the hole is subjected to a tensile force per unit thickness  $P$  acting on its edge at right angles to the plane of the crack, then the stress  $s$  in equations (2.1) and (2.2) is replaced by the 'bearing stress'  $P/D$  and  $\sigma_{\max}$  becomes

$$\sigma_{\max} = K_t \left( \frac{P}{D} \right) \quad . \quad (2.11)$$

Equation (2.4) for the short crack limit is unchanged. For this loading the limit of the stress intensity factor at very long crack-lengths is that of an isolated crack of length  $2a$  subjected to a force per unit thickness  $P$  acting on the crack face perpendicular to the crack plane. The distance between the point of application of  $P$  and the crack tip (or tips) is the same as the perpendicular distance between the line of

application of  $P$  and the crack tip (or tips) when the force was applied at the edge of the hole. If the hole is symmetrical about the line of application of  $P$  then, for one crack of length  $\ell$ ,  $K$  is given (Case 1.1.12, Ref 2) by

$$\lim_{\ell/D \rightarrow \infty} \{K\} = \frac{P}{2\sqrt{\pi a}} \sqrt{\frac{R}{R+\ell}} \quad , \quad (2.12)$$

and, for two cracks of length  $\ell_1$  and  $\ell_2$ ,  $K$  is given (Case 1.1.12, Ref 2) by

$$\lim_{\ell_2/D \rightarrow \infty} \{K\} = \frac{P}{2\sqrt{\pi a}} \sqrt{\frac{R+\ell_1}{R+\ell_2}} \quad , \quad (\text{for the crack of length } \ell_2) \quad (2.13)$$

where  $R = D/2$ . The limit for  $Y$  is given by

$$\lim_{\ell/D \rightarrow \infty} \{Y\} = \frac{R}{\pi\sqrt{a\ell}} \sqrt{\frac{R}{R+\ell}} \quad (2.14)$$

for one crack, and

$$\lim_{\ell_2/D \rightarrow \infty} \{Y\} = \frac{R}{\pi\sqrt{a\ell_2}} \sqrt{\frac{R+\ell_1}{R+\ell_2}} \quad (2.15)$$

for the crack of length  $\ell_2$  when there are two cracks.

Simple expressions for the stress intensity factors, for both one and two cracks, can be obtained by using equations (2.4) and (2.14) or (2.15) in equation (2.1); for one crack,  $Y$  is given by

$$\text{and } \left. \begin{aligned} Y &= 1.12 K_t && \text{for 'short' cracks} \\ Y &= \frac{1}{\pi} \sqrt{\frac{2}{\lambda(\lambda+1)(\lambda+2)}} && \text{for 'long' cracks} \end{aligned} \right\} \quad (2.16)$$

where  $\lambda = \ell/R$ ; for two cracks,  $Y$  is given, for the crack of length  $\ell_2$ , by

$$\left. \begin{aligned} Y &= 1.12 K_t && \text{for 'short' cracks} \\ Y &= \frac{1}{\pi} \sqrt{\frac{2(\lambda_1+1)}{\lambda_2(\lambda_2+1)(\lambda_2+\lambda_1+2)}} && \text{for 'long' cracks} \end{aligned} \right\} \quad (2.17)$$

where  $\lambda_1 = \ell_1/R$  and  $\lambda_2 = \ell_2/R$ .

If a uniform pressure  $p$  acts on the upper surface of the hole, then  $s$  is replaced by  $p$  in equations (2.1) and (2.2). Equations (2.11) to (2.17) are still applicable with  $P/D$  replaced by  $p$ .

### 2.1.3 Residual strength and fatigue crack growth calculations

The stress intensity factors derived above are used in two main ways in fracture mechanics calculations: (i) to determine the residual static strength of a cracked component and to compare the strength with that required to withstand the most severe service loading with adequate safety factors and (ii) to determine whether a cracked, but safe, component will become unsafe due to crack growth under fatigue conditions. The residual strength  $s_r$  is obtained by equating the stress intensity factor to the appropriate material constant  $K_{Ic}$  or  $K_c$ , *eg*

$$K = Ys_r \sqrt{\pi \ell} = K_c . \quad (2.18)$$

If  $s_r$  is greater than the maximum service stress (safety factors may be included) then the component has adequate strength. However cracks grow longer under the common service conditions of varying stress (fatigue); in practical cases the function  $Y$  in equation (2.18) will be such that an increase in crack-length  $\ell$  results in a decrease in the strength  $s_r$ . There will thus be a critical crack-length beyond which the crack will grow rapidly and the component will become unsafe.

The rate of growth of cracks is determined by the stress intensity factor. It is necessary to be able to calculate how long (how many stress cycles) it will take for a crack to grow to an unsafe length. The calculation of growth-times, usually expressed in terms of cycles of applied stress, requires the knowledge of a crack growth law. A law which is applicable to constant amplitude fatigue loading and which relates the growth rate per fatigue cycle to the stress intensity factor will be used in this thesis. For many materials crack growth in fatigue can be approximately described by a power law<sup>18</sup>; this can be written as

$$\frac{d\ell}{dN} = C(\Delta K)^m \quad (2.19)$$

where  $d\ell/dN$  is the increase in crack-length per cycle of stress,  $C$  and  $m$  are constants (dependent on material) and  $\Delta K$  is the range of stress intensity factor, which is defined as

$$\Delta K = K_{\max} - K_{\min} , \quad (2.20)$$

where  $K_{\max}$  and  $K_{\min}$  are respectively the maximum and minimum values of the stress intensity factor during a fatigue cycle. The number of cycles  $\Delta N$  required for a crack of initial length  $\ell_i$  to reach a final length  $\ell_f$  can be obtained by integrating equation (2.19); it is given by

$$\Delta N = \frac{1}{C} \int_{\ell_i}^{\ell_f} \frac{d\ell}{(\Delta K)^m} . \quad (2.21)$$

The initial crack-length  $\ell_i$  will depend on the actual application: it should not be less than the smallest crack-length that can be reliably detected using standard non-destructive inspection methods or it could be an actual crack-length detected in a routine inspection; it might be the largest flaw-size likely to result from a given manufacturing or fabrication technique, a size which might therefore be adopted as a standard length and specified by damage-tolerant design requirements. The final crack-length  $\ell_f$  would be that length, less some safety factor, at which rapid crack growth occurs and so the component can no longer be guaranteed safe without either repair or replacement.

Typically the power  $m$  is in the range 2 to 4 for common airframe alloys. Although the total life, for a given stress level, decreases the greater  $m$  is, a larger proportion of the lifetime, *ie* the majority of the stress cycles, is generally spent while the crack-length is close to the lower limit  $\ell_i$ . The effect is more pronounced for small  $\ell_i$  because  $\Delta K$  is smaller and the crack grows more slowly. This dependence of  $\Delta N$  on  $m$  is illustrated in Fig 2.2 for the case of a crack growing from a hole in a sheet subjected to a uniform uniaxial, alternating tensile stress remote from the hole. The ratio  $\Delta N_L / \Delta N_R$  is plotted as a function of  $L/R$ ;  $\Delta N_L$  and  $\Delta N_R$  are the numbers of cycles required for a crack to grow from an initial length of  $0.01R$  to a final length of  $L$  and  $R$  respectively. These results were obtained using the numerical solution of Tweed and Rooke<sup>19</sup> for the  $\Delta K$  values and integrating equation (2.21) numerically. From Fig 2.2 it can be seen that  $\Delta N_L = 0.5\Delta N_R$  when  $L = 0.44R$  for  $m = 1$ , when  $L = 0.32R$  for  $m = 2$ , when  $L = 0.16R$  for  $m = 3$ , and when  $L = 0.04R$  for  $m = 4$ . In order that full allowance can be made for short-crack behaviour in determining  $\Delta N$  the simple expressions used for  $K$  must be accurate at short crack-lengths; otherwise damage-tolerant airframe designs may lead to structural inefficiencies.

The use of approximate expressions for  $Y$  in the calculation of residual strengths and fatigue lifetimes introduces errors into the results for these quantities. The magnitude of these errors is related to the magnitude of the error in  $Y$ . If  $\delta Y$  is the error in  $Y$  etc, then, from equation (2.18), the error in residual strength  $s_r$  is given by

$$\frac{\delta s_r}{s_r} = \left( \frac{\delta K_c}{K_c} - \frac{1}{2} \frac{\delta \ell}{\ell} \right) - \frac{\delta Y}{Y}, \quad (2.22)$$

where all errors are considered small (*ie*  $|\delta Y/Y| \ll 1$ ). Equation (2.22) shows that an error of  $\pm x\%$  in  $Y$  produces an additional error of  $\mp x\%$  in  $s_r$ . Thus an approximation which overestimates  $Y$  (*ie*  $\delta Y > 0$ ) will tend towards a safe underestimate of the strength  $s_r$ . The approximation suggested using the stress concentration factor  $K_t$  always overestimates  $Y$  in the important short crack region; that is, it always gives conservative estimates of residual strength.

The effect of errors in  $Y$  on fatigue lifetimes is more difficult to quantify since the calculation of  $\Delta N$  in equation (2.21) involves integrating  $Y^{-m}$ . Thus the results depend on the errors in  $Y$  over the whole range of crack growth and also depend on the constant  $m$ . The error in growth-rates depend on  $\delta Y$  in a simple way since, from equation (2.19),  $\delta(da/dN)$  is given by

$$\frac{\delta(da/dN)}{da/dN} = m \left[ \frac{\delta Y}{Y} + \frac{\delta s}{s} + \frac{1}{2} \frac{\delta \ell}{\ell} \right]. \quad (2.23)$$

Thus an error of  $\pm x\%$  in  $Y$  introduces an additional bigger error of  $\pm mx\%$  in the growth-rate. The effect of this increased error on  $\Delta N$  is mitigated by the fact that the larger  $m$  is, the more cycles are spent at shorter crack lengths where the errors in  $Y$  will be less. Equation (2.23) shows that an overestimate of  $Y$  will tend to overestimate  $da/dN$  and hence tend to produce a conservative underestimate of the lifetime; the  $K_t$  approximation does, in fact, always overestimate  $Y$ .

## 2.2 Applications of asymptotic stress analysis

Many cracks occur at the edges of filled holes, across which there is little load transfer and these can be represented by cracks at the edge of a circular hole (sections 2.2.1 and 2.2.2) or an elliptical hole (section 2.2.3). The holes are considered to be in large sheets which are loaded by uniform stresses remote from the cracks. Other cracks occur at holes which are subjected to loads at the edge of the holes.

Two extremes of loading are considered in section 2.2.4, namely, a point load and a uniform pressure. Cracks can also occur at stress concentrations in rotating machinery such as aero-engines. The case of a crack at the bore of a rotating annular disc is considered in section 2.2.5; the loading consists of body forces due to the rotation.

Accurate numerical solutions for the stress intensity factors are available for the configurations studied and are used as a basis for comparison with the approximate solutions.

### 2.2.1 One crack from a circular hole - remote loading

The opening mode stress intensity factor for a crack of length  $\ell$  at the edge of a circular hole of radius  $R$  (see Fig 2.3) can be written, following equation (2.1), as

$$K = Y\sigma\sqrt{\pi\ell} \quad , \quad (2.24)$$

where  $\sigma$  is the applied uniaxial tensile stress remote from the crack and  $Y$  is given by equation (2.10). For this configuration  $K_t = 3$  and  $2a = 2R + \ell$ , therefore equation (2.10) becomes

$$\text{and } \left. \begin{aligned} Y &= 3.36 && \text{for 'short' cracks} \\ Y &= \sqrt{\frac{2R + \ell}{2\ell}} && \text{for 'long' cracks.} \end{aligned} \right\} \quad (2.25)$$

The accurate results for  $Y$  obtained at discrete values of  $\ell/R$  by Tweed and Rooke<sup>19</sup> are shown in Fig 2.4 together with the two expressions for  $Y$  given by equation (2.25). From this figure it can be seen that the two expressions intersect at  $\ell/R = 0.092$ . The errors in  $Y$  are minimised by changing from the short crack expression to the long crack expression at this value of  $\ell/R$ ; for convenience in the crack growth calculations the changeover point was chosen to be  $\ell/R = 0.1$ . Thus for this configuration  $Y$  is given by

$$\text{and } \left. \begin{aligned} Y &= 3.36 \quad , && \ell/R \leq 0.1 \\ Y &= \sqrt{\frac{2R + \ell}{2\ell}} \quad , && \ell/R > 0.1 \quad . \end{aligned} \right\} \quad (2.26)$$

The percentage differences between the values of  $Y$  obtained from equation (2.26) and the accurate numerical results are shown in Fig 2.5; the percentage differences are defined as

$$\text{difference (\%)} = \frac{Y_{\text{app}} - Y_{\text{num}}}{Y_{\text{num}}} \times 100 . \quad (2.27)$$

It can be seen that the maximum difference ( $\sim 21\%$ ) occurs at the transition point,  $\ell/R = 0.1$ , but falls rapidly for both smaller and larger values of  $\ell/R$ . The effect on residual strength of these errors in  $Y$  is given by equation (2.22).

An approximate value  $\Delta N_{\text{app}}$  may be obtained from equation (2.21) by substituting the appropriate form of equation (2.26) into the expression for  $\Delta K$ ,

$$\Delta K = Y\Delta\sigma\sqrt{\pi\ell} , \quad (2.28)$$

and substituting this into the integrand of equation (2.21). The resulting integrals are known and the solutions are given in Appendix A. An accurate estimate  $\Delta N_{\text{num}}$  may be obtained from equation (2.21) by using the results of Tweed and Rooke<sup>19</sup> and integrating numerically. The ratio of  $\Delta N_{\text{app}}/\Delta N_{\text{num}}$  is shown in Fig 2.6 as a function of  $\ell_f/R$  for an initial crack-length  $\ell_i = 0.01R$  and  $m = 2, 3, 4$ . It can be seen that over most of the range (which includes all short cracks) this approximation gives a 'safe' underestimate of  $\Delta N$ ; the maximum underestimate is  $\sim 20\%$ .

The errors in  $\Delta N$ , due to using these approximations for the stress intensity factor, do not vary in a systematic manner as  $m$  increases. This is because as  $m$  increases the smaller values of  $\Delta K$ , *ie* those for shorter cracks, dominate in the evaluation of  $\Delta N$  (see equation (2.21)); the errors in the K-approximation are smaller for shorter cracks. Thus the magnitude of the errors will depend in a complex way on both the initial and the final crack-length as well as on  $m$ . From Fig 2.5 it can be seen that the maximum errors in  $K$  occur at  $\ell/R = 0.1$ . Since for  $\ell_i > 0.1R$  the largest errors are not in the range of integration in equation (2.21), and since for  $\ell_i < 0.1R$  the dominating effect of growth at the shortest lengths will mitigate the effects of the large errors at  $\ell_i \approx 0.1R$ , it follows that the most inaccurate values of  $\Delta N$  will be obtained when  $\ell_i \sim 0.1R$ . To illustrate this  $\Delta N$  has also been obtained for an initial crack-length of  $0.1R$ ; the ratio  $\Delta N_{\text{app}}/\Delta N_{\text{num}}$  is shown in Fig 2.7. The errors, which are larger for bigger values of  $m$  are greater than those for  $\ell_i/R = 0.01$  (see Fig 2.6). For  $\ell_f/R \geq 0.2$  the error lies between  $\pm 12\%$  for  $m = 2$ ,  $\pm 17\%$  for  $m = 3$ , and  $\pm 25\%$  for  $m = 4$ . For shorter cracks ( $\ell_f/R \leq 0.35$ )  $\Delta N$  is underestimated and for longer cracks overestimated.

The initial growth between  $\ell_f/R = 0.1$  and 0.2 is underestimated by up to 60%.

### 2.2.2 Two cracks from a circular hole - remote loading

In many practical cases there may be two cracks, one each side of the hole, which may not be of equal length. Fig 2.8 shows this with two cracks of length  $\ell_A$  and  $\ell_B$ ; the crack-tips A and B have stress intensity factors  $K_A$  and  $K_B$  respectively. The following analysis considers tip B only for various values of the ratio  $\ell_A/\ell_B$ . In practice the longer crack is the more dangerous because it has the larger stress intensity factor<sup>20</sup>, *ie*

$$K_B > K_A \quad \text{if} \quad \ell_B > \ell_A . \quad (2.29)$$

The opening mode stress intensity factor for crack-tip B can be written, following equation (2.1), as

$$K_B = Y_B \sigma \sqrt{\pi \ell_B} , \quad (2.30)$$

where  $\sigma$  is the applied uniaxial tensile stress remote from the crack and now replaces  $s$  in equations (2.1) and (2.2) and  $Y_B$  is given by equation (2.10) with appropriate expressions for  $K_t$  and  $a$ . The stress concentration factor  $K_{tB}$  at the edge of the hole opposite A when  $\ell_B = 0$  is a function of  $\ell_A$ ; a curve of  $K_{tB}$  vs  $\ell_A$ , derived from the work of Tweed and Rooke<sup>20</sup> is shown in Fig 2.9. The total crack-length  $2a$  is given by

$$2a = \ell_A + 2R + \ell_B . \quad (2.31)$$

Hence equation (2.10) becomes

$$\left. \begin{aligned} Y_B &= 1.12K_{tB} && \text{for } \ell_B/R \leq 0.1 \\ \text{and} \\ Y_B &= \sqrt{\frac{\ell_A + 2R + \ell_B}{2\ell_B}} && \text{for } \ell_B/R > 0.1 . \end{aligned} \right\} \quad (2.32)$$

The transition at  $\ell_B/R = 0.1$  was chosen to be close to the intersection of the two curves as in the previous example (see section 2.2.1).

The percentage differences (as defined by equation (2.27) between the approximate values of  $Y_B$  and the numerical results<sup>20</sup> are shown in Fig 2.10 for  $\ell_A/R = 0.0$  and 1.0. Examination of the numerical results

shows that for  $\ell_A/R \leq 1$  the function  $Y_B/K_{tB}$  is independent of  $\ell_A$  over the range  $0 \leq \ell_B/R \leq 0.1$ . Thus the percentage difference shown in Fig 2.10, for  $\ell_B/R \leq 0.1$ , is identical with that for a single crack ( $\ell_A = 0$ ) shown in Fig 2.5. For  $\ell_B/R > 0.1$  the curve for  $\ell_A/R = 0$  is also identical with that shown in Fig 2.5. The maximum difference is therefore again about 21% at  $\ell_B/R = 0.1$ ; the maximum difference for  $\ell_A/R = 1.0$  is about 3% higher. Curves of  $\ell_A/R > 1.0$  have been omitted since the concern is with  $\ell_B > \ell_A$  and therefore only values of  $\ell_B/R > \ell_A/R$  need be considered and it can be seen from Fig 2.10 that differences are small ( $\leq 4\%$ ) for  $\ell_B/R \geq 1.0$ .

For short cracks ( $\ell_B/R \leq 0.1$ ) the errors introduced into calculations of residual strength and growth-times by the use of these approximations for  $Y_B$  are the same as for a single crack from a circular hole (section 2.2.1, Figs 2.6 and 2.7). For long cracks ( $\ell_B/R > 0.1$ ) the errors in the residual strength will depend on both  $\ell_A/R$  and  $\ell_B/R$  (see Fig 2.10). Initially ( $\ell_B/R \leq 0.2$ ) the errors will be a few per cent larger but for  $\ell_B/R \geq 0.2$  the errors will be less than those for the single crack ( $\ell_A/R = 0$ ). The errors in growth-times for long cracks will be dependent on both  $\ell_A/R$  and  $\ell_B/R$  but will not differ greatly from those for a single crack (Figs 2.6 and 2.7). This is because the percentage differences in  $Y_B$  for  $\ell_A/R \neq 0$  are only a few per cent different from those for  $\ell_A/R = 0$ , and since they are sometimes larger and sometimes smaller the effects will tend to cancel out if crack growth extends beyond  $\ell_B/R \geq 0.2$ . As in the single-crack case the maximum errors will occur if the initial crack-length is about  $0.1R$ .

### 2.2.3 Two cracks from an elliptical hole - remote loading

In order to demonstrate the wide applicability of the approximations suggested in the previous two sections (2.2.1 and 2.2.2), the problem of two equal-length cracks at the edge of an elliptical hole is considered in this section. The two cracks of length  $\ell$  are at the ends of one of the axes of the ellipse; the axis with the cracks is of length  $2c$  and the other axis of length  $2h$ . A uniform uniaxial tensile stress  $\sigma$  is applied at right angles to the crackline remote from the hole (see Fig 2.11). Newman<sup>21</sup> has obtained stress intensity factors as a function of crack-length for this configuration; he considered five values of  $h/c$ , viz 0.25, 0.5, 1.0, 2.0 and 4.0.

As before, the opening mode stress intensity factor can be written, replacing  $s$  by  $\sigma$  in equation (2.1), as

$$K = Y\sigma\sqrt{\pi\ell} \quad , \quad (2.33)$$

where  $Y$  is given by equation (2.10). The stress *concentration* factor  $K_t$  on the  $c$ -axis for an uncracked ellipse is given by

$$K_t = 1 + 2 \frac{c}{h} \quad . \quad (2.34)$$

The total crack-length is given by

$$a = c + \ell \quad . \quad (2.35)$$

In order to use equation (2.10) the transition point from 'short' cracks to 'long' cracks is considered to be a function of the radius of curvature  $\rho$  of the ellipse at the points from which the cracks originate. The parameter  $\rho$  is given by:

$$\rho = \frac{h^2}{c} \quad . \quad (2.36)$$

In the previous sections, for cracks at the edge of circular holes, the transition point was expressed in terms of the radius  $R$  of the hole. For the case  $h/c = 1$  the ellipse becomes a circle and  $\rho = R$ , therefore to ensure that the transition occurs at the same place as in sections 2.2.1 and 2.2.2 it is chosen to occur at  $\ell/\rho = 0.1$ . Thus the approximate expression for  $Y$  is given by

$$\text{and } \left. \begin{array}{l} Y = 1.12K_t \quad \text{for } \ell/\rho \leq 0.1 \\ Y = \sqrt{\frac{\ell + c}{\ell}} \quad \text{for } \ell/\rho > 0.1 \end{array} \right\} \quad (2.37)$$

The percentage differences (equation (2.27)) between the above approximation and the numerical results<sup>21</sup> are plotted in Fig 2.12 as a function of  $\ell/\rho$  for the different values of  $h/c$ . For  $\ell/\rho < 0.1$  the differences are independent of  $h/c$  and identical to those for cracks from circular holes (Figs 2.5 and 2.10). For  $\ell/\rho > 0.1$  the differences are a function of the ratio  $h/c$ . The maximum difference occurs at  $\ell/\rho = 0.1$  and increases as  $h/c$  decreases. In most practical problems  $h/c \geq 1$ , however if  $h/c$  is small, then  $\rho (= h^2/c)$  is small and practical values of  $\ell/\rho$  will probably be greater than 0.1. The error introduced into the residual strength by the use of these approximations is given by equation (2.22).

Since the radius of curvature  $\rho$  varies as  $h/c$  varies, direct comparison of crack growth-times  $\Delta N$  cannot easily be made if the results are plotted as a function of  $l/\rho$ . For this reason crack growth-times have been calculated, in terms of  $l/c$ , *ie* the ratio of the crack-length to the semi-axis of the ellipse. From the numerical data available (Newman<sup>21</sup>) the smallest starting crack that can be considered is  $l_i = 0.02c$ . An approximate value  $\Delta N_{app}$  may be obtained in a similar way to that in section 2.2.1; again the necessary integrals in equation (2.21) are known; the solutions are given in Appendix B. An accurate estimate  $\Delta N_{num}$  may be obtained from equation (2.21) by using the results of Newman<sup>21</sup> and by integrating numerically. The ratio  $\Delta N_{app}/\Delta N_{num}$  is shown in Figs 2.13 to 2.15 assuming three different forms of the crack growth law ( $m = 2, 3$  or  $4$  in equation (2.19)). Each graph contains curves for the different values of  $h/c$ ; the transition from the short crack approximation ( $l/\rho < 0.1$ ) to the long crack approximation ( $l/\rho > 0.1$ ) occurs at different values of  $l_f/c$  on the different curves because  $\rho$  is a function of  $h/c$ .

Comparison of Figs 2.13 to 2.15 show that the approximate growth-times are predominantly conservative, *ie* safe, since the number of stress cycles is underestimated. It can also be seen that the errors tend to increase as  $m$  increases with a maximum of  $\sim 50\%$  for  $h/c = 0.5$  at  $m = 4$  and  $l_f/c = 0.04$ . The errors shown are always a maximum for  $h/c = 0.5$  at the shortest crack-length shown; this is because the starting crack-length of  $l_i = 0.02c$  is very close to the transition point of  $l/\rho = 0.1$  ( $l_i/c = 0.025$ ) and the errors in the stress intensity factor are a maximum. On average curves for the smallest value of  $h/c$  (0.25) and the largest (4.0) show the least deviation from unity which indicates that for both smaller and larger values of  $h/c$  outside the range 0.25 to 4.0 the approximations used would be even better.

#### 2.2.4 One crack from a circular hole - local loading

Cracks can grow from holes which are subjected to loads at their perimeters. Such holes frequently occur in structural components, *eg* bolted joints, pin-loaded lugs. Approximations similar to those used in the previous sections are applied to loaded holes in this section. The configuration of an infinite sheet containing a circular hole with a single radial crack at its edge is considered. The perimeter of the hole is subjected to two types of loading, either a localized radial force per unit thickness,  $P$  acting at right angles to the crack, or a

uniform pressure  $p$  acting over a semicircular arc with the resultant force per unit thickness ( $= 2pR$ ) in the same direction as  $P$  (see Fig 2.16a). In a real component the loading would consist of a variable pressure acting over part of the hole perimeter, rather than a force  $P$  localized at one point.

The opening mode stress intensity factor for a crack of length  $\ell$  at the edge of a circular hole, of radius  $R$ , subjected to local forces (see Fig 2.16) can be written as in equation (2.1)

$$K = Ys\sqrt{\pi\ell} \quad (2.38)$$

where  $Y$  is given by equation (2.16). The 'stress'  $s$  takes different forms depending on the loading on the hole: for a point force/unit thickness  $P$ ,  $s = P/2R$ ; for a uniform pressure  $p$  acting on half of the hole perimeter  $s = p$  (see Fig 2.16a). The stress concentration factor which appears in the short crack approximation in equation (2.16) is given, for the force  $P$ , by  $K_t = 2/\pi$ , and for the pressure  $p$ , by  $K_t = 0.5$ . The equivalent cracks for the long crack approximation are shown in Fig 2.16b.

The approximate values of  $Y$  obtained from equation (2.16) can be compared with accurate numerical values obtained by Tweed and Rooke<sup>20</sup>; this is done in Fig 2.17 where the percentage differences, as defined in equation (2.27) are plotted as a function of  $\ell/R$  for both the force  $P$  and the pressure  $p$ . In order to minimise the errors involved in using these approximations the transitions from the short crack to the long crack expressions should occur at different values of  $\ell/R$  for the two force distributions. For the point load  $P$  the maximum difference is  $\sim 30\%$  if the transition is at  $\ell/R \simeq 0.15$ , and for the pressure  $p$  the maximum is  $\sim 45\%$  if the transition is at  $\ell/R \simeq 0.25$ . These maximum differences are greater than those for remote loading (see Figs 2.5, 2.10 and 2.12) which are  $\sim 20\%$ . However differences greater than 20% occur only over small regions, viz from  $\ell/R = 0.1$  to 0.2 for the force  $P$  and from  $\ell/R = 0.1$  to 0.5 for the pressure  $p$ . Outside these regions the percentage differences are comparable to those for remote loading. The errors introduced into the residual strength by the use of these approximations will again be given by equation (2.22).

In order to simplify the calculations of  $\Delta N$  the transition from the short crack approximation to the long crack approximation was taken at the same value of  $\ell/R$ , namely  $\ell/R = 0.2$ , for both types of loading. Equation (2.16) therefore becomes, for the force  $P$ ,

$$\begin{array}{l}
 Y = \frac{2.24}{\pi} \quad \text{for } \ell/R \leq 0.2 \\
 \text{and} \\
 Y = \frac{1}{\pi} \sqrt{\frac{2}{\lambda(\lambda+1)(\lambda+2)}} \quad \text{for } \ell/R > 0.2,
 \end{array}
 \left. \vphantom{\begin{array}{l} Y = \frac{2.24}{\pi} \\ Y = \frac{1}{\pi} \sqrt{\frac{2}{\lambda(\lambda+1)(\lambda+2)}} \end{array}} \right\} (2.39)$$

and for the pressure  $p$ ,

$$\begin{array}{l}
 Y = 0.56 \quad \text{for } \ell/R \leq 0.2 \\
 \text{and} \\
 Y = \frac{1}{\pi} \sqrt{\frac{2}{\lambda(\lambda+1)(\lambda+2)}} \quad \text{for } \ell/R > 0.2.
 \end{array}
 \left. \vphantom{\begin{array}{l} Y = 0.56 \\ Y = \frac{1}{\pi} \sqrt{\frac{2}{\lambda(\lambda+1)(\lambda+2)}} \end{array}} \right\} (2.40)$$

An approximate value  $\Delta N_{\text{app}}$  may be obtained in a similar way to that in section 2.2.1; again the integrals appearing in equation (2.21) are known and are given in Appendix C. An accurate estimate  $\Delta N_{\text{num}}$  may be obtained from equation (2.21) by the numerical integration of the results of Tweed and Rooke<sup>20</sup>. Both  $\Delta N_{\text{app}}$  and  $\Delta N_{\text{num}}$  for  $\ell_i/R = 0.01$  have been calculated as a function of  $\ell_f/R$  for  $m = 2, 3$  and  $4$ . Fig 2.18 shows the ratio of  $\Delta N_{\text{app}}/\Delta N_{\text{num}}$  for the force  $P$  and Fig 2.19 the same ratio for the pressure  $p$ . Figs 2.18 and 2.19 show that the approximations are predominantly conservative, *ie* safe, since the time is underestimated for  $\ell_f/R \leq 1.0$  for a force  $P$ , and for  $\ell_f/R \leq 3$  for a pressure  $p$ . The errors are generally larger than those for a crack at the edge of a hole in a sheet loaded remote from the crack (see Fig 2.6). As in the case of remote loading errors would be at maximum if the starting crack-length  $\ell_i$  occurred at the transition from the short crack to the long crack approximation (see Figs 2.6 and 2.7). However the maximum errors of  $\sim 50\%$  are within the likely errors that can result from material variations, *ie* variations of a factor of two or more in crack growth-rates. The bigger errors at long cracks are due to the fact that  $K$  decreases and hence  $da/dN$  decreases and therefore an appreciable part of the fatigue life is spent while the cracks are long, which is in contrast to the behaviour for remote loading. In practice the presence of other boundaries would cause  $K$  to increase when the crack-tip approached them.

### 2.2.5 Cracks at the bore of a rotating annular disc

Cracks can sometimes arise in structures that have rotating components such as turbine discs in aero-engines. In this section both one and two cracks at the bore of a rotating annular disc are considered; the disc has an inner radius of  $R_i$  and an outer radius of  $R_o$  and is

rotating at an angular velocity  $\omega$  (see Fig 2.20a). This problem has been studied by Grandt<sup>22</sup> using a superposition technique with results from a finite element analysis.

The approximations developed in the previous sections, based on the short crack and long crack limits, can be used to derive a stress intensity factor for this configuration. The behaviour of short cracks will be controlled by the maximum stress, perpendicular to the crackline, at the bore of the disc. In plane stress the maximum stress is given (cf equation (2.3))

$$\sigma_{\max} = K_t p_0 \quad (2.41)$$

where

$$p_0 = \frac{3 + \nu}{8} d \omega^2 R_o^2, \quad (2.42)$$

and

$$K_t = 2 \left[ 1 + \frac{(1 + \nu)}{(3 + \nu)} \frac{R_i^2}{R_o^2} \right], \quad (2.43)$$

where  $d$  is the material density and  $\nu$  is Poisson's ratio<sup>23</sup>. The long crack approximation is obtained by replacing the crack(s) plus the hole by a single crack in a solid rotating disc of radius  $R_o$ . In the one-crack case the replacement crack is of length  $2R_i + \ell$  and is located eccentrically in the disc (see Fig 2.20b). In the two-crack case the replacement crack is of length  $2R_i + 2\ell$  and is located centrally in the disc (see Fig 2.20b). The stress intensity factors for both an eccentric and a central crack in a rotating solid disc were obtained from Rooke and Tweed<sup>24</sup>.

The geometry factors  $Y$  are defined by equation (2.1) with  $s$  replaced by  $p_0$ . The values of  $Y$  obtained from both the short and long crack approximations are shown in Fig 2.21 together with the results of Grandt<sup>22</sup>; the results were obtained for  $R_i/R_o = 0.5$  and  $\nu = 0.3$ . The percentage differences, as defined in equation (2.27) are shown in Fig 2.22 as a function of  $\ell/(R_o - R_i)$  for both one and two cracks. For one crack,  $\ell/(R_o - R_i) \leq 0.8$ , the differences lie between +8% and -4% if the transition from the short crack to the long crack approximation occurs at  $\ell/(R_o - R_i) \approx 0.5$ . In fact, the short crack approximation gives differences between +8% and -9% for  $\ell/(R_o - R_i) \leq 0.7$ . For two cracks,  $\ell/(R_o - R_i) \leq 0.8$ , the differences are larger, lying between +13% and -19% if the transition occurs at  $\ell/(R_o - R_i) = 0.35$ . The differences are positive for small cracks in both cases, hence

estimates of both the residual strength and the crack growth-time  $\Delta N$  will be conservative. The percentage errors in residual strength from using these approximations will be the same magnitude as the percentage differences in  $Y$  shown in Fig 2.22. The numerical data available is not sufficient for a detailed analysis of the likely errors in  $\Delta N$  calculations. However since the differences in  $Y$  for this configuration are comparable, in particular are small at short crack-lengths, with those for cracks at the edges of holes (see Figs 2.5, 2.10, 2.12 and 2.17) it follows that differences in growth-times will be comparable with those for cracks at holes (see Figs 2.6 and 2.7, 2.13 to 2.15, 2.18 and 2.19). Thus for this configuration also the errors in a fracture mechanics analysis introduced through using an approximate stress analysis will in most cases be less than those due to other sources.

### 2.3 Discussion

The errors introduced into fracture mechanics analyses by using a simple stress-analysis to calculate the stress intensity factor have been quantified, for several cases of cracks at stress concentrations. It is therefore now possible to compare these errors with those due to other sources such as uncertainties in load or material variability and to assess their relative importance in any given analysis. From the results given it is seen that in many cases the uncertainties in static residual strength and crack growth-times in fatigue, due to the approximate stress analysis, are less than those due to external sources. The configurations considered contain few boundaries in the vicinity of the crack, but the same techniques could be used where the crack interacts with many boundaries. The problems of the crack interacting with each of the boundaries separately would be solved using the approximate stress analysis methods and the results combined using the compounding method<sup>12</sup> (see Chapters 3 to 9).

The approximate method chosen consists of a combination of the asymptotic expressions for the 'short crack' and the 'long crack' limits. The short crack limit is controlled by the maximum stress at the point of initiation of the crack and this is usually characterized by the stress *concentration* factor  $K_t$ . The long crack limit is controlled by the overall length of the crack(s) plus hole. From a study of plots of these two expressions as a function of crack-length the optimum length for changing from one expression to the other can be chosen; this optimum value of the crack-length would be chosen so as to minimize the errors in the stress intensity factor. Errors could be further reduced

by considering some form of interpolation between two limits. Interpolation between limits has been used by Benthem and Koiter<sup>25</sup> to obtain accurate values of the stress intensity factor for some common test configurations. The transition points used in this study were not necessarily the optimum points, but were chosen in order to facilitate comparison with existing numerical results. Dowling<sup>26</sup> has independently suggested that the intersection point of the two limiting functions should be used as a transition point.

One particular advantage of the approximations chosen is that the stress intensity factor is overestimated at short crack-lengths and so the calculated residual strengths and growth-times  $\Delta N$  are conservative. It is important that fracture mechanics analyses should be conservative since safety is paramount. However over-conservative design can result in unacceptable weight penalties so that it is also important that errors due to approximate analysis be as small as possible particularly when the cracks are small - the  $K_t$  approximation satisfies these requirements.

Errors at short crack-lengths could be further reduced by using the tip stress or the mean stress instead of the maximum stress<sup>10</sup>. The tip stress is the stress at the site of the crack-tip in the uncracked body, and the mean stress is the average stress over the crack site in the uncracked body. Both these approximations have the disadvantages that the detailed stress distribution along the crack site must be known and that the results may not be conservative. For many configurations which are susceptible to cracking the stress *concentration* factors are known, but the detailed stress field is not. The existence of residual stresses at the edges of holes can readily be included in the methods considered by including them in the definition of the maximum stress.

The optimum position for the transition from the short crack approximation to the long crack approximation depends on the type of loading. For a crack of length  $\ell$  at the edge of a hole of radius  $R$ , the optimum occurs at  $\ell/R \simeq 0.1$  for remote loading, at  $\ell/R \simeq 0.15$  for localized loading on the perimeter of the hole and at  $\ell/R \simeq 0.25$  for a pressurized hole. The difference between the approximate and the numerical stress intensity factors was greater for a hole with two cracks than for a hole with one crack in the case considered (remote loadings). The differences were larger for loads at the hole edge than for remote loading, although in all cases the largest differences (>10%) are confined to a narrow band near the transition from short cracks to long cracks. The errors in crack growth-times  $\Delta N$  are a

function of the initial crack-length as well as the final crack-length; the errors are a maximum when the initial crack-length is close to the length at which the maximum error in the stress intensity factor occurs. The variations of the growth-times derived, assuming a power law dependence on  $K$ , from the numerical results are larger for loading at the hole than for remote loading. If the initial crack-length is one hundredth of the hole radius and the final crack-length up to five times the radius the variations are between -20% and +10% for remote loading (see Fig 2.6), between -20% and +50% for a localized force on the hole (see Fig 2.18) and between -25% and +40% for an internal pressure in the hole (see Fig 2.19).

These variations will usually be less than the variations in the crack growth-rates due to uncertainties in both materials data and applied stresses. The approximate results are always conservative for the shorter cracks, *ie* if the final crack-length is less than  $0.6R$  ( $m = 2,3$ ) or less than  $2R$  ( $m = 4$ ) for remote loading, less than  $R$  (all  $m$ ) for a localized force and less than  $3R$  (all  $m$ ) for an internal pressure. The dependence on  $m$  is not straightforward, but the errors are usually largest for  $m = 4$  over the whole range of crack-length for remote loading and at long crack-lengths for loading at the edge of the hole.

Examination of Fig 2.12 suggests that the radius of curvature of the ellipse  $\rho$  at the position of the cracks takes the place of the radius of the circular hole in determining the transitions from 'short' to 'long' cracks, *ie* the transition occurs at  $\ell/\rho = 0.1$  for all ellipses. The percentage differences in the normalized stress intensity factors near the transition increase as the ellipse becomes narrower ( $h/c$  decreasing). However very small values of  $h/c$  imply small values of  $\rho$  and practical crack-lengths  $\ell$  will result in large values of  $\ell/\rho$  where the differences are small. The growth-times obtained for an initial crack-length of  $0.02c$  and final lengths up to  $1.4c$  are conservative over the whole range for  $h/c = 0.5, 1, 2$  and  $4$ ; the results for  $h/c = 0.25$  are slightly non-conservative (a few per cent) for  $\ell_f/c \geq 0.1$  (see Figs 2.13 to 2.15). In general the variations from the numerical results increase as  $m$  increases; they are between +3% and -23% for  $m = 2$ , +3% and -46% for  $m = 3$ , and +4% and -54% for  $m = 4$ . The largest errors are for  $h/c = 0.5$  because  $\ell_i/c = 0.02c$  for that ellipse corresponds to an initial crack-length very close to the transition between the short and long crack approximations. The errors are

smallest for the two extreme cases  $h/c = 4$  and  $0.25$  - they will be smaller still for  $h/c > 4$  and  $h/c < 0.25$  .

Baratta and Neal<sup>27</sup> have shown that the stress *concentration* factor at a U-shaped notch is the same as that of an elliptical notch if the radius of curvature and the notch-length are the same; the stress field through which a crack would grow must therefore be very similar for the different notches. Therefore approximations based on  $K_t$  for the stress intensity factor of short cracks will be similar in accuracy for both types of notches. For long cracks the type of the notch will be less important in determining  $K$  . The transition from 'short' to 'long' cracks will, again, be determined by the radius of curvature at the end of the notch.

Recently, Murakami<sup>28</sup> has calculated stress intensity factors for cracks at semi-circular notches in the edge of strips subjected to uniform stress. Comparison of his results with approximations obtained using the method described here show errors of the same order as those for a cracked hole (Fig 2.5). Thus the approximate methods suggested here will produce useful engineering estimates of strength and fatigue lifetimes for cracks from notches of differing geometries for which the stress *concentration* factor is known.

In section 2.2.5 the approximate stress analysis used to derive stress intensity factors for cracks at the edge of holes in the absence of other boundaries was applied to a rotating disc with one or two cracks at the bore. For this configuration the geometry factor does not decrease continuously as the crack-length increases, as in previous sections, but decreases initially and then rises again because of the interaction between the crack-tip and the outer boundary of the disc. Despite the more complex behaviour of  $Y$  the simple stress analysis gives a good approximation (see Fig 2.22) and would lead to reasonable estimates of growth-times in fatigue. The short crack approximation overestimates the stress intensity, hence calculations of residual strength and growth-times  $\Delta N$  will be conservative for short cracks.

#### 2.4 Conclusions

(1) Structural components often contain stress concentrators, such as holes and notches, at which cracks are initiated; approximate stress intensity factors for these cracks can be obtained by a simple combination of the 'short crack' and 'long crack' limits.

(2) The errors introduced due to the approximations are in general no more than (and they are often less than) those due to the uncertainties in service loads and material properties.

(3) Static strength calculations of components with short cracks are always conservative, *ie* they err on the side of safety; and because much of the fatigue life of a component is spent while the cracks are short the calculated lifetime is usually also conservative.

(4) These approximations are particularly applicable to damage-tolerant design calculations which are concerned with short cracks; and the built-in safety-factor will not incur excessive weight penalties since the errors are small in this region.

(5) Any approximate method of stress analysis which results in errors in stress intensity factors similar to those discussed in this chapter, will be acceptable for most engineering applications.

CHAPTER 3  
CRACKS NEAR BOUNDARIES<sup>12</sup>

The tip of a growing crack is often close to structural boundaries (see Figs 1.1 to 1.18) and this will influence the stress intensity factor. In this chapter a method is developed which takes into account the effects on the crack of nearby boundaries. Both the proximity to the crack-tip and the shape of the boundary are important. The shape of the boundary is described by the radius of curvature of that part of the boundary which is nearest to the crack. Configurations in which the boundary intersects the crack are considered in later chapters. Stress intensity factors for many simple configurations are already available<sup>2-4</sup> but these configurations seldom model adequately real engineering structures. The compounding method developed here is a quick and versatile way of extending these solutions to other, more complex, configurations for which the stress intensity factors are not known. An empirical method which was used by Figge and Newman<sup>29</sup>, Smith<sup>30</sup> and Liu<sup>31</sup>, is a special case of compounding but its generality appears not to have been realized or investigated.

In this chapter only two-dimensional configurations are considered. Although, the method may also be used to obtain solutions to complex three-dimensional configurations, applications are restricted by the small number of ancillary solutions available for simple three-dimensional configurations. The compounding method is developed, tested against known solutions (section 3.2.1) and used to solve a previously unsolved problem (section 3.2.2).

### 3.1 The compounding method

A configuration containing a crack may have several boundaries, *eg* holes, other cracks or sheet edges; all these will influence the stress intensity factor at the tip of the crack under consideration. The principle of the compounding method presented here is to obtain a solution for the stress intensity factor by separating the complex configuration containing a crack into a number of simpler ancillary configurations which have known solutions. Each ancillary configuration will, usually, contain only one boundary which interacts with the crack. The contributions to the final stress intensity factor are compounded neglecting any effects due to boundary-boundary interaction. The error term, due to neglecting these effects, is formally derived in Appendix D.

Consider the configuration shown in Fig 3.1a containing a crack near to a stress free boundary  $B_1$ ; the configuration is subjected to an applied stress system  $S_0$  on its boundary  $B_0$  which is remote from the crack. Let the stress intensity factor at one of the crack tips be denoted by  $K_1$ . If the stress free boundary  $B_1$  were absent from the configuration, stresses  $S_1$  would occur at the site of  $B_1$ ; the stress intensity factor, in the absence of internal boundaries, is now given by  $\bar{K}$  (Fig 3.1b). The original configuration can be obtained by the superposition of

- (i) the cracked configuration with applied stress  $S_0$  on  $B_0$  without an internal boundary (Fig 3.1b); and
- (ii) the cracked configuration with zero stress on  $B_0$  and  $-S_1$  on  $B_1$  (see Fig 3.1c).

Thus the stress intensity  $K_1$  is given by

$$K_1 = \bar{K} + K_1^* \quad (3.1)$$

where  $K_1^*$  is the stress intensity factor when the only applied stress is  $-S_1$  on  $B_1$ . Similarly, for a second boundary,  $B_2$  say, the stress intensity factor would be given by

$$K_2 = \bar{K} + K_2^* \quad (3.2)$$

If the two boundaries  $B_1$  and  $B_2$  are present together (Fig 3.2a), the resultant stress intensity factor  $K_r$  is given by the superposition of Fig 3.2b&c as

$$K_r = \bar{K} + K_r^* \quad (3.3)$$

where  $K_r^*$  is the stress intensity factor when the configuration has zero stress on  $B_0$ , and stresses  $-S_1$  and  $-S_2$  on  $B_1$  and  $B_2$  respectively (Fig 3.2c).

If the two boundaries do not interact with each other then, by superposition,  $K_r^*$  is given by

$$K_r^* = K_1^* + K_2^* \quad (3.4)$$

If they do interact there will be an extra term which is denoted by  $K_e$ , *ie*

$$K_r^* = K_1^* + K_2^* + K_e \quad (3.5)$$

Combining equations (3.1), (3.2), (3.3) and (3.5) gives

$$K_r = K_1 + K_2 - \bar{K} + K_e \quad (3.6)$$

Thus the stress intensity factor for a crack in a configuration with multiple internal boundaries can be expressed in terms of stress intensity factors derived from configurations with single internal boundaries, apart from a correction term. In general for  $N$  boundaries  $B_n$  ( $n = 1, 2, \dots, N$ ), the resultant stress intensity factor is given by

$$\left. \begin{aligned} K_r &= \bar{K} + \sum_{n=1}^N (K_n - \bar{K}) + K_e \\ \text{or} \\ Q_r &= 1 + \sum_{n=1}^N (Q_n - 1) + Q_e \end{aligned} \right\} \quad (3.7)$$

where  $Q$  denotes a normalized stress intensity factor<sup>†</sup> such that  $Q_r = K_r/\bar{K}$ ,  $Q_n = K_n/\bar{K}$  and  $Q_e = K_e/\bar{K}$ ;  $Q_e$  is the correction term due to the interaction of the  $N$  boundaries. If  $Q_e$  can be estimated or can be shown to be small ( $\ll 1$ ), then equation (3.7) can be used to build up solutions to complex configurations from known simpler ones.

An empirical method, which has been used<sup>29-31</sup> to obtain approximate stress intensity factors, states that in the case of two boundaries

$$Q_r = Q_1 \times Q_2 \quad (3.8)$$

If we write  $Q_1 = 1 + \alpha$  and  $Q_2 = 1 + \beta$ , then  $\alpha$  and  $\beta$  are usually less than unity. It follows from equation (3.8) that  $Q_r$  is given by

$$Q_r = 1 + \alpha + \beta + \alpha\beta \quad (3.9)$$

Equation (3.7) for two boundaries becomes

$$Q_r = 1 + \alpha + \beta + Q_e \quad (3.10)$$

Thus equations (3.9) and (3.10) are the same but for a correction term  $\alpha\beta$  or  $Q_e$  and the empirical expression, equation (3.8) is seen to be a special case of equation (3.7). If the correction term is small the two methods will give virtually the same result. However, this will not be so if  $\alpha, \beta \gtrsim 1$ , and the meaning of the term  $\alpha\beta$  is undefined.

<sup>†</sup> The function  $Q$  is a generalization of the geometry factor  $Y$  introduced in Chapter 2; in some configurations  $Q$  could be identical to  $Y$ , but this will not be so in general.

The correction term  $Q_e$  can be expressed formally using the Schwarz alternating technique which has been described by Sokolnikoff<sup>32</sup> and used to determine stress intensity factors by Smith, *et al*<sup>33</sup> and also used in papers by Kanazawa, *et al*<sup>34</sup>. The term  $Q_e$  can be expected to be small provided that the boundaries are not too close to each other. A derivation of the correction term for the special case  $N = 2$  is contained in Appendix D (Fig 3.3).

### 3.2 Application to plane sheets

In this section approximate compounded solutions are compared with known solutions for three different types of boundary. These boundaries, each characterized by different radii of curvature  $\rho$ , are (see section 3.2.1) another crack ( $\rho = 0$ ), a circular hole ( $\rho = \text{hole radius}$ ) and a straight edge ( $\rho = \infty$ ). Boundaries with a large radius of curvature will have an effect over a larger distance than boundaries with a small radius.

The approximate formula, for  $N$  boundaries,

$$Q_r = 1 + \sum_{n=1}^N (Q_n - 1) \quad (3.11)$$

is used to compound stress intensity factors for configurations with known solutions and, by comparison, it is shown that  $Q_e$  (the term omitted from equation (3.11)) is small (*ie*  $\ll 1$ ). The magnitude of  $Q_e$  will depend on the number, nearness and shape of the boundaries. As errors in  $Q_r$  due to using equation (3.11) will increase as  $N$  increases multiple boundaries are also considered.

In section 3.2.2 an approximate stress intensity factor is obtained for a crack in a half-plane between a hole and the edge of the half-plane.

#### 3.2.1 Test solutions

The configurations shown in Figs 3.4 to 3.6 for which solutions are known, are used as test cases to illustrate and assess the method. These represent widely different boundary effects, namely a pair of boundaries of infinite, finite or zero radius of curvature in the path of the crack.

Consider the configuration shown in Fig 3.4 for a crack located eccentrically in a finite width sheet subjected to a uniaxial tensile

stress. Fig 3.7 shows the appropriate ancillary configurations, for which the stress intensity factors are given in Case 1.1.11, Ref 2. The normalized stress intensity factors  $Q_r$  for the crack in Fig 3.4 are obtained by compounding from equation (3.11) with  $N = 2$ , *ie*

$$Q_r = Q_1 + Q_2 - 1 \quad . \quad (3.12)$$

For tip A in Fig 3.4,  $Q_1$  and  $Q_2$  are the normalized stress intensity factors at the left hand tip in Fig 3.7a&b respectively and, for tip B,  $Q_1$  and  $Q_2$  are the normalized stress intensity factors for the right hand tip in Fig 3.7a&b respectively. Comparison of Figs 3.4 and 3.7 shows that we require  $c = b$  and  $d = b_1 + e$ : in this configuration  $\bar{K} = \sigma\sqrt{\pi a}$ . Values of the opening mode normalized stress intensity factor  $Q_r$  ( $= K_I/\sigma\sqrt{\pi a}$ ) obtained from equation (3.12) are compared in Table 3.1 with the results given in Case 1.1.5, Ref 2 for  $a/b \leq 0.7$  and  $e/b_1 = 0.0$  and  $0.8$ .

Table 3.1

Comparison of values of  $K_I/(\sigma\sqrt{\pi a})$  for an eccentric crack in a finite width sheet subjected to a uniaxial tensile stress

$\frac{a}{b}$	$e/b_1 = 0.0$		$e/b_1 = 0.8$			
	Tips A and B		Tip A		Tip B	
	Compounded results	Case 1.1.5 (Ref 2)	Compounded results	Case 1.1.5 (Ref 2)	Compounded results	Case 1.1.5 (Ref 2)
0.0	1.000	1.000	1.000	1.000	1.000	1.000
0.1	1.005	1.005	1.003	1.003	1.002	1.003
0.2	1.020	1.021	1.011	1.014	1.009	1.012
0.3	1.047	1.05	1.03	1.03	1.02	1.03
0.4	1.09	1.10	1.05	1.07	1.04	1.05
0.5	1.15	1.18	1.09	1.11	1.06	1.08
0.6	1.23	1.29	1.15	1.19	1.08	1.11
0.7	1.34	1.48	1.24	1.30	1.11	1.15

In a similar manner solutions are obtained for configurations in Figs 3.5 and 3.6; the required ancillary solutions were obtained from Case 1.3.5 and Case 1.2.2 in Ref 2. Compounded results for the test case in Fig 3.5 ( $b/R = 1$ ) and the test case in Fig 3.6 (middle crack of three) are shown in Table 3.2 and compared with the solutions given in Case 1.3.7 and Case 1.2.8 respectively in Ref 2.

Table 3.2

Comparison of values of  $K_I/(\sigma\sqrt{\pi a})$  for the configurations  
in Figs 3.5 and 3.6

$\frac{a}{b}$	Fig 3.5 ( $b/R = 1$ )		Fig 3.6 (middle crack of three)	
	Compounded results	Case 1.3.7 (Ref 2)	Compounded results	Case 1.2.8 (Ref 2)
0.0	1.44	1.47	1.00	1.00
0.1	1.45	1.47	1.00	1.00
0.2	1.46	1.49	1.01	1.01
0.3	1.49	1.52	1.02	1.02
0.4	1.53	1.56	1.05	1.05
0.5	1.59	1.63	1.08	1.08
0.6	1.68	1.72	1.12	1.13
0.7	1.81	1.87	1.19	1.20
0.8	2.02	2.12	1.31	1.33
0.9	2.43	2.64	1.57	1.60

Errors in the stress intensity factors obtained for the configurations in Figs 3.4 to 3.6 are summarized in Table 3.3 and indicate two trends. Firstly errors increase as the crack-length increases relative to the distance to a boundary. Secondly at a fixed crack-length errors tend to increase with increasing boundary radius. Thus it appears that for  $a/b$  up to 0.8 the errors are probably  $<10\%$  for straight boundaries,  $<5\%$  for circular boundaries (two radii apart) and 1.5% for other crack boundaries.

Table 3.3

Percentage errors for the compounding method

$\frac{a}{b}$	Percentage error		
	Straight boundaries (Fig 3.4)	Circular boundaries (Fig 3.5)	Crack boundaries (Fig 3.6)
0.0	0.0	2.1	0.0
0.2	0.2	2.1	0.0
0.4	1.6	2.0	0.0
0.6	4.3	2.4	0.5
0.8	17.9	5.0	1.4

As an example of a solution to a problem involving more than two boundaries, consider the configuration in Fig 3.6 with an odd number ( $>3$ ) of cracks. The factor  $Q_r$  for the middle crack, with  $N = 5, 7$  and 11 in equation (3.11) can be compounded from the same ancillary

solution, Case 1.2.2, Ref 2, as was used for the three-crack problem. The results are given in Table 3.4 and compared with the known solution given in Case 1.2.8, Ref 2. It is seen that, at any fixed crack-length, the errors increase with the number of cracks; this illustrates the effect of the increasing interaction between boundaries which has not been taken into account in equation (3.11).

Table 3.4

Comparison of values of  $K_I/(\sigma\sqrt{\pi a})$  for the central crack of an odd number of collinear cracks subjected to a uniform tensile stress

$\frac{a}{b}$	5 cracks			7 cracks			11 cracks		
	Compounded results	Case 1.2.8 (Ref 2)	Error %	Compounded results	Case 1.2.8 (Ref 2)	Error %	Compounded results	Case 1.2.8 (Ref 2)	Error %
0.0	1.00	1.00	0.0	1.00	1.00	0.0	1.00	1.00	0.0
0.2	1.01	1.01	0.0	1.01	1.02	0.1	1.02	1.02	0.1
0.4	1.06	1.06	0.3	1.06	1.06	0.4	1.06	1.07	0.7
0.6	1.15	1.16	1.4	1.16	1.17	1.4	1.16	1.19	2.0
0.8	1.36	1.41	4.1	1.37	1.46	5.8	1.38	1.49	7.3

It can therefore be concluded that the errors due to neglecting boundary interactions are small (a few per cent). Such errors are within the allowable tolerances for many engineering applications.

### 3.2.2 A solution for two different boundaries

No comparison solution is available for this problem of a crack in the vicinity of a hole in a half-plane subjected to a uniaxial tensile stress (Fig 3.8), but it illustrates how the relative effects of boundaries can change as the distance from the crack-tip changes. The ancillary solutions required for this problem are given in Cases 1.1.11 and 1.3.5 in Ref 2. Compounded stress intensity factors at both crack-tips are shown in Fig 3.8 for  $R/b = 1$ . Three ratios of the distance between the crack and the straight boundary  $c$  and the distance between the crack and the hole  $b$  are considered, namely  $c/b = 0.5, 1$  and  $2$ . For  $c/b = 0.5$  the tip adjacent to the straight boundary (tip B) has a higher stress intensity factor for short cracks ( $a/b < 0.35$ ). As  $a/b$  increases the tip nearer to the hole (tip A) has the higher stress intensity factor. This behaviour is due to the tip A entering the highly stressed region in the vicinity of the hole whilst tip B, although very close to the straight boundary, is for  $a/b > 0.35$  in a region of lower stress resulting in a lower stress intensity factor. For the other values of  $c/b$  considered the crack-tip adjacent to the

hole is more critical for all  $a/b$ . If the straight boundary is remote from the hole ( $c/b = 2$  say) the stress intensity factor for the tip at B initially reduces slightly as  $a/b$  increases since the stress field due to the hole is decreasing. For larger  $a/b$  the effect of the straight boundary causes the stress intensity factor to increase. Consideration of the errors estimated in section 3.2.1 suggests that this solution is probably accurate to better than 10%, *ie* adequate for most engineering purposes.

### 3.3 Discussion and conclusions

The compounding method has been shown (section 3.2) to produce approximate stress intensity factors for cracks in the vicinity of multiple boundaries in plane unstiffened sheets. The errors in the approximations increase as the length of the crack increases, as the number of boundaries increases, and as the radii of curvature of the boundaries increase. This method can be used to solve many plane crack problems, *eg* with the ancillary configurations used in section 3.2 approximate stress intensity factors can be determined for a crack between holes of unequal radii unequally spaced on either side of the crack and also any number of equal length, unequally spaced collinear cracks. This latter configuration can be extended by using results in Savin<sup>35</sup> to any number of unequal length, unequally spaced collinear cracks. Results for these ancillary configurations and many others have been collected together and presented as curves of  $K/\bar{K}$  by Rooke and Cartwright<sup>2</sup>.

The accuracy of the method is adequate for most engineering applications: the errors in the stress intensity factors are of the same order as those considered in Chapter 2, therefore the uncertainties in fracture mechanics calculations (residual strength and fatigue lifetimes) will be no more than and often less than those due to uncertainties in loading or material properties.

CHAPTER 4CRACK(S) AT AN UNLOADED HOLE<sup>36</sup>

With the advent of the damage tolerant design philosophy for airframes the assumption is made that small cracks exist at the start of service life; this implies that, unless the growth behaviour of small cracks can be predicted, over-conservative safety factors may have to be used. This can mean either structural weight penalties or pessimistic estimates of lifetimes and inspection intervals. Regions of high stress, such as those at the edge of a hole or cut-out are likely sites for cracks. When these cracks are small the stress intensity factor varies rapidly with crack-length. Both this rapid variation and the power law dependence (see Chapter 2) imply that a considerable fraction of the fatigue life of a structure with a cracked hole is spent while the crack is small. Hence the reliable estimation of lifetime requires accurate estimation of stress intensity factors for short cracks.

Some stress intensity factors for simple configurations of cracks at the edges of holes are available, however the solutions that are needed in practice are usually for complex configurations having other boundaries near the cracked hole, and these are not generally available. The theory of compounding developed in the previous chapter is further developed in this chapter and the method is used to calculate stress intensity factors for cracks at the edges of holes. In the original development of the compounding theory none of the boundaries crossed the crack. However in this case the crack starts at a boundary, namely the edge of the hole. A modification to the theory is needed and the concept of the 'equivalent crack' is introduced in section 4.1.

It was shown in Chapter 3 that the compounding method gave acceptable results for plane problems in which the interaction between the boundaries had a negligible effect on the stress intensity factors. However when a hole with a crack is near another boundary this interaction may not be negligible and a method of estimating its effect, by using the known stress *concentration* factor for the uncracked configuration, is presented in section 4.2. It will be seen that this is a powerful addition to the compounding technique since it ensures accuracy at small crack-lengths.

The procedure is tested in section 4.3 by comparing the compounded solution for two cracks of equal length at a central hole in a strip, subjected to uniaxial tension remote from the crack, with a numerical

solution given in Case 1.3.1, Ref 2; the differences between the solutions are small (a few per cent). Solutions are obtained for two other configurations in section 4.4, namely, a crack at the edge of a hole located eccentrically in a strip and a crack at the edge of a hole near another circular hole. In all cases opening mode stress intensity factors ( $K_I$ ) are calculated.

It should be noted that the application of the compounding method to cracks at the edges of holes requires not only the existence of stress intensity factors for a few simple geometries to be known, but also stress *concentration* factors for the original uncracked configurations. Many stress *concentration* factors have been collected together by Peterson<sup>17</sup>.

#### 4.1 Equivalent crack concept

If a boundary intersects the crack, *eg* the crack is at the edge of a hole, the effects of the other boundaries cannot usually be evaluated because there are unlikely to be solutions to the ancillary configurations. It is necessary to simplify the ancillary configurations by replacing the crack and its intersecting boundary by an 'equivalent crack'. This fictitious or equivalent crack is defined in terms of the stress intensity factor of the original crack at the boundary in the absence of all other boundaries. The location of the equivalent crack with respect to the boundaries, is determined by reference to the original configuration.

##### 4.1.1 One crack at the edge of a circular hole

Let us consider a radial crack of length  $l$  at the edge of a circular hole of radius  $R$  in a sheet subjected to a uniform uniaxial tensile stress  $\sigma$  remote from the hole. The stress acts in a direction perpendicular to the crack. The hole is located between two boundaries  $B_1$  and  $B_2$  such that the distance, along the crackline, from the centre of the hole to  $B_1$  is  $b_1$ , and to  $B_2$  is  $b_2$  (see Fig 4.1).

In accordance with the procedures in the previous chapter for compounding stress intensity factors, the above configuration is represented by several simpler ancillary configurations. The first ancillary configuration will be that of a radial crack at the edge of a hole in a large sheet subjected to the remote stress  $\sigma$  acting perpendicular to the crackline (see Fig 4.2a). Let the stress intensity factor of the

crack in this configuration be  $K_0$ . The normalized stress intensity factor  $Q_0$  is defined by

$$Q_0 = \frac{K_0}{\bar{K}}, \quad \bar{K} = \sigma\sqrt{\pi a} . \quad (4.1)$$

The configuration of the crack at the edge of the hole must be simplified before the interactions between the crack tip and the boundaries  $B_1$  and  $B_2$  can be evaluated since there are few ancillary solutions for a crack at the edge of a hole in the presence of other boundaries. It is therefore postulated that the hole/crack combination can be replaced by an 'equivalent crack' for the purposes of evaluating the effects of boundaries other than the hole. The interactions between the boundaries and the tip A of the equivalent crack are assumed to be the same as the interactions between the boundaries and tip A of the original crack.

The equivalent crack is defined such that it has the same stress intensity factor  $K_0$  as the crack at the edge of the hole in the absence of all boundaries. This implies the same crack-tip shape, since the opening of the crack in the vicinity of the tip is proportional to the stress intensity factor. The distance of the tip of the equivalent crack from the boundaries is determined (see later) by the distance of the original tip from the boundaries.

The equivalent crack is postulated to be an isolated crack of length  $2a'$  in a large sheet subjected to a uniform tensile stress  $\sigma$  acting remote from the crack and perpendicular to it; the length  $a'$  is determined by the condition that the stress intensity factor must be equal to  $K_0$ , *ie*

$$K = \sigma\sqrt{\pi a'} = K_0 . \quad (4.2)$$

The combination of equations (4.1) and (4.2) leads to

$$a' = Q_0^2 a . \quad (4.3)$$

The equivalent crack must conform with certain physical limits if it is to be an adequate replacement for the original crack: they are

- (i) as the original crack-length  $l$  tends to zero, the equivalent crack-length  $a'$  must also tend to zero; and

(ii) when the radius of the hole is small compared to the original crack-length, the hole/crack combination behaves like an isolated crack of total length  $a + R \simeq a$ , and the equivalent crack must do the same.

From equation (4.3) it follows that:

$$\lim_{\ell \rightarrow 0} \{a'\} = a \lim_{\ell \rightarrow 0} \{Q_0^2\} = 0, \quad (4.4)$$

since from Case 1.3.3, Ref 2, it follows that

$$\lim_{\ell \rightarrow 0} \{Q_0\} = 0, \quad (4.5)$$

therefore condition (i) above is satisfied. Also, from equation (4.3),

$$\lim_{a/R \rightarrow \infty} \{2a'\} = 2a \lim_{a/R \rightarrow \infty} \{Q_0^2\} = a, \quad (4.6)$$

since from Case 1.3.3, Ref 2, it follows that

$$\lim_{a \rightarrow R} \{Q_0\} = \frac{1}{\sqrt{2}}, \quad (4.7)$$

therefore condition (ii) is satisfied.

Thus, in order to evaluate the stress intensity factor for the crack in Fig 4.1, solutions to the ancillary configurations shown in Fig 4a-c are needed. The dimensions  $b'_1$  and  $b'_2$  shown in Fig 4.2b&c are related to  $b_1$  and  $b_2$  in the original configuration (Fig 4.1), by considering the distance from tip A to the boundaries. The distance  $b'_1$  in Fig 4.2b is determined by the condition that the distance from tip A to the boundary  $B_1$ , along the crackline, must be the same in the ancillary configuration as in the original configuration. Comparison of Figs 4.1 and 4.2b shows that

$$b'_1 - a' = b_1 - a. \quad (4.8)$$

If a similar condition is used to determine  $b'_2$ , namely that the distance from tip A to boundary  $B_2$  should be the same, then

$$b'_2 + a' = b_2 + a. \quad (4.9)$$

However this condition can lead to overestimating the effect of  $B_2$  in some circumstances. If  $2a' > (a + R)$ , then the uncracked ligament

between  $B_2$  and the nearer tip B of the equivalent crack is less in the ancillary configuration than in the original if  $b'_2$  is determined by equation (4.9). This would lead to an overestimate of the effect of  $B_2$  on the stress intensity factor particularly if  $B_2$  is close to the hole. To avoid this, equation (4.9) is used when  $2a' < (a + R)$  and the condition that the distance between tip B and boundary  $B_2$  should be the same as the distance between the edge of the hole and  $B_2$  is used when  $2a' > (a + R)$ . This condition leads to

$$b'_2 - a' = b_2 - R, \quad 2a' > (a + R). \quad (4.10)$$

Since  $a' = Q_0^2 a$ , the three conditions can be written as:

$$\left. \begin{aligned} b'_1 - a' &= b_1 - a, & \text{all } Q_0; \\ b'_2 + a' &= b_2 + a, & Q_0^2 \leq \frac{1}{2} \left(1 + \frac{R}{a}\right); \\ b'_2 - a' &= b_2 - R, & Q_0^2 > \frac{1}{2} \left(1 + \frac{R}{a}\right). \end{aligned} \right\} \quad (4.11)$$

The introduction of the equivalent crack leads to a modification of the basic compounding formula given by equation (3.7) in the previous chapter. The compounding equation becomes

$$K_r = K_0 + \sum_{n=1}^N (K'_n - K_0) + K_e, \quad (4.12)$$

where  $K'_n$  is the stress intensity factor of the equivalent crack of length  $2a'$  in the presence of the nth boundary only. By normalizing with respect to  $\bar{K}$  as before, and by using equation (4.1), the normalized resultant stress intensity factor becomes

$$Q_r = Q_0 \left[ 1 + \sum_{n=1}^N (Q'_n - 1) \right] + Q_e \quad (4.13)$$

where

$$Q'_n = \frac{K'_n}{K_0} = \frac{K'_n}{\sigma \sqrt{\pi a'}}. \quad (4.14)$$

#### 4.1.2 Two equal-length cracks at the edge of a circular hole

In this section we consider two diametrically opposite radial cracks of equal length  $\ell$  at the edge of a circular hole of radius  $R$  in a sheet subjected to a uniform uniaxial tensile stress  $\sigma$  acting remote from the hole in a direction perpendicular to the crackline. There are two boundaries  $B_1$  and  $B_2$  in the vicinity of the hole (see Fig 4.3). The first ancillary configuration is that of two diametrically opposite radial cracks of equal length at the edge of a hole in a large sheet with a uniform uniaxial tensile stress acting perpendicular to the crackline remote from the hole. Let the stress intensity factor for tip A be  $K_0$  (the value for tip B will be the same in this case). The other ancillary configurations required are the same as shown in Fig 4.2b&c.

The equivalent crack is again of length  $2a'$  and is given by equation (4.3).

The equivalent crack satisfies the required physical limits:

$$\lim_{\ell \rightarrow 0} \{a'\} = a \lim_{\ell \rightarrow 0} \{Q_0^2\} = 0, \quad (4.15)$$

since, from Case 1.3.3, Ref 2,

$$\lim_{\ell \rightarrow 0} \{Q_0\} = 0, \quad (4.16)$$

and

$$\lim_{a/R \rightarrow \infty} \{2a'\} = 2a \lim_{a/R \rightarrow \infty} \{Q_0^2\} = 2a, \quad (4.17)$$

since, from Case 1.3.3, Ref 2,

$$\lim_{a/R \rightarrow \infty} \{Q_0\} = 1. \quad (4.18)$$

The distances  $b_1$  and  $b_2$  are determined by similar conditions to those used in the previous section:

- (i) tip A is the same distance from  $B_1$  in both the ancillary configurations and the original;
- (ii) tip A is the same distance from  $B_2$  in both configurations if  $a' < a$ ; or
- (iii) tip B is the same distance from  $B_2$  in both configurations if  $a' > a$ .

That is,

$$\left. \begin{aligned} b_1' - a' &= b_1 - a, & \text{all } Q_0 \\ b_2' + a' &= b_2 + a, & Q_0 \leq 1 \\ \text{and} \\ b_2' - a' &= b_2 - a, & Q_0 > 1. \end{aligned} \right\} \quad (4.19)$$

The compounding equations for determining the stress intensity factors will again be given by equations (4.12) to (4.14).

#### 4.1.3 Two unequal-length cracks at the edge of a circular hole

If the configuration described in the previous section has two cracks of unequal lengths,  $\ell_A$  and  $\ell_B$ , at the edge of the hole (see Fig 4.4), then the definition of the equivalent crack will depend on which tip is under consideration. The different tips will have different stress intensity factors. The first ancillary configuration to be considered is that of the hole with two unequal cracks in a sheet with a uniform uniaxial tensile stress  $\sigma$  remote from the hole, acting perpendicular to the crackline. Let the stress intensity factors at tip A and tip B be  $K_{OA}$  and  $K_{OB}$  respectively. If tip A is the tip under consideration, then the equivalent crack-length  $a_A'$  is defined by

$$a_A' = Q_{OA}^2 a \quad \text{with} \quad Q_{OA} = \frac{K_{OA}}{\bar{K}}, \quad (4.20)$$

$$\text{where} \quad 2a = a_A + a_B = \ell_A + \ell_B + 2R. \quad (4.21)$$

If tip B, then the equivalent crack-length  $a_B'$  is defined by

$$a_B' = Q_{OB}^2 a \quad \text{with} \quad Q_{OB} = \frac{K_{OB}}{\bar{K}}. \quad (4.22)$$

The normalized stress intensity factors  $Q_{OA}$  and  $Q_{OB}$  have been evaluated by Tweed and Rooke<sup>20</sup>. The crack-lengths  $a_A'$  and  $a_B'$  satisfy the required physical limits at both long and short crack-lengths. The distance from the centres of the equivalent cracks to the boundaries  $B_1$  and  $B_2$  in the ancillary configurations are determined by similar conditions to those given in the previous section. Thus, for tip A

$$\begin{array}{l}
 b_1' - a_A' = b_1 - a_A , \\
 b_2' + a_A' = b_2 + a_A , \\
 b_2' - a_A' = b_2 - a_B ,
 \end{array}
 \left. \begin{array}{l}
 \text{all } Q_{OA} \\
 Q_{OA} \leq 1 \\
 Q_{OA} > 1 ;
 \end{array} \right\} \quad (4.23)$$

and

and for tip B

$$\begin{array}{l}
 b_2' - a_B' = b_2 - a_B , \\
 b_1' + a_B' = b_1 + a_B , \\
 b_1' - a_B' = b_1 - a_A ,
 \end{array}
 \left. \begin{array}{l}
 \text{all } Q_{OB} \\
 Q_{OB} \leq 1 \\
 Q_{OB} > 1 .
 \end{array} \right\} \quad (4.24)$$

and

The stress intensity factors are again determined from equations (4.12) to (4.14) for either tip A or tip B.

#### 4.2 Boundary-boundary interactions

In the plane problems considered in Chapter 3, it was shown that boundary-boundary interaction effects were small, and that only small errors resulted from neglecting  $Q_e$ , the contribution to the stress intensity factors arising from such effects. However for cracks at the edges of holes near other boundaries this may not be the case, and  $Q_e$  in equation (4.13) may not be small. An indication of the likely importance of  $Q_e$  may be obtained by considering the stress at the site of the crack in the uncracked configuration. If the value of this stress in the configuration with all the boundaries present is markedly different from that with no boundaries, then boundary-boundary interactions will be important. If they are important in the uncracked configuration, then they will be important in the cracked configuration also. For cracks at holes, the stress at the crack site is often expressed in terms of the stress *concentration* factor  $K_t$  on the boundary of the hole.

In Chapter 2 a close relationship was demonstrated between the stress *concentration* factor in the uncracked configuration and the stress intensity factor of short cracks. This relationship will be used here to ensure that the calculation of  $Q_e$  leads to accurate values of  $Q_r$  at short cracks. The contribution of  $Q_e$  to  $Q_r$  is less significant as the crack-length increases.

In the derivation of the compounding method in Chapter 3, the term  $Q_e$  was shown to arise because stresses induced on any one boundary site by the presence of the other boundaries, were not allowed for. The formal relationship between these stresses and  $Q_e$  was described in Appendix D using an alternating technique. In general the evaluation of  $Q_e$ , by such a technique, is too time-consuming and costly; therefore a simpler approximate procedure is developed in this section. The unknown distribution of these stresses around the hole boundary is replaced by two equal and opposite localized forces  $P_e$  acting, on the hole perimeter, perpendicular to the crackline (see Fig 4.5). The magnitude of  $P_e$  is chosen so that the sum of the maximum tensile stresses ( $\sigma_{\max}$ ) for all the ancillary configurations without cracks, is equal to that in the real configuration without a crack. In general the maximum stress occurs at the edge of the hole at the site of the crack.

In practice the magnitude of  $P_e$  is determined by considering the limiting values of the stress intensity factors for small cracks. For a short crack (length  $\ell$ ) at the edge of a hole (radius  $R$ ) in the region of maximum stress ( $\sigma_{\max}$ ) the stress intensity factor ( $K$ ) becomes, as  $\ell$  tends to zero<sup>†</sup>

$$\lim_{\ell/R \rightarrow 0} \{K\} = 1.12\sigma_{\max}\sqrt{\pi\ell} = 1.12K_t\sigma\sqrt{\pi\ell} \quad (4.25)$$

where 1.12 is the usual correction factor for a crack at a stress-free edge, and  $K_t$  is the stress *concentration* factor. The limits are determined for each stress intensity factor in the compounding equation

$$K_r = K_0 \left[ 1 + \sum_{n=1}^N (Q'_n - 1) \right] + K_e \quad (4.26)$$

The limiting values of  $K_r$ ,  $K_0$  and  $Q'_n$  can be determined in terms of known quantities and that of  $K_e$  can be expressed in terms of the unknown force  $P_e$ .

For cracks at the edge of a hole in a large sheet subjected to a uniaxial tensile stress  $\sigma$  the stress intensity factor ( $K_0$ ) becomes

---

<sup>†</sup> It is assumed that any other cracks that are present, will tend to zero length at least as fast as the crack under consideration.

$$\lim_{\ell/R \rightarrow 0} \{K_0\} = 1.12 \times 3\sigma\sqrt{\pi\ell} \quad (4.27)$$

since  $\sigma_{\max} = 3\sigma$ . For cracks at the edge of a hole subjected to localized forces  $P_e$  the stress intensity factor  $K_e$  becomes

$$\lim_{\ell/R \rightarrow 0} \{K_e\} = 1.12 \times \frac{2P_e}{\pi R} \sqrt{\pi\ell}, \quad (4.28)$$

since  $\sigma_{\max} = 2P_e/(\pi R)$ . Because  $a' \rightarrow 0$  as  $\ell \rightarrow 0$  (ie  $a/R \rightarrow 1$ ), it follows that

$$\lim_{\ell/R \rightarrow 0} \{K'_n\} = \lim_{a' \rightarrow 0} \{K'_n\} = \sigma'_n \sqrt{\pi a'} = \frac{\sigma'_n}{\sigma} K_0. \quad (4.29)$$

The stress  $\sigma'_n$  is the stress at the centre of the crack site in the uncracked ancillary configuration containing the  $n$ th boundary; it may be written in terms of the applied stress  $\sigma$ , as

$$\sigma'_n = M'_n \sigma, \quad (4.30)$$

where  $M'_n$  is the magnification factor on the stress due to the presence of the  $n$ th boundary a distance  $b'_n$  away.  $M'_n$  may be greater or less than unity.

Substitution of equations (4.27) to (4.30) into equation (4.26) gives

$$\lim_{\ell/R \rightarrow 0} \{K_r\} = 1.12\sigma\sqrt{\pi\ell} \left\{ 3 \left[ 1 + \sum_{n=1}^N (M'_n - 1) \right] + \frac{2P_e}{\pi R\sigma} \right\}. \quad (4.31)$$

However the limiting value for the stress intensity factor ( $K_r$ ) for small cracks in the original configuration must be given by

$$\lim_{\ell/R \rightarrow 0} \{K_r\} = 1.12K_t\sigma\sqrt{\pi\ell} \quad (4.32)$$

where  $K_t$  is the stress *concentration* factor in the original uncracked configuration. Comparison of equations (4.31) and (4.32) show that, for the two expressions to be equivalent, we must have

$$3 \left[ 1 + \sum_{n=1}^N (M'_n - 1) \right] + \frac{2P_e}{\pi R\sigma} = K_t. \quad (4.33)$$

This determines  $P_e$  as

$$P_e = \frac{\pi}{2} \Delta R \sigma \quad (4.34)$$

where

$$\Delta = K_t - 3 \left[ 1 + \sum_{n=1}^N (M'_n - 1) \right] . \quad (4.35)$$

In the special case when the only other boundaries are a pair of straight edges, *ie* a hole in a strip,  $M'_n = 1$  and

$$\Delta = K_t - 3 . \quad (4.36)$$

In other cases  $M'_n$  can be obtained from the stress distribution in the uncracked ancillary configurations or from the stress intensity factors for the ancillary configurations, since it follows from the definition of  $Q'_n$  and equation (4.30) that

$$\lim_{a' \rightarrow 0} \{Q'_n\} = M'_n . \quad (4.37)$$

The function  $\Delta$  introduced in equation (4.34) and defined in (4.35) depends only on parameters of the uncracked configuration and hence  $P_e$  which is proportional to  $\Delta$  depends only on the uncracked configuration. Thus the force  $P_e$  to be used in the calculation of  $Q_e$  is a constant for any given configuration, and does not depend on the crack-length. In the special case of straight boundaries perpendicular to the crackline, the function  $\Delta$  is particularly easy to interpret; it is, see equation (4.36), just the difference in the stress *concentration* factors at the edge of the hole with the other boundaries present or absent. Thus the magnitude of  $Q_e$  which is proportional to  $P_e$  is determined by the stress concentration factors in the uncracked configuration.

If the boundaries are not straight, equation (4.35) must be used to determine the function  $\Delta$ ; it can be written

$$\Delta = K_t - 3 - 3 \sum_{n=1}^N (M'_n - 1) . \quad (4.38)$$

The first two terms are just the difference in the stress *concentration* factors as before, but now  $\Delta$  contains an extra term which will reduce  $\Delta$  if  $M'_n$  is greater than unity: a reduction in  $\Delta$  means a reduction in  $Q_e$ . The extra term arises because if the nth boundary is curved, eg a hole, it will affect the stress distribution at the site of the equivalent crack. When the contribution to the stress intensity factor is calculated for the nth ancillary configuration it will include this effect. This change in stress distribution is (see Appendix D) also the source of the boundary-boundary interactions. Thus in the case of the curved boundaries some of the contribution to  $Q_r$  due to boundary-boundary interactions may be automatically included in the terms  $Q'_n$  and therefore the contributions from  $Q_e$  will be less. This effect will be demonstrated in later examples in this thesis.

The stress intensity factor for cracks at the edge of a circular hole subjected to localized loads has been obtained by Tweed and Rooke<sup>20</sup>;  $Q_e$  can be derived from their results which are given as  $K/(p_0\sqrt{\pi\ell})$  where  $p_0 = P_e/(2R)$ ; thus

$$\frac{K_e}{\bar{K}} = Q_e = \left[ \frac{K}{p_0\sqrt{\pi\ell}} \right] \frac{P_e\sqrt{\pi\ell}}{2R} \times \frac{1}{\sigma\sqrt{\pi a}} \quad (4.39)$$

By using equation (4.34) in equation (4.39) we obtain

$$\frac{Q_e}{\Delta} = \frac{\pi}{4} \sqrt{\frac{\ell}{a}} \left[ \frac{K}{p_0\sqrt{\pi\ell}} \right] \quad (4.40)$$

Plots of  $Q_e/\Delta$  as a function of  $a/R$  are shown in Fig 4.6 for a single crack and for two equal-length cracks.

### 4.3 Test configuration: cracks at a central hole in a strip

In this section the stress intensity factor is evaluated for the crack-tip A in the configuration shown in Fig 4.7. The compounding method as modified in the two previous sections is used, and the results are compared with known results given in Case 1.3.1, Ref 2.

Two radial cracks each of length  $\ell$  are situated (see Fig 4.7) at opposite ends of a diameter of a hole of radius  $R$ ; the distance between the tips is  $2a$ , and the hole is located centrally in a long strip, of width  $2b$ , such that the crackline is perpendicular to the strip axis. The strip is subjected, remote from the cracks, to a uniform uniaxial

tensile stress  $\sigma$  in the direction of its axis. The ancillary configurations required are shown in Fig 4.8. The strip edge nearer to tip A is  $B_{+1}$  and the other edge is  $B_{-1}$  (of boundaries  $B_1$  and  $B_2$  in section 4.1)<sup>†</sup>.

The resultant normalized stress intensity factor is calculated from equation (4.13) which, for this case, becomes ( $n = \pm 1$ )

$$Q_r = Q_0 [Q'_{+1} + Q'_{-1} - 1] + Q_e \quad (4.41)$$

where  $Q_0$  is the normalized stress intensity factor for two cracks at the edge of a hole, in the absence of all other boundaries, and  $Q'_{\pm 1}$  are the normalized stress intensity factors for a crack of length  $2a'$  near to the edge of a uniformly stressed sheet;  $Q'_{+1}$  is for the boundary nearer to the tip being considered (tip A in Fig 4.8) and  $Q'_{-1}$  for the boundary farther away from the tip. It follows from equation (4.19) that the distances  $b'_{+1}$  and  $b'_{-1}$  from the centre of the equivalent crack to the near boundary and to the far boundary respectively are given by

$$\left. \begin{aligned} b'_{+1} - a' &= b - a, & \text{all } Q_0 \\ b'_{-1} + a' &= b + a, & Q_0 < 1 \\ \text{and} \\ b'_{-1} - a' &= b - a, & Q_0 > 1 \end{aligned} \right\} \quad (4.42)$$

The values of  $Q'_{\pm 1}$  are given in Case 1.1.11, Ref 2, as a function of  $a'/b'_{\pm 1}$ . From equation (4.42) and the definition of the equivalent crack it follows that

$$\left. \begin{aligned} \frac{a'}{b'_{+1}} &= Q_0^2 \left[ \frac{b}{a} - (1 - Q_0^2) \right]^{-1} \\ \frac{a'}{b'_{-1}} &= Q_0^2 \left[ \frac{b}{a} + \left| (1 - Q_0^2) \right| \right]^{-1} \end{aligned} \right\} \quad (4.43)$$

<sup>†</sup> Labelling boundaries with positive and negative integers has been introduced here, because it will be convenient when there are many boundaries (see later) crossing the crackline on both sides of the crack.

The boundary-boundary interaction term  $Q_e$  was obtained from Fig 4.6; in this configuration  $\Delta$  is  $(K_t - 3)$ , since the other boundaries are straight (see equation (4.36)). The values of  $K_t$  corresponding to the  $b/R$  ratios used are tabulated in Table 4.1.

Table 4.1

Stress concentration factors for a central hole  
in a uniformly stressed strip

b/R	10	5	4	3	2.5	2
$K_t$	3.03	3.14	3.24	3.47	3.74	4.32

The resultant stress intensity factor can now be obtained using equation (4.41); the contribution to  $Q_r$  from  $Q_e$  is significant for small values of  $b/R$  (at  $b/R = 2$ ,  $Q_e \leq 0.3Q_r$ ). The results for  $Q_r$  are plotted in Fig 4.9 as a function of  $a/R$ . For  $a/R$  greater than the values shown a good approximation may be obtained by using the long crack limit described in Chapter 2, *ie* replacing the cracked hole by a crack of length  $2a$  and using the solution for a cracked strip (Case 1.1.1, Ref 2). The results for  $b/R = 10$  differ by less than 1% from the results for  $b/R = \infty$  (*ie* an infinitely wide strip).

The cracked hole in a strip has been studied by Newman using a collocation technique; his results are reported in Case 1.3.1, Ref 2. The differences between the compounded  $Q_r$  and Newman's results are tabulated in Table 4.2.

Table 4.2

$Q_r$  values for two equal-length cracks at the edge of a central hole  
in a uniformly stressed strip

$\frac{a}{R}$	b/R = 4			b/R = 2		
	Compound	Newman	% diff	Compound	Newman	% diff
1.02	-	-	-	0.655	0.653	<1
1.04	0.661	0.659	<1	0.895	0.882	1
1.08	0.862	0.851	1	1.19	1.14	4
1.20	1.11	1.08	3	1.63	1.50	9
1.40	1.22	1.18	4	1.95	1.82	7
1.60	1.25	1.22	3	-	-	-
2.00	1.28	1.28	<1	-	-	-

It can be seen from Table 4.2 that the differences between the two solutions become larger as the hole radius increases. However even for a hole with a diameter equal to half the strip-width ( $b/R = 2$ ) the maximum difference is less than 10%.

#### 4.4 Other configurations

In this section two configurations will be considered in order to further illustrate the equivalent crack concept, and the role of boundary-boundary interactions. The two configurations are a radial crack at the edge of a hole which is located off the centre line in a strip, and a radial crack at the edge of a hole which is near another hole in a large sheet (see Fig 4.10). The stress intensity factors are calculated, using the compounding method, for these two configurations. It is shown that for long cracks a good approximation to the stress intensity factor may be obtained by using the long crack limit (described in Chapter 2) modified by the presence of the extra boundaries.

##### 4.4.1 Crack at an off-centre hole in a strip

A radial crack of length  $l$  (tip to hole-centre distance =  $a$ ) is situated (see Fig 4.10a) at the edge of a circular hole (radius  $R$ ) in a long strip of width  $2b$ ; the centre of the hole is a distance  $b_{+1}$  from the nearer edge of the strip, and  $b_{-1}$  from the farther edge. The crack is perpendicular to the axis of the strip which is subjected to a uniform uniaxial tensile stress  $\sigma$  remote from the crack. The ancillary configurations required are shown in Fig 4.11.

The resultant normalized stress intensity factor is again given by equation (4.41), where  $Q_0$  is the stress intensity factor for a single radial crack at the edge of the hole, in the absence of all other boundaries, and  $Q'_{\pm 1}$  are the same as before. It follows from equation (4.11) that the distances  $b'_{+1}$  and  $b'_{-1}$ , from the centre of the equivalent crack to the near boundary and to the far boundary respectively, are given by

$$\left. \begin{aligned} b'_{+1} - a' &= b_{+1} - a, & \text{all } Q_0 \\ b'_{-1} + a' &= b_{-1} + a, & 2a' < a + R \\ b'_{-1} - a' &= b_{-1} - R, & 2a' > a + R. \end{aligned} \right\} \quad (4.44)$$

and

The values of  $Q'_{\pm 1}$  are again given in Case 1.1.11, Ref 2, as a function of  $a'/b'_{\pm 1}$ ; from equation (4.44) and the definition of the equivalent crack-length, it follows that

$$\left. \begin{aligned} \frac{a'}{b'_{+1}} &= Q_0^2 \left[ \frac{b_{+1}}{a} - (1 - Q_0^2) \right]^{-1}, & \text{all } Q_0, \\ \frac{a'}{b'_{-1}} &= Q_0^2 \left[ \frac{b_{-1}}{a} + (1 - Q_0^2) \right]^{-1}, & 2a' < a + R, \\ \text{and} \\ \frac{a'}{b'_{-1}} &= Q_0^2 \left[ \frac{b_{-1}}{a} - \left( \frac{R}{a} - Q_0^2 \right) \right]^{-1}, & 2a' > a + R. \end{aligned} \right\} \quad (4.45)$$

The derivation of  $Q_e$  was given in section 4.2 and the values required may be obtained from Fig 4.6 providing that the function  $\Delta$  is known. In this case, since other boundaries are straight,  $\Delta$  is given by equation (4.36) as  $(K_t - 3)$ . The configurations studied in this section are described by  $b/R = 5$  and  $b_{+1}/R = 5, 4$  and  $3$  with the corresponding stress concentration factors,  $K_t = 3.14, 3.22$  and  $3.42$ .

The resultant stress intensity factor for this configuration can now be obtained using equation (4.41); the contribution to  $Q_r$  from  $Q_e$  is a maximum of 15% for  $b_{+1}/R = 3$ , 6% for  $b_{+1}/R = 4$ , and 4% for  $b_{+1}/R = 5$ . The results are plotted as  $Q_r$  vs  $a/R$  in Fig 4.12. Also included are results (dashed curve) obtained by assuming that the hole plus crack can be replaced by a crack of length  $(a + R)$  the near tip of which is the same distance from the boundary as the original tip. It can be seen that this approximation, as expected (see Chapter 2), approaches the compounded results at large values of  $a/R$ .

#### 4.4.2 Crack at a hole near another hole

A radial crack of length  $\ell$  (tip to hole-centre distance =  $a$ ) is situated (see Fig 4.10b) at the edge of a circular hole of radius  $R_1$  which is located near another hole of radius  $R_2$ ; the crack lies between the holes along the line joining the centres which are a distance  $c$  apart. The distance from the centre of the cracked hole to the edge of the uncracked hole (boundary  $B_1$ ) is  $b_1$  ( $b_1 = c - R_2$ ). The sheet containing the holes is subjected, remote from them, to a uniform uniaxial tensile stress  $\sigma$  acting in a direction perpendicular to the crack. The ancillary configurations required are shown in Fig 4.13.

The resultant normalized stress intensity factor is calculated from equation (4.13) which becomes ( $N = 1$ )

$$Q_r = Q_0 Q_1' + Q_e, \quad (4.46)$$

where  $Q_0$  is the normalized stress intensity factor for a radial crack at the edge of a hole in an infinite sheet subjected to a uniform uniaxial tensile stress, and  $Q_1'$  is the normalized stress intensity factor for the equivalent crack of length  $2a'$  near a hole of radius  $R_2$ . The distance between the centre of the crack and the edge of the hole is  $b_1'$  (see Fig 4.13). To ensure that the distance from the tip to the boundary  $B_1$  is the same as in the original configuration, we need

$$b_1' - a' = b_1 - a, \quad (4.47)$$

ie

$$\frac{a'}{b_1'} = Q_0^2 \left[ \frac{b_1}{a} - 1 + Q_0^2 \right]^{-1}. \quad (4.48)$$

The stress intensity factor for a crack near a hole in a uniformly stressed sheet has been given by Isida (see Case 1.3.5, Ref 2). The results depend upon the ratio  $R_2/c'$  ( $c' = b_1' + R_2$ ) which is given by

$$\frac{R_2}{c'} = \frac{R_2}{a} \left[ \frac{b_1}{a} - 1 + Q_0^2 + \frac{R_2}{a} \right]^{-1}. \quad (4.49)$$

The derivation of  $Q_e$  was given in section 4.2 and the values required may be obtained from Fig 4.6 provided that the function  $\Delta$  is known. In this case  $\Delta$  is given by equation (4.35) as

$$\Delta = K_t - 3M_1', \quad (4.50)$$

where  $M_1'$  is the magnification factor on the applied stress as a distance  $c_0'$  from the centre of an uncracked hole of radius  $R_2$ ; it is given<sup>23</sup> by

$$M_1' = 1 + \frac{1}{2} \left( \frac{R_2}{c_0'} \right)^2 + \frac{3}{2} \left( \frac{R_2}{c_0'} \right)^4, \quad (4.51)$$

for this configuration,  $c_0'$  is the distance to the centre of the equivalent crack when its length tends to zero; in other words (see Fig 4.13),

$$c'_0 = \lim_{a' \rightarrow 0} \{c'\} = b_1 + R_2 - R_1 \quad (4.52)$$

The configurations considered in this report are for  $b_1/R_1 = 4$ , and  $R_2/R_1 = 1, 5$  and  $10$ ; the appropriate stress *concentration* factors and the corresponding values of  $\Delta$  are given in Table 4.3.

Table 4.3

Stress concentration factors for a circular hole near another hole in a uniformly stressed sheet

$R_2/R_1$	$M'_1$	$K_t$	$\Delta$
1	1.037	3.02	-0.09
5	1.424	3.82	-0.45
10	1.821	5.10	-0.36

Since  $\Delta$  is negative the correction term  $Q_e$  will be negative; this is because the replacement of the original cracked hole by an equivalent crack in the stress field modified by the second hole leads to an overestimate of the stress intensity factor.  $|Q_e|/Q_r \lesssim 3\%$  for  $R_2/R_1 = 1$ ,  $\lesssim 12\%$  for  $R_2/R_1 = 5$ , and  $\lesssim 8\%$  for  $R_2/R_1 = 10$ .

The resultant stress intensity factor for this configuration can now be obtained from equation (4.46). The results are plotted as  $Q_r$  vs  $a/R_1$  in Fig 4.14. Also included in Fig 4.14 are results (dashed curve) obtained by using the 'long-crack' approximation developed in Chapter 2, and allowing for the existence of another boundary, *ie* by assuming that the hole plus crack can be replaced by a crack of length  $(a+R)$ , the near tip of which is the same distance from the other hole as the original tip. It can be seen that this approximation may be adequate for long cracks ( $a/R_1 \gtrsim 1.5$ ), but as expected, is not suitable for short cracks since it tends to the wrong limit.

#### 4.5 Discussion and conclusions

The compounding technique for calculating approximate stress intensity factors has been applied to cracks at the edge of circular holes which interact with other boundaries. A systematic way is presented of calculating the effect of boundary-boundary interactions, which had been neglected in Chapter 3. In the case of two equal length cracks at the edge of a circular hole located centrally in a uniformly stressed strip the compounded results can be compared with a known numerical solution. This comparison (Table 4.2) shows two trends

similar to those observed in Chapter 3; the probable errors in the compounded solutions tend to increase as the crack-length increases and as the boundaries become closer together. For practical configurations the errors are  $\lesssim 10\%$  and this is usually adequate for most engineering applications.

Two new configurations of a radial crack at the edge of a hole have been considered; in one case the hole is located eccentrically in a uniformly loaded strip, in the other case the hole is near another hole in a uniformly stressed sheet. The approximation of replacing the hole plus the crack by a crack of the same overall length can be made for long cracks ( $a/R > 2.5$  for the eccentric hole in a strip and  $a/R > 1.5$  for a cracked hole near another hole); it becomes unsatisfactory for close boundaries (Fig 4.12).

The importance of accuracy for small cracks was discussed at the beginning of this chapter in the context of damage-tolerant design concepts. The modifications to the compounding techniques, developed in this chapter, are particularly useful in this respect, since they ensure that the errors in the stress intensity factor will be least when the crack is small. This advantage arises from the use of the stress *concentration* factor for the uncracked hole to ensure that the solution has the correct asymptote as the crack-length tends to zero. In the next chapter this powerful addition to the compounding technique will be exploited further, to solve problems of cracks growing from arrays of holes such as may occur in riveted structures.

## CHAPTER 5

CRACKS AT UNLOADED HOLES IN AN ARRAY OF HOLES<sup>36,37</sup>

In this chapter the compounding method is applied to problems of cracks at the edges of holes in a row of holes in a uniformly stressed sheet. This configuration is representative of some airframe components. For example, cracks may develop at a rivet hole in a longitudinal stiffener in a pressure cabin, in which the major in-plane loading arises from the hoop stress, with little in-plane load transfer through a rivet. An analogous situation may arise in a wing skin in which a chordwise crack may develop at a rib/skin fastener under wing bending fatigue loads. Fatigue stresses which act in a direction perpendicular to the row of holes will cause the cracks to grow along the line of holes.

In section 5.1, the configuration is considered of one or two cracks at the edge of only one of the holes in a row of holes and it is shown how compounding is used to obtain the stress intensity factor. In practice, cracks may develop at the edge of more than one hole. Therefore in section 5.2 a more general problem is considered of cracks at each hole in a row of holes. The presence of additional cracks causes the stress intensity factor to increase, thereby leading to an increase in fatigue growth rates and a consequent reduction in fatigue lifetimes; the magnitudes of these effects are examined in section 5.3.

In order to apply the compounding method to such configurations the stress intensity factors are required for the following ancillary configurations; an isolated hole with one or two cracks (Case 1.3.3, Ref 2) and a crack near an isolated hole (Case 1.3.5, Ref 2). The boundary-boundary interaction term is estimated in the way described in section 4.2 and hence gives accurate solutions for short crack-lengths. The importance of accuracy for short cracks lies in the fact that a major portion of the structure's useful fatigue lifetime is spent when the crack is short.

5.1 Crack(s) at one of the holes in a row of holes<sup>36</sup>

The structural configuration studied in this section is that of a row of holes, of radius  $R$ , in an infinite sheet uniformly stressed remote from and perpendicular to the line of holes (see Fig 5.1). Two configurations are considered, either one or two radial cracks at one of the holes. In both cases the cracks are along the line of the holes and  $a$  is the distance from the centre of the hole to the tip of the crack. In order to calculate the effect of the other holes on the crack

the hole plus the crack(s) must be replaced by an equivalent crack, using the procedure developed in section 4.1.

If the holes on the side of tip A (Fig 5.1) are labelled  $n = +1, +2$  etc, and the holes on the other side labelled  $n = -1, -2$  etc, then equation (4.13) for the normalized resultant stress intensity factor for tip A becomes

$$Q_r = Q_0 \left[ 1 + \sum_{n=-\infty}^{n=\infty} (Q'_n - 1) \right] + Q_e, \quad n \neq 0, \quad (5.1)$$

where  $Q_0$  is the normalized stress intensity factor for one or two cracks at the edge of a hole in the absence of all other boundaries, and  $Q'_n$  is that for the equivalent crack in the presence of the  $n$ th boundary (hole) only.

The boundary-boundary interaction may be obtained from values of  $Q_e/\Delta$ , for a hole with one or two cracks, given in Fig 4.6. The function  $\Delta$  is given by equation (4.35). Thus the complete compounding formula is given by

$$Q_r = Q_0 \left[ 1 + \sum_{n=-\infty}^{n=\infty} (Q'_n - 1) \right] + \left[ K_t - 3 \left( 1 + \sum_{n=-\infty}^{n=\infty} (M'_n - 1) \right) \right] \left( \frac{Q_e}{\Delta} \right), \quad (5.2)$$

where the summations exclude  $n = 0$ .

The ancillary configurations required for the evaluation of  $Q_0$  and  $Q'_n$  are shown in Fig 5.2. Values for  $Q_0$ , for both one and two cracks, are given in Case 1.3.3, Ref 2, and values of  $Q'_n$  in Case 1.3.5, Ref 2. In order to evaluate  $Q'_n$ , the length of the equivalent crack  $a'$  and the distances from the boundaries  $b'_n$  must be known. The length of the equivalent crack is again given by equation (4.3) and  $b'_n$  is obtained from equation (4.11), for one crack, as

$$\left. \begin{aligned} b'_n - a' &= b_n - a, & \text{all } Q_0, \quad n > 0, \\ b'_n + a' &= b_n + a, & Q_0^2 \leq \frac{1}{2} \left( 1 + \frac{R}{a} \right), \quad n < 0, \\ b'_n - a' &= b_n - R, & Q_0^2 > \frac{1}{2} \left( 1 + \frac{R}{a} \right), \quad n < 0, \end{aligned} \right\} \quad (5.3)$$

where  $b'_n = |n|b - R$ . For two cracks  $b'_n$  is obtained from equation (4.19) as

$$\left. \begin{aligned} b'_n - a' &= b_n - a, & \text{all } Q_0, n > 0, \\ b'_n + a' &= b_n + a, & Q_0 \leq 1, n < 0, \\ b'_n - a' &= b_n - a, & Q_0 > 1, n < 0. \end{aligned} \right\} \quad (5.4)$$

The values of  $K_t$  required in order to calculate the boundary-boundary interaction term are given in Table 5.1, for the values of  $b/R$  studied in this section<sup>17</sup>.

Table 5.1

Stress concentration factors for a hole  
in a periodic row of holes

$b/R$	3.0	3.5	4.0	5.0	10
$K_t$	3.92	3.44	3.24	3.10	3.01

The values of  $M'_n$  are obtained from the limiting values of  $Q'_n$  according to equation (4.37).

The resultant normalized stress intensity factor  $Q_r$  can now be obtained from equation (5.2); the results are plotted in Figs 5.3 and 5.4 for one and two cracks respectively. In both cases it was found that  $(Q'_n - 1)$  was negligible for  $|n| > 2$  and that  $Q_e$  was small (*ie*  $Q_e < 5\% Q_r$ ).

## 5.2 Cracks at every hole in a row of holes<sup>37</sup>

In the previous section the compounding method was applied to the problem of one or two cracks at the edge of a hole which is in a row of holes in a uniformly stressed sheet<sup>36</sup>; the stress which acts in a direction perpendicular to the row of holes causes the cracks to grow along the line of holes. This may occur in components having rows of rivet holes, *eg* the fuselage or wing-skin of an aeroplane. When the holes are periodically spaced as they frequently are, the stress fields at each hole are similar and hence cracks may occur at several holes during service life. These cracks will grow due to fatigue loads; the rate at which any one grows will be influenced by the presence of the others. If the cracks are collinear they will grow faster than similar isolated cracks and hence the fatigue lifetime will be shortened.

In this section the compounding method is used for calculating the stress intensity factor for a crack at the edge of a hole in a row of holes any number of which have cracks at the edges. The cracks are collinear, lying along the line of the holes and perpendicular to the principal stress direction. The solution to the general problem of cracks of arbitrary length at the edges of holes of arbitrary diameter is stated first, and then the stress intensity factors are determined for the special case of a periodic configuration, *ie* the cracks are all the same length, the holes are all the same radius and spaced a uniform distance apart.

In the configurations studied in this section, the stress intensity factor  $K_r$  for the crack under consideration will be affected by the presence both of the holes and of other cracks. In the previous section only one hole had a crack at its edge; this hole/crack configuration was replaced by an equivalent crack, and the contribution to  $K_r$  of the interaction of this crack with the other holes was considered. However, if the other holes have cracks at their edges there are additional interactions between the equivalent crack and these other cracks. In order to evaluate these interactions, each hole/crack configuration must, in turn, be replaced by an equivalent crack which interacts with the original equivalent crack. In general the lengths of the equivalent cracks will be all different.

### 5.2.1 General configuration of holes with cracks

The most general configuration of a row of holes each with two cracks of unequal lengths is shown in Fig 5.5; the holes may have different radii and may be unequally spaced along the row. The holes are in a sheet which is subjected to a uniform uniaxial tensile stress remote from the line of holes, and which acts in a direction perpendicular to the line of holes. Let the crack under consideration be the right-hand crack (tip A) at the edge of a hole of radius  $R_0$ ; it is of length  $l_{0,R}$  and the left-hand crack at the same hole is of length  $l_{0,L}$ . The holes to the right of this hole are labelled with positive integers such that the  $n$ th is of radius  $R_n$  and its left-hand crack is of length  $l_{n,L}$  and its right-hand crack of length  $l_{n,R}$ . A corresponding notation with negative integers is used for holes to the left of the hole of radius  $R_0$ . The distances of the left and right crack tips from the centre of their hole are given by  $a_{n,L} = l_{n,L} + R_n$  and  $a_{n,R} = l_{n,R} + R_n$  for all  $n$ . In order to apply the compounding method to this configuration, stress intensity factors for three ancillary configurations are required. These are:

- (i) two cracks of unequal length at the edge of a hole in a uniformly stressed sheet (see Fig 5.6);
- (ii) a crack near a hole in a uniformly stressed sheet (see Fig 5.7a&b);
- (iii) two collinear cracks of unequal length in a uniformly stressed sheet (see Fig 5.8a&b).

The first of these configurations has been studied by Tweed and Rooke<sup>20</sup>. Results for the stress intensity factor for the second configuration are available, Case 1.3.5, Ref 2, in a form suitable for use with the compounding method; results for the third configuration, are available in Case 1.2.3, Ref 2.

For the general configuration described in Fig 5.5, the resultant stress intensity factor  $K_r$  for the right-hand crack (tip A) at the edge of the hole of radius  $R_0$  is given by:

$$K_r = K_0 + \sum_{n=-\infty}^{n=\infty} (K'_n - K_0) + \sum_{n=-\infty}^{n=\infty} (K''_n - K_0) + K_e, \quad n \neq 0, \quad (5.5)$$

where  $K_0$  = the stress intensity factor for tip A in Fig 5.6 in the absence of all other boundaries;  $K'_n$  = the stress intensity factor for tip A of the equivalent crack of length  $2a'_{0,R}$ , in Fig 5.7a&b, near a hole of radius  $R_n$ ;  $K''_n$  = the stress intensity factor for tip A of the equivalent crack of length  $2a'_{0,R}$  in Fig 5.8a&b, near another equivalent crack of length  $2a'_{n,L}$  (if  $n$  is positive) or  $2a'_{n,R}$  (if  $n$  is negative);  $K_e$  = the contribution to the stress intensity factor because of the disturbance of the stress field caused by interactions between the holes.

The equivalent crack-lengths in Figs 5.7 and 5.8 are defined, according to the definitions in section 4.1, as follows:

$$\sigma\sqrt{\pi a'_{0,R}} = K_0 = Q_0 \bar{K}, \quad (5.6)$$

similarly

$$\left. \begin{aligned} \sigma\sqrt{\pi a'_{n,R}} &= K_{n,R} = Q_{n,R} \bar{K}, \\ \sigma\sqrt{\pi a'_{n,L}} &= K_{n,L} = Q_{n,L} \bar{K}, \end{aligned} \right\} \quad (5.7)$$

and

where  $K_{n,L}$  is the stress intensity factor for the left-hand tip at the hole of radius  $R_n$  in the absence of all other boundaries,  $K_{n,R}$  is for the right-hand crack, and  $\bar{K}$  is the stress intensity factor for an isolated crack of length  $2a_{0,R}$  in a uniform tensile stress field of  $\sigma$ , *ie*

$$\bar{K} = \sigma\sqrt{\pi a_{0,R}} . \quad (5.8)$$

If equation (5.5) is normalized with respect to  $\bar{K}$ , it becomes

$$Q_r = Q_0 \left[ 1 + \sum_{n=-\infty}^{n=\infty} (Q'_n - 1) + \sum_{n=-\infty}^{n=\infty} (Q''_n - 1) \right] + Q_e , \quad n \neq 0 , \quad (5.9)$$

where  $Q_r = K_r/\bar{K}$ ,  $Q'_n = K'_n/K_0$ ,  $Q''_n = K''_n/K_0$  and  $Q_e = K_e/\bar{K}$ . If only one hole has cracks, then  $(Q''_n - 1)$  is zero for all  $n$ , and equation (5.9) reduces to equation (5.1).

Values of  $Q_0$ ,  $Q_{n,L}$  and  $Q_{n,R}$  are given by Tweed and Rooke<sup>20</sup>. In order to use the values of  $Q'_n$  given in Case 1.3.5, Ref 2, the distances  $b'_{0,n}$  and  $b'_{n,0}$  between the centre of the equivalent crack and the hole in Fig 5.7a&b must be defined. This is done by following the principles laid down in section 4.1, and comparing the configurations in Fig 5.5 and Fig 5.7a&b.

Thus equation (4.23) becomes:

$$\left. \begin{array}{l} \text{for } n > 0 \quad b'_{0,n} - a'_{0,R} = b_{0,n} - a_{0,R} , \quad \text{all } Q_0 , \\ \text{and for } n < 0 \quad b'_{n,0} + a'_{0,R} = b_{n,0} + a_{0,R} , \quad Q_0 \leq 1 , \\ \text{or} \quad b'_{n,0} - a'_{0,R} = b_{n,0} - a_{0,L} , \quad Q_0 > 1 . \end{array} \right\} (5.10)$$

To obtain the values of  $Q''_n$  from Case 1.2.3, Ref 2 the distances  $d'_{0,n}$  and  $d'_{n,0}$  between the centres of the two equivalent cracks in Fig 5.8a&b must be defined. Again the principles of section 4.1 are followed and the configurations in Figs 5.5 and 5.8a&b compared to give,

$$\left. \begin{aligned}
 d'_{0,n} - a'_{0,R} - a'_{n,L} &= b_{0,n} - a_{0,R} - a_{n,L}, & \text{all } Q_0, \quad n > 0, \\
 d'_{n,0} + a'_{0,R} - a'_{n,R} &= b_{n,0} + a_{0,R} - a_{n,R}, & Q_0 \leq 1, \quad n < 0, \\
 \text{and} \\
 d'_{n,0} - a'_{0,R} - a'_{n,R} &= b_{0,n} - a_{0,L} - a_{n,R}, & Q_0 > 1, \quad n > 0.
 \end{aligned} \right\} \dots\dots (5.11)$$

The final term  $Q_e$  in equation (5.9) is obtained by assuming that the effects of the boundary-boundary interactions can be approximated by the effects of forces per unit thickness  $P$  acting on the hole of radius  $R_0$ ; this configuration is shown in Fig 5.9. The force  $P$  is given by

$$\frac{2P}{\pi R_0 \sigma} = K_t - 3 \left[ 1 + \sum_{n=-\infty}^{n=\infty} (M'_n - 1) \right], \quad n \neq 0, \quad (5.12)$$

where  $K_t$  is the stress *concentration* factor at the edge of the hole in the row of holes with no cracks and  $M'_n$  is the magnification of the stress a distance  $b'_{0,n}$  away from the  $n$ th hole in the absence of all other holes and cracks (for details of the derivation see section 4.2). From equation (4.37) it follows that the value of  $M'_n$  is equal to the value of  $Q'_n$  as  $a'_{0,R}$  tends to zero; it is assumed that other cracks are negligible when  $a'_{0,R}$  is small.

### 5.2.2 Periodic configuration of holes with cracks

In this section the special case is considered of a periodic array of holes, namely, each hole has the same radius  $R$  and is at a fixed distance  $b$  from its nearest neighbours; at each hole there are two cracks of equal length. The configuration is shown in Fig 5.10 where  $R_n = R$ ,  $b_{0,n} = b_{n,0} = |n|b$  and  $a_{n,L} = a_{n,R} = a$  for all values of  $n$ .

The resultant stress intensity factor is again given by equation (5.5), but now  $K_0$  = the stress intensity factor for a pair of cracks at the edge of a hole in the absence of all other boundaries;  $K'_n$  = the stress intensity factor for tip A of the equivalent crack of length  $2a'$  near a hole of radius  $R$ ;  $K''_n$  = the stress intensity factor for tip A of the equivalent crack of length  $2a'$  near another equivalent crack of the same length;  $K_e$  = the contribution to the stress intensity factor because of the disturbance of the stress field caused by interactions between the holes. All the equivalent cracks are the same length  $2a'$ , defined by

$$\sigma\sqrt{\pi a'} = K_0 ; \quad (5.13)$$

since

$$K_{n,R} = K_{n,L} = K_0 , \quad (5.14)$$

it follows that

$$a'_{n,R} = a'_{n,L} = a'_0 = a' . \quad (5.15)$$

For the periodic configuration the normalization factor  $\bar{K}$ , the stress intensity factor for an isolated crack of length  $2a$  in a uniform tensile stress field of  $\sigma$ , is given by

$$\bar{K} = \sigma\sqrt{\pi a} . \quad (5.16)$$

The normalized compounding equation is given by equation (5.9).

Values of  $Q_0$  are given by Tweed and Rooke<sup>20</sup>,  $Q'_n$  are given by Case 1.3.5, Ref 2, and  $Q''_n$  by Case 1.2.3, Ref 2. The parameters required for  $Q'_n$  are obtained from equation (5.10); for this periodic configuration we have,

$$a' = Q_0^2 a , \quad (5.17)$$

$$\text{and } \left. \begin{aligned} b'_{0,n} &= nb - a(1 - Q_0^2) , & n > 0 , \\ b'_{n,0} &= |n|b + a \left| (1 - Q_0^2) \right| , & n < 0 . \end{aligned} \right\} \quad (5.18)$$

The parameters required for  $Q''_n$ , in addition to  $a'$ , are

$$\left. \begin{aligned} d'_{0,n} &= nb - 2a(1 - Q_0^2) , & \text{all } Q_0 , n > 0 , \\ d'_{n,0} &= |n|b , & Q_0 \leq 1 , n < 0 , \\ d'_{n,0} &= |n|b + 2a(Q_0^2 - 1) , & Q_0 > 1 , n < 0 . \end{aligned} \right\} \quad (5.19)$$

Results for the stress intensity factor for a periodic array of holes with equal length cracks have been obtained and are shown in Fig 5.11 for various values of  $b/R$ . Also shown for comparison is the Westergaard solution (Case 1.2.8, Ref 2) for a periodic array of collinear cracks with no holes ( $R = 0$ ). It can be seen that the stress intensity factor firstly increases rapidly from zero at the edge of the hole and then approaches the curve for collinear cracks as the cracks

lengthen. The deviation of  $Q_r$  from the normalized stress intensity factor for  $R = 0$  is within  $\pm 8\%$  if the crack is more than 15% of the radius, *ie*  $a/R > 1.15$ , and  $a/b < 0.4$ .

The stress intensity factor for a crack in the presence of other cracks is larger than that for one of a pair of cracks at one of the holes in a periodic array; and the effect increases as the length of the crack increases. The results obtained above are compared in Fig 5.12 with those for a pair of cracks obtained in the previous section. The ratio of  $K_m/K_s$  is plotted as a function of  $a/b$  for various values of  $b/R$ ;  $K_m$  and  $K_s$  are respectively the stress intensity factors for two cracks at each hole and for two cracks at one hole. It can be seen that  $K_m$  becomes larger than  $K_s$  as  $a/b$  increases from zero and at large  $a/b$ , results for all  $b/R$  tend to similar values.

### 5.3 Fatigue crack growth

The increase in stress intensity factor due to the presence of many cracks leads to an increase in the rate at which the cracks will grow under fatigue loadings. Since the rate at which cracks grow is strongly dependent on the value of the stress intensity factor, small increases in  $K$  can lead to large increases in rate. Hence a significant shortening of the fatigue life of a structure can occur if many cracks are present.

It is often assumed<sup>18</sup> that the growth rate  $(da/dN)$  of a crack of length  $2a$  can be simply represented by a power dependence on the range of the stress intensity factor  $(\Delta K)$  applied to the cracked structure. Thus

$$\frac{da}{dN} = C(\Delta K)^p, \quad (5.20)$$

where  $C$  and  $p$  are material constants and  $N$  is the number of cycles of stress. The range of the stress intensity factor will be given by

$$\Delta K = Q\Delta\sigma\sqrt{\pi a}, \quad (5.21)$$

where  $\Delta\sigma$  is the range of applied stress.

It follows from equations (5.20) and (5.21) that the growth rate for many cracks  $(da/dN)_m$  in terms of that for just two cracks  $(da/dN)_s$  is given by

$$\frac{(da/dN)_m}{(da/dN)_s} = \left(\frac{Q_m}{Q_s}\right)^p \quad (5.22)$$

The ratio  $(Q_m/Q_s)$  of the normalized stress intensity factors is the same as the ratio of  $K_m/K_s$  plotted in Fig 5.12. As seen from equation (5.22) the ratio of the rates depends on the value of  $p$ . Typically, for aluminium alloys,  $p$  is between 2 and 4. Results for the increased rate due to many cracks are shown in Fig 5.13 for  $p = 2, 3$  and 4, and  $b/R = 8$ ; this value of  $b/R$  is typical of many aerospace riveted structures. It is seen from Fig 5.13 that the rate of growth increases as both  $p$  and  $a/b$  increase. The rate for many cracks is double that for just two cracks at  $a/b = 0.415$  for  $p = 2$ , at  $a/b = 0.365$  for  $p = 3$  and at  $a/b = 0.33$  for  $p = 4$ .

#### 5.4 Discussion and conclusions

The compounding method isolates the effects of the component boundaries and considers, in turn, how they each influence the stress intensity factor. Which boundaries are important in affecting the resultant stress intensity factor in the periodic configuration (see section 5.2.2), depend on the length of the crack. For short cracks the row of holes which determine the stress *concentration* factor  $K_t$  also determines the stress intensity factor, since

$$\lim_{a \rightarrow R} \{K_r\} = K_t \sigma \sqrt{\pi(a-R)} = K_t \sigma \sqrt{\pi \ell} \quad (5.23)$$

The presence of the other cracks has only a small effect; at  $\ell/R = 0.01$  the effect is less than 10% of that due to the holes. But it becomes more important as the cracks grow and at  $\ell/R = 0.1$  the effect of the other cracks is about equal to that of the holes. At longer crack-lengths the effect of the other cracks dominates, particularly for values of  $b/R$  commonly used in aerospace structures (*ie*  $b/R \geq 8$ ). The effect of the boundary-boundary interaction through the term  $Q_e$  was negligible for all the configurations considered.

The formula, given in equation (5.5) for calculating  $K_r$  contains two summations over all boundaries. In practice only boundaries close to the crack significantly affect the stress intensity factor; for all values of  $b/R$ , the only important boundaries are  $n = \pm 1$  and  $n = \pm 2$ . The contribution from  $n = \pm 2$  is usually about one-tenth of that due to  $n = \pm 1$ . For the periodic configuration,  $K_e$  due to the interaction of the holes is negligible; this is because of the use of the ancillary

configuration of the equivalent crack near a neighbouring hole, takes into account most of the stress disturbance due to the presence of the holes.

For practical configurations ( $b/R > 8$ ), the stress intensity factor  $K_r$  for short cracks ( $l/R < 0.2$ ) differs by less than 3% from the value of  $K_0$  for cracks at the edge of an isolated hole<sup>20</sup>. Fig 5.11 shows that  $K_r$  for long cracks ( $l/R > 0.2$ ) differs by less than 7% from the Westergaard solution  $K$  (Case 1.2.8, Ref 2). These two limiting cases suggest a simple approximate procedure for estimating the stress intensity factor

$$\left. \begin{aligned} K_r &= K_0, & 0 < a/R \leq 0.2. \\ \text{and} \\ K_r &= K_w = \sigma \left\{ b \tan\left(\frac{\pi a}{b}\right) \right\}^{\frac{1}{2}}, & 0.2 < a/R. \end{aligned} \right\} (5.24)$$

It has been demonstrated in Chapter 2 that such approximations are adequate for fatigue crack growth calculations in many engineering applications. The tendency for  $K_r$  to fall below  $K_w$  for  $a/b > 0.25$  is probably due to an underestimate of  $K_r$ ; it is shown in Chapter 3 that, in the simple case of collinear cracks, the compounding method underestimates the resultant stress intensity factor.

It was seen in section 5.3 that the presence of many cracks can significantly increase the rate of growth of a crack under fatigue loadings. The largest increases occur for the largest values of  $p$ , the exponent in equation (5.20). Such increases can lead to large reductions in fatigue life of a cracked structure. Thus with periodic cracks, not only has the crack less distance to travel (half-way between the holes) but it is travelling faster.

The results given in Figs 5.11 to 5.13 are for the special case of holes of equal radius in a periodic array with two collinear cracks of equal lengths at each hole. Stress intensity factors can also be calculated (see section 5.2.1) for the general case of collinear cracks of unequal length at holes of unequal radius in a non-periodic array.

Many aircraft components will have holes of equal size and in a periodic array (*eg* row of rivet holes), but the cracks will be of unequal length; with tensile loading remote from the cracks the longest crack will have the largest stress intensity factor.

## CHAPTER 6

CRACKS AT LOADED HOLES

In the previous chapter the compounding method was used to evaluate the stress intensity factor for cracks at the edge of unloaded holes, arranged in a row. As well as unloaded holes in structures, there are also many cases of loaded holes, *eg* pin-loaded lugs or fastener holes where load is transmitted through the fastener to the sheet. In this chapter the opening-mode stress intensity factor is evaluated for two cracks at the edge of each loaded hole in a row of fastener holes. The concept of the 'equivalent crack-length', needed in Chapters 4 and 5 to make it possible to calculate the effects of boundaries on the stress intensity factor, is not appropriate for cracks at loaded holes. A new concept of the 'equivalent load' will be introduced and described in section 6.1 of this chapter.

In section 6.2 the opening-mode stress intensity factors are obtained for two equal-length cracks at each hole in a periodic row of holes; the holes are subjected to a uniform internal pressure. The results are compared with those obtained by Parker<sup>38</sup>; the agreement is good. A more complex configuration is studied in section 6.3, where the row of holes is near a boundary and the pressure on the hole perimeter is not uniform. In all cases considered in this chapter the loading on the hole perimeter is symmetric about the diameter perpendicular to a line joining the centres of the holes in a row.

6.1 Equivalent loading on crack

In the definition of the equivalent crack, given in equation (4.2), the stress  $\sigma$  can be interpreted as a uniform pressure acting on the crack faces. This follows from the fact that an isolated crack of length  $2a'$  subjected to a uniform internal pressure  $p$  has a stress intensity factor given by

$$K = p\sqrt{\pi a'} \quad . \quad (6.1)$$

Thus if the pressure  $p$  is equal to the stress  $\sigma$ , then the stress intensity factor is  $K_0$ , the same as for the equivalent crack defined by equation (4.2). For cracks growing from loaded holes, the definition of the equivalent crack must contain information about both the loading on the hole and the remote loading. In fact, if the loads on the hole are in equilibrium, the remote stress  $\sigma$  may be zero and equation (4.2) is then clearly not applicable as a definition of  $a'$ .

Three different loading cases are considered for two radial cracks at the edge of a hole in a sheet. In section 6.1.1 the only loads are self-equilibrated loads acting on the perimeter of the hole. A case when the loads on the hole have a non-zero resultant is considered in section 6.1.2; the other boundaries are considered so remote that the stress on them required to satisfy overall equilibrium is negligible. Finally in section 6.1.3 the case is considered when the boundary stresses are not negligible and must be included in the determination of the stress intensity factor.

It is necessary to redefine the equivalent crack when considering cracks at loaded holes, so that known physical limits are reproduced. A new concept of 'equivalent loads' acting on the faces of the equivalent crack is introduced: the loaded hole and the original crack(s) are replaced by an equivalent crack, of the same overall length as the original crack(s) plus hole, but with equivalent loads acting at right angles to the two crack faces. The loads (force per unit thickness) are determined by the condition that the equivalent crack has the same stress intensity factor  $K_0$  as the original crack at the loaded hole in the absence of all the other boundaries. The effect of these other boundaries is then accounted for by the compounding procedure.

#### 6.1.1 Self-equilibrated loads on the perimeter of the hole

Consider a circular hole, defined in cylindrical polar coordinates  $(r, \theta)$  by  $r = R$ ,  $0 \leq \theta < 2\pi$ , which is loaded by a pressure  $p(\theta)$ , see Fig 6.1; the pressure distribution is symmetrical about  $\theta = 0$ , that is,  $p(\theta) = p(-\theta)$ . Two radial cracks of length  $\ell$  are located at the edge of the hole along  $\theta = 0$  and  $\theta = \pi$  respectively, so that the tip-to-tip distance is  $2a$  where  $a = R + \ell$ . Fig 6.1 also shows the equivalent crack, which is an isolated crack of the same length  $2a$  with two opposing forces of equal magnitude  $P'$  acting perpendicular to the crack at its centre. The force  $P'$  is defined by the condition given above as

$$\frac{P'}{\sqrt{\pi a}} = K_0, \quad (6.2)$$

since the left-hand side of equation (6.2) is the stress intensity factor of an isolated crack subjected to localized forces  $P'$ .

The force  $P'$  has the following limiting values, as shown below:

$$\lim_{\ell \rightarrow 0} \{P'\} = 0 \quad \text{and} \quad \lim_{\ell \rightarrow \infty} \{P'\} = P, \quad (6.3)$$

where  $P$  is the resultant force acting on one half of the hole perimeter, perpendicular to the crackline. This force results from the pressure  $p(\theta)$  for  $0 \leq \theta < \pi$ ; it is given by

$$P = R \int_0^{\pi} p(\theta) \sin \theta \, d\theta \quad . \quad (6.4)$$

The first limit in equation (6.3) follows directly from equation (6.2) since  $P \propto K_0$  and since  $K_0$  must be zero when there is no crack ( $\ell = 0$ ). Thus the equivalent crack becomes, when  $\ell = 0$ , an unloaded crack of length  $2R$ . Since it is unloaded it will not interact with the boundaries; therefore  $K_n$  will be zero for all values of  $n$  and hence the resultant stress intensity factor  $K_r$  will be zero as required.

When the crack is long ( $\ell \gg R$ ) the presence of the hole at the centre of the crack has little effect on the value of the stress intensity factor; its value tends towards that for a crack with two equal and opposite forces  $P$  acting at the centre of the crack. Thus the limiting value for the stress intensity factor  $K_0$  for such a crack is given by

$$\lim_{\ell \rightarrow \infty} \{K_0\} = \frac{P}{\sqrt{\pi a}} \quad , \quad (6.5)$$

where  $P$  is defined in equation (6.4). Comparison of equations (6.2) and (6.5) leads to the second limit given in equation (6.3).

In the case of two cracks of unequal length at the edge of the hole the equivalent load will depend on which crack tip is under consideration. Consider a circular hole defined as before with a symmetrical pressure distribution  $p(\theta)$ , but with two cracks of different lengths located at the edge of the hole along  $\theta = 0$  and  $\theta = \pi$  respectively. Let the crack with tip A be of length  $\ell_A$  from the edge of the hole to the tip and the crack with tip B be of a length  $\ell_B$  (see Fig 6.2). The tip-to-tip distance is  $2a$  where

$$2a = a_A + a_B \quad (6.6)$$

$$\text{with} \quad a_A = \ell_A + R \quad \text{and} \quad a_B = \ell_B + R \quad . \quad (6.7)$$

If tip A is the tip under consideration the equivalent crack is of length  $2a$  with two opposing forces of equal magnitude  $P'_A$  acting perpendicular to the crack at a distance  $a_A$  from tip A and  $a_B$  from tip B. The stress intensity factor for tip A of the equivalent crack is given, in Case 1.1.12, Ref 2, by

$$K = \frac{P'_A}{\sqrt{\pi a}} \sqrt{\frac{a_B}{a_A}} . \quad (6.8)$$

If this is to be equal to the stress intensity factor  $K_{0A}$  of the original tip A in the absence of all boundaries except the loaded hole, then it follows that

$$P'_A = K_{0A} \sqrt{\pi a} \sqrt{\frac{a_A}{a_B}} . \quad (6.9)$$

For tip B the equivalent load  $P'_B$  is determined in a similar manner, and is given by

$$P'_B = K_{0B} \sqrt{\pi a} \sqrt{\frac{a_B}{a_A}} , \quad (6.10)$$

where  $K_{0B}$  is the stress intensity factor for tip B in the absence of all boundaries other than the loaded hole.

#### 6.1.2 Resultant load on the perimeter: zero stress on sheet boundary

If there is a resultant load on the perimeter of the hole, then the two equivalent loads will not be equal in magnitude. Since, in this case, the boundaries are far removed from the hole and hence large in extent, the remote stresses required for equilibrium are small and will not affect the stress intensity factor. Consider such a loaded hole with two cracks of length  $l$  (tip-to-tip distance of  $2a$ ). The equivalent crack is of length  $2a$  with opposing forces of  $P'_1$  and  $P'_2$  acting at the centre. The stress intensity factor of such a crack is given by

$$K = \frac{P'_1 + P'_2}{2\sqrt{\pi a}} . \quad (6.11)$$

Thus for the crack to be equivalent, it follows that the equivalent loads are given by

$$P'_1 + P'_2 = 2K_0 \sqrt{\pi a} . \quad (6.12)$$

The case for two cracks of unequal length at a hole with a resultant load on its perimeter, can be treated in a similar way to that above for a zero resultant.

### 6.1.3 Resultant load on the perimeter: finite stress on sheet boundary

If boundaries are not remote from the hole the stress intensity factor will be affected by both the boundary stresses needed to balance the resultant load on the hole perimeter and any externally applied boundary stresses which exist. Both of these effects must be included in  $K_0$  and in the definition of the equivalent crack.

In general there will be an integral relationship, between the resultant force on the hole and the boundary stresses - the integral of the stresses around the boundary must balance the loads on the hole perimeter. In the special case of a uniform normal stress  $\sigma$  acting on a boundary parallel to the cracks, this becomes

$$\sigma W = P \quad . \quad (6.13)$$

The significance of the length  $W$  will depend on the actual configuration: for a loaded hole in a strip (see Fig 6.3a),  $W$  is the width of the strip; for an infinite array of periodically spaced loaded holes (see Fig 6.3b),  $W$  is the spacing between the hole centres.

In Chapters 4 and 5 the ancillary configuration for a crack at the edge of a hole, used for the determination of  $K_0$ , was obtained by removing all other boundaries (cracks, holes and edges). The removal of all these boundaries did not alter the boundary conditions; in the case of the loaded holes this may not be so. Consider the configurations in Fig 6.3a&b. If the boundaries are removed by letting  $W \rightarrow \infty$ , then it follows from equation (6.13) that  $\sigma \rightarrow 0$  in order to maintain equilibrium if the force  $P$  is held fixed. Thus in the limit the stress will be too small to affect the stress intensity factor, and  $K_0$  will be a function of  $P$  and crack-length only. This ancillary configuration of a crack at the edge of a hole with a single load  $P$  on its perimeter is not therefore suitable for evaluating  $K_0$ ; the uniform stress  $\sigma$  will have a large effect on the stress intensity factor and must be included in  $K_0$ , the major contribution to  $K_r$ .

It is necessary to consider ancillary configurations in which the forces and stresses are symmetric about the crackline, so that both the boundary forces and the boundary stresses are separately in equilibrium. Removal of boundaries to obtain a configuration suitable for evaluating  $K_0$  does not now affect the boundary conditions. The opening mode stress intensity factor for an asymmetric configuration can be obtained from a

combination of symmetric configurations by applying the principle of superposition. For instance, the stress intensity factor for the asymmetric configuration shown in Fig 6.3a is the same if the force  $P$  is replaced by two equal and opposite radial forces of  $P/2$  acting on opposite sides of the hole perpendicular to the crackline, and if the tensile stress  $\sigma$  at one end of the strip is replaced by tensile stresses of  $\sigma/2$  at both ends of the strip. Similarly the forces  $P$  and the stress  $\sigma$  in the periodic configuration shown in Fig 6.3b would be replaced by two equal and opposite forces  $P/2$  on each hole and stresses  $\sigma/2$  on the two boundaries remote from the holes.

The ancillary configuration required for the determination of  $K_0$  for these symmetric configurations is obtained by removing all boundaries, as in Chapter 4, except the hole with the two cracks under consideration. Thus the ancillary configuration contains two equal length cracks at the edge of a hole with two equal and opposite radial forces  $P/2$  acting on the perimeter perpendicular to the crackline; the hole is in a sheet which is subjected to a uniform tensile stress of  $\sigma/2$  acting perpendicular to the crackline remote from the hole. This ancillary configuration, which contains no other boundaries, is shown in Fig 6.3c. Since  $K_0$  must be the same for both the symmetric and the antisymmetric configurations, it follows that the same ancillary configuration must be used.

By using the principle of superposition  $K_0$  may be determined from two simpler configurations for which the stress intensity factors are known. These two configurations are obtained from Fig 6.3c by considering the effect of the forces  $P/2$  and the stresses  $\sigma/2$  separately. Let  $K_\sigma$  be the stress intensity factor for the ancillary configuration when there are no forces acting ( $P = 0$ ), and let  $K_P$  be the stress intensity factor when there are no stresses acting ( $\sigma = 0$ ); therefore

$$K_0 = K_P + K_\sigma . \quad (6.14)$$

At long crack-lengths the effect of the hole on  $K_0$  is negligible;  $K_P$  tends to the limit  $P/(2\sqrt{\pi a})$ , and  $K_\sigma$  tends to the limit  $\sigma\sqrt{\pi a}/2$ . Therefore it follows that

$$\lim_{a \rightarrow \infty} \{K_0\} = \frac{1}{2} \left( \frac{P}{\sqrt{\pi a}} + \sigma\sqrt{\pi a} \right) . \quad (6.15)$$

The above procedure for obtaining the ancillary configuration for  $K_0$  is not limited to the case of a localized load  $P$  on the hole perimeter. The same arguments apply for any distribution of pressure  $p(\theta)$  around the perimeter. The force  $P$  is now the resultant force acting on the perimeter and is given by equation (6.4). The ancillary configuration for  $K_0$  will now have a distribution of pressure on the perimeter of the hole given by  $p(\theta)/2$  for  $0 \leq \theta < \pi$  and  $p(-\theta)/2$  for  $0 > \theta \geq -\pi$ .

The equivalent crack is derived from the ancillary configuration for  $K_0$  by replacing the hole plus the cracks by a crack of length  $2a$ , subjected to two opposing forces  $P'/2$ , in a sheet subjected to a uniform tensile stress  $\sigma'/2$  acting, remote from the crack, in a direction perpendicular to the crack. Again, by using the principle of superposition, the forces and stresses may be considered separately. When the forces  $P'/2$  act alone, the stress intensity factor is  $P'/(2\sqrt{\pi a})$ , and when the stresses  $\sigma'/2$  act alone, the stress intensity factor is  $\sigma'\sqrt{\pi a}/2$ . The values of  $P'$  and  $\sigma'$  are determined by the condition that the stress intensity factor of the isolated equivalent crack is  $K_0$ , *ie*

$$\frac{1}{2} \left( \frac{P'}{\sqrt{\pi a}} + \sigma' \sqrt{\pi a} \right) = K_0 \quad (6.16)$$

For long crack-lengths, the comparison of equations (6.15) and (6.16) shows that  $P' \rightarrow P$  and  $\sigma' \rightarrow \sigma$ . Since in the original configuration  $P = \sigma W$  in order to maintain equilibrium, it follows that, in the ancillary configurations, equilibrium is maintained by  $P' = \sigma' W$ . This relationship between  $P'$  and  $\sigma'$  combined with equation (6.16) determines these two unknowns; thus

$$\frac{P'}{2\sqrt{\pi a}} \left( 1 + \frac{\pi a}{W} \right) = K_0, \quad \text{or} \quad \frac{\sigma' \sqrt{\pi a}}{2} \left( \frac{W}{\pi a} + 1 \right) = K_0 \quad (6.17)$$

In the above  $\sigma'$  was considered as a remote stress. It may be convenient for some configurations to consider  $\sigma'$  as a uniform pressure acting on the crack faces - this is permissible since the stress intensity factor of the equivalent crack is identical (see equation (6.1)). The principle of superposition makes it possible to interpret the equivalent crack in another way. Since the opening-mode stress intensity factor for an isolated crack of length  $2a$ , subjected to two equal and opposite forces of magnitude  $P'/2$  is  $P'/(2\sqrt{\pi a})$ , and since that for a similar crack subjected to a pressure of  $\sigma'/2$  is  $(\sigma'\sqrt{\pi a})/2$ , then it

follows that the stress intensity factor for a crack subjected to both loadings is the same as that given by equation (6.16). Thus the equivalent crack may be interpreted as an isolated crack subjected to a uniform pressure  $\sigma'/2$  on its faces and two equal and opposite forces  $P'/2$  acting perpendicular to its faces at the centre of the crack. This interpretation will be needed in one of the ancillary configurations used in section 6.3.

## 6.2 Cracks at pressurized holes

In order to test procedures, outlined in the previous section, for applying the compounding method to configurations with loaded holes, the opening-mode stress intensity factor will be evaluated for a configuration with a known solution<sup>38</sup>. The configuration consists of a periodic row of internally pressurized holes, of radius  $R$ , spaced a distance  $2b$  apart. The pressure  $p$  is a radial pressure acting uniformly on the perimeter of each hole. At the edge of each hole are two cracks of equal length which lie along the line of centres; each crack is of length  $\ell$  measured from the edge of the hole to the crack-tip. The total distance between the tips of the two cracks at any one hole is  $2a$  ( $= 2\ell + 2R$ ). Although all the crack tips have the same value of the stress intensity factor in this configuration, it is convenient to consider a particular tip, namely the one labelled  $A$  in Fig 6.4a&b. The hole associated with crack tip  $A$  is labelled  $n = 0$ ; holes on the same side as tip  $A$  are labelled with positive integers, i.e.  $n = +1, +2$  etc, and holes on the other side with negative integers.

The compounding equation required for this configuration is the modified version, based on equation (4.12). In this case  $K_0$  is the stress intensity factor for two diametrically opposite cracks of equal length at the edge of a circular hole subjected to a uniform radial pressure  $p$ . This configuration has been studied by Tweed and Rooke<sup>20</sup>.

The equivalent crack is a crack of length  $2a$  with two opposing forces of magnitude  $P'$  acting perpendicular to the crack at its centre. The equivalent load  $P'$  is given by equation (6.2). The interactions of the equivalent crack with the other boundaries are evaluated by first replacing each pressurized hole with its two cracks by another equivalent crack of length  $2a$  with forces  $P'$  acting on it. Since all the holes are similar with similar loading and similar cracks it follows that all the equivalent cracks will be similar. Thus the ancillary configuration used in evaluating the effects of the boundaries on tip  $A$  is a periodic set of loaded cracks spaced a distance  $2b$  apart; each crack

is subjected to two opposing forces  $P'$  acting perpendicular to the crackline (see Fig 6.4b). The stress intensity factor  $K'$  for this configuration is given in Case 1.2.9, Ref 2. It follows that  $K'$  contains all the contributions from every  $K'_n$  in equation (4.12); in fact

$$\sum_{n=-\infty}^{n=\infty} (K'_n - K_0) = K' - K_0, \quad n \neq 0. \quad (6.18)$$

Therefore the compounding equation becomes

$$K_r = K' + K_e, \quad (6.19)$$

where  $K'$  is a function of  $P'$  ( $= K_0 \sqrt{\pi a}$ ).

Equation (6.19) can be written in terms of normalized stress intensity factors  $Q$ . The normalizing constant for  $K'$  is  $P'/\sqrt{\pi a}$ , that is the stress intensity factor for an isolated crack subjected to two opposing forces of magnitude  $P'$ . Thus

$$Q' = \frac{K'}{P'/\sqrt{\pi a}} = \frac{K'}{K_0}. \quad (6.20)$$

It follows that  $Q'$  is independent of  $P'$  since both  $K'$  and  $K_0$  are proportional to  $P'$ . Thus equation (6.19) becomes

$$K_r = K_0 Q' + K_e. \quad (6.21)$$

It is convenient to normalize equation (6.21) with respect to  $\bar{K}$ , the stress intensity factor for an isolated crack subjected to a uniform pressure  $p$  on its faces, which is given by

$$\bar{K} = p\sqrt{\pi a}. \quad (6.22)$$

Thus equation (6.21) becomes

$$Q_r = Q_0 Q' + Q_e, \quad (6.23)$$

where  $Q_r = K_r/\bar{K}$ ,  $Q_0 = K_0/\bar{K}$  and  $Q_e = K_e/\bar{K}$ .

The contribution to  $K_r$  from the boundary-boundary interactions, which are all included in  $Q_e$ , is evaluated (see section 4.2) by

considering the effect of two additional opposing forces of magnitude  $P_e$  acting radially on the hole ( $n = 0$ ) in a direction through its centre and perpendicular to the crack. The forces  $P_e$  are determined by the requirement that  $K_r$  approaches the correct limiting value as the crack-length tends to zero, *ie*

$$\lim_{\ell \rightarrow 0} \{K_r\} = 1.12 \sigma_{\infty} \sqrt{\pi \ell} \quad , \quad (6.24)$$

where  $\sigma_{\infty}$  is the maximum stress, which occurs at the edge of the hole at the crack-site in an infinite row of pressurized holes, and the factor 1.12 is the usual free edge correction.

In order to consider the limiting behaviour of equation (6.21), the following limits are required:

$$\lim_{\ell \rightarrow 0} \{K_0\} = 1.12 \sigma_0 \sqrt{\pi \ell} \quad , \quad (6.25)$$

where  $\sigma_0$  is the maximum stress at the crack-site at the edge of an isolated pressurized hole;

$$\lim_{\ell \rightarrow 0} \{Q'\} = \lim_{a \rightarrow R} \{Q'\} = Q'\left(\frac{R}{b}\right) \quad , \quad (6.26)$$

where  $Q'(R/b)$  is the normalized stress intensity factor for a crack in an infinite row of collinear cracks of length  $2R$  a distance  $2b$  apart subjected to two equal and opposite forces at the crack centre;

$$\lim_{\ell \rightarrow 0} \{K_e\} = 1.12 \times \frac{2P_e}{\pi R} \sqrt{\pi \ell} \quad , \quad (6.27)$$

where  $2P_e/(\pi R)$  is the maximum stress at the crack-site at the edge of an isolated hole of radius  $R$  subjected to two opposing radial forces  $P_e$  acting perpendicular to the crackline.

Substitution of equation (6.24) to (6.27) into equation (6.21) gives

$$\sigma_{\infty} = \sigma_0 Q'\left(\frac{R}{b}\right) + \frac{2P_e}{\pi R} \quad . \quad (6.28)$$

For a uniform pressure  $p$  in the holes, we have  $\sigma_0 = p$  and  $\sigma_{\infty} = K_t p$  where  $K_t$  is the stress *concentration* factor<sup>17</sup>. Thus equation (6.28) can be written

$$P_e = \frac{\pi R p}{2} \left[ K_t - Q' \left( \frac{R}{b} \right) \right] . \quad (6.29)$$

Since, for a uniform pressure acting on the hole perimeter, the resultant force  $P$  is given by

$$P = 2pR , \quad (6.30)$$

it follows from equation (6.25) that

$$\frac{P_e}{P} = \frac{\pi}{4} \left[ K_t - Q' \left( \frac{R}{b} \right) \right] . \quad (6.31)$$

Values of  $Q_e$  can be obtained from Ref 20 where the normalized stress intensity factor  $K_e / (p_e \sqrt{\pi \ell})$  has been evaluated; the bearing pressure  $p_e$  is given by

$$p_e = \frac{P_e}{2R} . \quad (6.32)$$

We can write

$$Q_e = \frac{K_e}{p \sqrt{\pi a}} = \left( \frac{K_e}{p_e \sqrt{\pi \ell}} \right) \sqrt{\frac{\ell}{a}} \left( \frac{P_e}{2Rp} \right) = \left( \frac{K_e}{p_e \sqrt{\pi \ell}} \right) \sqrt{\frac{\ell}{a}} \left( \frac{P_e}{P} \right) , \quad (6.33)$$

where  $P_e/P$  is given by equation (6.31).

It follows from equations (6.23) and (6.33) that the smaller the value of the ratio  $P_e/P$ , the smaller is the boundary-boundary contribution to  $Q_r$ .

The normalized stress intensity factor  $Q_r$  has been evaluated from equation (6.23), with  $Q_0$  and  $Q_e$  obtained from Ref 20 and  $Q'_1$  from Case 1.2.9, Ref 2, for  $b/R = 10, 4$  and  $2$ . The results are compared with those obtained by Parker<sup>38</sup>. To facilitate comparison it is convenient to plot  $K_r / (p \sqrt{\pi \ell}) = Q_r \sqrt{a/\ell}$  as a function of  $a/b$ ; the comparison is shown in Fig 6.5. Over most of the range, the differences are between 2% and 5%. The major differences, up to 8%, are at the shortest crack-lengths. However at short crack-lengths Parker's method, mapping collocation, is known to become increasingly inaccurate, whereas the compounding method is constrained to approach known limits at  $\ell = 0$ .

The contribution to  $Q_r$  from the boundary-boundary interaction term  $Q_e$  increases as  $b/R$  decreases. The biggest contribution occurs at the shortest crack-lengths. The ratio  $P_e/P$  given by equation (6.31)

can be used to give a rough estimate of the maximum value of  $Q_e/Q_r$ . For instance, at  $b/R = 10$  we have  $P_e/P = 0.02$  and  $Q_e/Q_r \lesssim 0.03$ ; at  $b/R = 4$  we have  $P_e/P = 0.11$  and  $Q_e/Q_r \lesssim 0.12$ ; at  $b/R = 2$  we have  $P_e/P = 0.42$  and  $Q_e/Q_r \lesssim 0.33$ .

### 6.3 Loaded holes near a boundary

In this section the opening-mode stress intensity factors are evaluated for cracks at loaded holes which are close to a boundary (the edge of the sheet). The holes are of radius  $R$  and are spaced a distance  $W$  apart in a row parallel to the edge of the sheet; the distance from the edge of the sheet to the line of hole centres is  $h$  (see Fig 6.6). Each hole is subjected to a distribution of pressure  $p(\theta)$  on the side of the hole nearer to the boundary. Two cracks of equal length are located at the edge of each hole along the line passing through the hole centres. The cracks are of a length  $\ell$  measured from the edge of the hole, and the distance between crack tips at the same hole is  $2a (= 2\ell + 2R)$ . The forces on the hole are balanced by a uniform stress  $\sigma$  acting remote from the holes in a direction perpendicular to the cracks. In order to maintain equilibrium it follows that

$$\sigma W = P \quad (6.34)$$

where  $P$  is the resultant force on one hole due to the internal pressure  $p(\theta)$ , and is given by equation (6.4).

If the two cracks at each hole (see Fig 6.6) are taken to lie along  $\theta = 0$  and  $\theta = \pi$  respectively, then the pressure distribution used in this section is given by

$$p(\theta) = p_m \sin \theta, \quad 0 \leq \theta \leq \pi. \quad (6.35)$$

Therefore the pressure is a maximum equal to  $p_m$  at  $\theta = \pi/2$ , *ie* the point on the perimeter of the hole nearest to the edge of the sheet. From equations (6.4) and (6.35) it follows that the resultant force  $P$  acts along the line  $\theta = \pi/2$ , and is given by

$$P = \frac{\pi}{2} R p_m. \quad (6.36)$$

The compounding equation required to evaluate the opening-mode stress intensity factor for the crack-tip labelled A in Fig 6.6 is given by equation (4.12). The ancillary configurations required to evaluate  $K_0$ ,  $K_1'$  and  $K_2'$  are shown in Fig 6.7a-c. The compounding equation becomes

$$K_r = K_1' + K_2' - K_0 + K_e \quad (6.37)$$

The ancillary configurations needed for the determination of  $K_0$  are derived from Fig 6.3c and are shown in Fig 6.7a. They are (i) two equal length cracks at the edge of a hole which is subjected to a loading  $p_m \sin(\theta)/2$  for  $0 \leq \theta < \pi$  and  $-p_m \sin(\theta)/2$  for  $0 > \theta \geq -\pi$ ; (ii) two equal length cracks at the edge of a hole in a sheet that is subjected to a uniform stress  $\sigma/2$  remote from the hole. The stress intensity factors for both configurations were obtained using the method of Tweed and Rooke<sup>20</sup>; the loading function required for the pressure distribution given by equation (6.35) is obtainable from Rooke and Tweed<sup>39</sup>.

The value of  $K_1'$  for the ancillary configuration shown in Fig 6.7b is not directly available but can be obtained from known solutions by using the principle of superposition. The stress intensity factor  $K_{11}'$  is known<sup>2</sup> for an infinite array of equally spaced collinear cracks of length  $2a$ , each subjected to two equal and opposite forces  $P'$  acting perpendicular to the crack faces. Also the stress intensity factor  $K_{12}'$  is known<sup>2</sup> for an infinite array of equally spaced collinear cracks of length  $2a$  in an infinite sheet subjected to a uniform uniaxial stress  $\sigma'$  acting perpendicular to the line of cracks and remote from them. The principle of superposition, illustrated in Fig 6.8, leads to

$$K_1' = \frac{1}{2}(K_{11}' + K_{12}') \quad (6.38)$$

The stress intensity factor  $K_2'$  is not known for the ancillary configuration shown in Fig 6.7c, but it can be obtained from known solutions by a combination of compounding and superposition. By using compounding as illustrated in Fig 6.9a,  $K_2'$  can be expressed in terms of  $K_0$  and  $K_h'$ , where  $K_h'$  is the stress intensity factor for the equivalent crack located centrally parallel to the edges of a strip of width  $2h$ . Thus

$$K_2' = \frac{1}{2}(K_h' + K_0) \quad (6.39)$$

Equation (6.39) omits the boundary-boundary interaction term  $K_e'$ ; it will be included with all the others into the  $K_e$  term given in equation (6.37). The factor  $K_h'$  is not directly available, but can be obtained from known<sup>2</sup> results by application of the principle of superposition. This is illustrated in Fig 6.9b and leads to

$$K'_h = K'_{21} + K'_{22} ; \quad (6.40)$$

$K'_{21}$  is the stress intensity factor for a crack of length  $2a$  located centrally, parallel to the edges of a strip of width  $2h$ , with the crack subjected to two equal and opposite forces  $P'/2$  acting perpendicular to the faces at the centre of the crack;  $K'_{22}$  is the stress intensity factor for a similar crack in a similar strip with the crack subjected to a normal pressure  $\sigma'/2$  acting on its faces. The values of  $K'_{21}$  and  $K'_{22}$  can be obtained from Ref 2.

Thus from equations (6.39) and (6.40) we have

$$K'_2 = \frac{1}{2}(K'_{21} + K'_{22} + K_0) . \quad (6.41)$$

Finally by substituting equation (6.38) and (6.41) into equation (6.37), the compounding equation becomes

$$K_r = \frac{1}{2}(K'_{11} + K'_{12} + K'_{21} + K'_{22} - K_0) + K_e . \quad (6.42)$$

It is convenient to write equation (6.42) in terms of normalized stress intensity factors, because these are the functions given in Ref 2. The functions required are

$$\left. \begin{aligned} Q_{11} &= \frac{K'_{11}}{P'/\sqrt{\pi a}} , & \text{Case 1.2.9, Ref 2;} \\ Q_{12} &= \frac{K'_{12}}{\sigma'\sqrt{\pi a}} , & \text{Case 1.2.8, Ref 2;} \\ Q_{21} &= \frac{K'_{21}}{P'/(2\sqrt{\pi a})} , & \text{Case 1.1.10, Ref 2;} \\ Q_{22} &= \frac{K'_{22}}{\sigma'\sqrt{\pi a}/2} , & \text{Case 1.1.6, Ref 2.} \end{aligned} \right\} \quad (6.43)$$

Substitution for  $P'$  and  $\sigma'$  in terms of  $K_0$  from equation (6.17) gives

$$\left. \begin{aligned} Q_{11} &= \frac{K'_{11}(1+\omega)}{2K_0} , & Q_{21} &= \frac{K_{21}(1+\omega)}{K_0} , \\ Q_{12} &= \frac{K'_{12}(1+\omega)}{2\omega K_0} , & Q_{22} &= \frac{K'_{22}(1+\omega)}{\omega K_0} , \end{aligned} \right\} \quad (6.44)$$

where  $\omega = \pi a/W$ . Substitution of equation (6.44) into equation (6.42) gives

$$K_r = \frac{K_0}{(1+\omega)} \left[ Q_{11} + \omega Q_{12} + \frac{1}{2}(Q_{21} + \omega Q_{22}) - \frac{1}{2}(1+\omega) \right] + K_e . \quad (6.45)$$

Equation (6.45) can be normalized with respect to  $\bar{K}$ , the stress intensity factor, for an isolated crack of length  $2a$  with a single force  $P$  acting perpendicular to one face at its centre, where  $\bar{K}$  is given by

$$\bar{K} = \frac{P}{2\sqrt{\pi a}} . \quad (6.46)$$

The resultant normalized stress intensity factor  $Q_r (= K_r/\bar{K})$  becomes

$$Q_r = \frac{Q_0}{(1+\omega)} \left[ Q_{11} + \omega Q_{12} + \frac{1}{2}(Q_{21} + \omega Q_{22}) - \frac{1}{2}(1+\omega) \right] + Q_e , \quad (6.47)$$

where  $Q_0 = K_0/\bar{K}$  and  $Q_e = K_e/\bar{K}$ .

The only unknown function on the right-hand side of equation (6.47) is  $Q_e$ , the effect of boundary-boundary interactions. The procedure for evaluating  $Q_e$  is similar to that used in section 6.2. The contribution to  $Q_r$  from these interactions is assumed to be equivalent to the effect of two additional opposing forces of magnitude  $P_e$  acting on the perimeter of the hole; these forces are determined by the requirement that

$$\lim_{\ell \rightarrow 0} \left\{ K_r \right\} = 1.12 \sigma_\infty \sqrt{\pi \ell} \quad (6.48)$$

where  $\sigma_\infty$  is the maximum stress at the crack site at the edge of a hole in an infinite row of pressurized holes when  $\ell = 0$ .

Equation (6.45) is the most appropriate form of  $K_r$  for examining the limiting behaviour as  $\ell \rightarrow 0$  or, since  $a = R + \ell$ , as  $a \rightarrow R$ . The limits required are:

$$\lim_{\ell \rightarrow 0} \{K_0\} = \lim_{\ell \rightarrow 0} \{K_p + K_\sigma\} = 1.12 \left( \sigma_0 + \frac{3\sigma}{2} \right) \sqrt{\pi \ell} \quad (6.49)$$

where  $\sigma_0$  is the maximum stress at the crack site at the edge of an isolated pressurized hole, and  $3\sigma/2$  is the maximum stress at the edge of an isolated unpressurized hole in a sheet subjected to a uniform stress  $\sigma/2$  ;

$$\lim_{\ell \rightarrow 0} \{K_e\} = 1.12 \frac{2P_e}{\pi R} \sqrt{\pi \ell} \quad , \quad (6.50)$$

see equation (6.27);

$$\lim_{a \rightarrow R} \{Q_{11}\} = Q_{11} \left( \frac{R}{W} \right) \quad , \quad (6.51)$$

where  $Q_{11}(R/W)$  is the value of  $Q_{11}$  for a periodic array of cracks of length  $2R$  subject to point forces;

$$\lim_{a \rightarrow R} \{Q_{12}\} = Q_{12} \left( \frac{R}{W} \right) \quad , \quad (6.52)$$

where  $Q_{12}(R/W)$  is the value of  $Q_{12}$  for a periodic array of cracks of length  $2R$  subjected to a uniform stress;

$$\lim_{a \rightarrow R} \{Q_{21}\} = Q_{21} \left( \frac{R}{h} \right) \quad , \quad (6.53)$$

where  $Q_{21}(R/h)$  is the value of  $Q_{21}$  for a crack of length  $2R$  , subjected to point forces, in a strip of height  $2h$  ;

$$\lim_{a \rightarrow R} \{Q_{22}\} = Q_{22} \left( \frac{R}{h} \right) \quad , \quad (6.54)$$

where  $Q_{22}(R/h)$  is the value of  $Q_{22}$  for a crack of length  $2R$  , subjected to a uniform pressure, in a strip of height  $2h$  .

Substitution of equations (6.48) to (6.54) in equation (6.45) gives

$$\sigma_\infty = \left( \sigma_0 + \frac{3\sigma}{2} \right) q(R) + \frac{2P_e}{\pi R} \quad , \quad (6.55)$$

where  $q(R)$  is given by

$$q(R) = \frac{1}{1 + (\pi R/W)} \left\{ Q_{11}\left(\frac{R}{W}\right) + \frac{\pi R}{W} Q_{12}\left(\frac{R}{W}\right) + \frac{1}{2} \left[ Q_{21}\left(\frac{R}{h}\right) + \frac{\pi R}{W} Q_{22}\left(\frac{R}{h}\right) \right] - \frac{1}{2} \left( 1 + \frac{\pi R}{W} \right) \right\}. \quad (6.56)$$

Equation (6.55) can be re-written as

$$\frac{2P_e}{\pi R p_m} = \frac{\sigma_\infty}{p_m} - \frac{(\sigma_0 + (3\sigma/2))}{p_m} q(R), \quad (6.57)$$

where  $p_m$  is the maximum pressure. Substitution of equations (6.34) and (6.36) into equation (6.57) gives

$$\frac{P_e}{P} = K_t^\infty - \left( \frac{2}{\pi} + \frac{3\pi R}{4W} \right) q(R) \quad (6.58)$$

where  $K_t^\infty = \sigma_\infty/p_m$  is the stress concentration factor at the edge of one of the holes in Fig 6.6 when the cracks are absent, and  $\sigma_0/p_m = 2/\pi$  (see Ref 39). The factor  $K_t^\infty$  can be obtained as a function of  $R/W$  and  $R/h$  from the work of Mori<sup>40,41</sup>.

Three configurations are studied in this report, namely  $R/W = 0.10, 0.15$  and  $0.20$ , with  $h/R = 3.0$ . The values of  $R/W$  span the practical range for arrays of fastener holes; the value of  $h/R$  is the largest for which  $K_t^\infty$  is available. The values of  $K_t^\infty$  for these configurations, and the ratios  $P_e/P$  are given in Table 6.1.

Table 6.1

Values of  $K_t^\infty$  and  $P_e/P$  for  $h/R = 3.0$

R/W	$K_t^\infty$	$P_e/P$
0.10	0.96	-0.043
0.15	0.99	-0.17
0.20	1.09	-0.26

With a knowledge of  $P_e/P$ , the contribution  $Q_e$  can be evaluated. It can be written

$$Q_e = \frac{K_e}{\bar{K}} = \frac{\bar{K}_e}{\bar{K}} \left( \frac{K_e}{\bar{K}_e} \right), \quad (6.59)$$

where  $\bar{K}_e$  is the limiting value of  $K_e$  as  $a \rightarrow \infty$ , and is given by

$$\bar{K}_e = \frac{P_e}{\sqrt{\pi a}}. \quad (6.60)$$

Substitution of equations (6.46) and (6.60) into equation (6.59) gives

$$Q_e = 2 \frac{P_e}{P} \left( \frac{K_e}{\bar{K}_e} \right). \quad (6.61)$$

The ratio  $K_e/\bar{K}_e$  can be derived from the work of Rooke and Tweed<sup>20</sup>. We can write

$$\frac{K_e}{\bar{K}_e} = p_0 \sqrt{\pi \ell} \left( \frac{K_e}{p_0 \sqrt{\pi \ell}} \right) \frac{1}{P_e / \sqrt{\pi a}}, \quad (6.62)$$

where the function in parentheses is evaluated in Ref 20 and  $p_0 = P_e / (2R)$ . Thus

$$\frac{K_e}{\bar{K}_e} = \frac{\pi \sqrt{a \ell}}{2R} \left( \frac{K_e}{p_0 \sqrt{\pi \ell}} \right), \quad (6.63)$$

and therefore, from equations (6.61) and (6.63) we have

$$Q_e = \frac{\pi \sqrt{a \ell}}{R} \left( \frac{K_e}{p_0 \sqrt{\pi \ell}} \right) \frac{P_e}{P}. \quad (6.64)$$

Equation (6.47) can now be evaluated to give the resultant normalized stress intensity factor  $Q_r$  as a function of crack-length for the three configurations considered in this report. In practical structures the load on the hole is often specified in terms of the 'bearing pressure'  $\sigma_b (= P/(2R))$ . The normalized stress intensity factor  $Q_r$  can be written in terms of the bearing pressure, as

$$Q_r = \frac{K_r}{P/(2\sqrt{\pi a})} = \left( \frac{\pi a}{R} \right) \frac{K_r}{\sigma_b \sqrt{\pi a}}. \quad (6.65)$$

Fig 6.10 shows a plot of  $K_r/(\sigma_b\sqrt{\pi a})$  against  $2a/W$  for  $R/W = 0.10$ ,  $0.15$ , and  $0.20$ , with  $h/R = 3.0$ . The curves are very steep for short cracks, indicating that  $K_r$  increases rapidly from zero as the crack-length increases from zero.

The contribution of  $Q_e$  to  $Q_r$  increases as  $R/W$  increases. As in the case of the uniformly pressurized hole (see section 6.2), the magnitude of  $P_e/P$  is a rough estimate of the maximum value of  $Q_e/Q_r$ . At  $R/W = 0.10$  we have  $P_e/P = -0.043$  and  $|Q_e/Q_r| \lesssim 0.05$ ; at  $R/W = 0.15$  we have  $P_e/P = -0.17$  and  $|Q_e/Q_r| \lesssim 0.19$ ; and at  $R/W = 0.2$  we have  $P_e/P = -0.26$  and  $|Q_e/Q_r| \lesssim 0.25$ . For the same hole spacing these values of  $Q_e/Q_r$  are larger than in the test configuration (section 6.2). This is because the presence of the edge near the holes introduces further boundary interactions into this configuration.

#### 6.4 Discussion and conclusions

It has been shown that a modification of the 'equivalent crack' concept, introduced for cracks at unloaded holes allows the compounding method to be extended to the calculation of the opening-mode stress intensity factors for cracks at loaded holes. The method gave results which agreed to within a few percent with those obtained by collocation for the special case of cracks at the edges of holes in a row of pressurized holes; and it has been used to obtain stress intensity factors for cracks at the edges of holes in a row of fastener holes near the edge of a sheet. A particular merit of this method is that accurate values of the stress intensity factor are obtained for short cracks where most of the life in fatigue is spent.

The geometric configurations considered in this report are periodically spaced rows of loaded holes with two cracks of equal length at each hole. The method is not limited, in principle, to periodic configurations, but may be limited by the lack of solutions for ancillary configurations. In a practical case, only some of the holes may have cracks, either one crack or two cracks of unequal length. In these cases the equivalent cracks can still be determined (see section 6.1) but the array of equivalent cracks is no longer periodic even if the original array of holes was. Thus the ancillary configuration of a periodic array of loaded cracks (Case 1.2.9, Ref 2) cannot be used to calculate the actual interaction between cracks, although it could be used to determine an upper bound to the interaction. In some instances

approximate estimates of the interaction may be made using the following ancillary configurations: two pressurized cracks of unequal length (Case 1.2.3, Ref 2); one loaded and one unloaded crack of equal length (Case 1.2.6, Ref 2).

CHAPTER 7A CRACK IN A STIFFENED SHEET<sup>42</sup>

In this chapter the compounding method is extended to obtain stress intensity factors for cracks in plane sheets having localized line stiffeners (see Fig 7.1a) - a geometrical configuration which models the locally stiffened metal-sheet construction widely used in many aircraft structural components (see Fig 7.1b). There are two cases to consider; if the component is made by integral machining or by bonding of the stiffeners to the sheet then the stiffeners are attached continuously along the sheet; or, if localized fasteners, *eg* rivets (see Fig 7.1a&b) are used then the attachment is at discrete points. In both cases, known solutions for cracks in sheets with a single stiffener are compounded to give approximate stress intensity factors for cracks in sheets with many stiffeners.

In order to make use of the compounding method, the stiffeners are considered as boundaries, and crack interactions with stiffeners are treated in the same way as crack interactions with boundaries were in earlier chapters. Where a crack is crossed by a stiffener, as often happens in practice, the crack plus the stiffener is replaced by an 'equivalent crack' as defined in Chapter 4. The accuracy of the method is assessed by comparing the solutions for some configurations having known results, see section 7.1, and the errors are shown to be small (a few percent). The method is used to obtain a new solution for the stress intensity factor for a crack located asymmetrically between two stiffeners in a periodic set (see section 7.2).

7.1 Theory of compounding applied to stiffened sheets

In order to extend compounding methods to obtain stress intensity factors for cracks in sheets with stiffeners, it is necessary to consider the development of the basic method since stiffeners, regarded as boundaries, are different from the boundaries previously considered. In developing the compounding method each additional boundary introduced was subjected to forces (usually of zero magnitude) which were independent of the crack shape or size. However the forces acting on stiffeners exist because of the mismatch in displacements between the sheet and the stiffener; this mismatch is due entirely to the presence of the crack in the sheet and is a function of the shape and size of the crack. Thus the effect, on the crack, of introducing an additional stiffener is modified by the stiffeners already present with the result that

boundary interactions are not necessarily negligible when the boundaries are stiffeners. This interaction is small if the crack is between stiffeners and may be ignored, but it must be taken into account if a stiffener crosses the crack since the shape of the crack is then much altered. The way in which this is taken into account is to use the concept of the equivalent crack that was developed in Chapter 4.

Consider a sheet with a periodic array of stiffeners spaced a distance  $b$  apart with a crack of length  $2a$  ( $a < b$ ) which is perpendicular to the stiffeners; the crack is located either mid-way between two stiffeners (Fig 7.2a), or centred on a stiffener (Fig 7.2b). A uniaxial tensile stress  $\sigma$  is applied to the sheet remote from and perpendicular to the crack. In order to maintain strain compatibility remote from the crack a stress of  $(E_2/E_1)\sigma$  is applied to each stiffener;  $E_1$  and  $E_2$  are the Young's moduli of the sheet and stiffener respectively. It is convenient to label the stiffeners  $S_n$  where  $n$  are positive integers to the right of the crack and negative integers to the left. The stiffener that crosses the crack in Fig 7.2b is labelled  $S_0$ .

In the case where the stiffener crosses the crack, the stress intensity factor is  $K_0$  in the absence of all other boundaries except  $S_0$ . The equivalent crack of length  $2a'$  is defined as in section 4.1.1, equations (4.1) to (4.3), that is

$$a' = Q_0^2 a, \quad (7.1)$$

where

$$Q_0 = \frac{K_0}{\bar{K}} \quad (7.2)$$

and

$$\bar{K} = \sigma\sqrt{\pi a}. \quad (7.3)$$

The effect of adding other stiffeners to the sheet containing the crack  $2a$  is assumed to be the same as the effect of adding stiffeners to an infinite sheet containing a crack of length  $2a'$ . The distance from the tips of the equivalent crack to the additional stiffeners are determined by similar conditions to those for a hole with two cracks, in a row of holes, and are given by equations (5.4). Namely

$$\left. \begin{aligned} b'_n - a' &= b_n - a, & \text{all } Q_0, n > 0, \\ b'_n + a' &= b_n + a, & Q_0 \leq 1, n < 0, \\ b'_n - a' &= b_n - a, & Q_0 > 1, n < 0, \end{aligned} \right\} (7.4)$$

where  $b_n$  is the distance from the centre of the original crack to the  $n$ th stiffener, and  $b'_n$  is the distance from the centre of the equivalent crack to the  $n$ th stiffener.

## 7.2 Application to periodically stiffened sheets

Poe<sup>43,44</sup> has obtained the stress intensity factors for cracks located in sheets with periodic arrays of riveted stiffeners (see also Case 2.2.3, Ref 2); the rivets are spaced a distance  $h$  apart along the stiffeners. The crackline is always perpendicular to the stiffeners and passes through a rivet site at each stiffener. The cracks are located either symmetrically between two stiffeners (unbroken, Case 2.2.3, Ref 2) or centred about a single stiffener (unbroken, Case 2.2.3, Ref 2, or broken, Ref 44). The configurations are shown in Fig 7.2a&b where the stiffeners are labelled with positive integers to the right and negative integers to the left of the crack. The ancillary configurations required are shown in Fig 7.3a&b; the stress intensity factors for these configurations have been obtained by Bloom and Sanders<sup>45</sup>. For the crack located between two stiffeners the solution to the ancillary configuration in Fig 7.3a only is required. In Fig 7.3a,  $c$  is equal to  $a$  and  $d$  is equal to  $b/2$  if no stiffeners cross the crack, whereas  $c$  is equal to  $a'$  and  $d$  is equal to  $b'_n$  if the stiffener  $S_0$  crosses the crack.

### 7.2.1 Test solutions

The first test configuration considered is that of a crack of length  $2a$  located symmetrically between two of the stiffeners a distance  $b$  apart. A tensile stress is applied to the sheet, remote from and perpendicular to the crack, and a stress of  $(E_2/E_1)\sigma$  is applied to the stiffeners in order to maintain strain compatibility remote from the crack. Because of symmetry only one tip of the crack (eg tip A in Fig 7.2a) needs to be considered. If the normalized stress intensity factor due to the  $n$ th stiffener is  $Q_n$  then the compounding formula follows from equation (3.7); it is

$$Q_r = 1 + \sum_{n=-\infty}^{n=\infty} (Q_n - 1) + Q_e, \quad n \neq 0. \quad (7.5)$$

Since no stiffeners cross the crack, the equivalent crack concept is not required for this configuration.

The values of  $Q_n$  which contribute most to  $Q_r$  come from the nearest pair of stiffeners ( $n = \pm 1$ ); the contribution from the next pair of stiffeners ( $n = \pm 2$ ) is negligible over most of the range of  $a/b$ , the maximum being  $< 1\%$  at  $a/b = 0.45$ . Contributions from all other stiffeners ( $|n| > 2$ ) have been neglected. The results<sup>43</sup> for the periodic configuration are plotted as functions of  $a/b$  for various  $h/b$  values and various values of a stiffness parameter in Case 2.2.3, Ref 2. The stiffness parameter  $s$ , is the ratio of the stiffness of the stiffener to that of the sheet, *ie*

$$s = \frac{AE_2}{btE_1} \quad (7.6)$$

where  $A$  is the cross sectional area of the stiffener and  $t$  the thickness of the sheet. Poe<sup>43,44</sup> uses the stiffness parameter  $\mu$  which is given by

$$\mu = \frac{s}{1 + s}. \quad (7.7)$$

The values of  $Q_n$  for the ancillary configurations have been obtained as functions of  $a/b$  for various values of  $h/a$  and the parameter  $\lambda$  which is defined as

$$\lambda = \frac{2E_1at}{AE_2} \quad (7.8)$$

and which can be written in terms of  $s$  as

$$\lambda = \frac{2}{s} \left( \frac{a}{b} \right). \quad (7.9)$$

In the equivalent crack configuration  $a'$  replaces  $a$  and  $\lambda'$  replaces  $\lambda$  for the contribution from the stiffeners which do not cross the cracks;  $\lambda'$  is given by

$$\lambda' = \frac{2}{s} \left( \frac{a'}{b} \right) = Q_0^2 \lambda \quad (7.10)$$

Bloom and Sanders<sup>45</sup> show that, for the values of  $\lambda$  and  $a/h$  over the range of  $a/b$  considered here, the results for  $Q_n$  ( $n = \pm 1, \pm 2$ ) are indistinguishable from those for continuously attached stiffeners ( $a/h = \infty$ ) obtained by Greif and Sanders<sup>46</sup>. Since more data are available on continuously attached stiffeners, curves of  $Q_n$  for both  $n > 0$  and  $n < 0$  were obtained from the work of Greif and Sanders reported in Case 2.1.3, Ref 2.

Compounded results for the normalized opening-mode stress intensity factor ( $Q_r = K_I / (\sigma\sqrt{\pi a})$ ) have been obtained from equation (7.5), neglecting  $Q_e$ , and they are compared, in Table 7.1 with those from Case 2.2.3, Ref 2, for the configuration with  $0.0 \leq a/b \leq 0.45$ , for  $s = 1.0$  and  $h/b = 1/12$ . The differences which are a measure of  $Q_e$ , are very small ( $< 1\%$ ) and are no greater than the possible inaccuracies in reading the graphical results. The differences will be even less for smaller values of  $s$  and larger values of  $h/b$  since the effect of the stiffener decreases in both cases. The value of  $s = 1.0$  was chosen since it is about the maximum value of  $s$  in aircraft applications

Table 7.1

Comparison of values of  $K / (\sigma\sqrt{\pi a})$  for a crack located symmetrically between two stiffeners in a periodically stiffened sheet  
( $s = 1.0$ ,  $h/b = 1/12$ )

a/b	Compounded results	Case 2.2.3 (Ref 2)
0.00	1.00	1.00
0.10	0.98	0.99
0.20	0.96	0.96
0.30	0.92	0.92
0.40	0.82	0.81
0.45	0.72	0.72
0.50	stiffener site	

The next test configuration considered is that of a crack of length  $2a$  located symmetrically about one of the stiffeners in a periodic array spaced a distance  $b$  apart (see Fig 7.2b). The stiffener across the crack can be either unbroken<sup>43</sup> or broken<sup>44</sup>. The resultant normalized stress intensity factor is given by equation (5.1), that is

$$Q_r = Q_0 \left[ 1 + \sum_{n=-\infty}^{n=\infty} (Q'_n - 1) \right] + Q_e, \quad n \neq 0. \quad (7.11)$$

where  $Q'_n$  is the normalized stress intensity factor for the equivalent crack in the presence of the  $n$ th stiffener only. The summation term contains the effects of stiffeners which do not cross the crack and which are spaced a distance  $b$  apart, except for the two nearest the crack which are a distance  $(b'_+ + b'_-)$  apart. The term in square brackets has the same form as the right-hand side of equation (7.5) without  $Q_e$ ; it was evaluated in the same manner and  $Q_0$  for both broken and unbroken stiffeners, was obtained from the work of Bloom and Sanders reported in Case 2.2.1, Ref 2. The results, neglecting  $Q_e$ , for the opening-mode stress intensity factor for  $s = 1.0$  for both the unbroken central stiffener ( $h/b = 1/12$ ) and the broken central stiffener ( $h/b = 1/6$ ) are shown in Table 7.2. The maximum difference between the compounded solutions and the numerical solutions due to  $Poe^{43,44}$  is 5% for  $0.25 < a/b < 0.90$ , thus neglecting  $Q_e$  introduces only small errors into  $Q_r$ .

Table 7.2

Comparison of values of  $K_I / (\sigma\sqrt{\pi a})$  for a crack located symmetrically about the central stiffener in a periodically stiffened sheet ( $s = 1.0$ )

$\frac{a}{b}$	Central stiffener unbroken ( $h/b = 1/12$ )		Central stiffener broken ( $h/b = 1/6$ )	
	Compounded results	Case 2.2.3 (Ref 2)	Compounded results	Ref 44
0.25	0.67	0.68	1.72	1.78
0.50	0.66	0.67	1.32	1.36
0.75	0.64	0.65	1.11	1.12
0.90	0.56	0.59	0.91	0.91
1.00		next stiffener		

The above configurations have also been studied for the case when the stiffeners are continuously attached to the sheet. The results are indistinguishable within the approximations used from those for riveted stiffeners except when the crack is very close to the stiffener, *ie* the distance between the crack tip and the stiffener is  $\lesssim h$ . Too few results are available, for the ancillary configuration when the crack tip is close to the stiffener, to enable this region to be investigated fully.

### 7.2.2 New solution

In this section the solution is derived for a crack which is located asymmetrically between two continuously attached stiffeners in a periodically stiffened sheet. A stress  $\sigma$  is applied to the sheet remote from and perpendicular to the crack; in order to maintain strain compatibility a stress  $(E_2/E_1)\sigma$  is applied to the stiffener remote from the crack. The stiffeners to the right of the crack are labelled with positive integers (+n) and those to the left with negative integers (-n); the distance from the centre of the crack to the nth stiffener to the right is  $b_{+n}$  and the distance to the nth stiffener to the left is  $b_{-n}$ . This configuration is shown in Fig 7.4a; the required ancillary configuration is shown in Fig 7.4b. The distance  $d$  from the centre of the crack to the stiffener in the ancillary configuration is  $b_{+n}$  for the stiffeners on the right and  $b_{-n}$  for stiffeners on the left of the crack. If the stiffeners are a distance  $b$  apart then

$$b_{+n} + b_{-n} = (2n - 1)b \quad ; \quad n=1,2,\dots,\infty. \quad (7.12)$$

The resultant normalized stress intensity factor is given in equation (7.5). Because of the asymmetry the two tips will have different stress intensity factors. The contributions from each stiffener ( $Q_{+n}$  or  $Q_{-n}$ ) for the tip under consideration can be obtained from Case 2.1.3, Ref 2. The results, for  $s = 1.0$ , for both tips are shown in Fig 7.5;  $K_I/(\sigma\sqrt{\pi a})$  is plotted as a function of  $a/b$  for various values of  $b_{+1}/b$ .

### 7.3 Discussion and conclusions

The compounding method has been applied to crack problems in periodically stiffened sheets; use of the equivalent crack concept is necessary if a stiffener crosses the crack. The errors in the stress intensity factors, caused by neglecting boundary-boundary interactions, increase as the crack-length increases and as the relative stiffness of the stiffener to that of the sheet increases. The maximum error for a wide range of crack-lengths and stiffness ratios is a few per cent (Tables 7.1 and 7.2) which is within normal engineering tolerances. The compounding method can be extended readily to other configurations, but direct application to some other stiffener configurations may be limited by the lack of data for the required ancillary configurations. For example data are required on small cracks near stiffeners (the difference between continuously attached and riveted stiffeners would

be important) and on cracks which are located asymmetrically behind a single stiffener.

An important consequence of the use of the compounding is that it is now necessary to have data for simple ancillary configurations only. The importance of design parameters such as distribution of stiffeners, relative stiffnesses, type of attachment, flexibility of rivets and sheet curvature can be studied using a simple structure with a single stiffener. Results for a structure with many stiffeners can be compounded from those for the simple structure. The method of compounding can be applied to problems with both plane boundaries and stiffeners, *eg* a crack in the vicinity of a cut-out in a sheet with many stiffeners.

## CHAPTER 8

MANY CRACKS IN A STIFFENED SHEET<sup>47</sup>

A common structural element used in airframes is the stiffened panel - a large sheet onto which stiffening elements are fastened at regular intervals. Because of the periodicity of the stiffeners and fasteners it is likely that simultaneous (or nearly simultaneous) initiation of cracks may occur at different stiffeners. Multiple cracking of this sort is more damaging than a single crack since it leads to greater reductions in both the strength and fatigue life of the structure. The most dangerous configuration is when the cracks are collinear, since the growth of the cracks may result in them linking up to form a single long crack leading to early failure. Stress intensity factors are known for many stiffened configurations with a single crack, but none are available if more than one crack is present.

The compounding method was shown in Chapter 7, to be applicable to problems involving single cracks in stiffened sheets. In this chapter, the compounding method is used to derive a stress intensity factor for a crack in a collinear array of cracks which are centred about adjacent stiffeners. The theory is developed in section 8.1 for cracks of arbitrary length at arbitrarily spaced stiffeners. The specific application to periodically stiffened sheets with periodic collinear cracks is considered in section 8.2. Results for the stress intensity factor are presented and compared with those for single cracks in order to estimate the effects of multiple cracking on residual strength and on the growth of fatigue cracks.

8.1 Development of theory

An array of collinear cracks at stiffeners in a stressed sheet is shown in Fig 8.1, where  $S_n$  is the  $n$ th stiffener of Young's modulus  $E_n$  and cross-sectional area  $A_n$ ,  $2a_n$  is the length of the crack which is symmetrical<sup>†</sup> about  $S_n$  and the bay-width  $b_{m,n}$  is the distance between the  $m$ th and the  $n$ th stiffeners ( $S_m$  and  $S_n$ ). The central stiffener is labelled  $S_0$ , and the other stiffeners  $S_n$  are to the right of  $S_0$  if  $n > 0$  and to the left if  $n < 0$ . The stiffeners are riveted onto the sheet with a distance  $h$  between adjacent rivets. The uniform stress in the sheet, of Young's modulus  $E$ , is  $\sigma$  and

---

<sup>†</sup> The method can be readily extended to consider non-symmetrical cracks in a similar way to that in section 5.2.1 for cracks at holes.

strain compatibility is maintained between the stiffeners and the sheet remote from the cracks. The crack tip under consideration in this analysis is the right-hand tip (labelled A in the figures) of the crack of length  $2a_0$  which is centred about the stiffener  $S_0$ .

In order to use the compounding procedure, stress intensity factors for three ancillary configurations for cracks in a sheet subjected to a remote stress  $\sigma$  are required. They are:

- (a) a single crack centred about a single stiffener in a sheet containing no other cracks or stiffeners (Fig 8.2);
- (b) a single crack at a distance from a single stiffener in a sheet containing no other cracks or stiffeners (Fig 8.3);
- (c) two collinear cracks a distance apart in an unstiffened sheet containing no other cracks (Fig 8.4).

The three ancillary configurations represent the interaction between the crack (original length  $2a_0$ ) and (a) the central stiffener  $S_0$ , (b) the other stiffeners  $S_n$ , and (c) the other cracks (original length  $2a_n$ ). Stress intensity factor solutions for these three configurations are known and are available in Ref 2.

Fig 8.2 shows a crack of length  $2a_0$  centred about and perpendicular to a stiffener  $S_0$  in a sheet subjected to a uniform stress  $\sigma$  remote from a crack and parallel to the stiffener. The stress in the stiffener, remote from the crack, is  $\sigma E_0/E$  in order to ensure strain compatibility. The stress intensity factor for this configuration is  $K_0$  and the normalized stress intensity factor is  $Q_0$ ; they are related by

$$K_0 = Q_0 \sigma \sqrt{\pi a_0} \equiv Q_0 \bar{K}_0, \quad (8.1)$$

where  $\bar{K}_0$  is the stress intensity factor for an isolated crack of length  $2a_0$  in a sheet subjected to a uniform stress  $\sigma$  remote from the crack.

Values of  $Q_0$ , for the stiffener  $S_0$  broken or unbroken, are given in Case 2.2.1, Ref 2, where  $Q_0$  is plotted as a function of  $a_0/h$  for various values of  $\lambda$ , a measure of the relative stiffnesses of the sheet and the stiffener and  $h$  is the rivet pitch. The parameter  $\lambda$  is given by

$$\lambda = \frac{2a_0 t E}{A_0 E_0} \quad (8.2)$$

where  $t$  is the thickness of the sheet. Values of  $Q_0$  are available only for  $\lambda > 0.5$ ; for smaller values of  $\lambda$ , *ie* short crack-lengths or small values of  $E/E_0$ , results obtained for a crack in a periodically stiffened sheet may be used (Case 2.2.3, Ref 2 for unbroken  $S_0$ , and Ref 44 for a broken  $S_0$ ). The parameters required to use these results are  $a_0/b$ ,  $h/b$  and  $s$  (or  $\mu$ ). These are obtained from the following relationships:

$$\frac{a_0}{b} = \left( \frac{a_0}{h} \right) \left( \frac{h}{b} \right), \quad (8.3)$$

$$s\lambda = 2 \frac{a_0}{b} \quad (8.4)$$

and

$$\mu = \frac{s}{1+s}. \quad (8.5)$$

The smallest value of  $h/b$  must be chosen from the results available and substituted into equation (8.3) to give  $a_0/b$  and hence  $s$  from equation (8.4) and  $\mu$  from equation (8.5).

In order to calculate the effects of the crack of length  $2a_0$  interacting with the other stiffeners and cracks it is necessary to replace the crack and stiffener  $S_0$  by an equivalent crack. The length of the equivalent crack  $2a'_0$  is determined in the same way as in the previous chapter (see also Fig 8.2b), that is,

$$a'_0 = Q_0^2 a_0. \quad (8.6)$$

Fig 8.3 shows two possible configurations of a crack of length  $2a'_0$  whose centre is a distance  $b'_{0,n}$  ( $n > 0$ ) or  $b'_{n,0}$  ( $n < 0$ ) from a stiffener  $S_n$  in a sheet subjected to a uniform stress  $\sigma$  remote from the crack and parallel to the stiffener. The stress in the stiffener, remote from the crack, is  $\sigma E_n/E$  in order to ensure strain compatibility. If the stress intensity factor for the equivalent crack in this configuration is  $K'_{sn}$  then the normalized stress intensity factor  $Q'_{sn}$  is defined by

$$K'_{sn} = Q'_{sn} \sigma \sqrt{\pi a'_0} = Q'_{sn} Q_0 \sigma \sqrt{\pi a_0} = Q'_{sn} Q_0 \bar{K}_0. \quad (8.7)$$

The values of  $Q'_{sn}$  are obtained from Case 2.2.2, Ref 2, the distances  $b'_{0,n}$  or  $b'_{n,0}$  shown in Fig 8.3 are determined from the condition that the distance from the appropriate tip of the crack to the stiffener must be the same in the ancillary configuration as in the original configuration (see Chapter 4); they are given by equation (5.10) with  $a'_{0,R} = a'_{0,L} = a'_0$ . In stiffener configurations,  $Q_0 < 1$  if  $S_0$  is unbroken, and  $Q_0 > 1$  if  $S_0$  is broken.

The normalized stress intensity factor  $Q'_{sn}$  (called  $K_I/K_0$ ) is plotted in Ref 2 as a function of  $a/b$  for various values of  $a/h$  and  $\lambda$ . In this determination  $a$  is  $a'_0$  and  $b$  is  $b'_{0,n}$  or  $b'_{n,0}$ ,  $h$  is the rivet spacing and  $\lambda$  is given by

$$\lambda = \frac{2a'_0 t E}{A_n E_n} . \quad (8.8)$$

Results given in Case 2.2.2, Ref 2, show that  $Q'_{sn}$  for a given value of  $\lambda$  is almost independent of  $a'_0/h$  for the small values of  $a'_0/b'_{0,n}$  which will usually be required. For  $a'_0/b'_{0,n} < 0.5$  results for continuously attached stiffeners ( $a'_0/h = \infty$ ) must be used; they are given in Case 2.1.3, Ref 2.

The interaction between the crack of length  $2a_0$  and the other cracks is considered by replacing each crack and stiffener pair by an equivalent crack of length  $2a'_n (= 2Q_n^2 a_n)$ ;  $Q_n$  is the normalized stress intensity factor for the crack of length  $2a_n$  centred about the stiffener  $S_n$  in the absence of all other cracks and stiffeners. Fig 8.4 shows the two possible configurations of a crack of length  $2a'_0$ , whose centre is a distance  $d'_{0,n}$  ( $n > 0$ ) or  $d'_{n,0}$  ( $n < 0$ ) from the centre of a crack of length  $2a'_n$ , in a sheet subjected to a uniform stress  $\sigma$  remote from and perpendicular to the cracks. If the stress intensity factor for the equivalent crack  $2a'_0$  in this configuration is  $K'_{cn}$  then the normalized stress intensity factor  $Q'_{cn}$  is defined by

$$K'_{cn} = Q'_{cn} \sigma \sqrt{\pi a'_0} = Q'_{cn} Q_0 \bar{K}_0 . \quad (8.9)$$

The values of  $Q'_{cn}$  are obtained from Case 1.2.3, Ref 2. The distances  $d'_{0,n}$  or  $d'_{n,0}$  shown in Fig 8.4 are determined from the condition that the distance between the appropriate tips of the two cracks being considered should be the same in the ancillary configurations as in the original configuration (see Chapter 4); they are given by

equation (5.11) with  $a'_{0,R} = a'_{0,L} = a'_0$  and  $a'_{n,R} = a'_{n,L} = a'_n$ . The factors  $Q_n$  ( $n \neq 0$ ) are less than unity since  $S_n$  is unbroken.

The resultant stress intensity factor  $K$  for the crack of length  $2a$  in the original configuration is given by

$$K_r = K_0 + \sum_{n=-\infty}^{n=\infty} (K'_{sn} - K_0) + \sum_{n=-\infty}^{n=\infty} (K'_{cn} - K_0) + K_e, \quad n \neq 0. \quad (8.10)$$

The first summation represents the interactions between the equivalent crack ( $2a'_0$ ) and all the stiffeners except  $S_0$ ; the second summation represents the interactions between the equivalent crack ( $2a'_0$ ) and all the other equivalent cracks ( $2a'_n$ ). The final term  $K_e$  represents any contribution to  $K_r$  due to interactions between the various stiffeners. This term would be difficult to evaluate, but the comparisons with known solutions in Chapter 7, suggest that the contribution would be small and it was therefore neglected in these calculations. The normalized stress intensity factor  $Q_r (= K_r/\bar{K}_0)$  is obtained from equation (8.10) as

$$Q_r = Q_0 \left[ 1 + \sum_{n=-\infty}^{n=\infty} (Q'_{sn} - 1) + \sum_{n=-\infty}^{n=\infty} (Q'_{cn} - 1) \right], \quad n \neq 0. \quad (8.11)$$

Thus  $Q_r$  has been expressed in terms of the known quantities  $Q_0$ ,  $Q'_{sn}$ ,  $Q'_{cn}$ .

## 8.2 Periodically stiffened sheets

To illustrate the effects of collinear cracks the special case is considered of an array of equally-spaced, identical stiffeners with equal-length cracks centred on each stiffener. The stress intensity factor is derived for the crack centred about the stiffener  $S_0$ , which may be broken or unbroken at the crackline. All the other stiffeners  $S_n$  ( $n \neq 0$ ) are unbroken. In this configuration  $a_n = a$ ,  $b_{n,n+1} = b$ ,  $E_n = E_s$  and  $A_n = A_s$  for all  $n$ .

The expression given in equation (8.10) for the stress intensity factor can be simplified in this configuration. If  $K_p$  is the stress intensity factor for a single crack centred about a stiffener in a periodic array of stiffness, then it follows from Chapter 7 that

$$K_p = K_0 + \sum_{n=-\infty}^{n=\infty} (K'_{sn} - K_0) , \quad n \neq 0 . \quad (8.12)$$

where an error term of order  $K_e$  has been omitted. The factor  $K_p$  is known; Case 2.2.3, Ref 2, applies if the stiffener associated with the crack is unbroken, Ref 44 applies if the stiffener is broken. Thus equation (8.11) becomes

$$Q_r = Q_p + Q_0 \sum_{n=-\infty}^{n=\infty} (Q'_{cn} - 1) , \quad n \neq 0 . \quad (8.13)$$

where  $Q_p = K_p/\bar{K}$ , the values of the  $Q$ 's required for equation (8.13) are obtained as follows:

(i)  $Q_p$  from Case 2.2.3, Ref 2, for  $S_0$  unbroken,

(ii)  $Q_p$  from Ref 44, for  $S_0$  broken,

(iii)  $Q_0$  from Case 2.2.1, Ref 2.

(iv)  $Q'_{cn}$  from Case 1.2.3, Ref 2.

Values of  $Q_r$  have been obtained from equation (8.13) for  $s = 1$  and  $h/b = 1/12$ , where  $s$  is the ratio of the stiffness of the stiffener to that of a sheet of width  $b$  and thickness  $t$ . The values of  $s$  and  $h/b$  chosen are the same as used in Chapter 7, and they represent the stiffest stiffener with the smallest rivet spacing likely to be used in airframe construction; such stiffeners will result in the biggest deviation of the stress intensity factor from that for a crack in an unstiffened sheet. Results for the opening mode stress intensity factor for many cracks in a stiffened sheet are plotted in Fig 8.5 for both  $S_0$  unbroken and  $S_0$  broken; for comparison  $Q_p$ , the normalized stress intensity factor for a single crack in a periodically stiffened sheet, is also plotted. From Fig 8.5 it can be seen that multiple cracking causes the stress intensity factor to increase. This increase is small ( $< 5\%$ ) for cracks less than about a quarter of the bay-width, but increases as the cracks become longer; at  $a/b = 0.45$  the increase is  $\sim 35\%$  if  $S_0$  is unbroken and  $\sim 25\%$  if  $S_0$  is broken.

The effects of many cracks on the rate of fatigue crack growth are more significant because of the power-law dependence (see also section 5.3) the growth-rate per cycle  $da/dN$  approximates to

$$\frac{da}{dN} \propto K^P , \quad (8.14)$$

where  $p$  is typically in the range 2 to 4 depending on the material. These effects are illustrated in Fig 8.6 for  $S_0$  unbroken, and Fig 8.7 for  $S_0$  broken; the ratio of the crack growth-rate for many cracks  $(da/dN)_m$  to that for a single crack  $(da/dN)_s$  is plotted as a function of  $a/b$ . It can be seen that the effects become more pronounced as  $p$  increases and are more significant at longer crack-lengths; for a crack a quarter of a bay-width the growth-rate is increased by  $\sim 20\%$  for both  $S_0$  broken and unbroken when  $p = 4$ . For  $a/b = 0.45$  the growth-rate is more than doubled for  $S_0$  broken and more than tripled for  $S_0$  unbroken when  $p = 4$ .

### 8.3 Conclusions

- (1) The compounding method can be used to calculate stress intensity factors for many collinear cracks in stiffened sheets.
- (2) The presence of many cracks increases the stress intensity factor particularly for long cracks.
- (3) This increase in the stress intensity factor results in an increased growth-rate of the cracks and hence a reduced lifetime in fatigue.

## CHAPTER 9

DESIGN STUDY - CRACKS AT A DOUBLE ROW OF HOLES<sup>48</sup>

In Chapters 5 and 8 it was shown that the presence of many cracks can be much more damaging than just a single crack, since the increased stress intensity factor results in an increased growth-rate and hence a reduced fatigue lifetime. In particular growth-rates may be increased by a factor of two or more when many cracks are present at the edges of the holes in a row of holes.

A typical configuration of this type, used in airframe construction, is a row of fastener holes, and one or more of these may have a crack at its edge at some time during its service life. In the damage-tolerant specification<sup>49</sup> it is assumed that there are cracks at the edge of each hole at the start of service life. It is further assumed that the distance from the edge of the hole to the crack tip is 1.25 mm at one of the holes, and is 0.125 mm at all the other holes. These crack sizes are used in the model configurations studied in this chapter, where the possibility is examined of reducing the deleterious effects of multiple cracks by arranging the holes in two parallel rows instead of in a single row, the number of holes being kept constant. It is found that the stress intensity factor and hence the crack growth-rate are reduced; and there is a greater reduction in  $K$  as the separation between the two rows is increased. The subsequent improvement in lifetime, *i.e.* the number of stress cycles required for a crack to grow to a given size, depends on both the initial crack-length assumed and the final length.

### 9.1 Evaluation of the stress intensity factor

A typical geometry for a double row of fastener holes is shown in Fig 9.1. Holes of radius  $R$  are spaced a distance  $2b$  apart in each row and the rows are a distance  $h$  apart.

The holes in one row are located symmetrically with respect to the holes in the other row, so that if  $h$  is reduced to zero there is only one row of holes and the distance between adjacent holes becomes  $b$ . Let a uniform tensile stress  $\sigma$  be applied remote from the holes in a direction perpendicular to the parallel rows. It is assumed that each hole has two cracks at its edge, one on either side of the diameter perpendicular to the direction of the applied stress, that is the cracks lie along two parallel lines through the hole centres. The total

crack-length from tip to tip is  $2a$ , the distance from the edge of the hole to the tip is  $l (= a - R)$ .

The assumption regarding the position of the cracks is a reasonable one for a single row of holes, since cracks will tend to grow from the regions of maximum stress concentration which occur at the ends of the diameter which is perpendicular to the stress direction. For two rows of holes the position of the maximum stress is offset round the perimeter towards the adjacent row. However, for the value of the hole-spacing analysed in this chapter ( $b/R = 8$ ) the offset is small; it is therefore a reasonable approximation to assume that the cracks will still lie along the lines through the hole centres. This is discussed more fully in section 9.3.

Because of the symmetry, the opening-mode stress intensity factor is the same for all crack-tips; however, it is convenient to consider one particular tip, labelled A in Fig 9.1. It is also convenient to label the hole with tip A by  $n = 0$ . Holes on the same side as tip A are labelled  $n = +1, +2, \dots$  in sequence and holes on the other side  $n = -1, -2, \dots$  (see Fig 9.1). Only opening-mode stress intensity factors will be considered in this chapter (see section 9.3).

The resultant stress intensity factor  $K_r$  is again given by equation (5.5) as

$$K_r = K_0 + \sum_{n=-\infty}^{n=\infty} (K'_n - K_0) + \sum_{n=-\infty}^{n=\infty} (K''_n - K_0) + K_e, \quad n \neq 0, \quad (9.1)$$

where  $K_0$  = the stress intensity factor for a pair of cracks at the edge of a hole in the absence of all other boundaries;  $K'_n$  = the stress intensity factor for tip A of the equivalent crack of length  $2a'$  near a hole of radius  $R$ ;  $K''_n$  = the stress intensity factor for tip A of the equivalent crack of length  $2a'$  near another equivalent crack of the same length;  $K_e$  = the contribution to the stress intensity factor owing to the disturbance of the stress field caused by interactions between the holes.

The equivalent half crack-length  $a'$  required in evaluating  $K'_n$  and  $K''_n$  is defined as before (see section 4.1) by

$$\sigma\sqrt{\pi a'} = K_0. \quad (9.2)$$

Equation (9.1) can be normalized with respect to  $\bar{K}$ , the stress intensity factor for an isolated crack of length  $2a$  in an infinite sheet subjected to a uniform uniaxial tensile stress  $\sigma$  remote from the crack; since  $\bar{K}$  is given by

$$\bar{K} = \sigma\sqrt{\pi a} \quad , \quad (9.3)$$

equation (9.1) becomes

$$Q_r = Q_0 \left[ 1 + \sum_{n=-\infty}^{n=\infty} (Q'_n - 1) + \sum_{n=-\infty}^{n=\infty} (Q''_n - 1) \right] + Q_e \quad , \quad n \neq 0 \quad , \quad (9.4)$$

where  $Q_r = K_r/\bar{K}$ ,  $Q_0 = K_0/\bar{K}$ ,  $Q'_n = K'_n/K_0$ ,  $Q''_n = K''_n/K_0$  and  $Q_e = K_e/\bar{K}$ .

Values of  $Q_0$  are given by Rooke and Cartwright (Case 1.3.3 of Ref 2). The values of  $Q'_n$  and  $Q''_n$  depend upon whether  $n$  is odd or even; if  $n$  is odd the boundaries are in the other row and hence not on the line of the crack; if  $n$  is even the boundaries are in the same row and on the line of the crack. For odd values of  $n$  the ancillary configurations needed for the compounding method are shown in Fig 9.2a-d and those for even values of  $n$  are shown in Fig 9.3a-d.

Values of  $Q'_n$  for  $n$  odd are not known for the two ancillary configurations shown in Fig 9.2a&b. However results in Chapter 5, for  $b/R = 8$ , indicate that  $(Q'_n - 1)$  for non-zero values of  $h$  will be negligible: for  $h = 0$ , a single row of holes,  $(Q'_n - 1) \ll 1$  for all crack-lengths, the maximum contribution to  $Q_r$  being  $\sim 2\%$  at  $a/b \sim 0.5$ . For  $h > 0$ , *ie* two rows of holes the contribution of  $Q'_n$  will be less. Values of  $Q''_n$  for  $n$  odd are given in Case 1.2.4 of Ref 2 for the two ancillary configurations shown in Fig 9.2c&d.

The distances  $b'_{0,n}$ ,  $b'_{n,0}$ ,  $d'_{0,n}$  and  $d'_{n,0}$  shown in Fig 9.2 are determined (see section 4.1) by the conditions that the appropriate distances between boundaries are the same in the ancillary configurations as they are in the original configuration. Thus we obtain

$$\left. \begin{aligned} b'_{0,n} &= nb - a(1 - Q_0^2) \quad , \quad n > 0 \\ b'_{n,0} &= |n|b - a \left| (1 - Q_0^2) \right| \quad , \quad n < 0 \end{aligned} \right\} \quad (9.5)$$

and

$$\left. \begin{aligned} d'_{0,n} &= nb - 2a(1 - Q_0^2) , & n > 0 \\ d'_{n,0} &= |n|b , & n < 0, Q_0 \leq 1 , \\ \text{and} \\ d'_{n,0} &= |n|b + 2a(Q_0^2 - 1) , & n < 0, Q_0 > 1 . \end{aligned} \right\} \quad (9.6)$$

Values of  $Q'_n$  for  $n$  even are given in Case 1.3.5 in Ref 2 for the ancillary configurations shown in Fig 9.3a&b. Since holes in the same row are spaced a distance  $2b$  apart, it follows that  $b'_{0,n}/R$  and  $b'_{n,0}/R$  are approximately equal to  $2b/R$ . Results in Chapter 5 show that  $(Q'_n - 1)$  is negligible for these values of  $b'_{0,n}/R$ . Values of  $Q''_n$  for  $n$  even are given in Case 1.2.2 in Ref 2 for the ancillary configurations shown in Fig 9.3c&d. At crack-lengths  $a/b < 0.4$  the contribution to  $Q_r$  is negligible, at longer crack-lengths the contribution is a few per cent. The expressions for  $b'_{0,n}$ ,  $b'_{n,0}$ ,  $d'_{0,n}$  and  $d'_{n,0}$  are given by equations (9.5) and (9.6) with  $b$  replaced by  $2b$ .

For a single row of holes with  $b/R = 8$ , it was shown in Chapter 5 that  $Q_e$  makes a negligible contribution to  $Q_r$ . For two parallel rows of holes, the stress concentration factor  $K_t$ , which determines  $Q_e$  will be less (see Peterson<sup>17</sup>). It therefore follows that  $Q_e$  is negligible for the configuration considered here. Thus the normalized resultant stress intensity factor can be evaluated from the following form of equation (9.4):

$$Q_r = Q_0 [Q''_{+1} + Q''_{-1} + Q''_{+2} + Q''_{-2} - 3] . \quad (9.7)$$

The contributions from boundaries with  $|n| > 2$  are all negligible.

Results for  $Q_r (= K_r / (\sigma\sqrt{\pi a}))$  are plotted in Fig 9.4 as a function of  $a/b$  for  $h/R = 2$  and  $4$ , together with the results for multiple cracks in a single row of holes ( $h/R = 0$ ), obtained in Chapter 5.

It can be seen that the stress intensity factor is less when the holes are in two parallel rows; and that  $K$  decreases as the separation of the rows is increased. This reduction in  $K$  is more significant for long cracks than for short cracks, for instance going from  $h/R = 0$  to  $h/R = 4$  gives reductions of 33% at  $a/b = 0.45$ , of 12% at  $a/b = 0.35$  and of 4% at  $a/b = 0.25$ .



In Chapter 5 the stress intensity factor ( $K_s$  say) was obtained for a pair of cracks at a single hole in an otherwise uncracked row of holes periodically spaced a distance  $b$  apart; in the same chapter it was seen that, for cracks of equal lengths at all the holes, the stress intensity factor ( $K_m$  say) was greater than  $K_s$  by up to a factor of 2. However, Fig 9.4 shows that  $K_m$  can be reduced by arranging the holes into two parallel rows. In fact, for large separations,  $K_m$  approaches a limit, for short cracks, which is less than  $K_s$ . This limiting value of  $K_m$  is the stress intensity factor for two cracks at every hole in a row of holes periodically spaced a distance  $2b$  apart. However, for the value of  $b/R$  used in this chapter, the difference between  $K_s$  and the limiting value of  $K_m$  is small ( $\sim 1-2\%$ ) and of the same order as the accuracy of the  $Q$ -terms in equation (9.7). Curves of  $K_m/K_s$  against  $a/b$ , for  $h/b = 0, 2$  and  $4$ , are shown in Fig 9.5; it is seen that for  $h/b = 4$ ,  $K_m$  exceeds  $K_s$  by less than 10% for all crack-lengths.

## 9.2 Growth of fatigue cracks

Because the stress intensity factor is decreased by having a double row of holes, the rate at which cracks grow when the component is subjected to fatigue loadings will also be reduced. Thus the time for the crack to grow from some initial size  $a_i$  to a final size  $a_f$  will increase with the row spacing  $h$ . Two values of  $a_i/b$  are considered in this chapter, they correspond to the maximum and minimum flaw sizes assumed in the damage-tolerant specification<sup>49</sup>.

### 9.2.1 Rates of crack growth

The rate of growth of fatigue cracks is controlled by the range of the applied stress intensity factor  $\Delta K (= K_{\max} - K_{\min})$ . Paris showed<sup>18</sup> that for simple loadings, the growth of fatigue cracks could be described by a power law, namely

$$\frac{da}{dN} = C(\Delta K)^p, \quad (9.8)$$

where  $da/dN$  is the increase in crack-length per cycle of stress, and  $C$  and  $p$  are constants (see section 5.3).

For the high-strength aluminium alloys used in aerospace,  $p$  is about 3. In order to estimate the variation of growth-rate with stress intensity factor, it will be assumed that  $p = 3$ .

Since  $\Delta K$  can be written as

$$\Delta K = Q\Delta\sigma\sqrt{\pi a} \quad (9.9)$$

where  $\Delta\sigma$  is the range of applied stress, it follows that

$$\frac{da}{dN} = C(\Delta\sigma\sqrt{\pi})^P (Q\sqrt{a})^P \quad (9.10)$$

If  $(da/dN)_m$  is the crack growth-rate for two cracks of length  $a$  at the edge of each hole in a double row and  $(da/dN)_s$  that for two cracks also of length  $a$  at the edge of just one hole in a single row, then it follows from equation (9.10) that

$$\frac{(da/dN)_m}{(da/dN)_s} = \left(\frac{Q_m}{Q_s}\right)^P, \quad (9.11)$$

where  $Q_m$  is the normalized stress intensity factor for multiple cracks in a double row of holes, and  $Q_s$  that for two similar cracks at one of the holes in a single row of holes.

The ratio of growth-rates given by equation (9.11) with  $p = 3$  is plotted in Fig 9.6 as a function of  $a/b$  for  $h/R = 0, 2$  and  $4$ . It is seen that the effect of multiple cracks on the growth-rate is reduced by arranging the holes in two rows. For  $h/r = 4$  the crack growth-rate  $(da/dN)_m$  is within 30% of  $(da/dN)_s$  for all crack-lengths. For multiple cracks in a single row of holes ( $h/R = 0$ ), the ratio of the crack growth-rates is much greater, 1.5 at  $a/b = 0.3$  and 2.5 at  $a/b = 0.4$ .

### 9.2.2 Fatigue lifetimes

The value of the fatigue lifetime  $\Delta N_{if}$ , defined as the number of cycles of stress for a crack to grow from an initial length  $a_i$  to a final length  $a_f$ , provides a measure of the safety and serviceability of a cracked airframe structural component. The lifetime  $\Delta N_{if}$  is given, from equation (9.8), by

$$\Delta N_{if} = \frac{1}{C} \int_{a_i}^{a_f} \frac{da}{(\Delta K)^P}, \quad (9.12)$$

which can be combined with equation (9.10) to give

$$\Delta N_{if} = \frac{1}{C(\Delta\sigma\sqrt{\pi})^p} \int_{a_i}^{a_f} \frac{da}{(Q\sqrt{a})^p} . \quad (9.13)$$

It is convenient to write equation (9.13) in terms of the dimensionless variable  $\alpha$  ( $= a/b$ ); thus

$$\Delta N_{if} = N_0 \int_{\alpha_i}^{\alpha_f} \frac{d\alpha}{(Q\sqrt{\alpha})^p} \quad (9.14)$$

where  $\alpha_i = a_i/b$ ,  $\alpha_f = a_f/b$ , and

$$N_0 = \frac{b}{C(\Delta\sigma\sqrt{\pi b})^p} . \quad (9.15)$$

In order to estimate the increase in lifetime obtained by arranging the holes in two rows, a simple periodic configuration was studied, having two cracks of the same length,  $\ell_i$ , either 1.25 mm or 0.125 mm, at every hole; these two values are the same as the maximum and minimum flaw sizes of the damage-tolerant specification<sup>49</sup>. Lifetimes could be calculated for cracks of arbitrary lengths at different holes, but a step-by-step procedure would be needed (see section 9.3).

If the row of holes is a row of fastener holes then a typical diameter of the holes for an aircraft structure would be  $\sim 6$  mm. The ratio of the length  $\ell_i$  ( $= a_i - R$ ) to the radius will be either  $\sim 0.4$  for the larger crack or  $\sim 0.04$  for the smaller crack. Since

$$\alpha = \frac{a}{b} = \frac{a}{R} \frac{b}{R} = \left(1 + \frac{\ell}{R}\right) \frac{b}{R} , \quad (9.16)$$

it follows that  $\alpha_i = 0.18$  or  $0.13$ . With these values of  $\alpha_i$  the integral in equation (9.14) was evaluated numerically, for  $p = 3$ , as a function of  $\alpha_f$ . The results are shown in Fig 9.7 for  $h/R = 0, 2$  and  $4$  when all the holes have cracks and for  $h = 0$  when only one of the holes has cracks. It can be seen that there is a significant increase in lifetime from having two rows of holes. However, more area may be needed if the fasteners are in a double row and designing for longer life may carry a weight penalty.

The lifetime depends on both  $a_i$  and  $a_f$ . Because growth is described by a simple power-law, most of the lifetime of a fatigue crack is spent while the crack is short,  $a \sim a_i$ . When  $a_i$  is small, the stress intensity factor is not very sensitive to the actual position of the boundaries; thus, the benefits of arranging the holes in two rows will be less for small  $a_i$  than for large  $a_i$ . These effects are shown in Fig 9.8 where the ratio  $(\Delta N)_m / (\Delta N)_s$  is plotted as a function of  $a_f/b$  for the two values of  $a_i/b$  and  $h/R = 0, 2$  and  $4$ :  $(\Delta N)_m$  is the lifetime for two cracks at every hole and  $(\Delta N)_s$  is the lifetime for two cracks at one hole only in a single row of holes. For  $h/R = 0$ , multiple cracks reduce the lifetime for  $a_i/b = 0.13$  by between 5% and 24% over the range  $a_f/b \leq 0.45$ ; for a double row of holes ( $h/R = 4$ ), the reduction is less than 10% over the same range of  $a_f/b$ . For  $a_i/b = 0.18$  the reduction in lifetime caused by multiple cracks in a single row ( $h/R = 0$ ) is between 17% and 35%; for a double row of holes ( $h/R = 4$ ), the reduction is between 9% and 18%. The region where  $(\Delta N)_m / (\Delta N)_s > 1$  occurs because  $K_m$  can be less than  $K_s$  for large values of  $h/R$  and small crack-lengths (see section 9.1).

### 9.3 Discussion

The model configurations studied in this chapter are simplified representations of practical crack configurations at a double row of holes.

The major simplifications are:

- (a) the neglecting of any effects on the rate or direction of crack growth due to the sliding-mode stress intensity factor;
- (b) the direction of crack growth in each row of holes is along the line through the centres of the holes;
- (c) all the cracks have the same length;
- (d) the growth of cracks in fatigue is described by a simple power law (see equation (9.8)), with the power  $p = 3$ ;

The consequences of these simplifying assumptions are now discussed in more detail.

- (a) The calculations in sections 9.1 and 9.2 refer to opening mode stress intensity factors  $K_I$  only. Because the configuration is not symmetric about either row of holes, there is a non-zero contribution to the sliding mode stress intensity factor  $K_{II}$ . The magnitude of  $K_{II}$  can be obtained from the results for the ancillary configuration

shown in Fig 9.2c&d of two parallel off-set cracks (see Case 1.2.4 in Ref 2). From these results it follows that, for the configurations studied in this chapter,  $|K_{II}| \ll K_I$ , and hence the effects of the sliding mode stress intensity factor are unlikely to be significant.

(b) Because of the reduction in symmetry due to having two rows of holes, the maximum stress concentration at each hole is no longer at the ends of the diameter which lies along the line of the centres of the holes. It is displaced round the perimeter of the hole towards the neighbouring row (see Peterson<sup>17</sup>); in principle, this may cause the crack to deviate from the path assumed in this chapter. However, for the configurations considered the deviations are small and can be neglected.

It might be thought that cracks will be initiated and grow towards each other along the line joining the centres of two adjacent holes, one in each row. That is the cracks will tend to grow at an angle of  $\theta = \pm \tan^{-1}(h/b)$  rather than in the assumed direction at right angles to the applied stress. For the values of  $h/b = 2$  and  $4$ , the angles  $\theta$  are approximately  $15^\circ$  and  $30^\circ$ . The resultant stress intensity factor  $K_r$  for this configuration can be obtained for results from the following ancillary configurations:

- (i) a radial crack at the edge of a circular hole in a sheet subjected to a uniform uniaxial tensile stress remote from and at an arbitrary angle to the crack (Tweed and Rooke<sup>50</sup>);
- (ii) a crack in the vicinity of a hole in a sheet subjected to the same remote stress (Case 1.3.5, Ref 2);
- (iii) a crack collinear with another crack in a sheet subjected to the same remote stress (Case 1.2.2, Ref 2).

In order to obtain results for ancillary configurations (ii) and (iii) the applied stress must be resolved into both normal and shear components parallel and perpendicular to the crack.

For this configuration with  $b/R = 8$  calculations show that the stress intensity factor is always less (10-50%) than that for cracks perpendicular to the direction of the applied stress. It is unlikely, since the maximum stress occurs at  $\theta \approx 0$  that cracks will be initiated at an angle  $\theta$  much different from zero, but, if cracks do occur, they will grow much more slowly.

The sliding mode stress intensity factor  $K_{II}$  is again much smaller than  $K_I$ .

(c) The requirement of the damage-tolerant specification<sup>49</sup> is to assume one long crack (1.25 mm) and all the rest short (0.125 mm). This could be studied using the above methods but with some loss of accuracy because solutions are not yet available for all of the required ancillary configurations<sup>†</sup>. In order to calculate the lifetime, a step-by-step procedure must be used as cracks of different lengths grow at different rates. To facilitate the calculations, a model configuration with all the cracks the same length has been studied in this chapter. However, it can be shown that  $K_r$  for the model configuration is greater than that for the configuration specified in Ref 49. The long crack ( $l_i = 1.25$  mm) has the largest stress intensity factor. If its tip-to-tip length is  $2a$ , then for a given value of  $a/b$  the distance from either tip of the long crack to the nearer tips of the smaller cracks ( $l_i = 0.125$  mm) is greater than in the model configuration ( $l_i = 1.25$  for all cracks). Hence the contribution of the smaller cracks to  $K_r$  for the long crack is less, and the limiting value of  $K_m$  as  $h/R$  increases, is less than  $K_s$  (see section 9.1) for a much larger range of  $a/b$ . Thus the stress intensity factor for the longer crack is less for all values of  $a/b$  than if the cracks were all the same length, and hence the crack growth-rates will be less and the lifetimes more.

(d) The fatigue calculations were done assuming a simple dependence of the crack growth-rate on the stress intensity factor and no load interaction effects. The calculations can still be done even when load interaction effects are present provided the crack growth-rate can still be expressed as a function of the stress intensity factor. The simple power-law used assumed that the power  $p = 3$ . If  $p > 3$  the percentage increase of lifetime that results from having two rows of holes, would therefore be greater than those calculated for  $p = 3$ . Since the magnitude of the effects on lifetime increases as the initial crack-length increases, it follows that such effects become increasingly important in the calculation of inspection intervals as the component nears the end of its life.

(e) Boundary-boundary interactions are negligible for the double row of holes and therefore the term  $Q_e$  is negligible in the calculation of

---

<sup>†</sup> The major ancillary configuration of two cracks of unequal length at the edge of a hole has been obtained by Tweed and Rooke<sup>20</sup>; but two parallel offset cracks of unequal length has not, although two collinear cracks of unequal length has (see Case 1.2.3 in Ref 2).

the normalized stress intensity factor. The term  $Q_e$  was found to be negligible (see section 5.4) for a single row of holes; it will be even smaller for the double row as the stress *concentration* factor is less<sup>17</sup>.

#### 9.4 Conclusions

(1) Arranging fastener holes in two rows instead of one reduces stress intensity factors when the holes are cracked. This results in slower fatigue crack growth and longer lifetimes.

(2) The benefits of having two rows of holes are small while the cracks remain small, but if damage-tolerant requirements impose a large initial crack-length, then the benefits are substantial.

CHAPTER 10CONCLUDING REMARKS

In this thesis a method called compounding was developed for obtaining stress intensity factors for cracks in complex geometrical configurations representing engineering structural components. The emphasis was in developing a method which is quick and easy to use, and therefore not costly; such a method is, of necessity, approximate. The errors arising from the use of such approximations in the fracture mechanics calculations of fatigue lifetimes and residual strength of cracked structures were investigated, by using a simple asymptotic method; thus the degree of approximation which produces acceptable errors, *ie* within engineering tolerances, was determined. These error levels were adopted as a guide in developing the compounding method to the required accuracy.

It was shown how the method is used to build up the stress intensity factor solutions for a geometrically complex, cracked configuration with many boundaries from the solutions for several simple cracked configurations. An advantage of this procedure is that the boundaries which are likely to be important design features, are readily identified. The versatility of the compounding method was demonstrated by applying it to several common structural configurations including cracks at rows of holes, loaded and unloaded, and cracks in reinforced structures.

The method, is particularly suitable for design studies of damage tolerant structures and the calculation of fatigue lifetimes; the configurations studied in this thesis, although only two-dimensional, are appropriate for many design problems. In principle the compounding method can be applied to three-dimensional problems, but many more stress intensity factor solutions to simple three-dimensional configurations are required before it can be widely used. However many three-dimensional configurations can be modelled by a two-dimensional configuration which retains the essential boundary features and which will give conservative estimates of residual strength and fatigue lifetimes.

## APPENDIX A

EVALUATION OF GROWTH-TIME INTEGRALS FOR A CIRCULAR HOLE

(See sections 2.2.1 and 2.2.2)

The number of cycles  $\Delta N$  required for a crack of initial length  $\ell_i$  to reach a final length  $\ell_f$  is given, by equation (2.21), as

$$\Delta N = \frac{1}{C} \int_{\ell_i}^{\ell_f} \frac{d\ell}{(\Delta K)^m} . \quad (\text{A-1})$$

For a crack of length  $\ell$  at the edge of a circular hole of radius  $R$  the stress intensity factor range  $\Delta K$  is given by

$$\Delta K = Y \Delta \sigma \sqrt{\pi \ell} ; \quad (\text{A-2})$$

the geometry factor  $Y$  is given, by equation (2.26), as

$$\left. \begin{aligned} Y &= 3.36 , & \ell/R &\leq 0.1 , \\ Y &= \sqrt{\frac{2R + \ell}{2\ell}} , & \ell/R &> 0.1 . \end{aligned} \right\} \quad (\text{A-3})$$

Therefore for  $\ell_f/R \leq 0.1$ , equation (A-1) becomes

$$\Delta N = \frac{1}{C(3.36\Delta\sigma\sqrt{\pi})^m} \int_{\ell_i}^{\ell_f} \frac{d\ell}{\ell^{m/2}} , \quad (\text{A-4})$$

and for  $\ell_i/R \geq 0.1$ , equation (A-1) becomes

$$\Delta N = \frac{2^{m/2}}{C(\Delta\sigma\sqrt{\pi})^m} \int_{\ell_i}^{\ell_f} \frac{d\ell}{(\ell + 2R)^{m/2}} . \quad (\text{A-5})$$

The integral in (A-4) is known; the specific integrals required for this application are as follows:

for  $m = 2$

$$\int_{\ell_i}^{\ell_f} \frac{d\ell}{\ell} = \ln\left(\frac{\ell_f}{\ell_i}\right),$$

for  $m = 3$

$$\int_{\ell_i}^{\ell_f} \frac{d\ell}{\ell^{3/2}} = 2 \left( \frac{1}{\sqrt{\ell_i}} - \frac{1}{\sqrt{\ell_f}} \right),$$

and for  $m = 4$

$$\int_{\ell_i}^{\ell_f} \frac{d\ell}{\ell^2} = \left( \frac{1}{\ell_i} - \frac{1}{\ell_f} \right).$$

(A-6)

Substitution of  $x = \ell + 2R$  into the integrand in equation (A-5) gives

$$\Delta N = \frac{2^{m/2}}{C(\Delta\sigma\sqrt{\pi})^m} \int_{x_i}^{x_f} \frac{dx}{x^{m/2}}, \quad (A-7)$$

where  $x_i = \ell_i + 2R$  and  $x_f = \ell_f + 2R$ . The form of the integral in equation (A-7) is identical with those given in equation (A-6).

By combining equations (A-4) and (A-5) the value of  $\Delta N$  can be calculated for any  $\ell_i$  and  $\ell_f$ .

## APPENDIX B

EVALUATION OF GROWTH-TIME INTEGRALS FOR AN ELLIPTICAL HOLE

(See section 2.2.3)

For cracks at the edge of an elliptical hole the equations required to calculate  $\Delta N$  are (see Appendix A) as follows:

$$\Delta N = \frac{1}{C} \int_{\ell_i}^{\ell_f} \frac{d\ell}{(\Delta K)^m}, \quad (B-1)$$

$$\Delta K = Y \Delta \sigma \sqrt{\pi \ell}, \quad (B-2)$$

and

$$\left. \begin{aligned} Y &= 1.12 \left[ 1 + 2 \frac{c}{h} \right], & \ell/R \leq 0.1, \\ Y &= \sqrt{\frac{\ell + c}{\ell}}, & \ell/R > 0.1. \end{aligned} \right\} (B-3)$$

Therefore for  $\ell_f/R \leq 0.1$  equation (B-1) becomes

$$\Delta N = \frac{1}{C \left[ 1.12 \left( 1 + 2 \frac{c}{h} \right) \Delta \sigma \sqrt{\pi} \right]^m} \int_{\ell_f}^{\ell_i} \frac{d\ell}{\ell^{m/2}} \quad (B-4)$$

and for  $\ell_i/R > 0.1$  equation (B-1) becomes

$$\Delta N = \frac{1}{C (\Delta \sigma \sqrt{\pi})^m} \int_{\ell_i}^{\ell_f} \frac{d\ell}{(\ell + c)^{m/2}}. \quad (B-5)$$

The integral in equation (B-4) is identical to that in equation (A-4) and the integral in equation (B-5) is the same as the integral in equation (A-5) if  $2R$  is replaced by  $c$ . Thus the solutions given in equation (A-6) are applicable to this case and therefore  $\Delta N$  for any values of  $\ell_i$  and  $\ell_f$  can be calculated by combining equations (B-4) and (B-5).

## APPENDIX C

EVALUATION OF GROWTH-TIME INTEGRALS FOR A LOADED CIRCULAR HOLE

(See section 2.2.4)

For a crack at the edge of a hole, loaded either by a force  $P$  or a pressure  $p$ , the equations required to calculate  $\Delta N$  are (see Appendix A) as follows:

$$\Delta N = \frac{1}{C} \int_{\ell_i}^{\ell_f} \frac{d\ell}{(\Delta K)^m}, \quad (C-1)$$

and

$$\Delta K = Y \Delta s \sqrt{\pi \ell}, \quad (C-2)$$

where  $s$  is a stress equal to either  $P/(2R)$  or  $p$ . The function  $Y$  is given by

$$\left. \begin{aligned} Y &= 1.12K_t && \text{for } \ell/R \leq 0.2 \\ Y &= \frac{1}{\pi} \sqrt{\frac{2}{\lambda(\lambda+1)(\lambda+2)}} && \text{for } \ell/R > 0.2. \end{aligned} \right\} (C-3)$$

For short cracks,  $\ell_f/R \leq 0.2$ , substitution of equation (C-3) into equation (C-2) and equation (C-2) into (C-1) leads to integrals identical to those in equation (A-4) in Appendix A; the solutions of the integrals are given in equations (A-6). For long cracks,  $\ell_i/R \geq 0.2$ , equation (C-1) becomes

$$\Delta N = \frac{1}{C} \left( \frac{1}{\Delta s \sqrt{\pi/2}} \right)^m I_m, \quad (C-4)$$

where

$$I_m = \int_{\lambda_i}^{\lambda_f} [(\lambda+1)(\lambda+2)]^{m/2} d\lambda, \quad (C-5)$$

with  $\lambda_i = \ell_i/R$  and  $\lambda_f = \ell_f/R$ .

The integrals  $I_m$  are, for  $m = 2, 3$  and  $4$ , given by

$$I_2 = \left[ \frac{\lambda^3}{3} + \frac{3\lambda^2}{2} + 2\lambda \right]_{\lambda_i}^{\lambda_f} \quad (C-6)$$

$$I_3 = \left[ \left( \frac{\lambda^2 + 3\lambda + 2}{8} - \frac{3}{64} \right) (2\lambda + 3) \sqrt{\lambda^2 + 3\lambda + 2} + \frac{3}{128} \ln \left[ 2\sqrt{\lambda^2 + 3\lambda + 2} + 2\lambda + 3 \right] \right]_{\lambda_i}^{\lambda_f} \quad (C-7)$$

$$I_4 = \left[ \frac{\lambda^5}{5} + \frac{3\lambda^4}{2} + \frac{13\lambda^3}{3} + 6\lambda^2 + 4\lambda \right]_{\lambda_i}^{\lambda_f} . \quad (C-8)$$

By combining the short-crack and the long-crack expressions,  $\Delta N$  may be calculated for any values of  $\lambda_i$  and  $\lambda_f$ .

## APPENDIX D

EVALUATION OF BOUNDARY-BOUNDARY INTERACTIONS

(See section 3.1)

Consider a region containing a crack near to two stress free boundaries  $B_1$  and  $B_2$ ; the region is subjected to an applied stress system  $S_0$  on its boundary  $B_0$  which is remote from the crack. This can be obtained using superposition as shown in Fig 3.2. To obtain the stress intensity factor for the configuration in Fig 3.2c use is made of the solution for a region containing a crack near a single internal boundary  $B$  subjected to an arbitrary point force  $F$ ; the region being bounded, remote from the crack, by an external boundary  $B_0$ .

If  $B$  becomes  $B_1$  and distributed point forces  $F = -S_1 dt_1$  are introduced,  $dt_1$  being a length of arc along  $B_1$ , the stress intensity factor obtained is  $K_1^*$  (Fig 3.3a). Similarly, if  $B$  becomes  $B_2$  and  $F = -S_2 dt_2$  the stress intensity factor obtained is  $K_2^*$  (Fig 3.3b). The first stage in obtaining the stress intensity factor when both boundaries are present comes from superimposing Fig 3.2a&b. This gives a stress intensity factor of  $K_1^* + K_2^*$  but additional perturbation stresses  $(\Delta S_1)_1$  and  $(\Delta S_2)_1$  are introduced on boundaries  $B_1$  and  $B_2$  respectively (Fig 3.3c). The stresses  $(\Delta S_1)_1$  which occur at the site of boundary  $B_1$  result from introducing boundary  $B_2$  and the stresses  $(\Delta S_2)_1$  which occur at the site of boundary  $B_2$  result from introducing boundary  $B_1$ . These perturbation stresses  $(\Delta S_n)_1$ ,  $n = 1, 2$ , are cancelled by superimposing the point force configuration, with  $F = -(\Delta S_1)_1 dt_1$  and  $-(\Delta S_2)_1 dt_2$  on  $B_1$  and  $B_2$  respectively, on to the configuration in Fig 3.2c which gives a stress intensity factor of  $K_1^* + K_2^* + (\Delta K_1)_1 + (\Delta K_2)_1$  and leaves reduced stresses  $(\Delta S_1)_2$  and  $(\Delta S_2)_2$  on  $B_1$  and  $B_2$  respectively (Fig 3.3d). This alternating sequence may be continued until at the  $j$ th stage the stresses  $(\Delta S_n)_j$ ,  $n = 1, 2$ , are as small as required. In the limit the resultant stress intensity factor  $K_r^*$  is given by

$$K_r^* = K_1^* + K_2^* + \sum_{j=1}^{\infty} \{(\Delta K_1)_j + (\Delta K_2)_j\} \quad . \quad (D-1)$$

On substituting equations (3.1) to (3.3) into equation (D-1) the normalized stress intensity factor with  $N = 2$  becomes, for the configuration in Fig 3.2a,

$$Q_r = Q_1 + Q_2 - 1 + \sum_{j=1}^{\infty} \{(\Delta Q_1)_j + (\Delta Q_2)_j\} \quad . \quad (D-2)$$

Comparison of equation (D-2) with equation (3.7) ( $N = 2$ ) shows that  $Q_e$  is the summation term. Thus if  $(\Delta S_n)_j$ ,  $n = 1, 2$ , can be evaluated then so can the interaction term  $Q_e$ . The sum of the terms giving  $Q_e$  will be smaller than  $Q_1$  and  $Q_2$  because it depends only on the perturbation stresses  $(\Delta S_n)_j$ ,  $n = 1, 2$ , which arise from the interaction between the two boundaries.

REFERENCES

- 1     W.T. Kirkby           Examples of aircraft failure.  
In Fracture Mechanics of Aircraft Structures;  
edited by H. Liebowitz.  
AGARDograph No.176, pp.8-13, AGARD, London (1974)
- 2     D.P. Rooke            Compendium of stress intensity factors.  
D.J. Cartwright        London, HMSO (1976)
- 3     H. Tada                The stress analysis of cracks handbook.  
P. Paris                Hellertown, Del Research Corp. (1973)  
G. Irwin
- 4     G.C. Sih               Handbook of stress intensity factors.  
Lehigh University (1973)
- 5     H. Liebowitz (Ed)   Fracture (in 7 volumes).  
New York, Academic Press (1968-70)
- 6     G.C. Sih (Ed)        Mechanics of fracture (6 volumes announced  
to date).  
Leyden, Noordhoff (1973- )
- 7     D.J. Cartwright      Evaluation of stress intensity factors.  
D.P. Rooke              In A General Introduction to Fracture Mechanics,  
edited by H.L. Cox, *et al*, pp.54-73, London,  
MEP (1978)
- 8     A.S. Kobayashi      Experimental techniques in fracture mechanics.  
Connecticut, SESA (1973)
- 9     A.R. Luxmore         Proceedings of 1st and 2nd International Con-  
D.R.J. Owen (Eds)      ferences on Numerical Methods in Fracture  
Mechanics.  
Swansea, University College (1978 and 1980)
- 10    D.P. Rooke            Simple methods of determining stress <sup>intensity</sup> factors.  
F.I. Baratta            Engineering Fracture Mechanics, 14, 397-426  
D.J. Cartwright        (1981)
- 11    D.P. Rooke            Asymptotic stress intensity factors for  
fatigue crack-growth calculations.  
Int. J. Fatigue, 2, 69-75 (1980)

REFERENCES (continued)

- 12 D.J. Cartwright     Approximate stress intensity factors compounded  
D.P. Rooke             from known solutions.  
Engineering Fracture Mechanics, 6, 563-571  
(1974)
- 13 T.R. Brussat         Fatigue crack growth in reinforced panels with  
S.T. Chiu              initial corner cracks.  
J.L. Rudd              Engineering Fracture Mechanics, 14, 665-683  
M. Creager             (1981)
- 14 N.F. Harper         The value of full scale testing.  
A.J. Troughton        In Fatigue Design Procedures, edited by  
E. Gassner and W. Schütz (Proc. 4th ICAF  
Symposium, Munich) London, Pergamon (1969)
- 15                     -                     Damage tolerant design handbook, Parts 1 and 2.  
Metals and Ceramics Information Centre, Battelle  
(1975)
- 16 S.R. Novak           Brittle fracture ( $K_{Ic}$ ) behaviour of cracks  
J.M. Barsom           emanating from notches.  
In Cracks and Fracture, edited by J.L. Swedlow  
and M.L. Williams, STP 601, ASTM, pp.409-443  
(1976)
- 17 R.E. Peterson       Stress concentration factors.  
New York, John Wiley & Sons (1974)
- 18 P.C. Paris           The fracture mechanics approach to fatigue.  
In Fatigue - An Interdisciplinary Approach,  
edited by J.J. Burke, N.L. Reed and V. Weiss,  
New York, Syracuse University Press, pp.107-132  
(1964)
- 19 J. Tweed             The distribution of stress near the tip of a  
D.P. Rooke             radial crack at the edge of a circular hole.  
Int. J. Engng. Sci., 11, 1185-1195 (1973)
- 20 J. Tweed             The elastic problem for an infinite solid con-  
D.P. Rooke             taining a circular hole with a pair of radial  
edge cracks of different lengths.  
Int. J. Engng. Sci., 14, 925-933 (1976)

REFERENCES (continued)

- 21 J.C. Newman An improved method of collocation for the stress analysis of cracked plates with various shaped boundaries.  
NASA TN D-6376 (1971)
- 22 A.F. Grandt Two dimensional stress intensity factor solutions for radially cracked rings.  
AFML-TR-75-121 (1975)
- 23 S. Timoshenko Theory of elasticity.  
J.N. Goodier 2nd edition, New York, McGraw-Hill (1951)
- 24 D.P. Rooke The stress intensity factors of a radial crack in a finite rotating elastic disc.  
J. Tweed Int. J. Engng. Sci., 10, 709-714 (1972)
- 25 J.P. Benthem Asymptotic approximations to crack problems.  
W.T. Koiter In Methods of Analysis and Solutions to Crack Problems, Chapter 3, Vol.1 in Ref 6 (1973)
- 26 N.E. Dowling Notched member fatigue life predictions combining crack initiation and propagation.  
Fatigue of Engng. Mat. and Struct. 2, 129-138 (1979)
- 27 F.I. Baratta Stress concentration factors in U-shaped and semi-elliptical edge notches.  
D.M. Neal J. Strain Analysis, 5, 121-127 (1970)
- 28 Y. Murakami A simple procedure for the accurate determination of stress intensity factors by finite element method.  
Engng. Fracture Mech., 8, 643-655 (1976)
- 29 I.E. Figge Fatigue crack propagation in structures with simulated rivet forces.  
J.C. Newman, Jr ASTM STP No.415, pp.71-93 (1967)
- 30 F.W. Smith Stress intensity factors for a semi-elliptical surface flaw.  
Boeing Company, Structural Development Research Memo 17 (1966)

REFERENCES (continued)

- 31 A.F. Liu Stress intensity factors for a corner flaw.  
Engng. Fracture Mech., 4, 175-179 (1972)
- 32 I.S. Sokolnikoff Mathematical theory of elasticity.  
pp.318-327, McGraw-Hill (1956)
- 33 F.W. Smith Stress intensity factors for semi-circular  
A.F. Emery cracks. Part 2 - Semi-infinite solid.  
A.S. Kobayashi J. Appl. Mech., 34, 953-959 (1967)
- 34 T. Kanazawa *et al* Some basic considerations on crack arresters,  
Parts I-V.  
J. Soc. Naval Architects of Japan (1964/67);  
RAE Library Translation 1648 (1972)
- 35 G.N. Savin Stress distribution around holes.  
'Naukova Dumka' Press, Kiev (1968);  
Translation: NASA TT F-607 (1970)
- 36 D.P. Rooke Stress intensity factors for cracked holes in  
the presence of other boundaries.  
In Fracture Mechanics in Engineering Practice,  
edited by P. Stanley, pp.149-163, London,  
Applied Science Pub. Ltd (1977)
- 37 D.P. Rooke Stress intensity factors for a crack at a row  
of holes.  
Int. J. Fracture, 18, R31-R36 (1982)
- 38 A.P. Parker Mechanics of fracture and fatigue in some  
common structural configurations.  
Technical Note MAT/18, RMCS Shrivenham (1979)
- 39 D.P. Rooke Stress intensity factors for a crack at the  
J. Tweed edge of a pressurized hole.  
Int. J. Engng. Sci., 18, 109-121 (1980)
- 40 K. Mori Stress distributions in a semi-infinite plate  
with a row of circular holes.  
Bull, Japan Soc. Mech. Engng., 15, 899-906  
(1972)
- 41 K. Mori Private communication.
- 42 D.P. Rooke The compounding method applied to cracks in  
D.J. Cartwright stiffened sheets.  
Engng. Fracture Mech., 8, 567-573 (1976)

REFERENCES (concluded)

- 43 C.C. Poe Stress intensity factor for a cracked sheet with riveted and uniformly spaced stringers. NASA TM R-358 (1971)
- 44 C.C. Poe The effect of broken stringers on the stress intensity factor for a uniformly stiffened sheet containing a crack. NASA TM X-71947 (1973)
- 45 J.M. Bloom The effect of a riveted stringer on the stress  
J.L. Sanders in a cracked sheet.  
J. Appl. Mech., 33, 561-570 (1966)
- 46 R. Greif The effect of a stringer on the stress in a  
J.L. Sanders cracked sheet.  
J. Appl. Mech., 32, 59-66 (1965)
- 47 D.P. Rooke Stress intensity factors for collinear cracks  
D.J. Cartwright in a stiffened sheet.  
Int. J. Fracture, 14, R237-240 (1978)
- 48 D.P. Rooke Fatigue lifetimes for cracks at a double row of holes.  
Proceedings of Symposium on 'The use of fracture mechanics in design', Institute of Physics, London, March 1982 (to be published)
- 49 United States Air Force Airplane tolerance requirements.  
Military Specification MIL-A-83444 (USAF) (1974)
- 50 J. Tweed The stress intensity factor for a crack at the  
D.P. Rooke edge of a loaded hole.  
Int. J. Solids Structures, 15, 899-906 (1979)

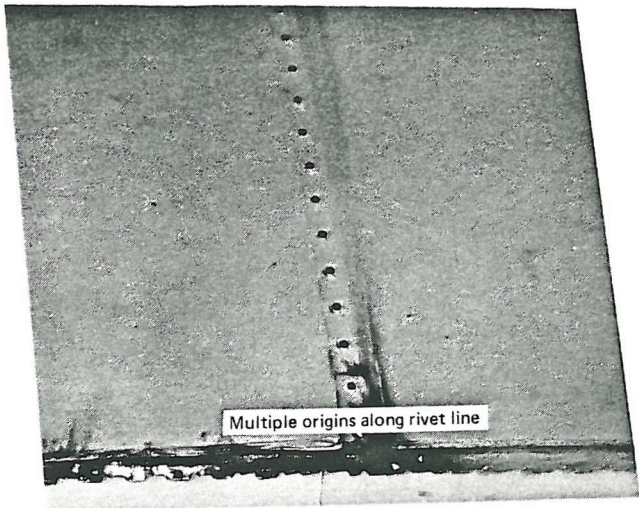


Fig 1.1 In service failure - pressure cabin skin

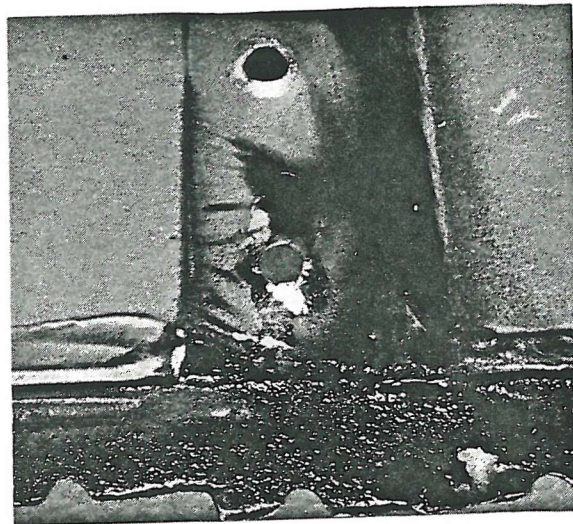


Fig 1.2 Pressure cabin skin failure - growth of damage along rivet line

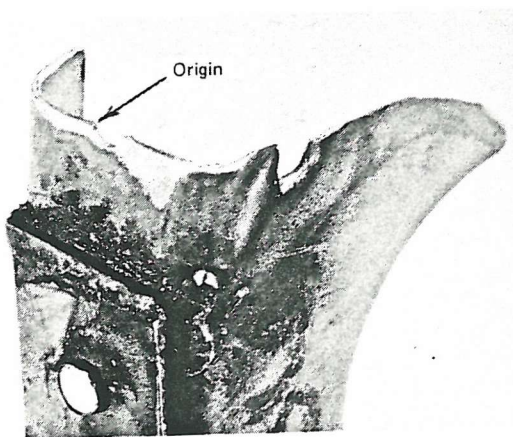


Fig 1.3 Pressure cabin failure - crack through underlying frame

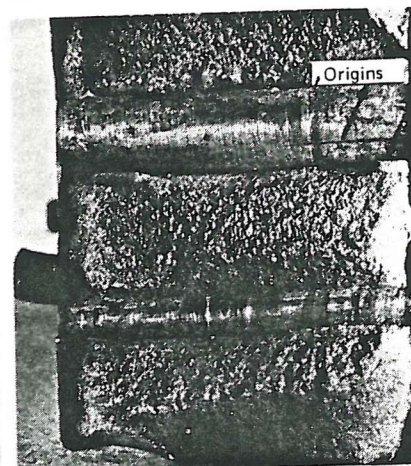
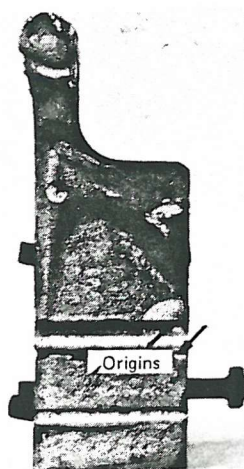


Fig 1.4 In service failure - mainplane spar boom

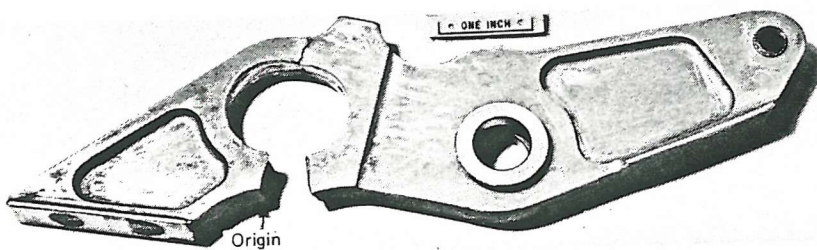


Fig 1.5 In service failure - landing gear door up-lock operating lever

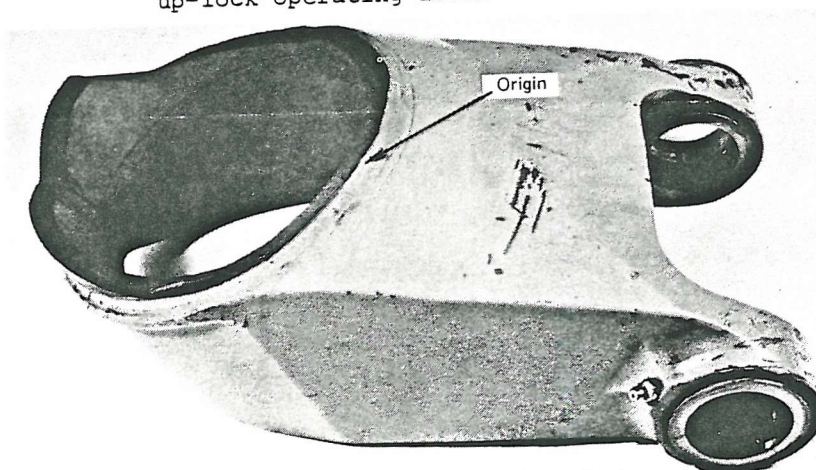


Fig 1.6 In service failure - pivot bracket

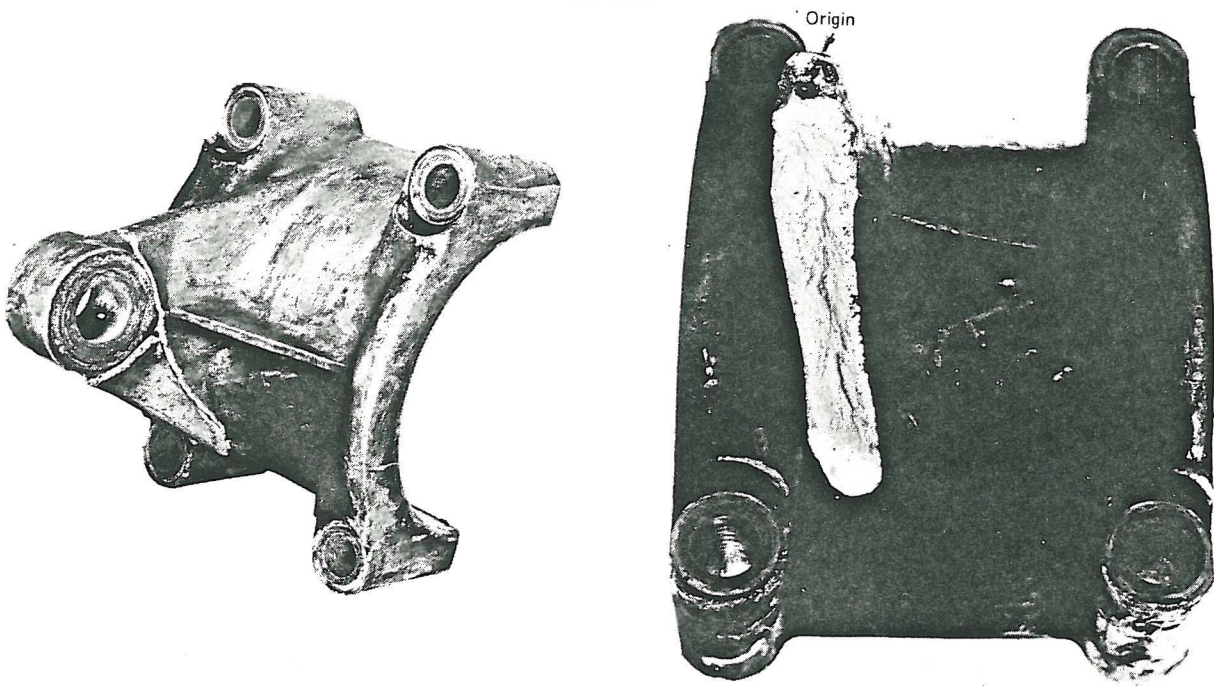


Fig 1.7 In service failure - half axle clamp

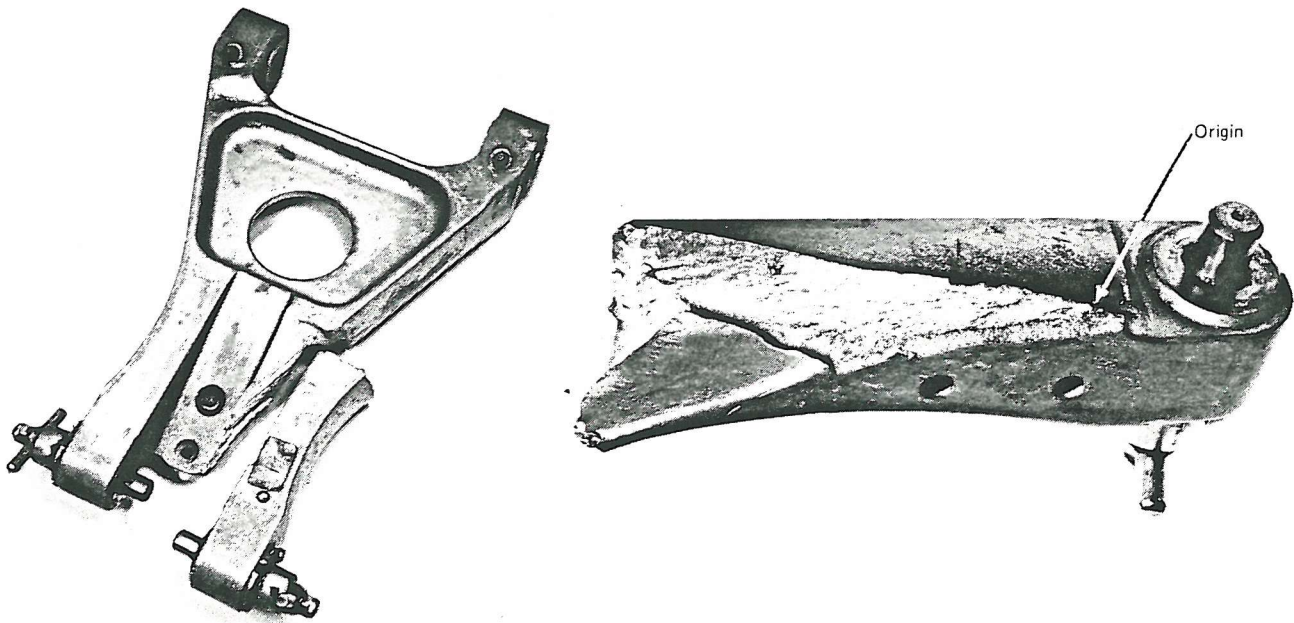


Fig 1.8 In service failure - undercarriage torque link



Fig 1.9 In service failure - nose-wheeling casting

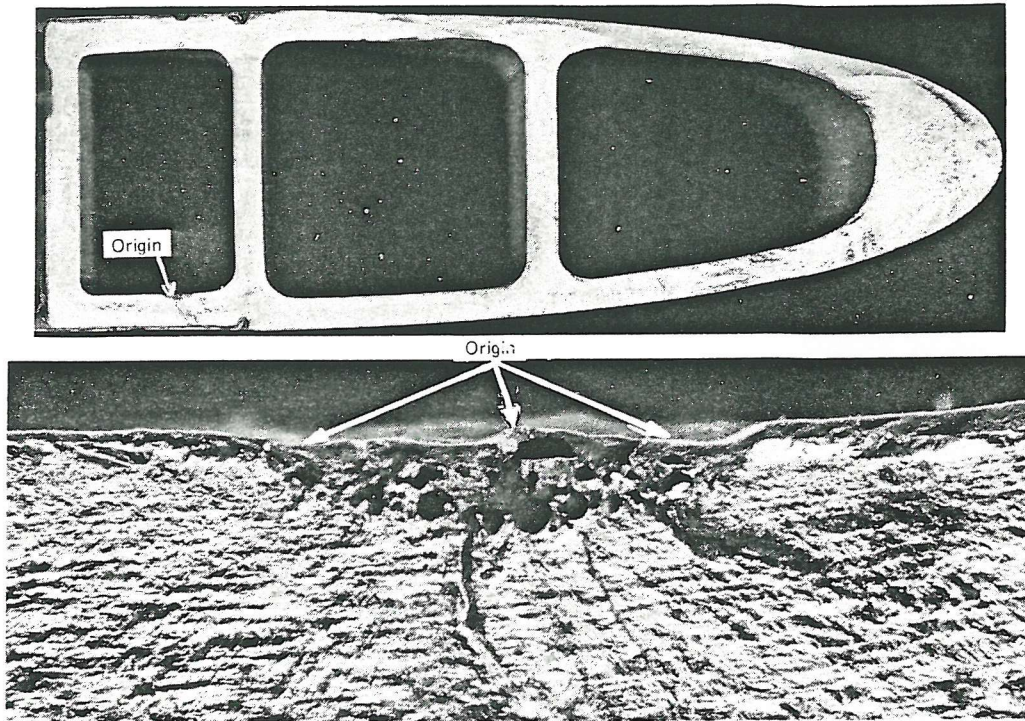


Fig 1.10 In service failure - helicopter rotor blade extrusion

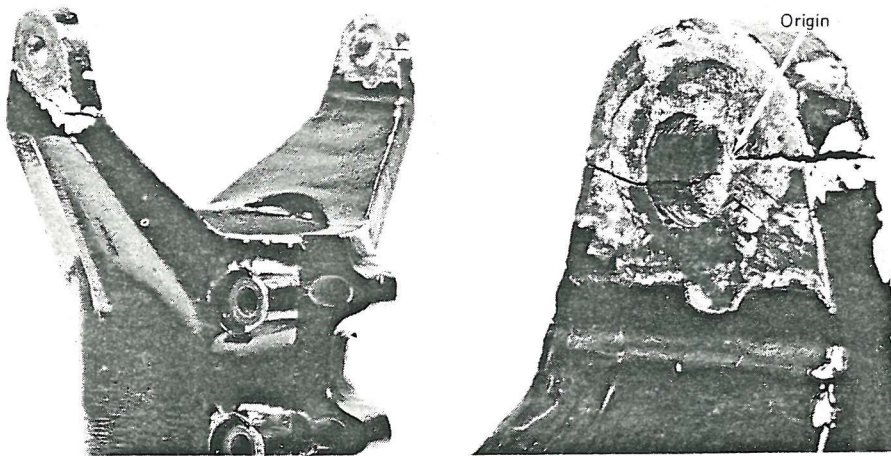


Fig 1.11 In service failure - helicopter rotor drive yoke

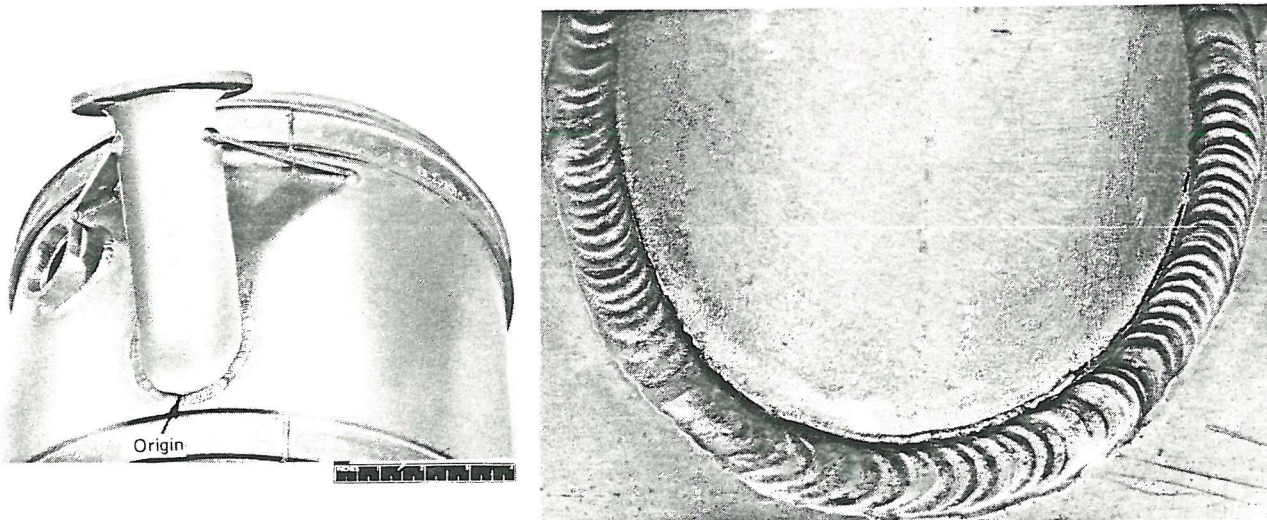


Fig 1.12 In service failure - hydraulic reservoir

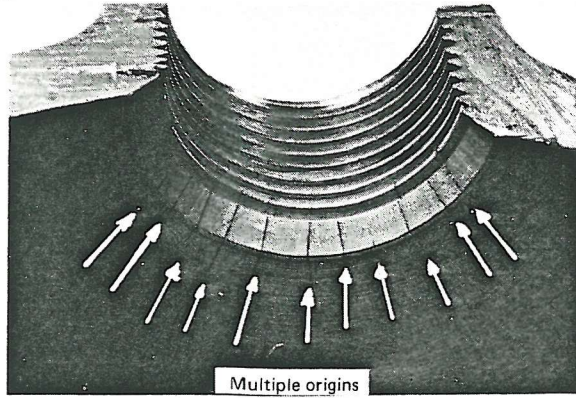
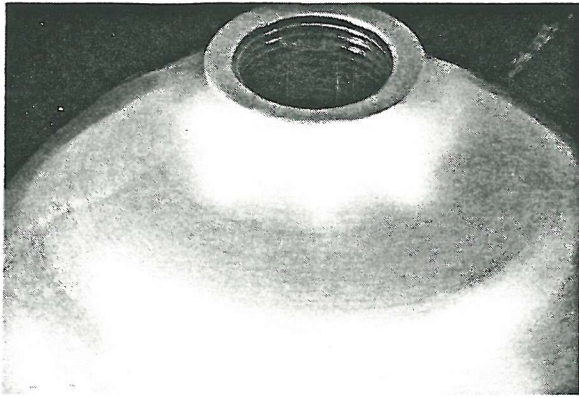


Fig 1.13 In service failure - air bottle

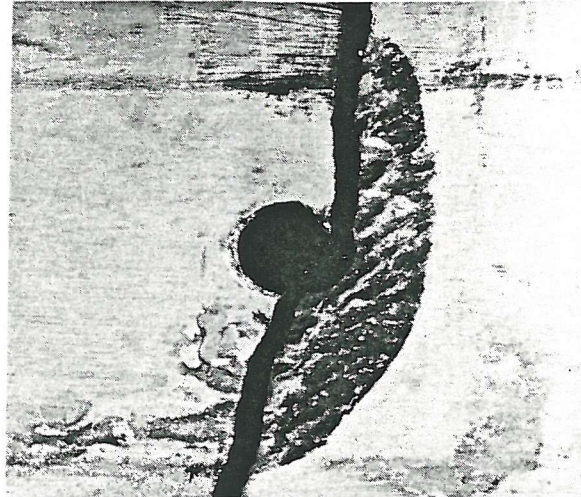
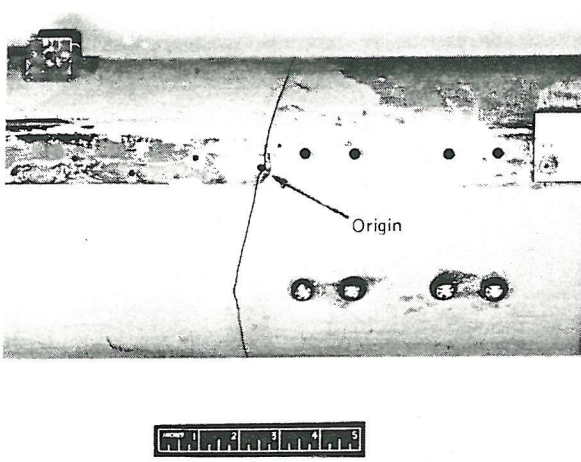


Fig 1.14 In service failure - tubular lift strut

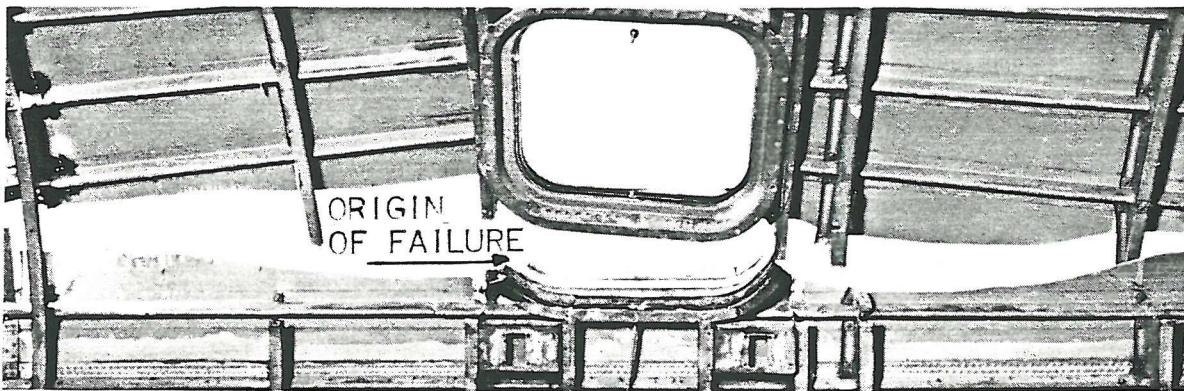


Fig 1.15 Failure in test - aircraft pressure cabin

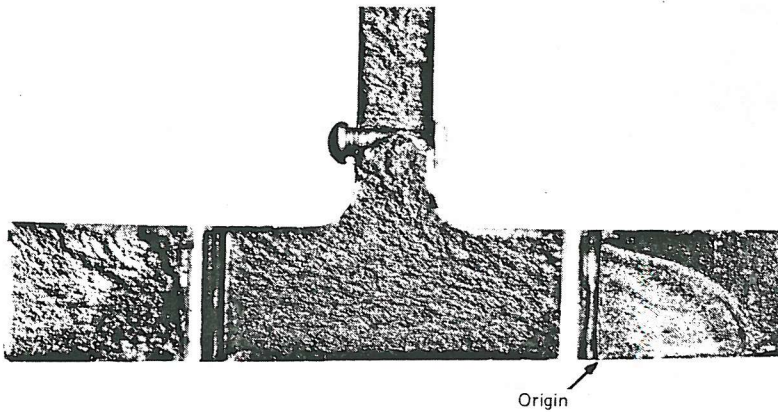


Fig 1.16 Failure in test - spar boom

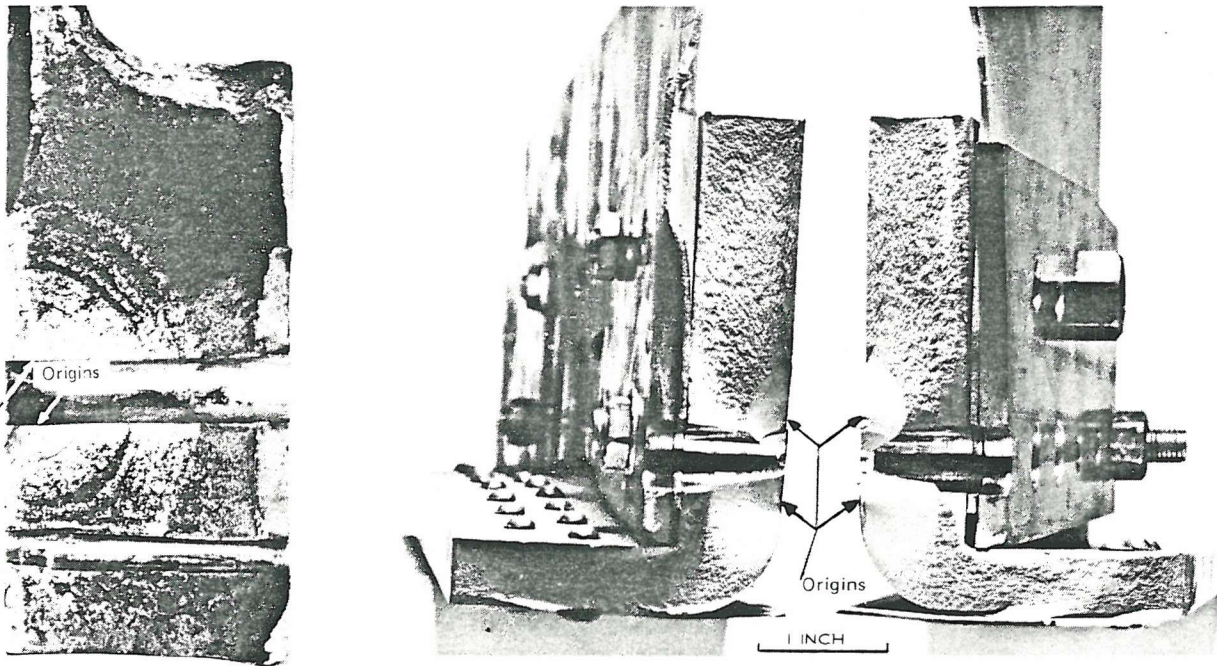
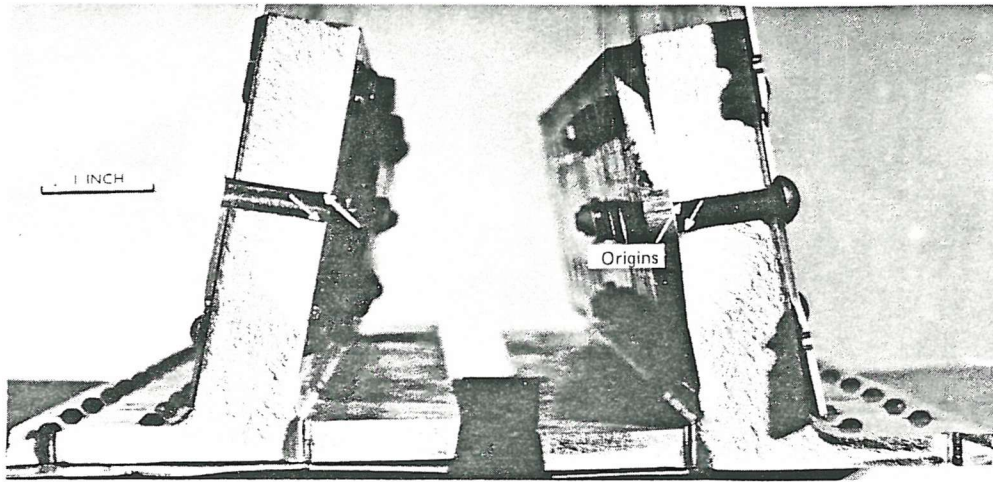


Fig 1.17 Failures in test - spar booms

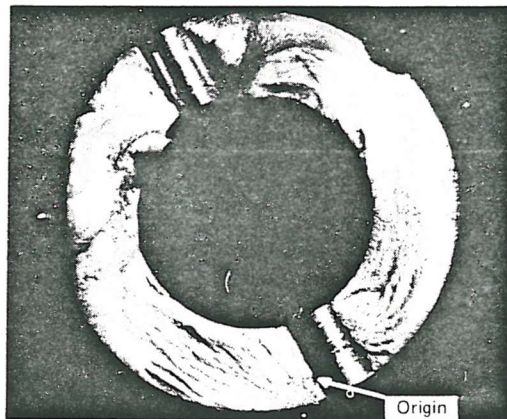
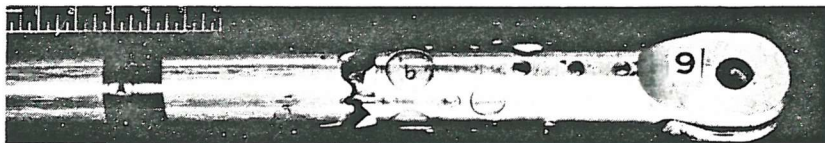


Fig 1.18 Failure in test - tubular control rod

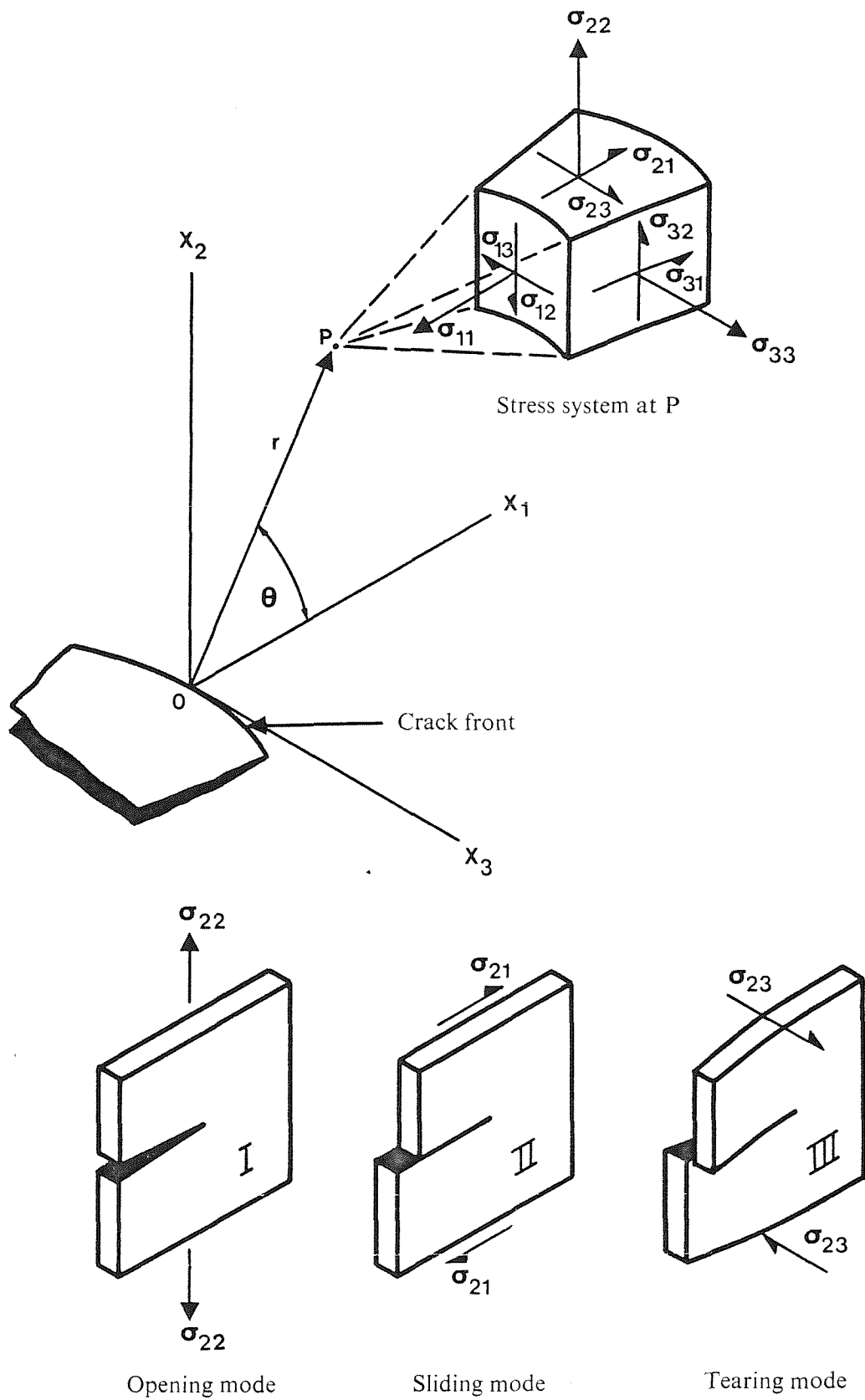


Fig 1.19 Crack coordinate system and modes of deformation

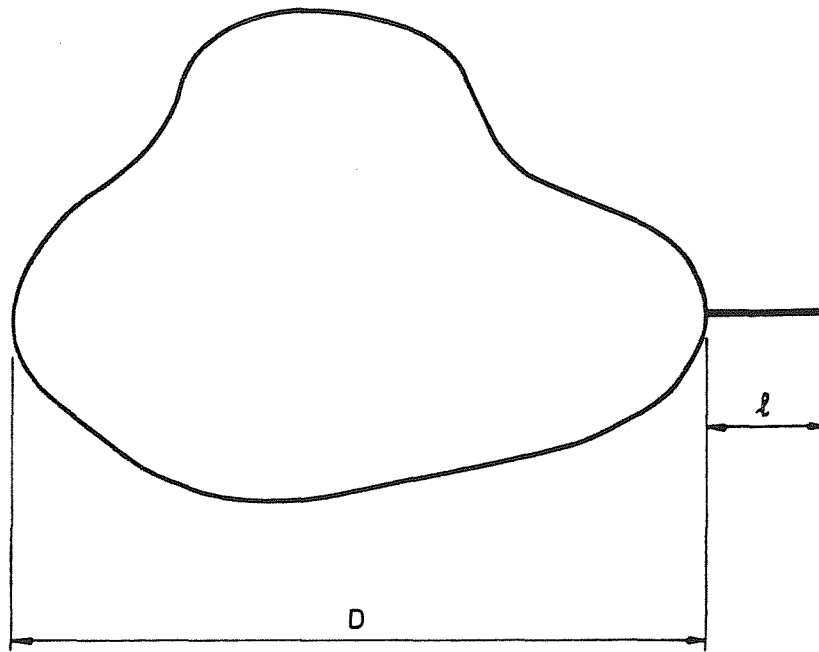


Fig 2.1 Crack at the edge of an arbitrarily shaped hole

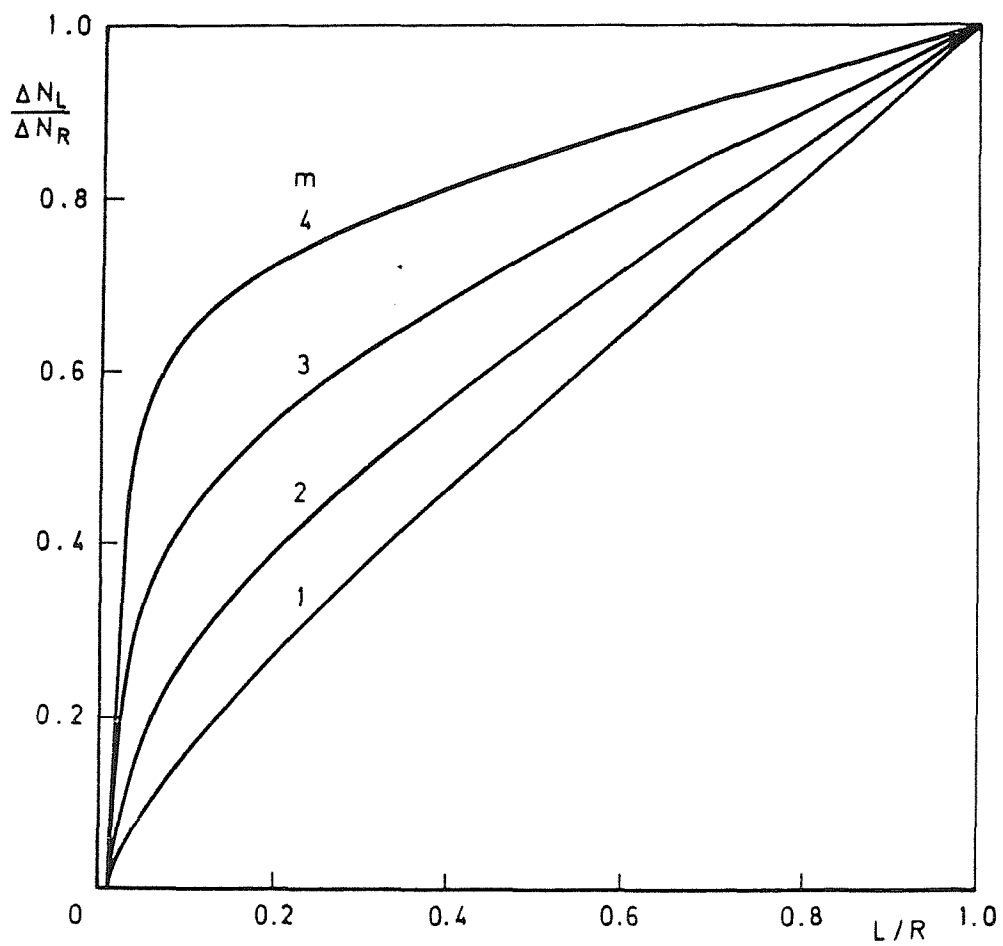


Fig 2.2 Ratio of crack growth-times for an initial crack length of  $0.01 R$

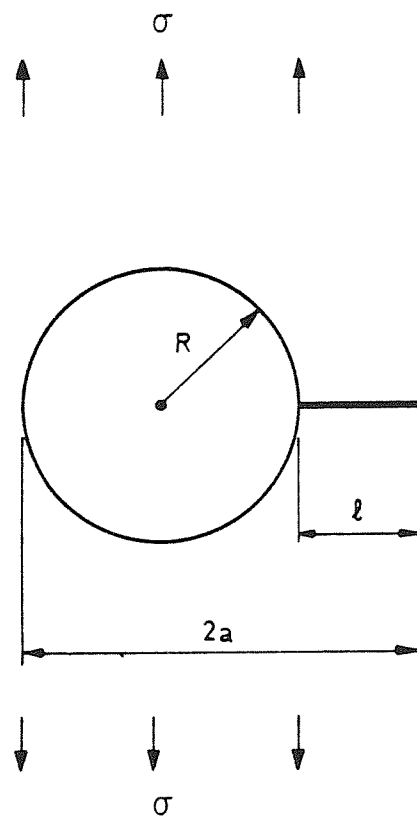


Fig 2.3 Crack at the edge of a hole in a uniformly stressed sheet

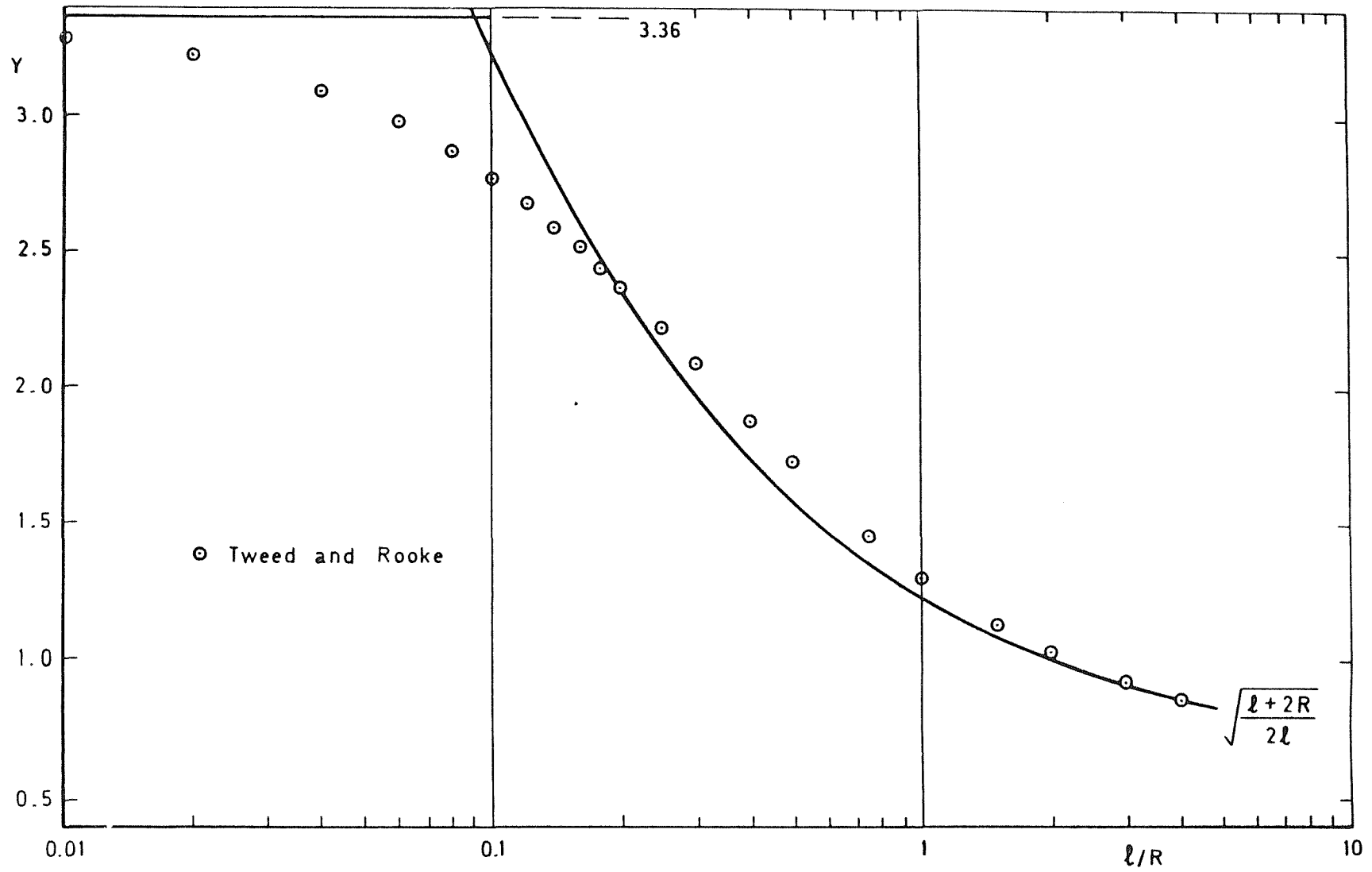


Fig 2.4 The geometry factor  $Y$  for a crack at the edge of a circular hole: remote tensile stress

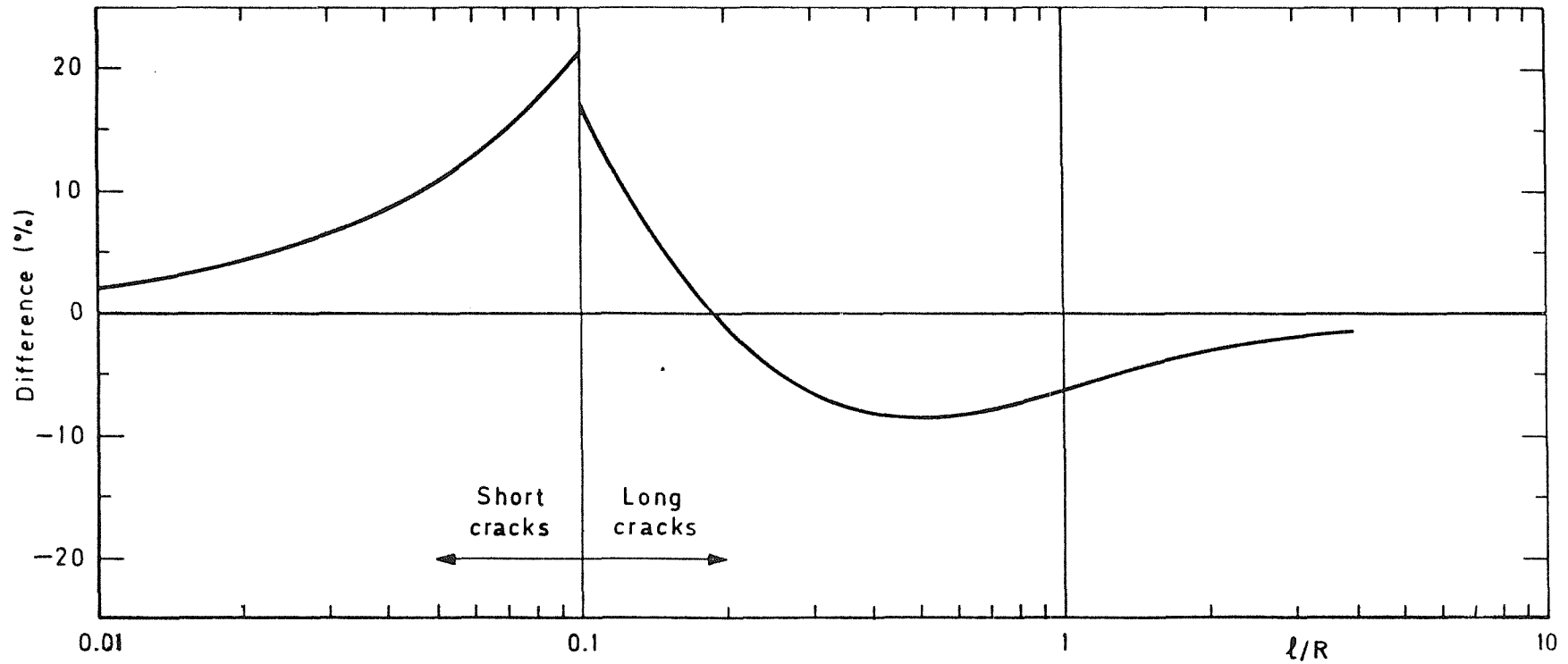


Fig 2.5 Percentage differences between approximate and numerical solutions for the stress intensity factor for a singly cracked hole - remote tensile stress

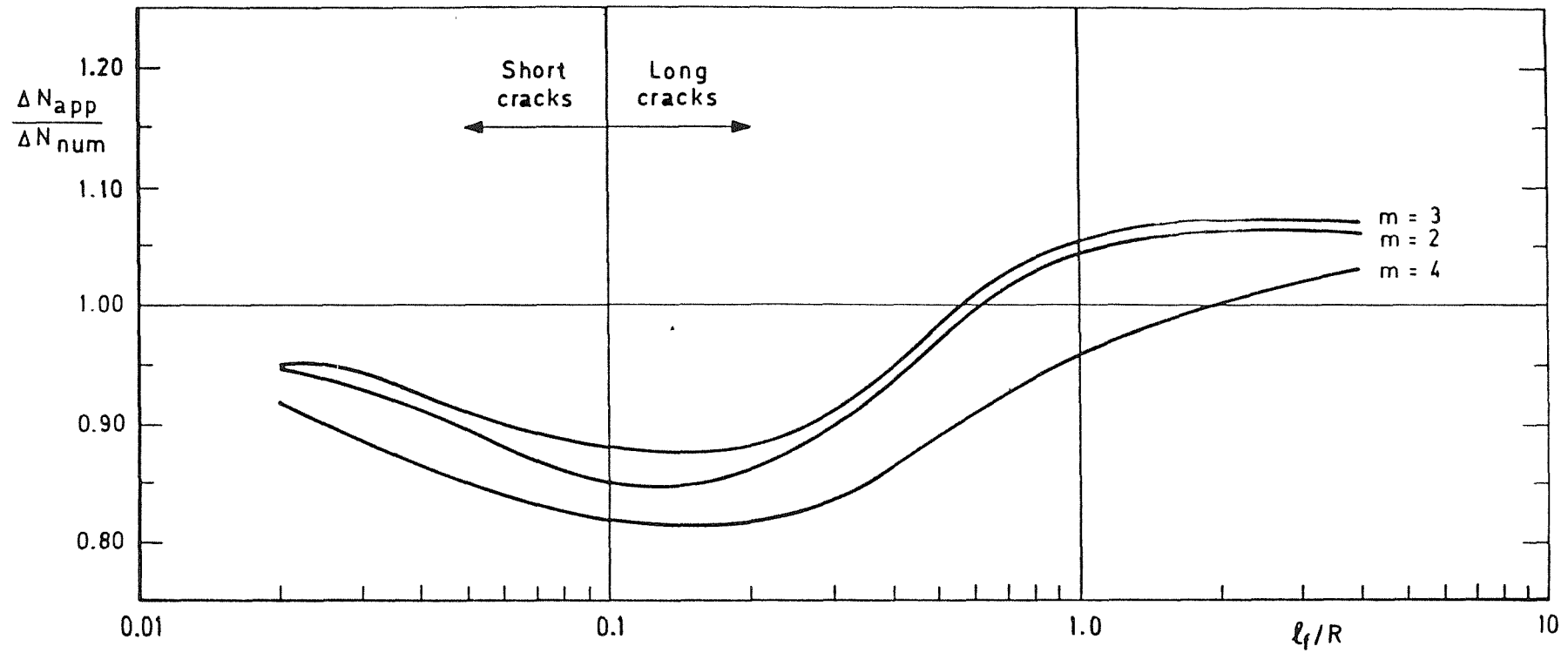


Fig 2.6 Ratio of growth-times for a crack at the edge of a circular hole - remote loading ( $\ell_i/R = 0.01$ )

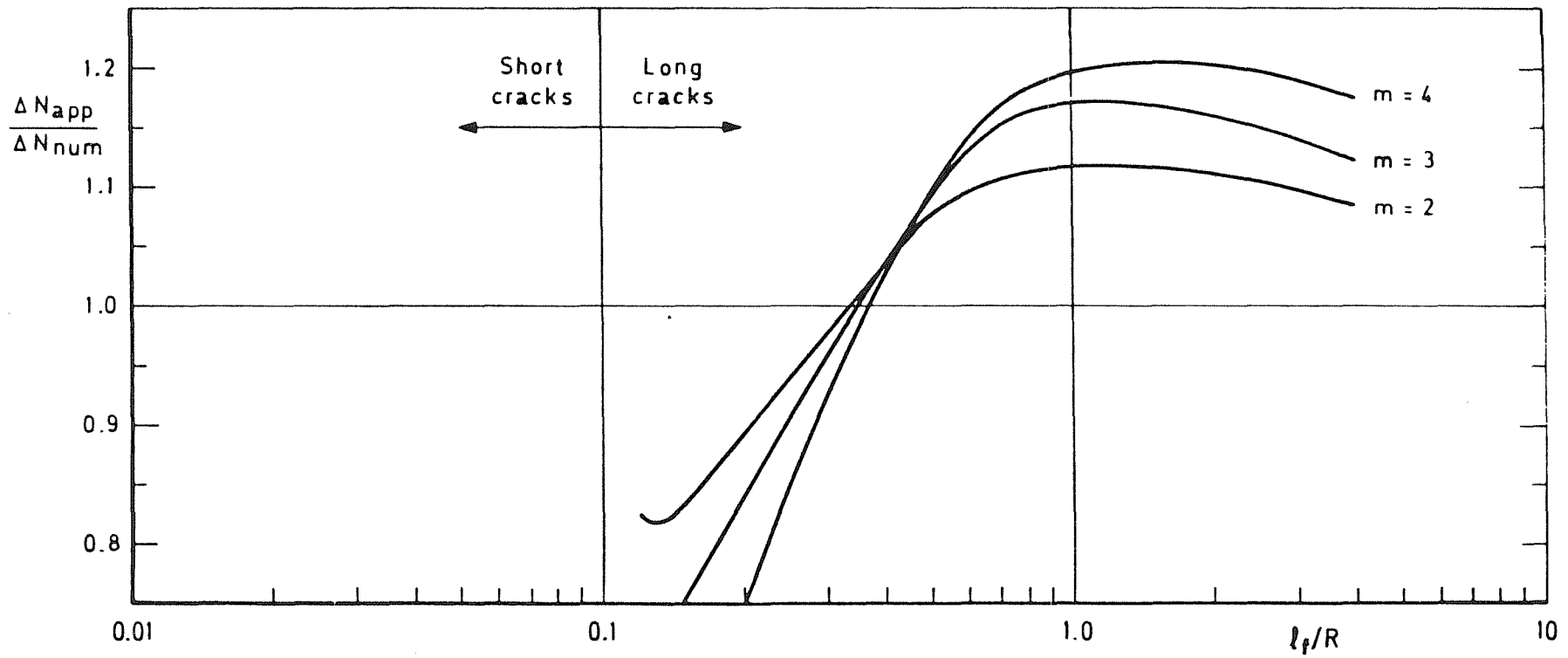


Fig 2.7 Ratio of growth-times for a crack at the edge of a circular hole - remote loading ( $\ell_i/R = 0.1$ )

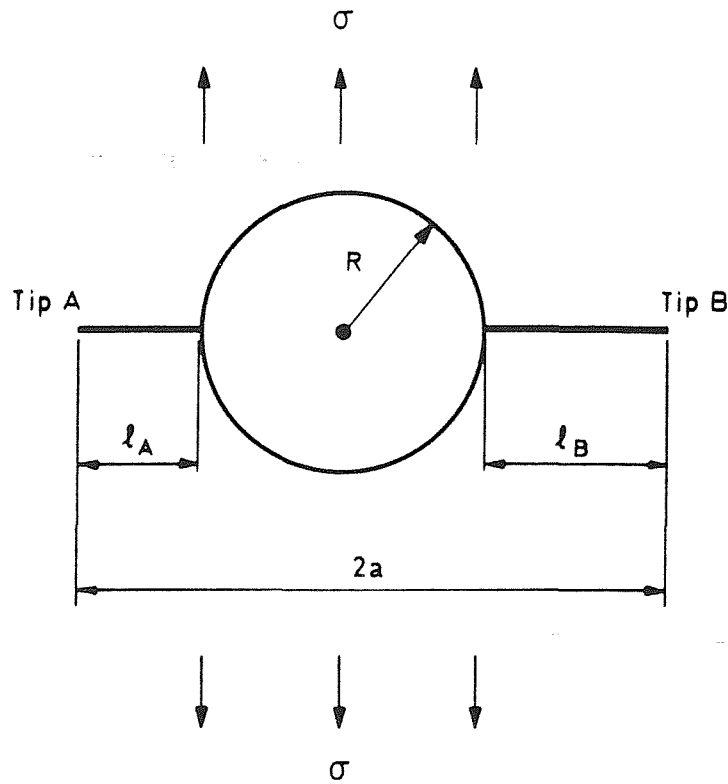


Fig 2.8 Two cracks at the edge of a circular hole in a uniformly stressed sheet

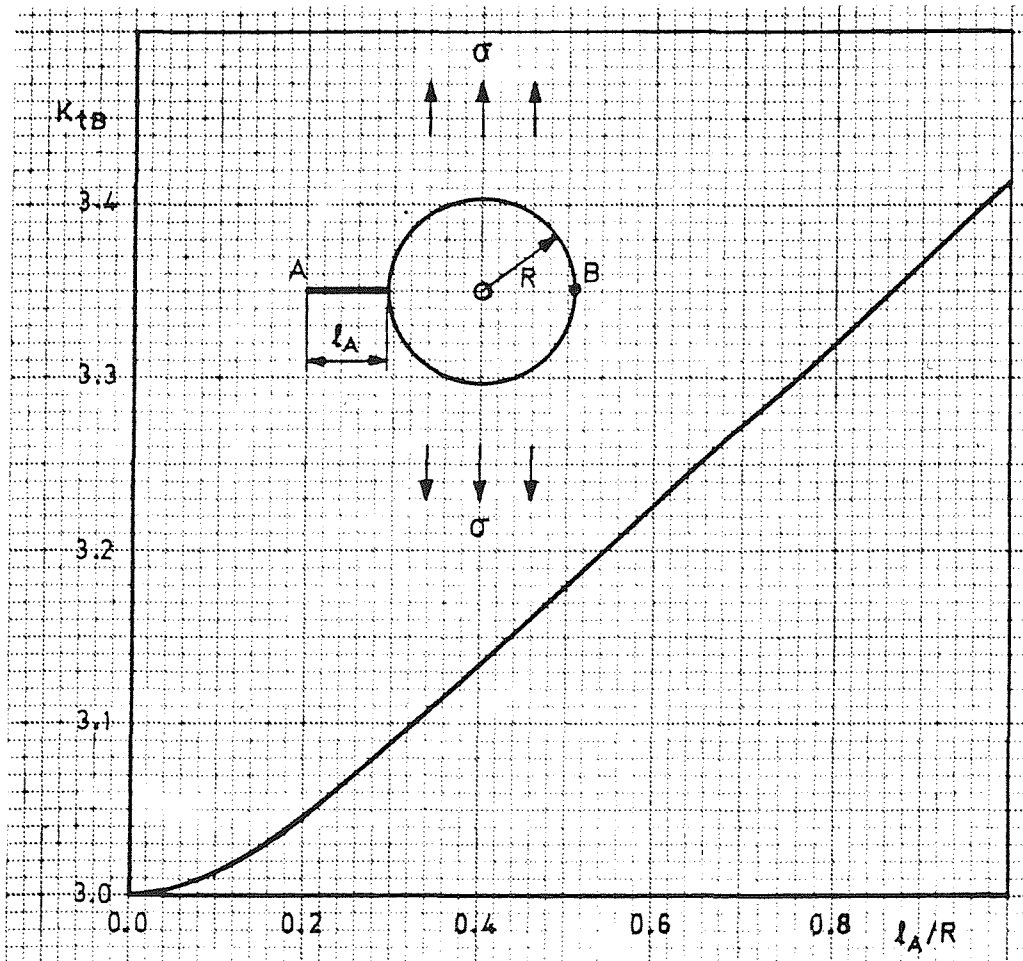


Fig 2.9 Stress concentration factor at B

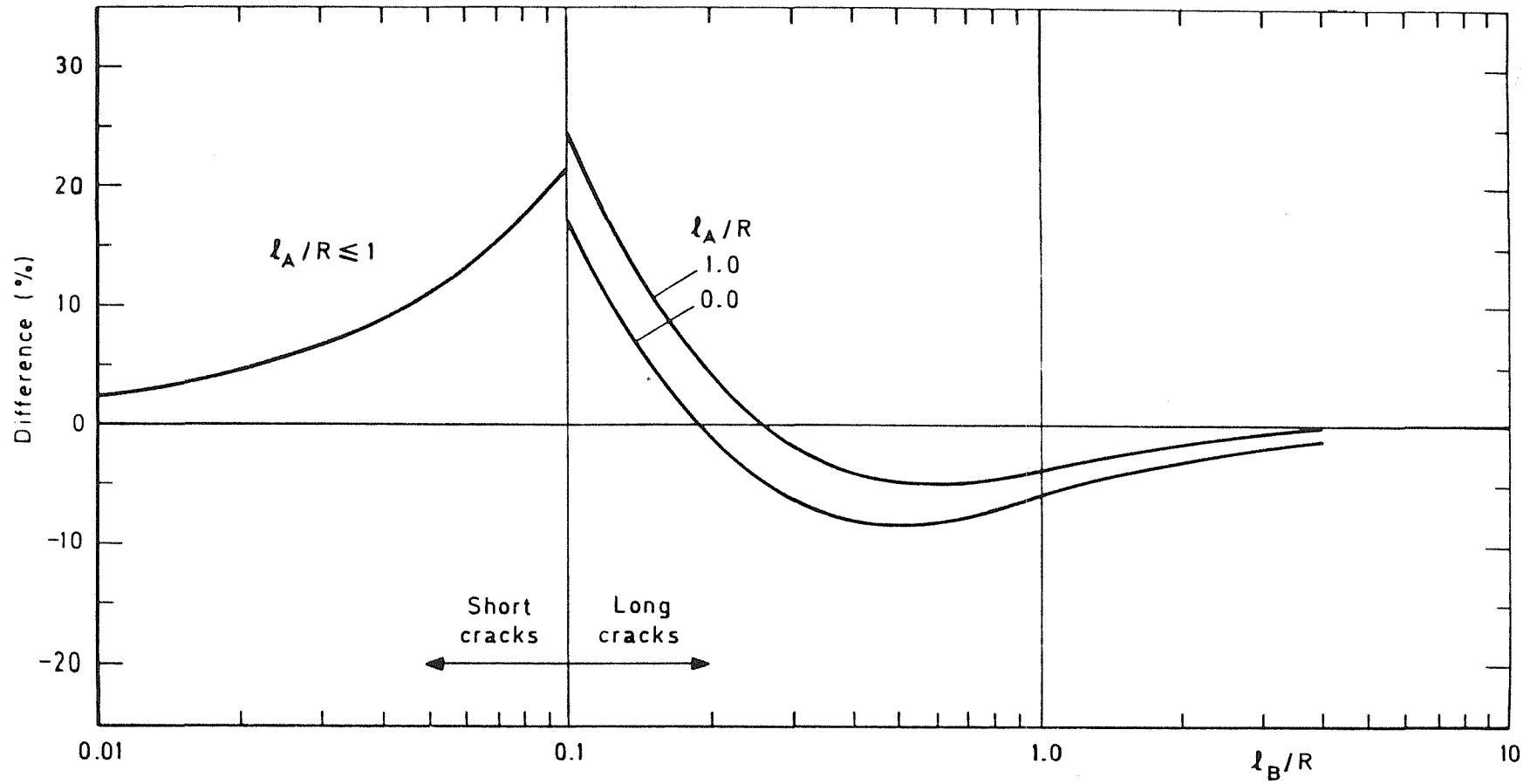


Fig 2.10 Percentage differences between approximate and numerical solutions for the stress intensity factor for a doubly cracked hole - remote loading

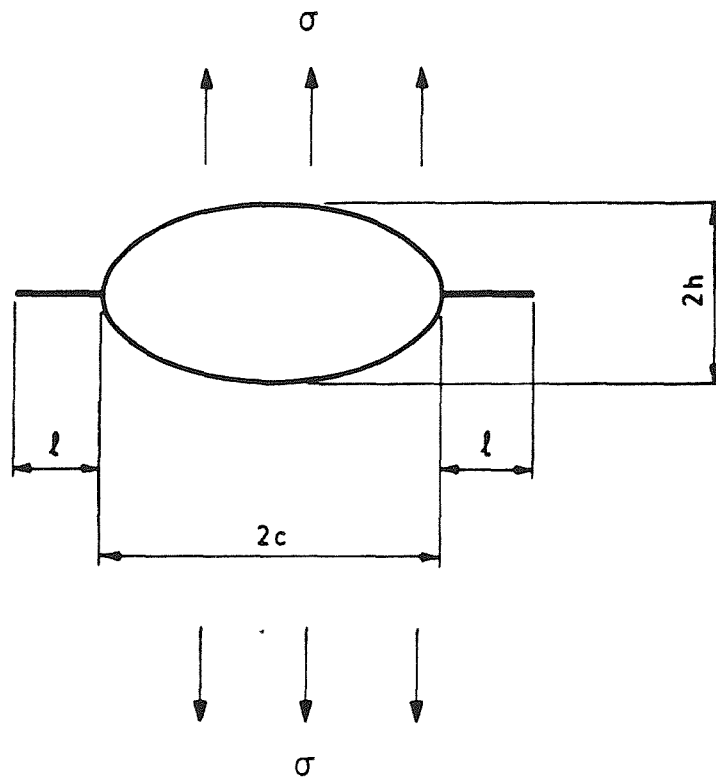


Fig 2.11 Two cracks at the edge of an elliptical hole in a uniformly stressed sheet

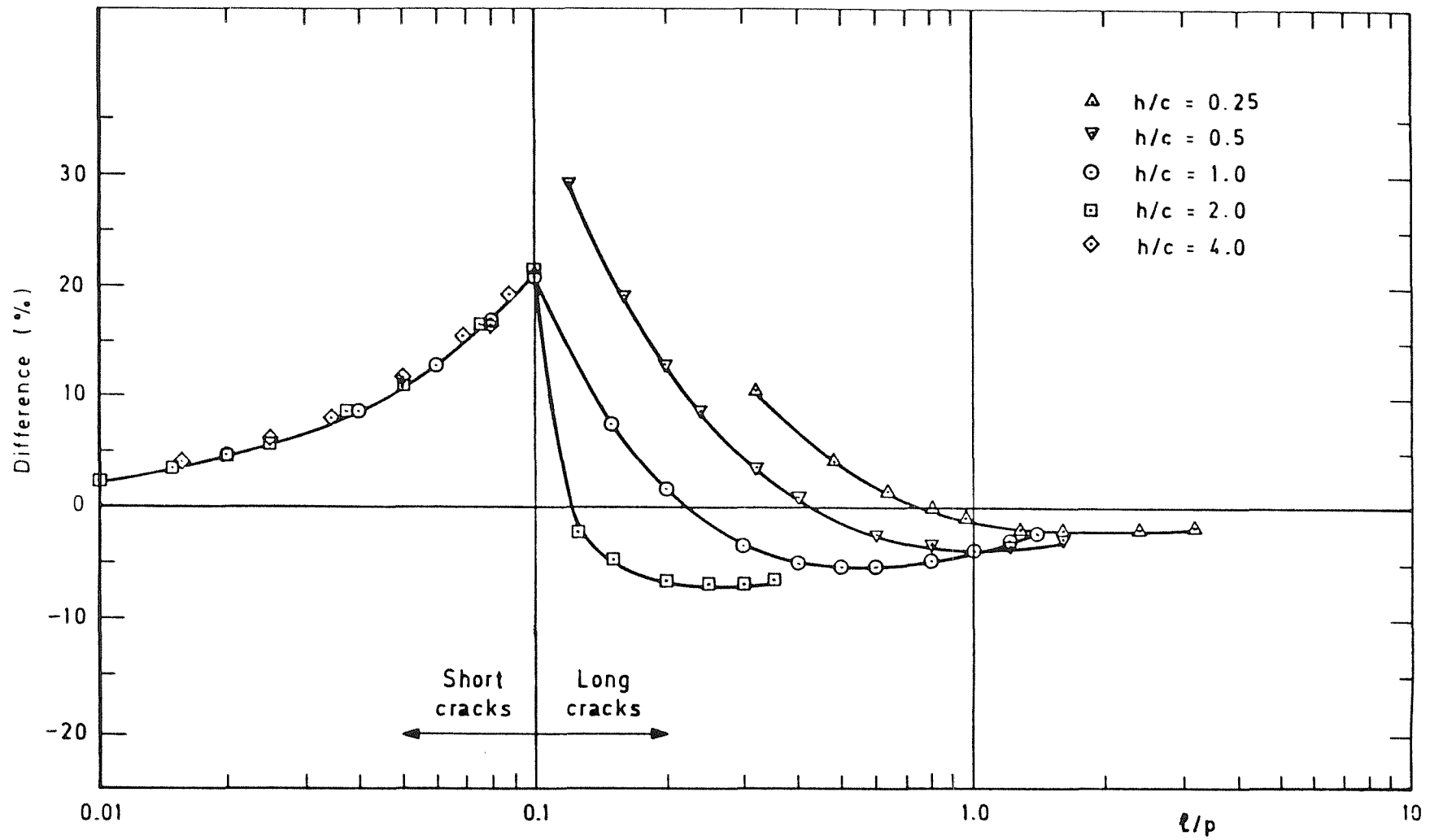


Fig 2.12 Percentage differences between approximate and numerical solutions for the stress intensity factor for two equal-length cracks at the edge of an elliptical hole - remote loading

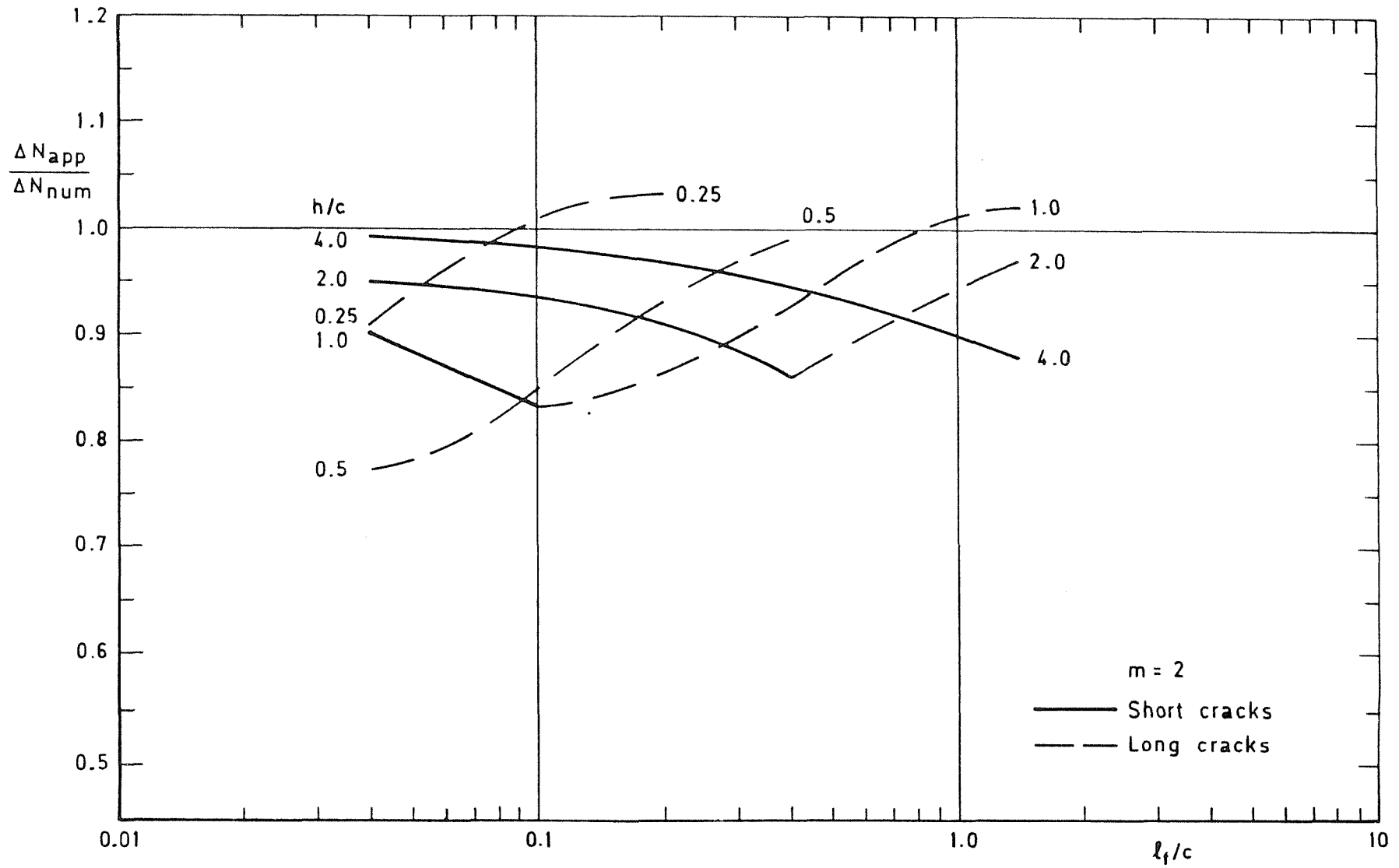


Fig 2.13 Ratio of growth-times for two cracks at the edges of an elliptical hole - remote loading ( $\ell_i/c = 0.02$ ,  $m = 2$ )

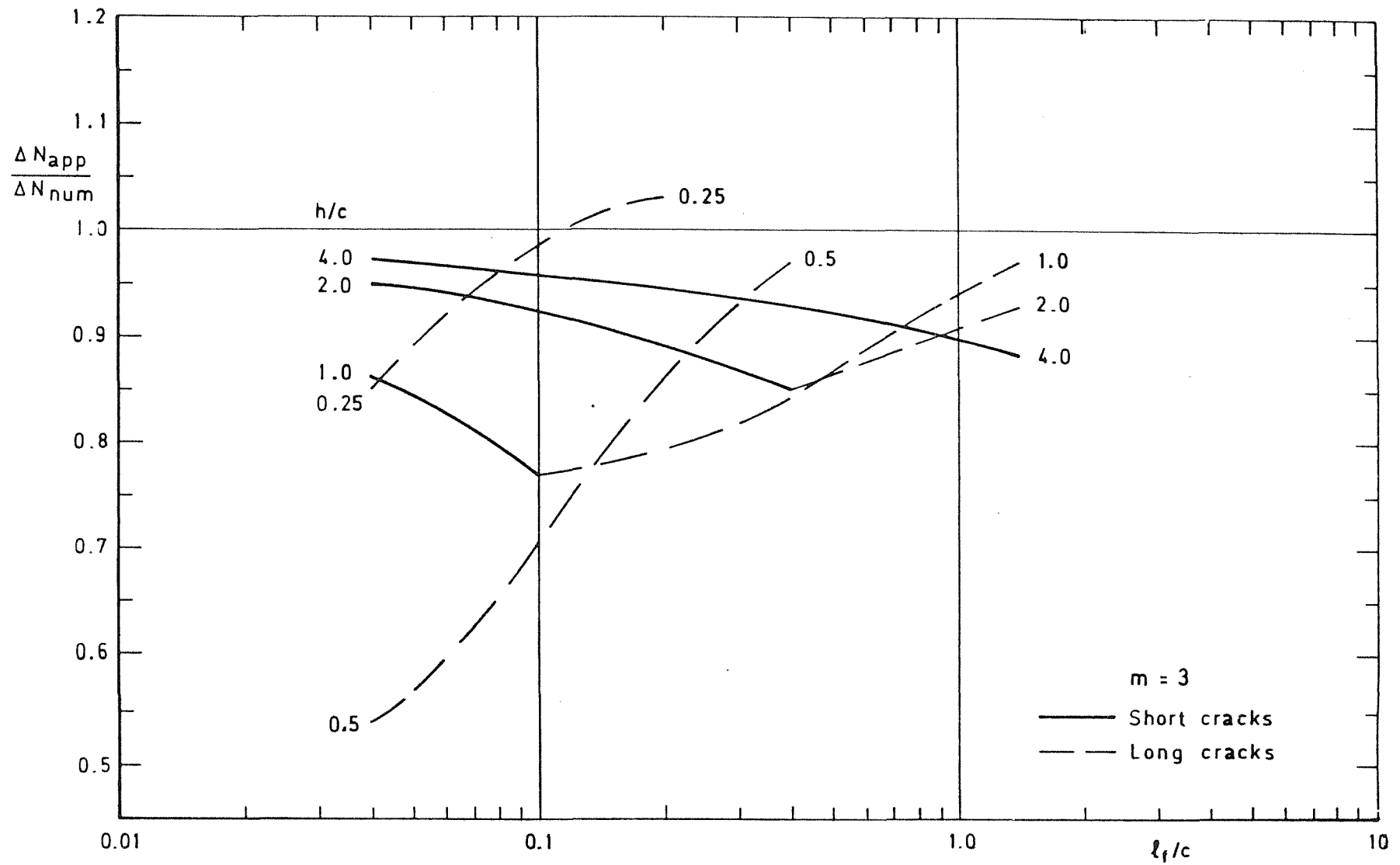


Fig 2.14 Ratio of growth-times for two cracks at the edges of an elliptical hole - remote loading ( $\ell_j/c = 0.02$ ,  $m = 3$ )

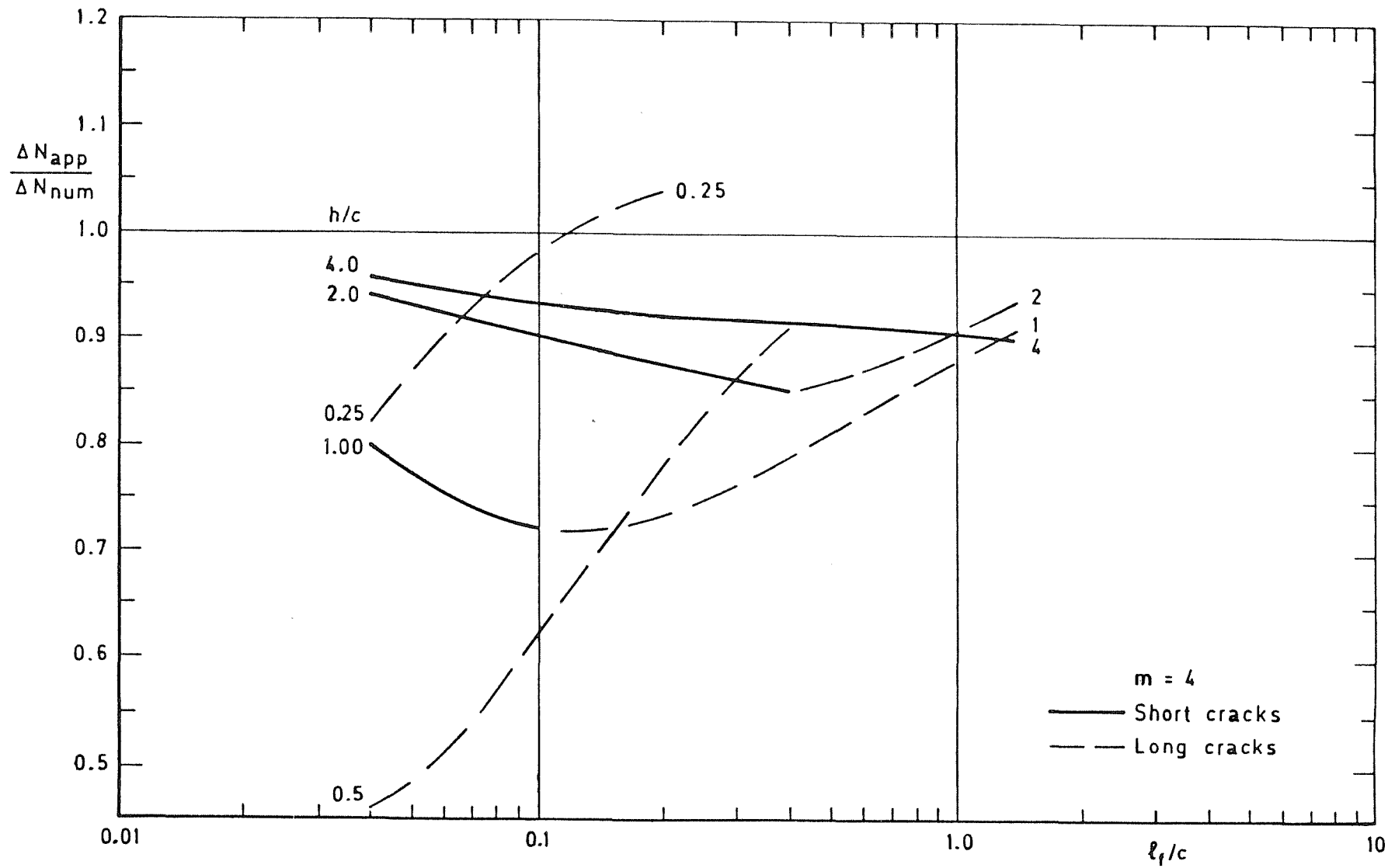


Fig 2.15 Ratio of growth-time for two cracks at the edges of an elliptical hole - remote loading ( $\ell_j/c = 0.02$ ,  $m = 4$ )

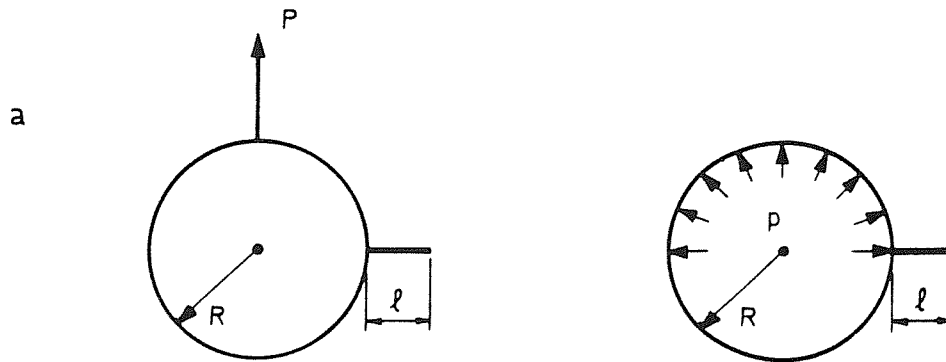


Fig 2.16a Crack at a hole subjected to either a localised force  $P$  or a pressure  $p$

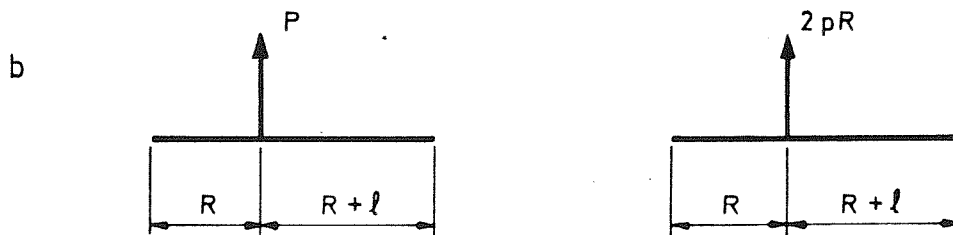


Fig 2.16b Equivalent cracks for long-crack approximation

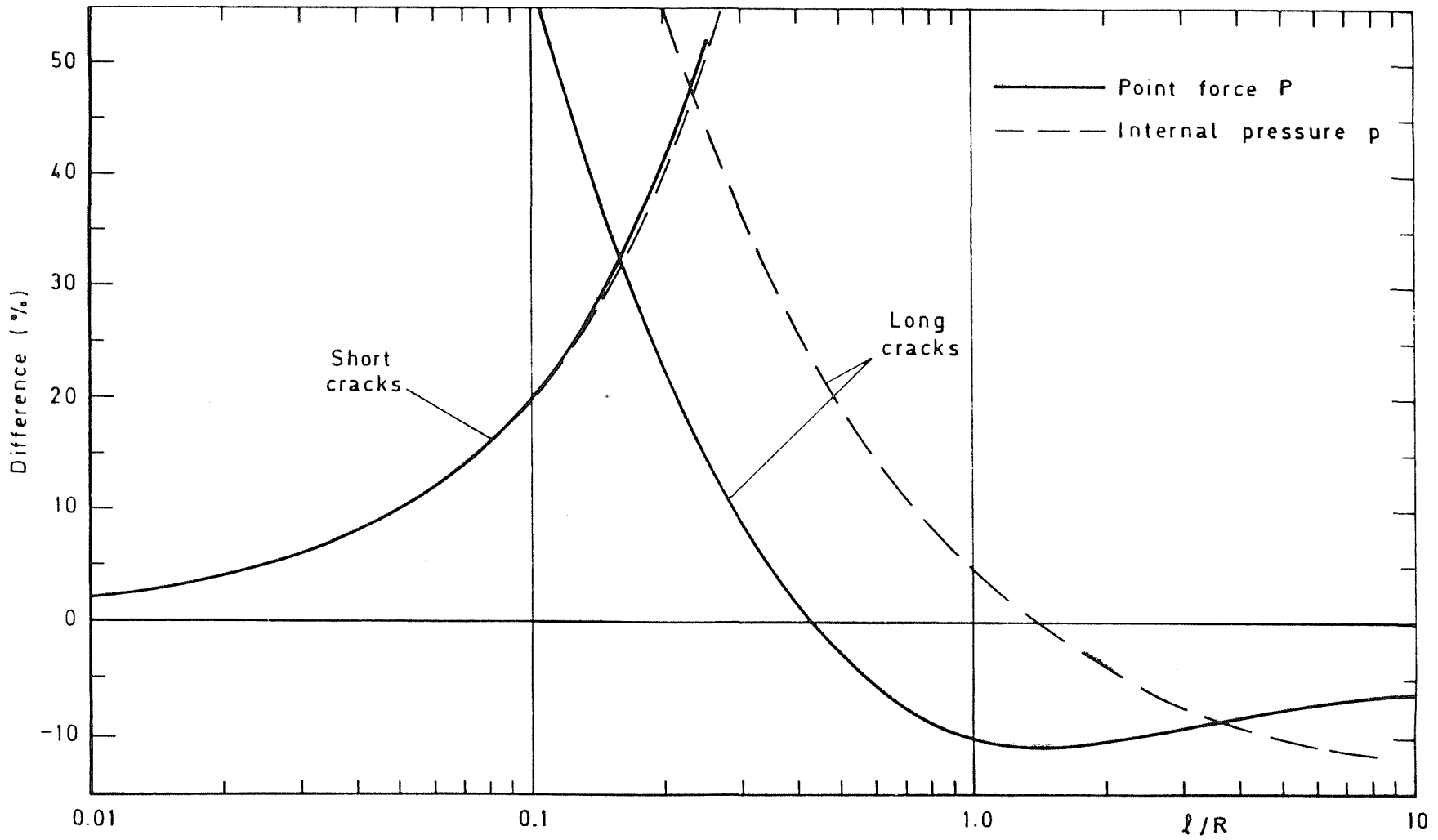


Fig 2.17 Percentage differences between approximate and numerical solutions for the stress intensity factor for a single cracked hole - local loading

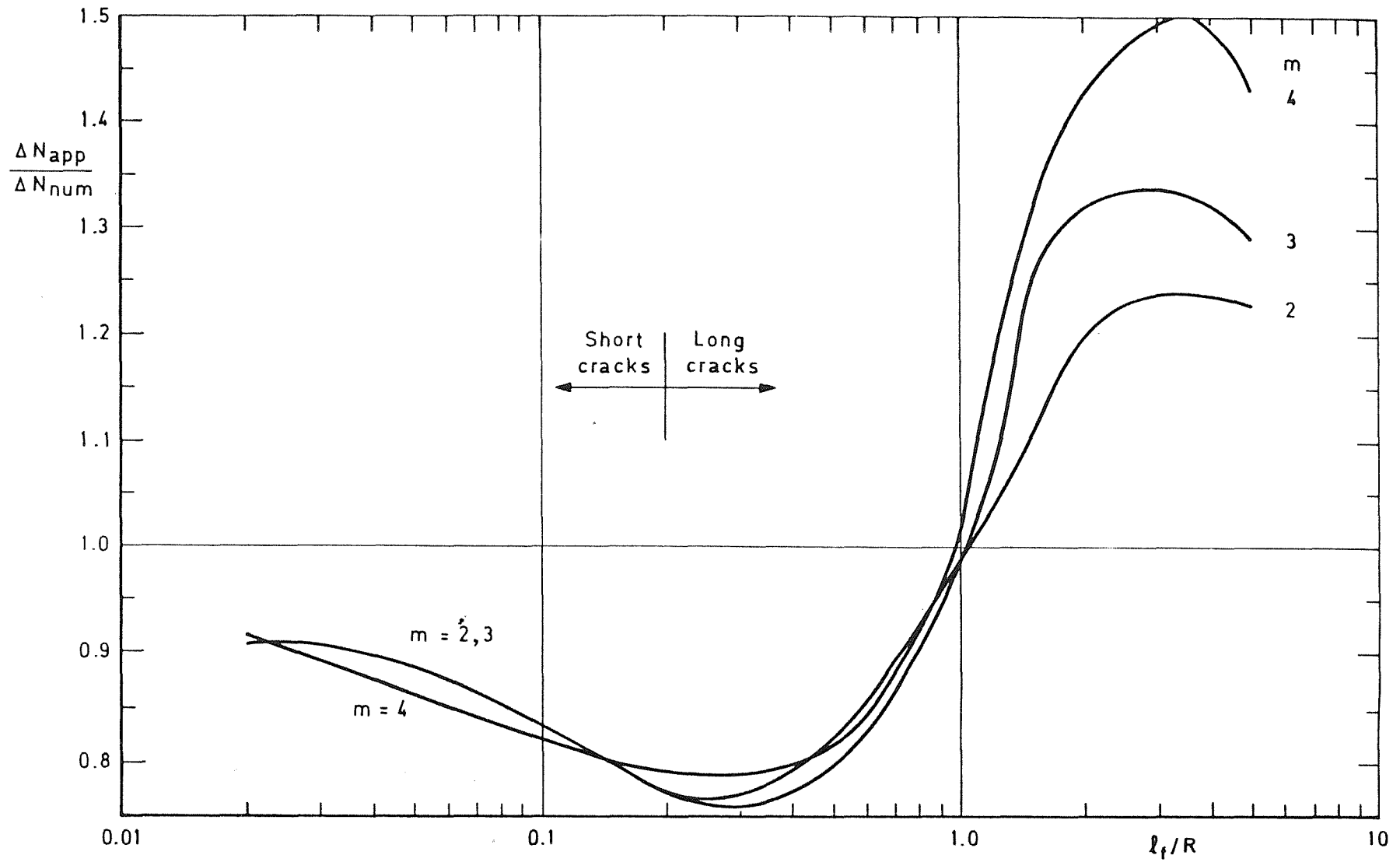


Fig 2.18 Ratio of growth-times for a crack at the edge of a circular hole - force  $P$  at the hole ( $l_i/R = 0.01$ )

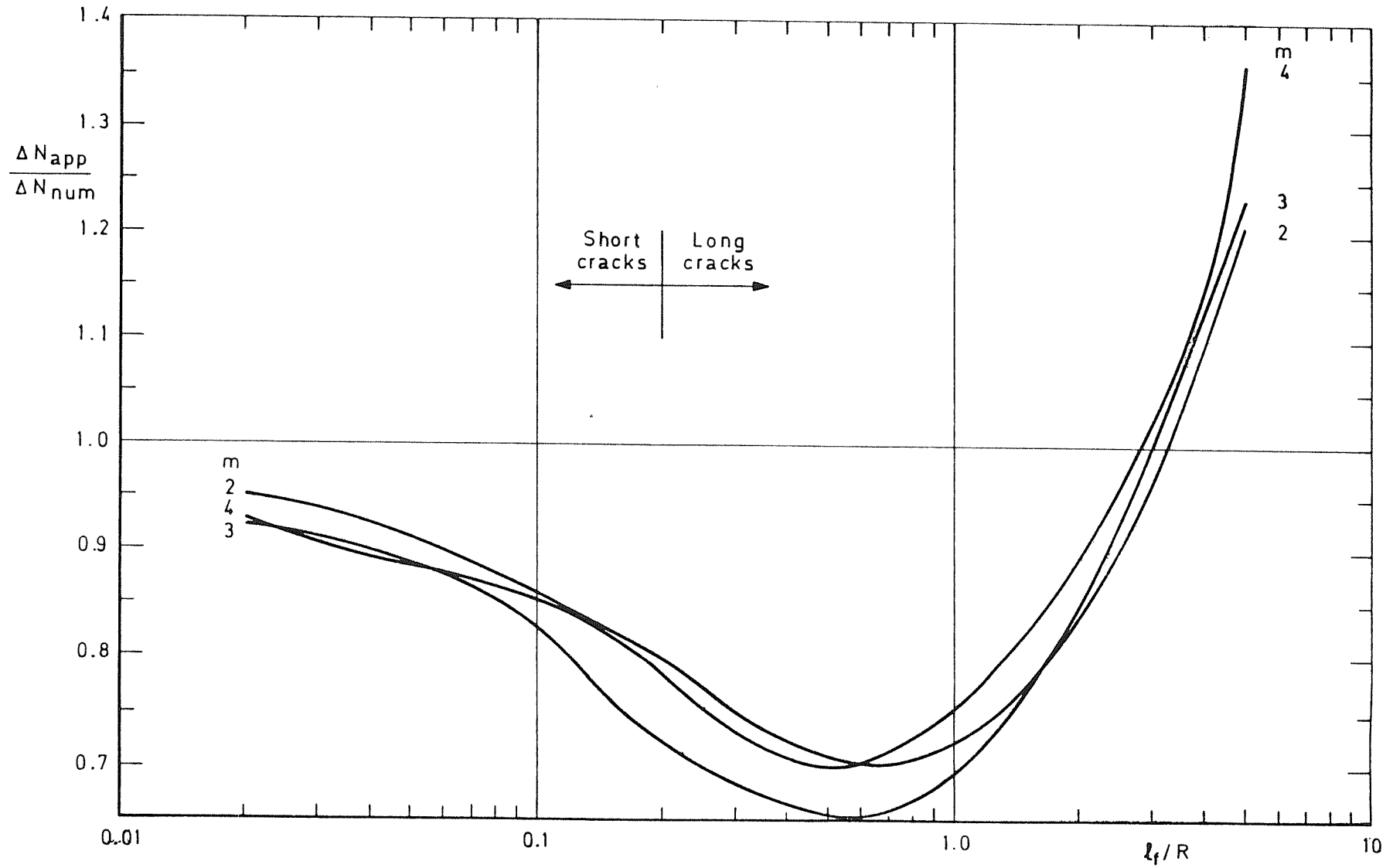


Fig 2.19 Ratio of growth-times for a crack at the edge of a circular hole - pressure  $p$  in the hole ( $\ell_i / R = 0.01$ )

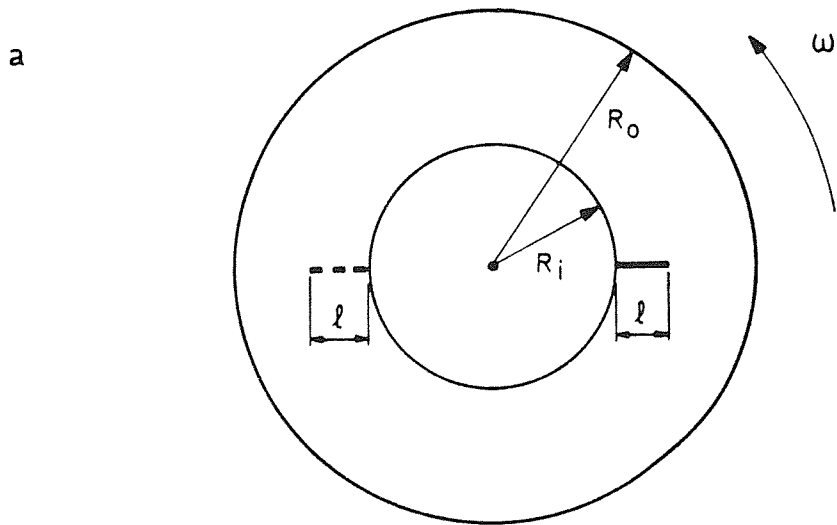


Fig 2.20a Crack(s) at the bore of a rotating disc

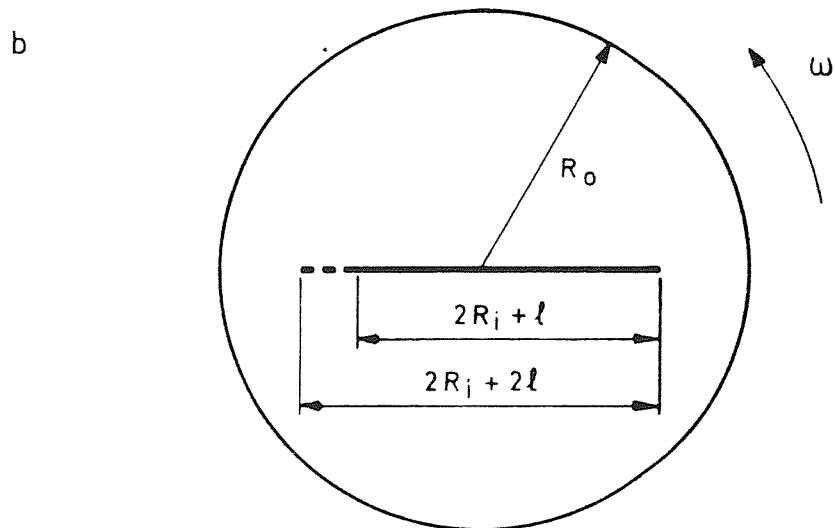


Fig 2.20b Equivalent crack for long crack approximation

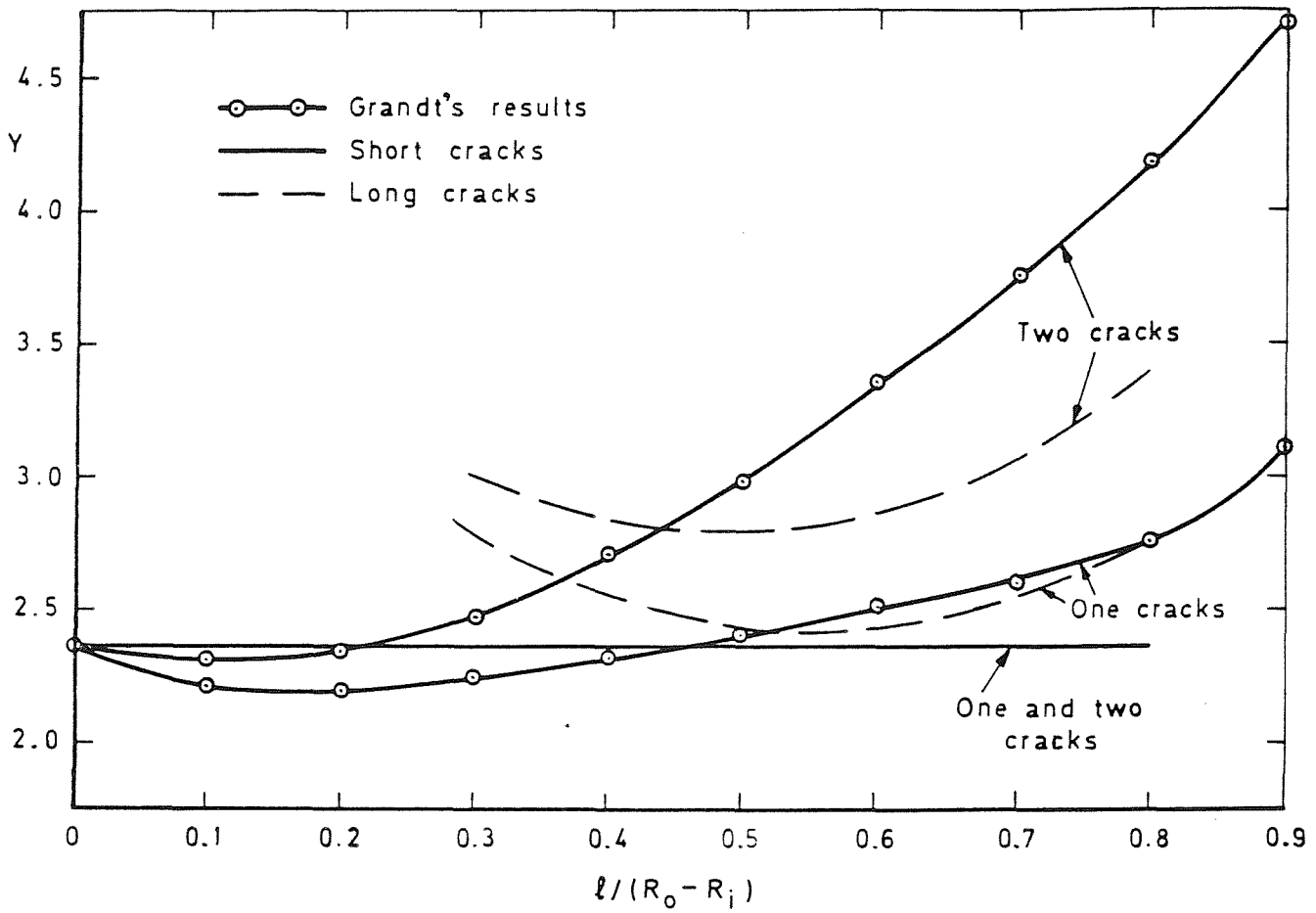


Fig 2.21 The geometry factor  $Y$  for a crack at the bore of a rotating disc ( $R_i/R_0 = 0.5$ ,  $\nu = 0.3$ )

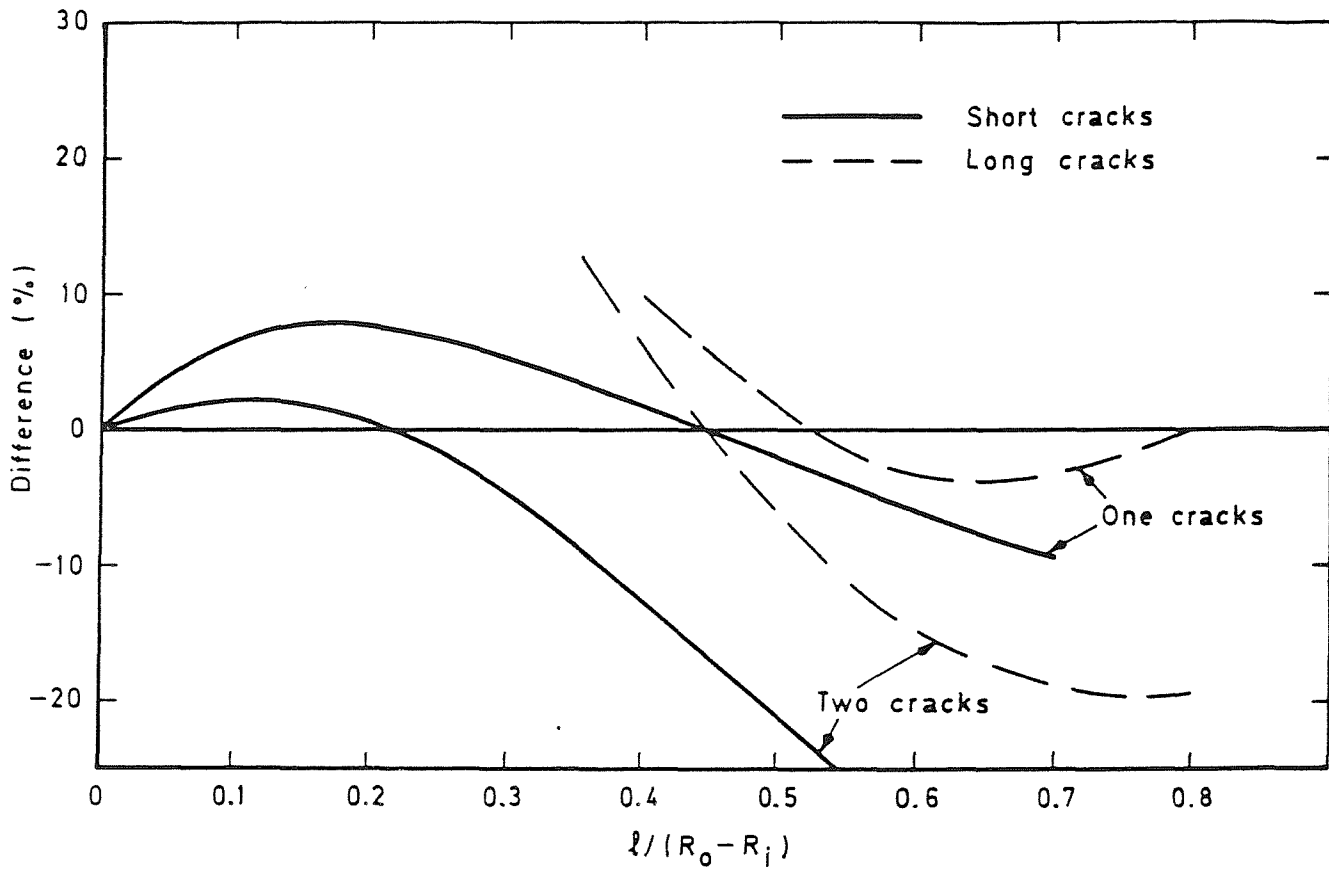


Fig 2.22 Percentage differences between approximate and numerical solutions for the stress intensity factor for a crack at the bore of a rotating disc ( $R_i/R_0 = 0.5$ ,  $\nu = 0.3$ )

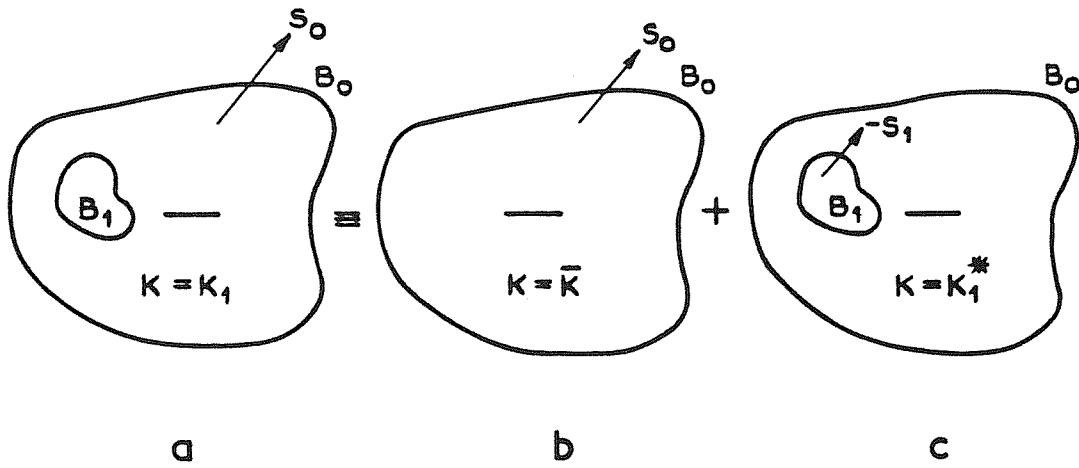


Fig 3.1 Superposition for a crack near one internal boundary

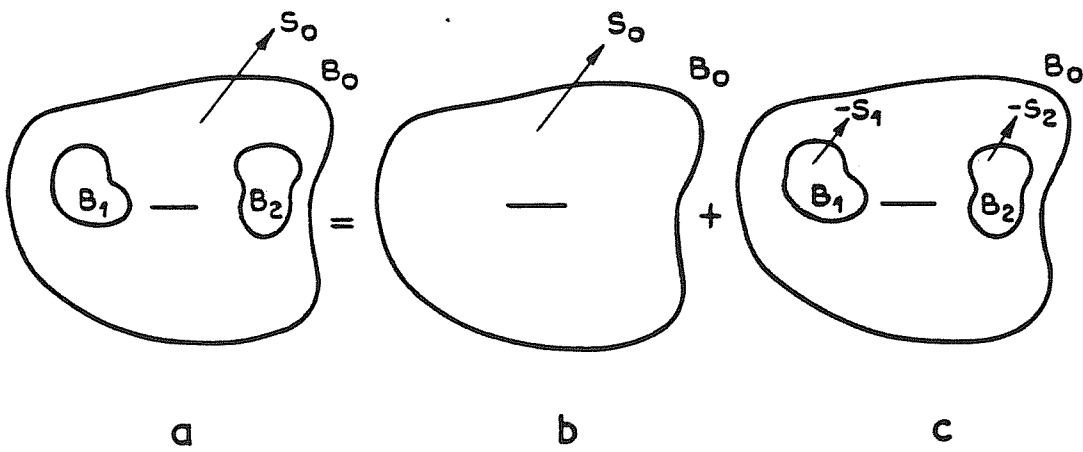


Fig 3.2 Superposition for a crack near two internal boundaries

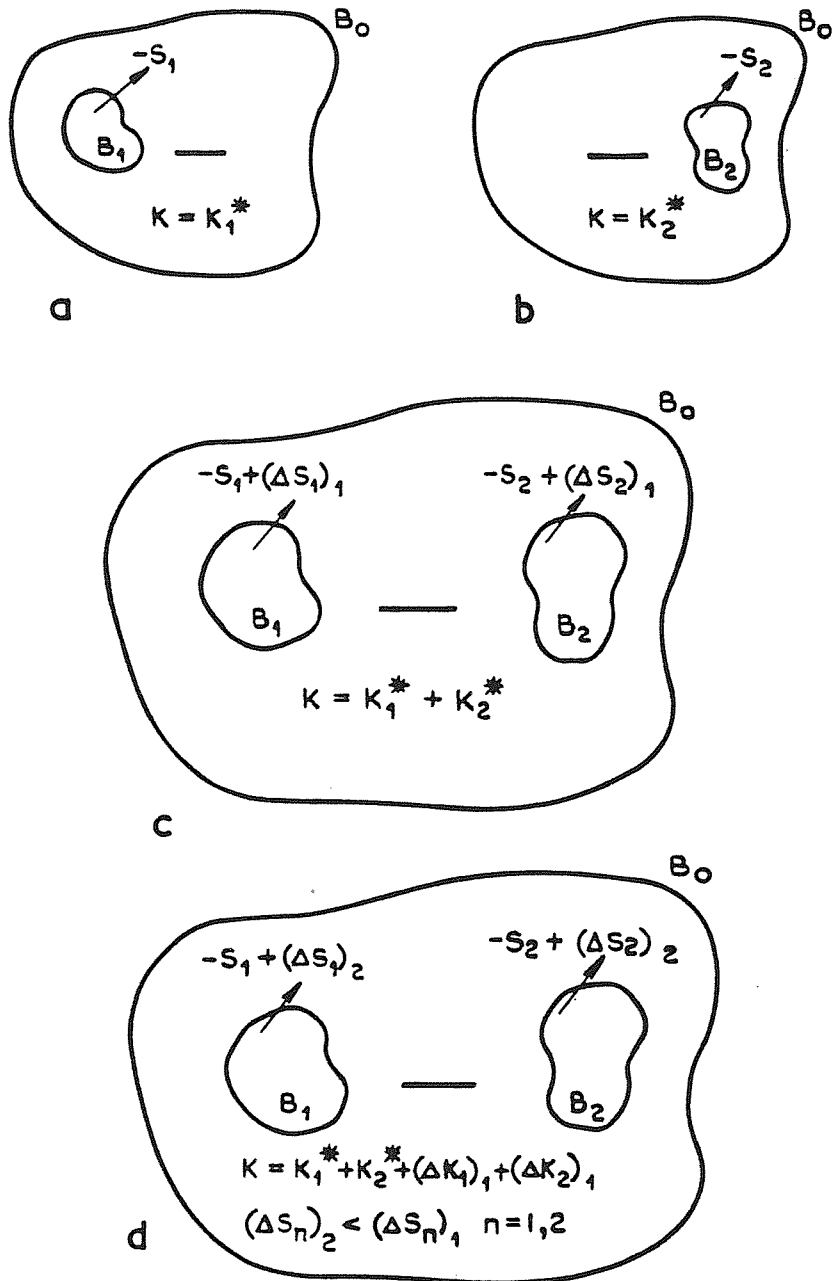


Fig 3.3 Stages in the Schwarz alternating technique for a crack near two boundaries

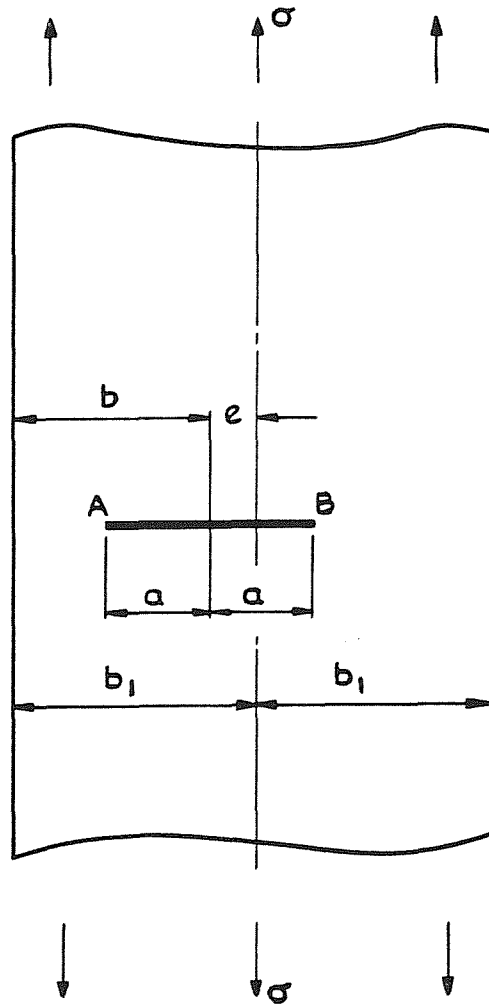


Fig 3.4 Eccentric crack in a finite width sheet subjected to a uniaxial tensile stress

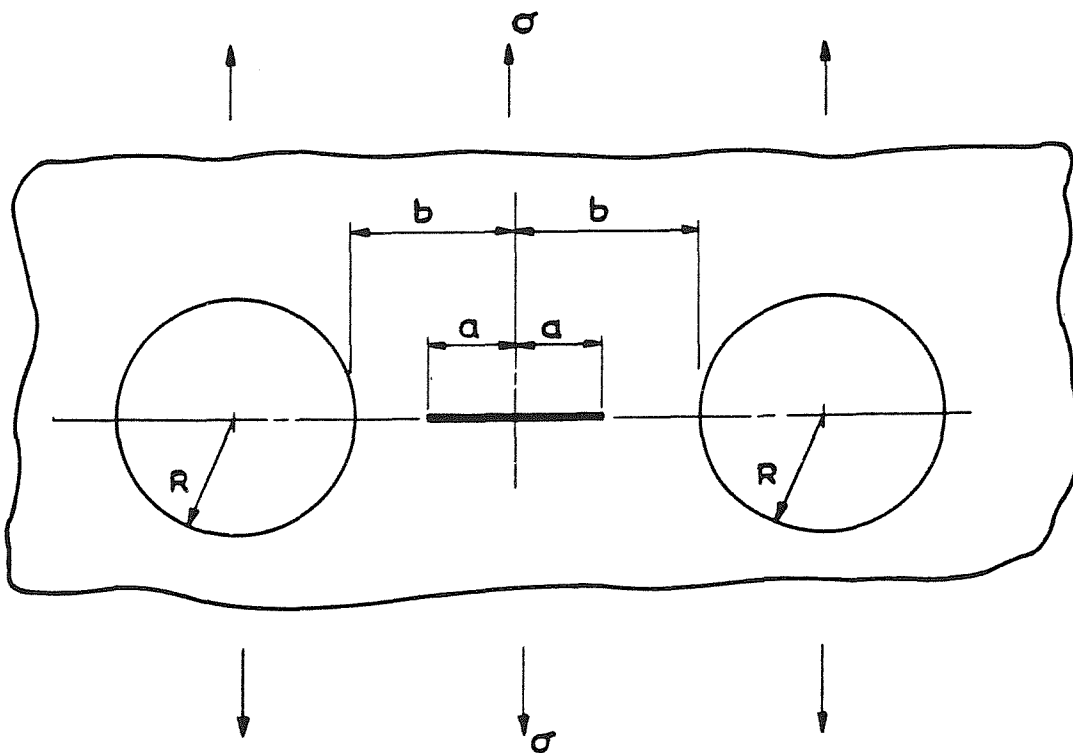


Fig 3.5 Crack between two holes in an infinite sheet subjected to a uniaxial tensile stress

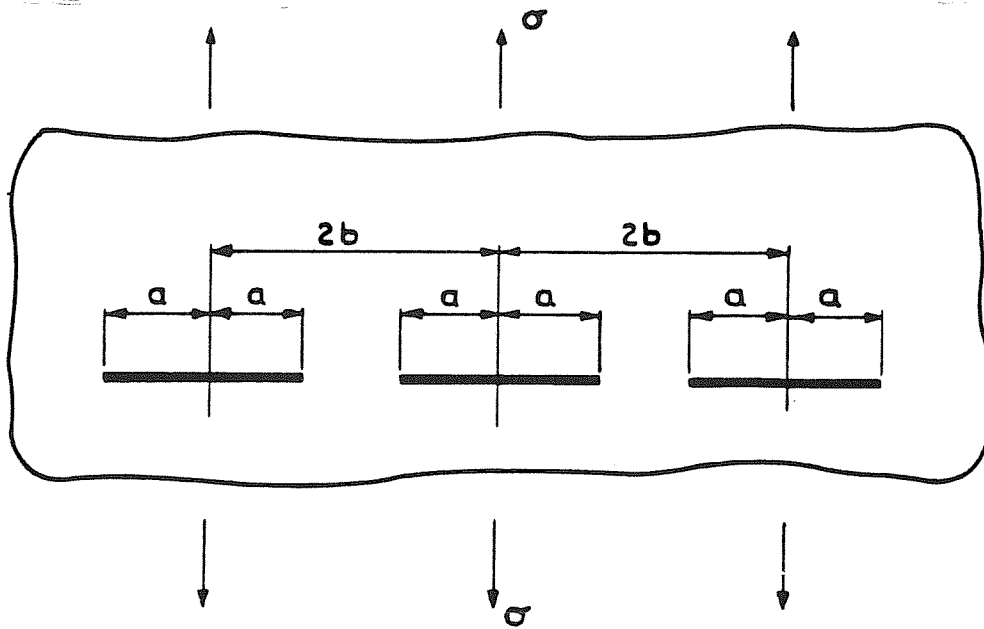


Fig 3.6 Odd number of collinear cracks in an infinite sheet subjected to a uniaxial tensile stress

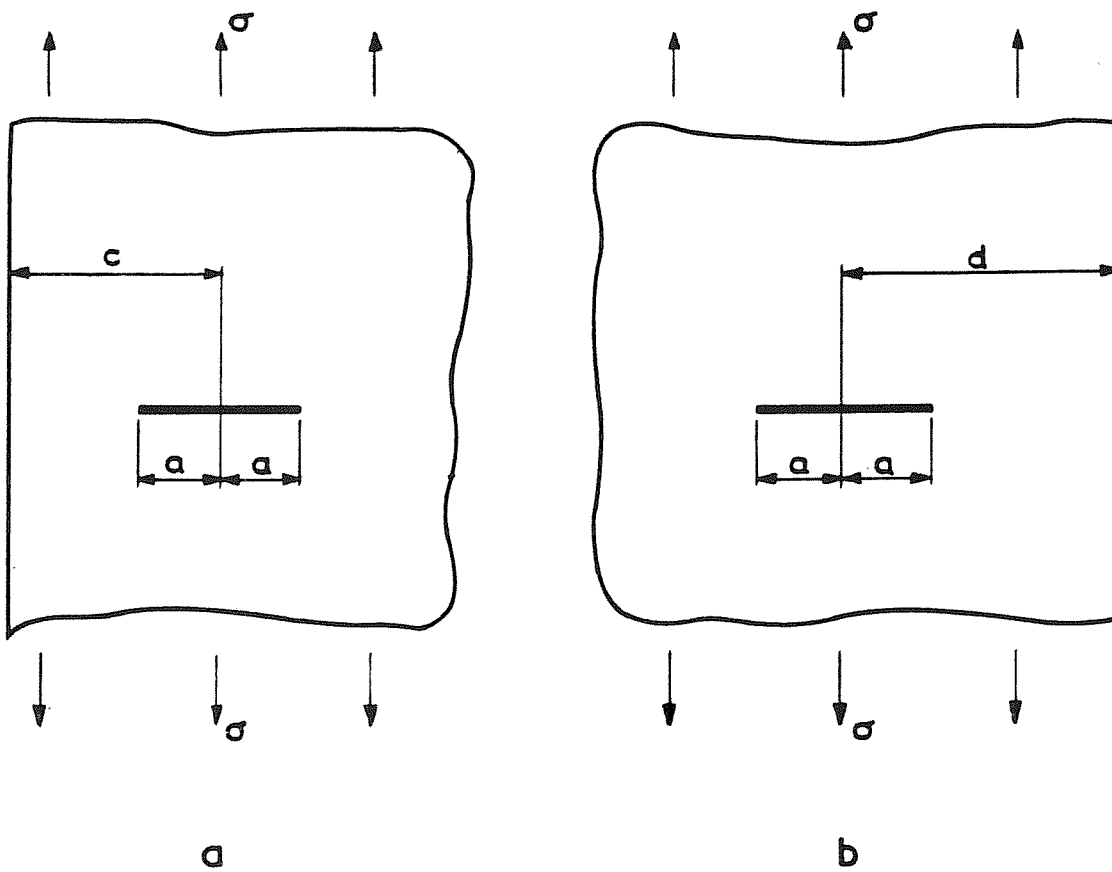


Fig 3.7 Crack near the edge of a half plane subjected to a uniform tensile stress; ancillary configuration for Fig 45 ( $d \geq c$ )

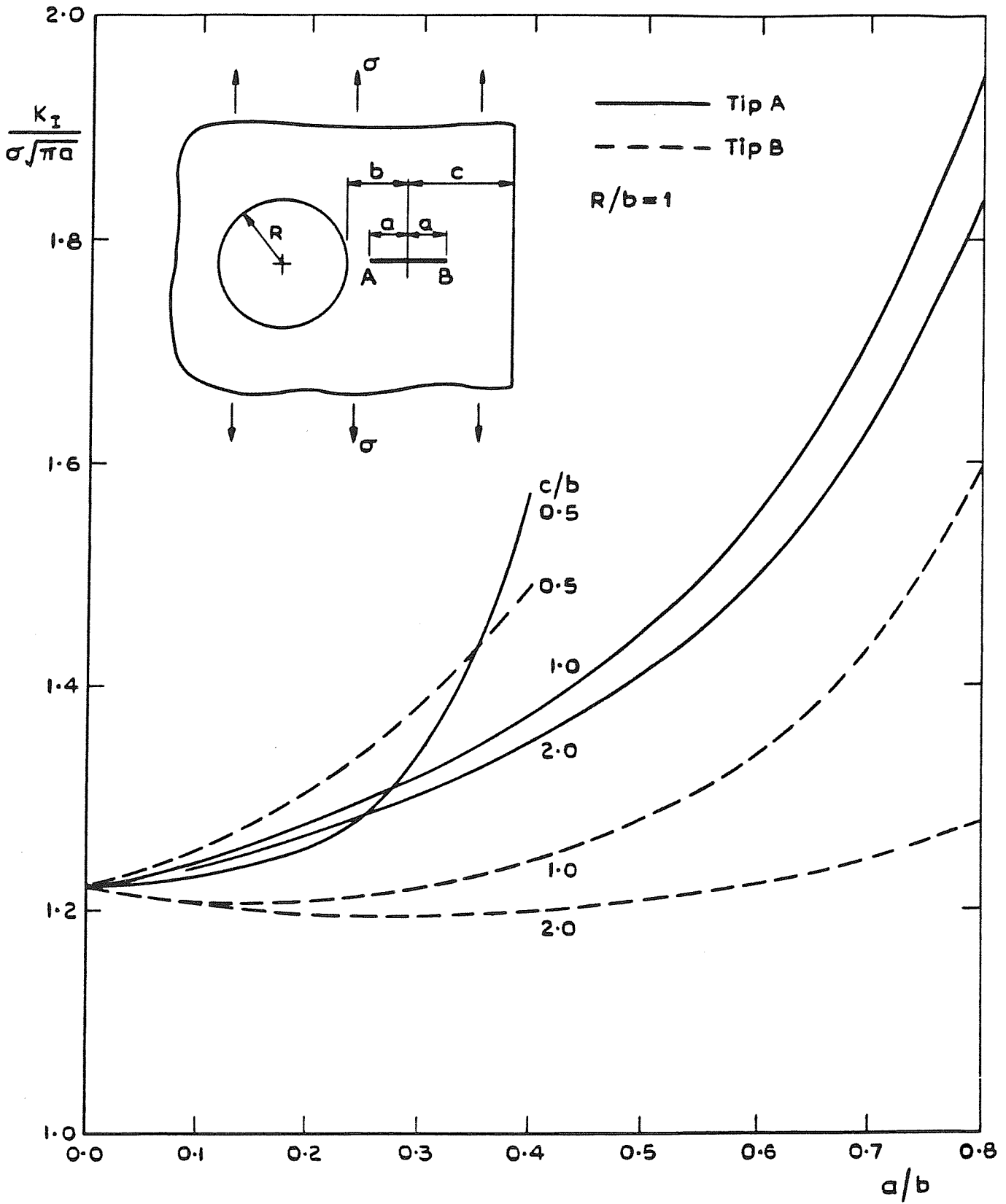


Fig 3.8 Stress intensity factors for a crack in the vicinity of a hole in a half plane subjected to a uniaxial tensile stress

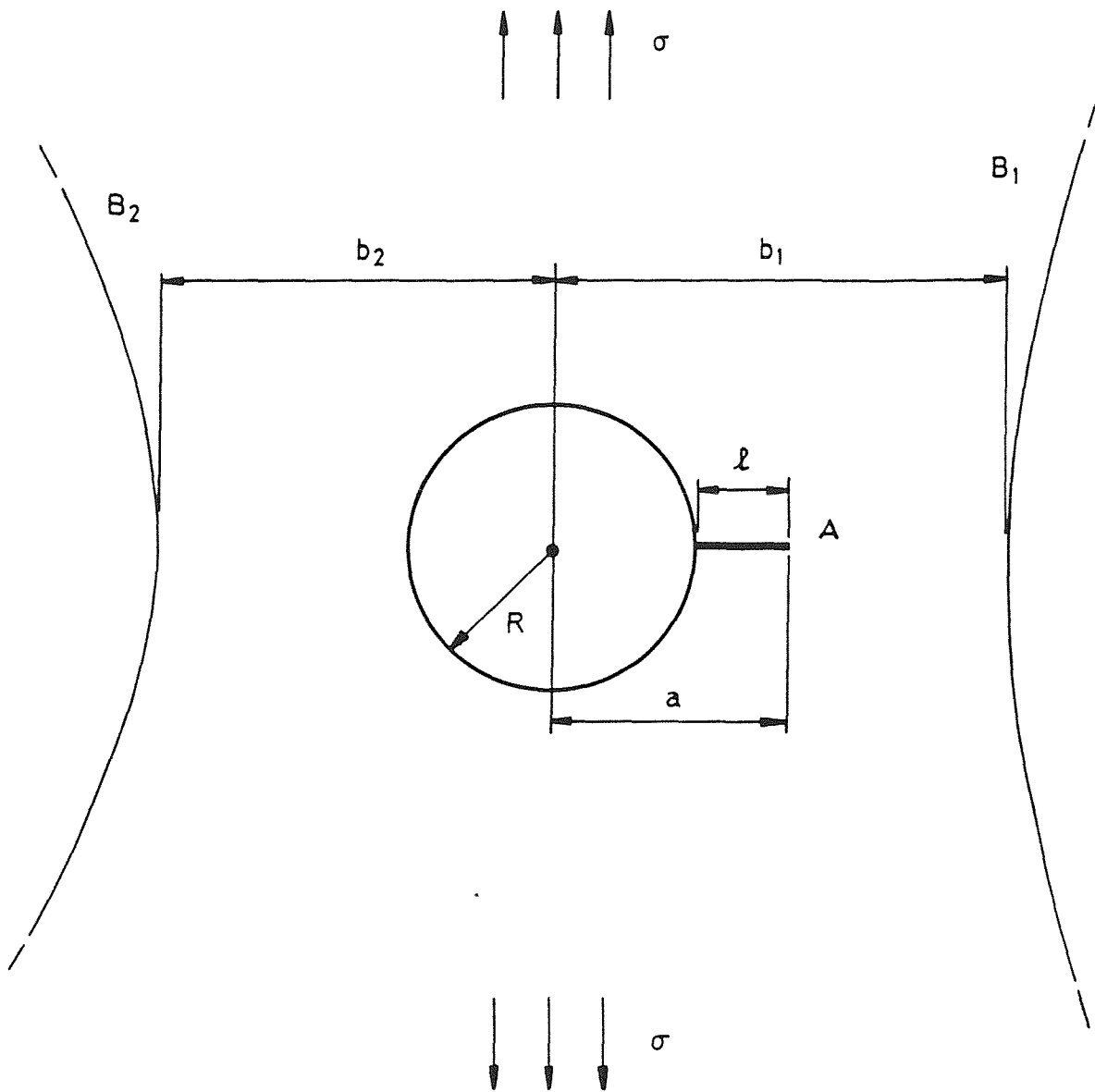


Fig 4.1 Radial crack at the edge of a circular hole between two boundaries

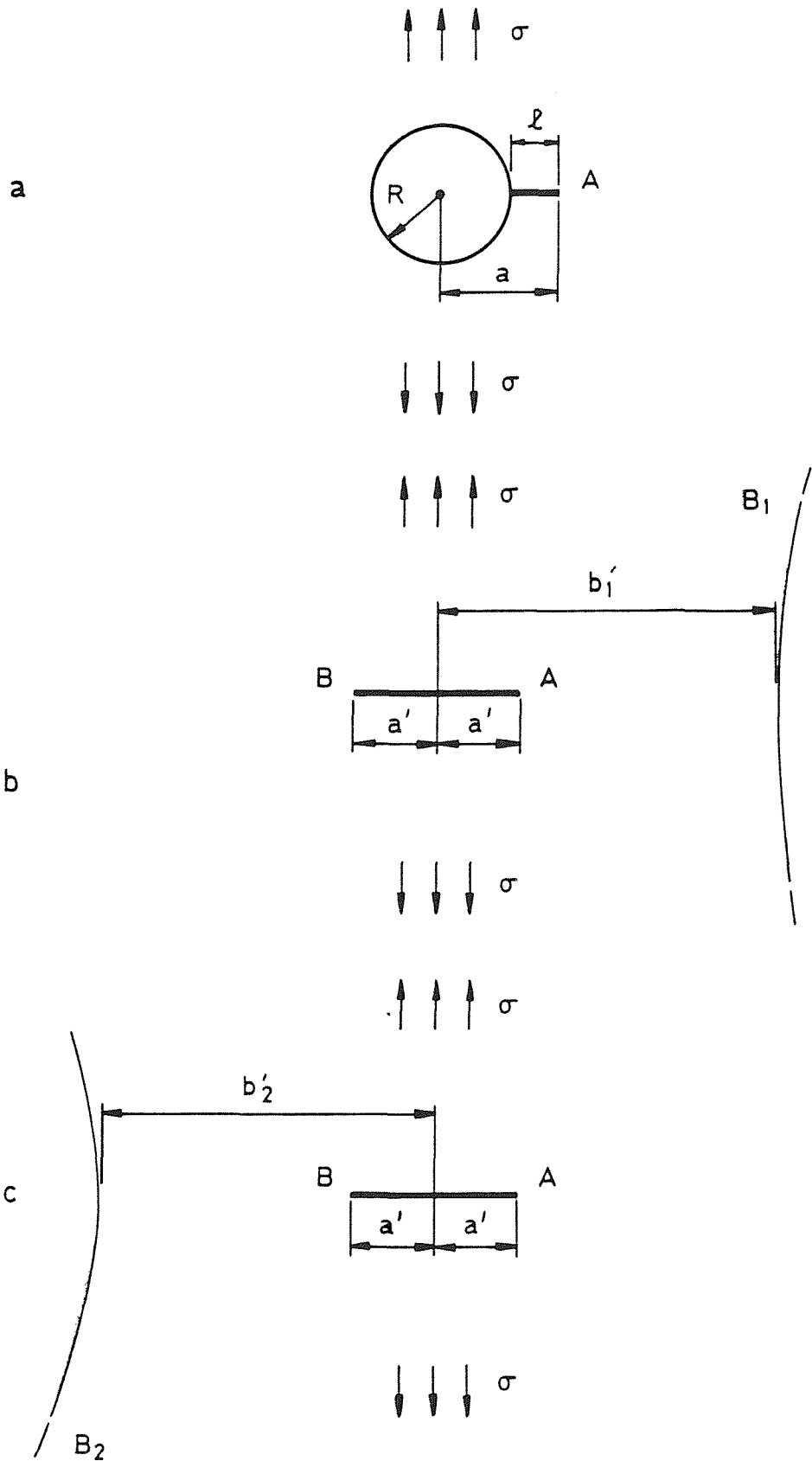


Fig 4.2 Ancillary configurations for a radial crack at the edge of a circular hole between two boundaries

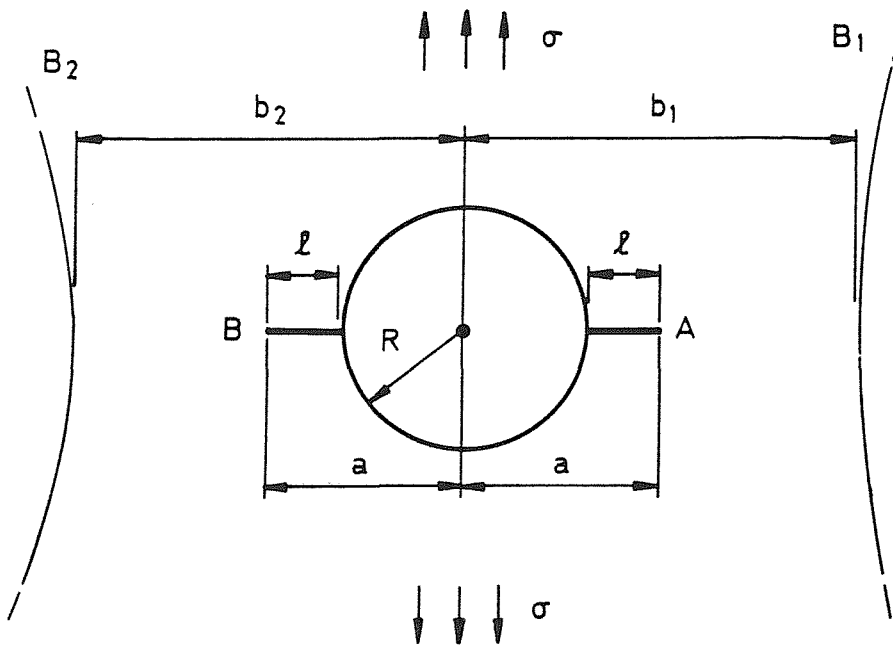


Fig 4.3 Two equal-length radial cracks at the edge of a circular hole between two boundaries

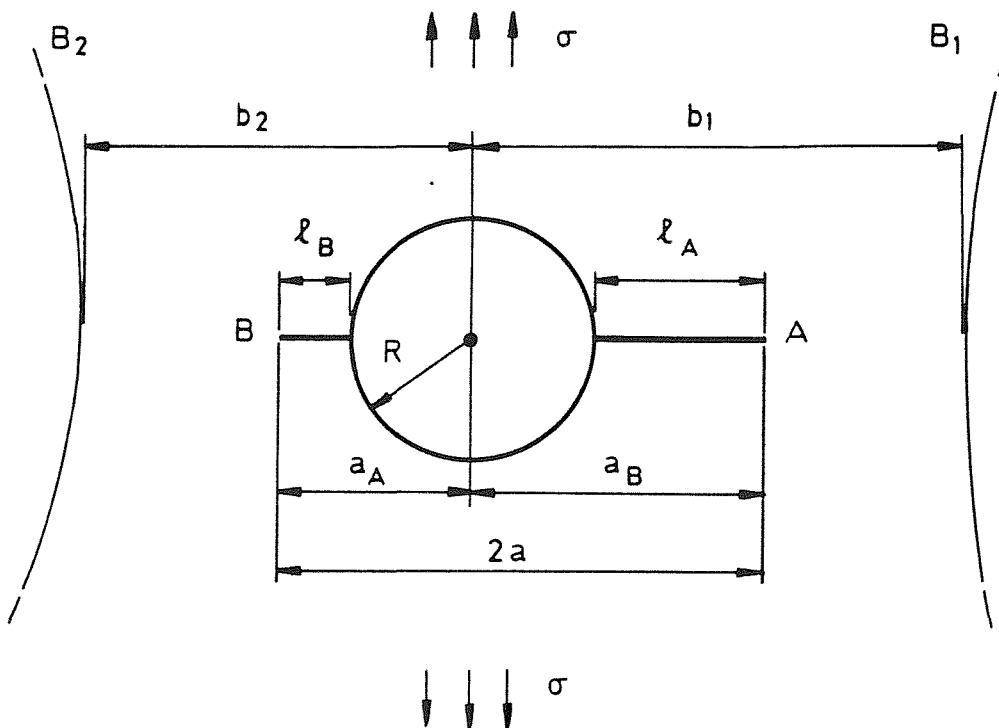


Fig 4.4 Two unequal-length radial cracks at the edge of a circular hole between two boundaries

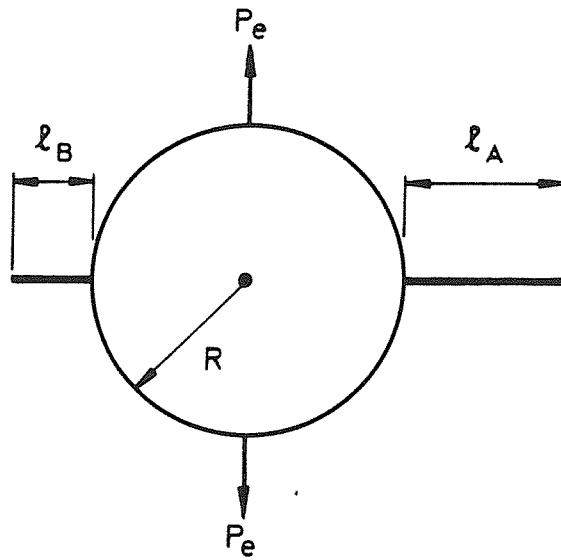


Fig 4.5 Localized radial forces acting on the hole perimeter, perpendicular to the crackline

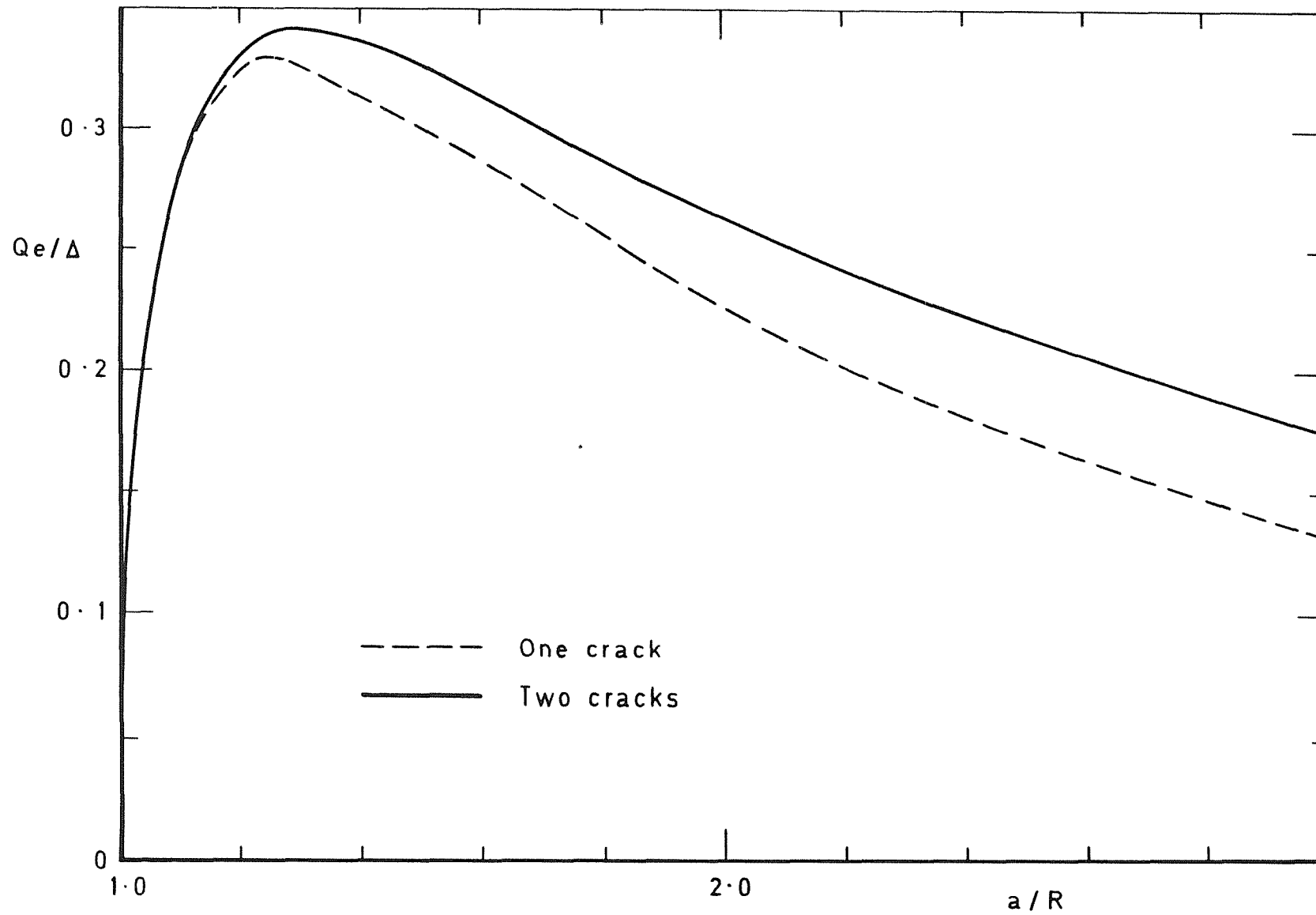


Fig 4.6 Correction to normalized stress intensity factors due to boundary-boundary interactions

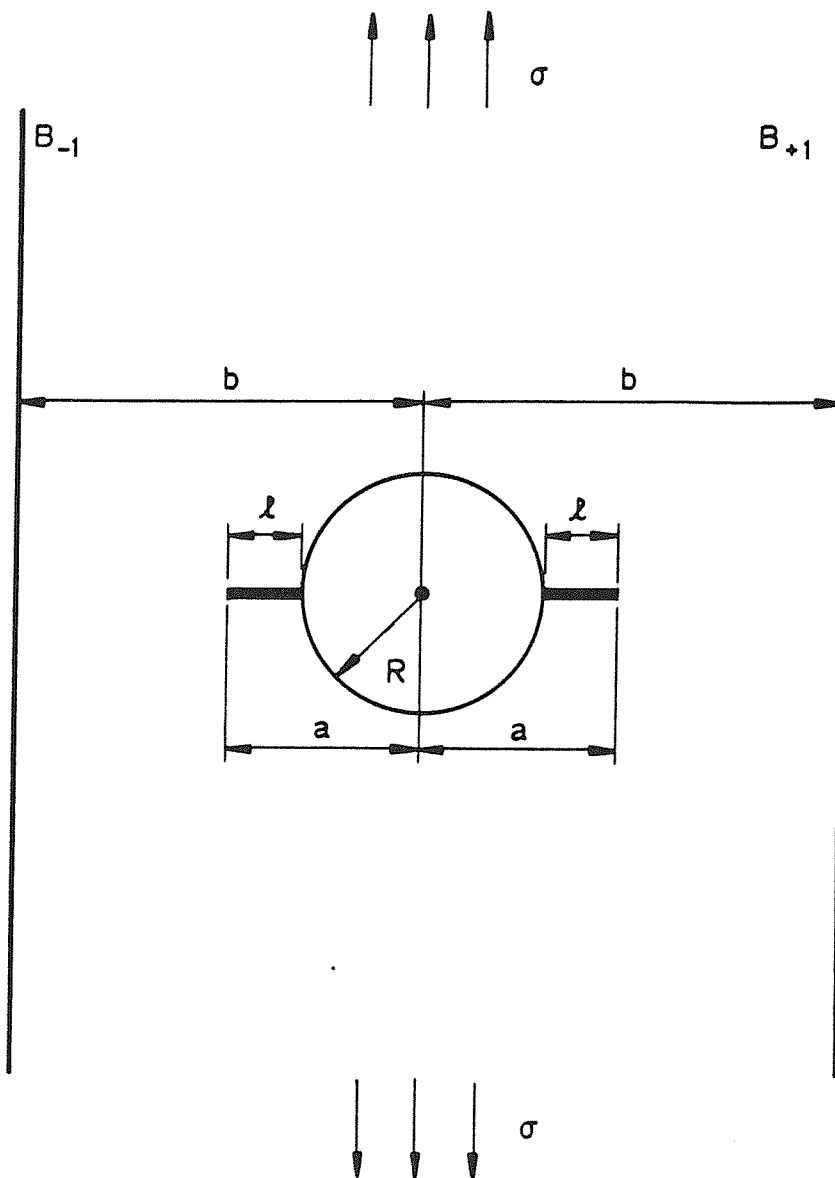


Fig 4.7 Two radial cracks at the edge of a hole in a uniformly stressed strip

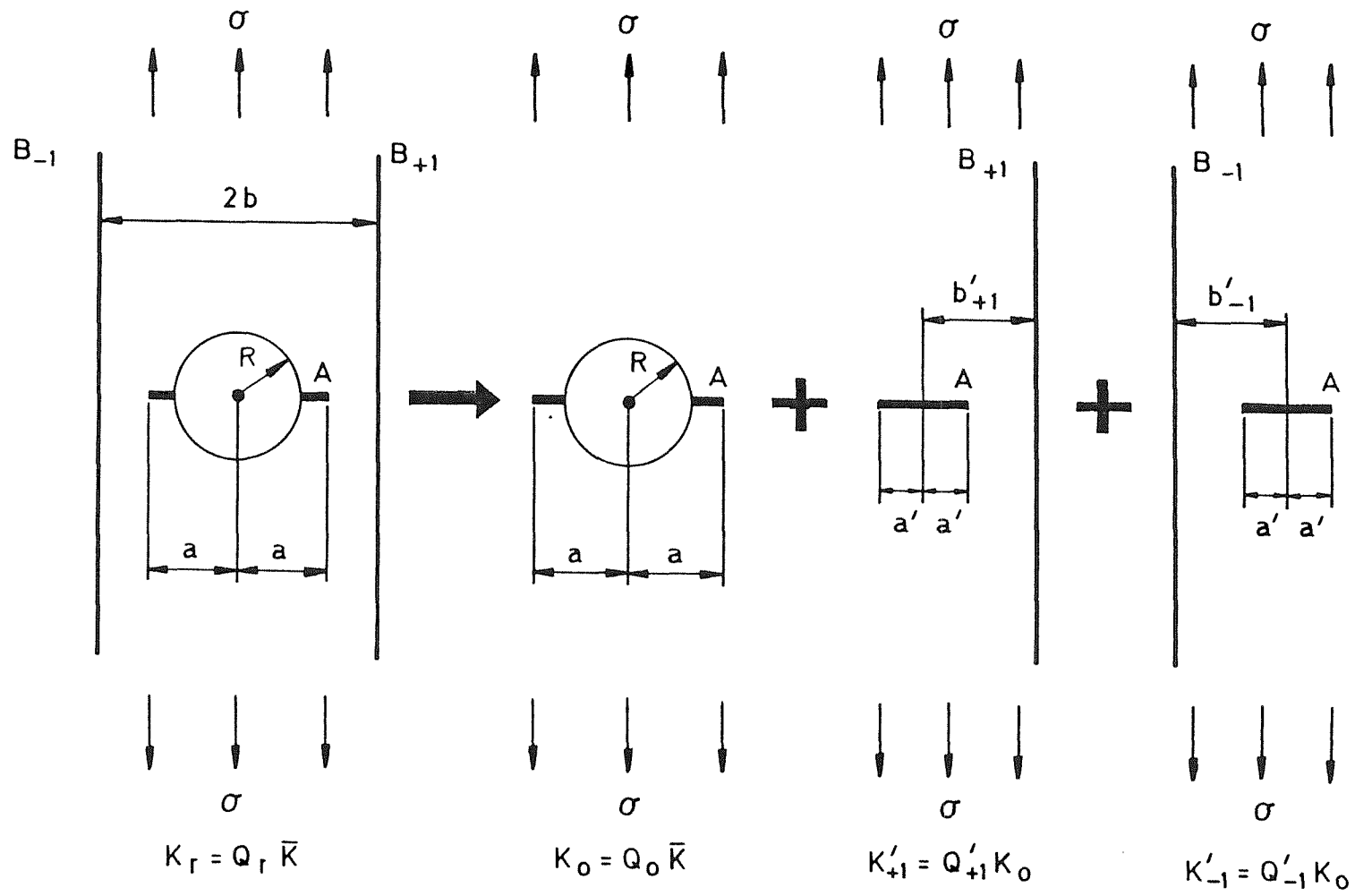


Fig 4.8 Ancillary configurations for two radial cracks at the edge of a circular hole in the middle of a strip

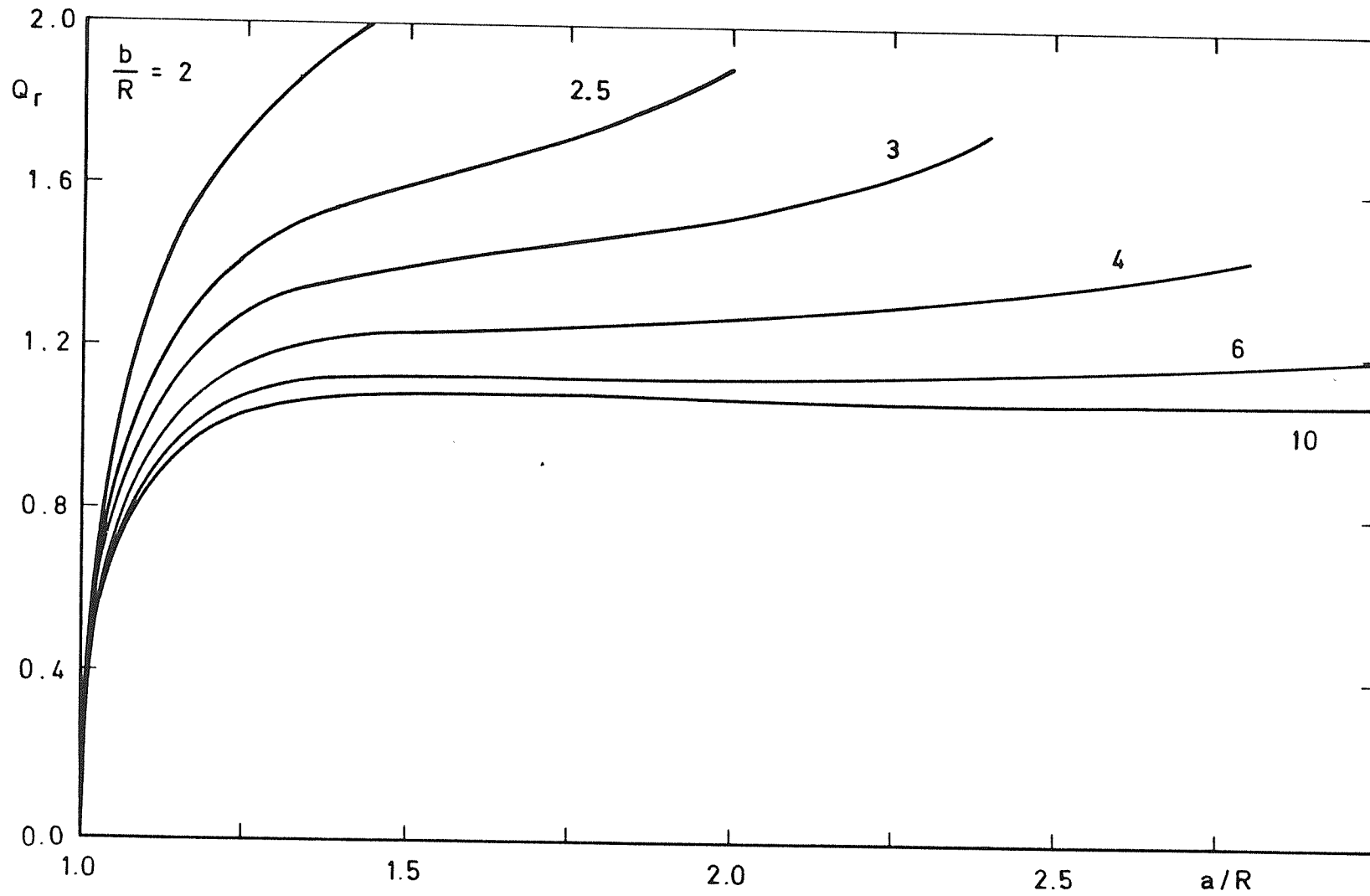


Fig 4.9 Normalized stress intensity factor for cracks at a hole in the centre of a strip

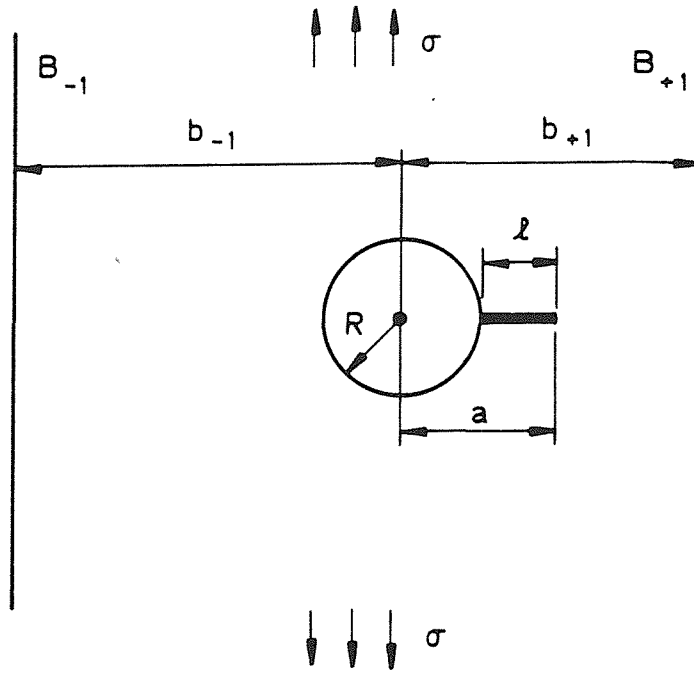


Fig 4.10a Radial crack at the edge of a circular hole near one edge of a strip

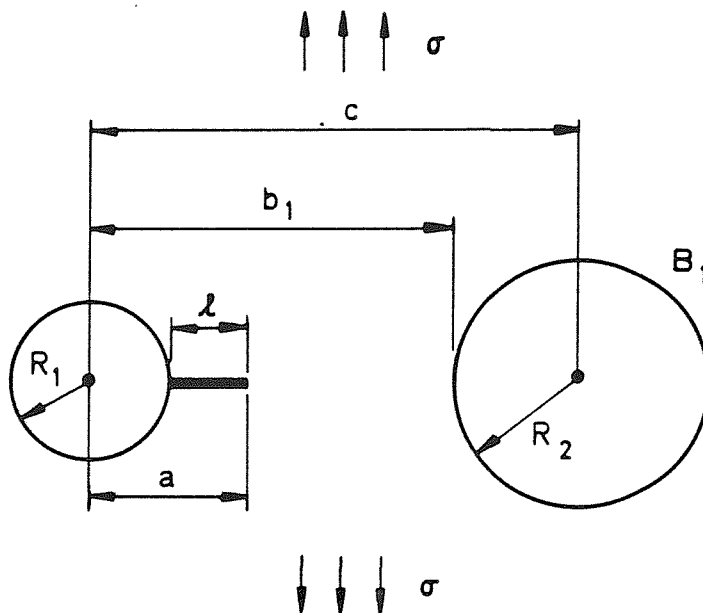


Fig 4.10b Radial crack at the edge of a circular hole near another circular hole

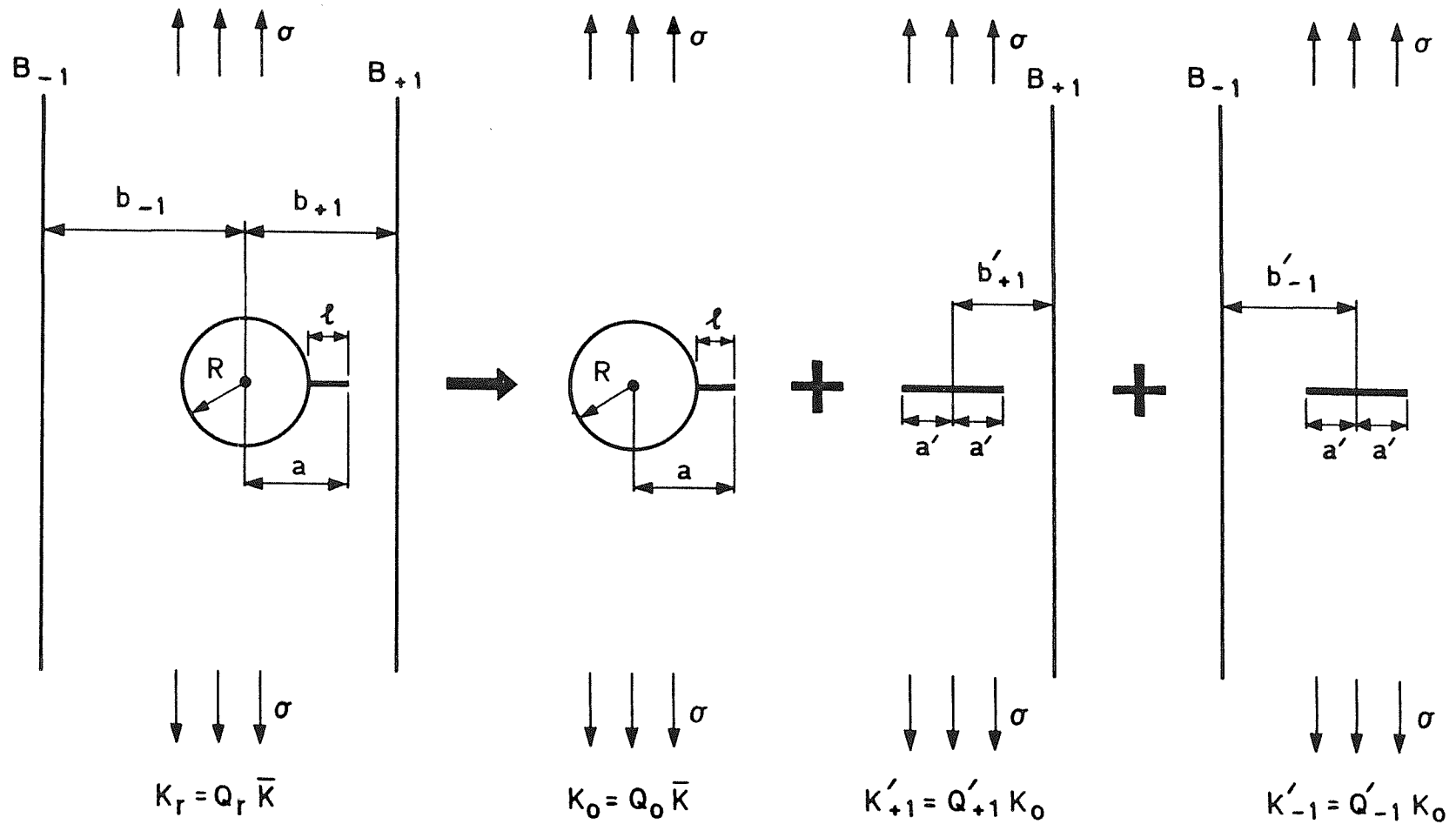


Fig 4.11 Ancillary configurations for a radial crack at the edge of a circular hole near one edge of a strip

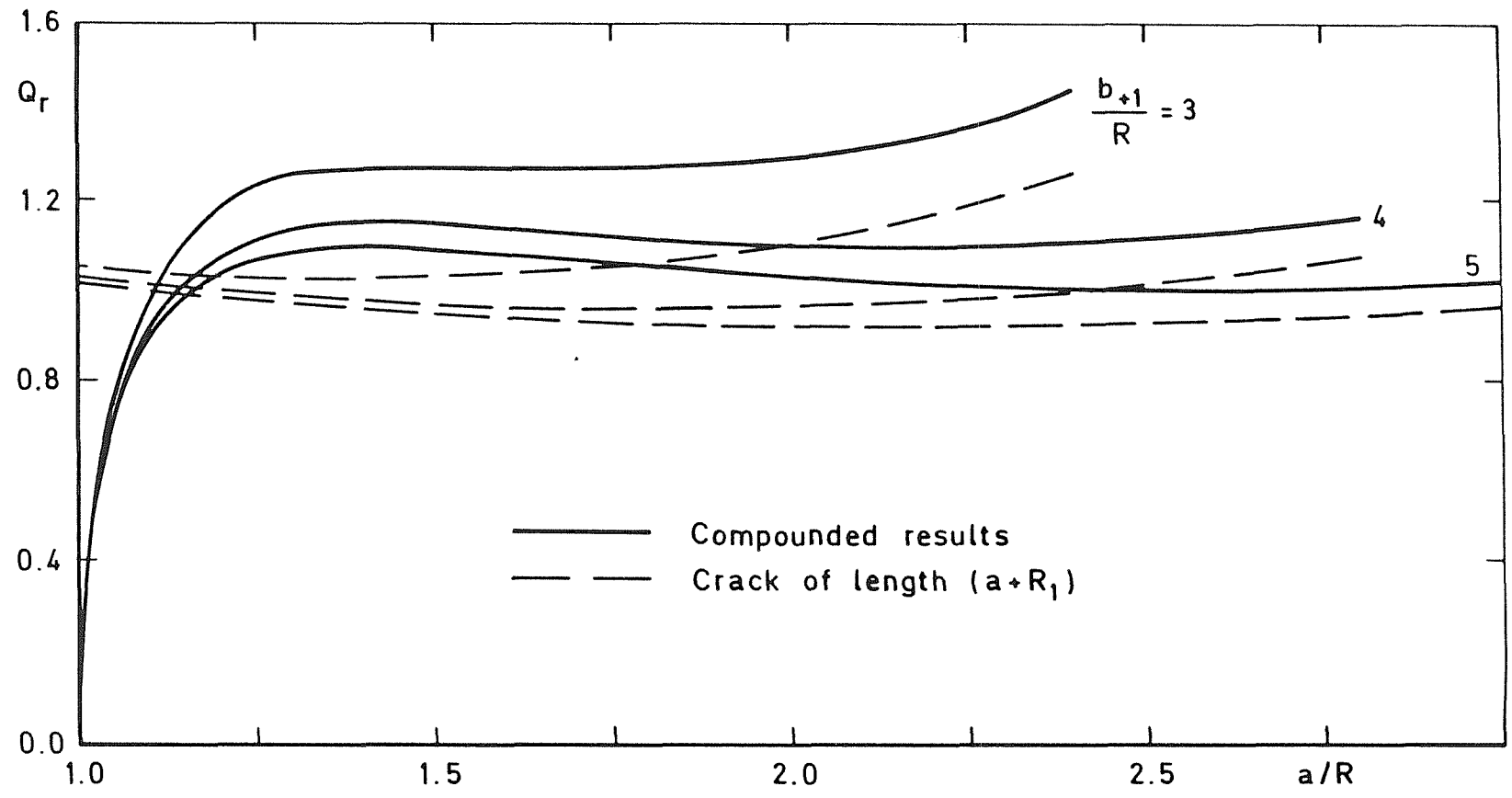


Fig 4.12 Normalized stress intensity factor for a radial crack at the edge of a circular hole near one edge of a strip

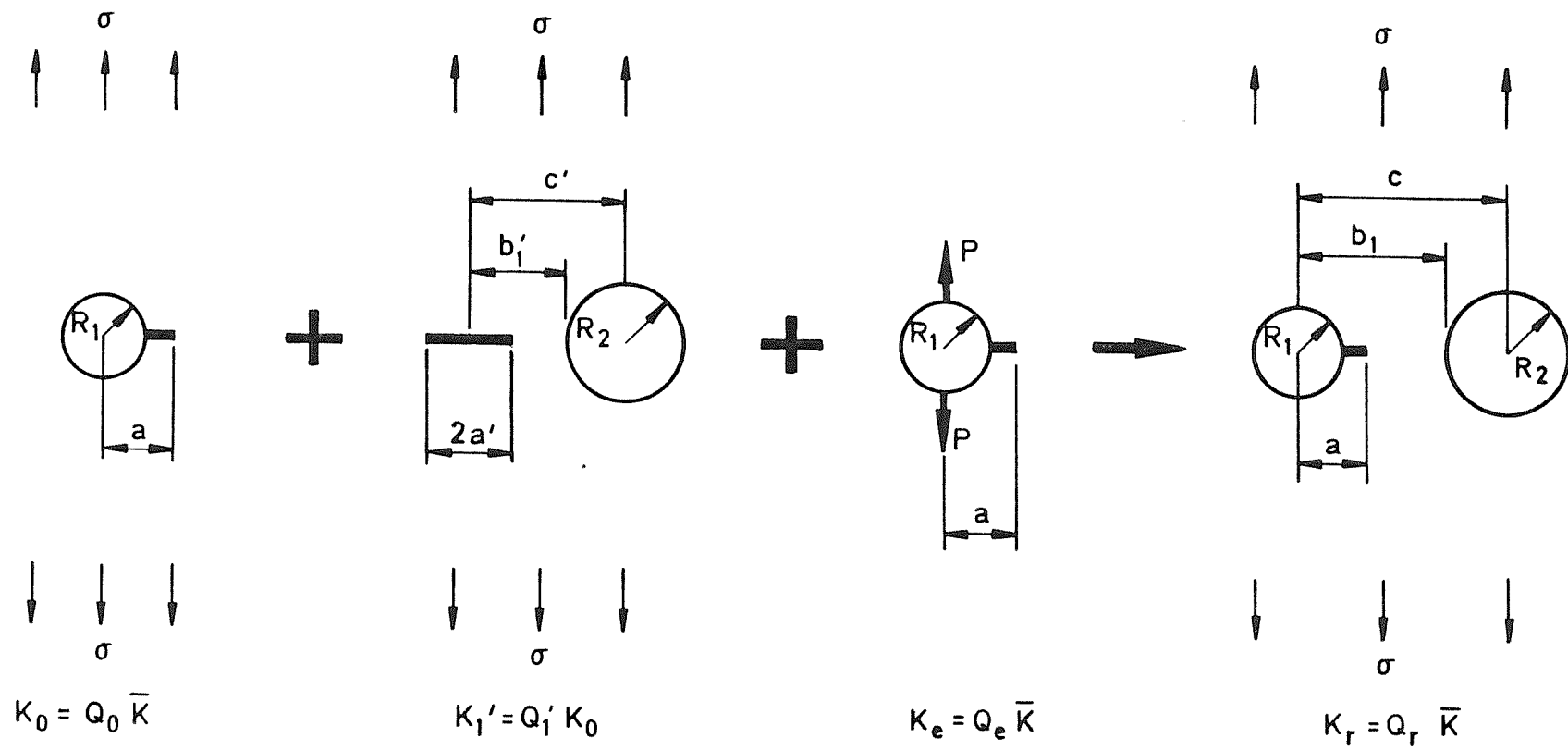


Fig 4.13 Ancillary configurations for a radial crack at the edge of a circular hole near another circular hole

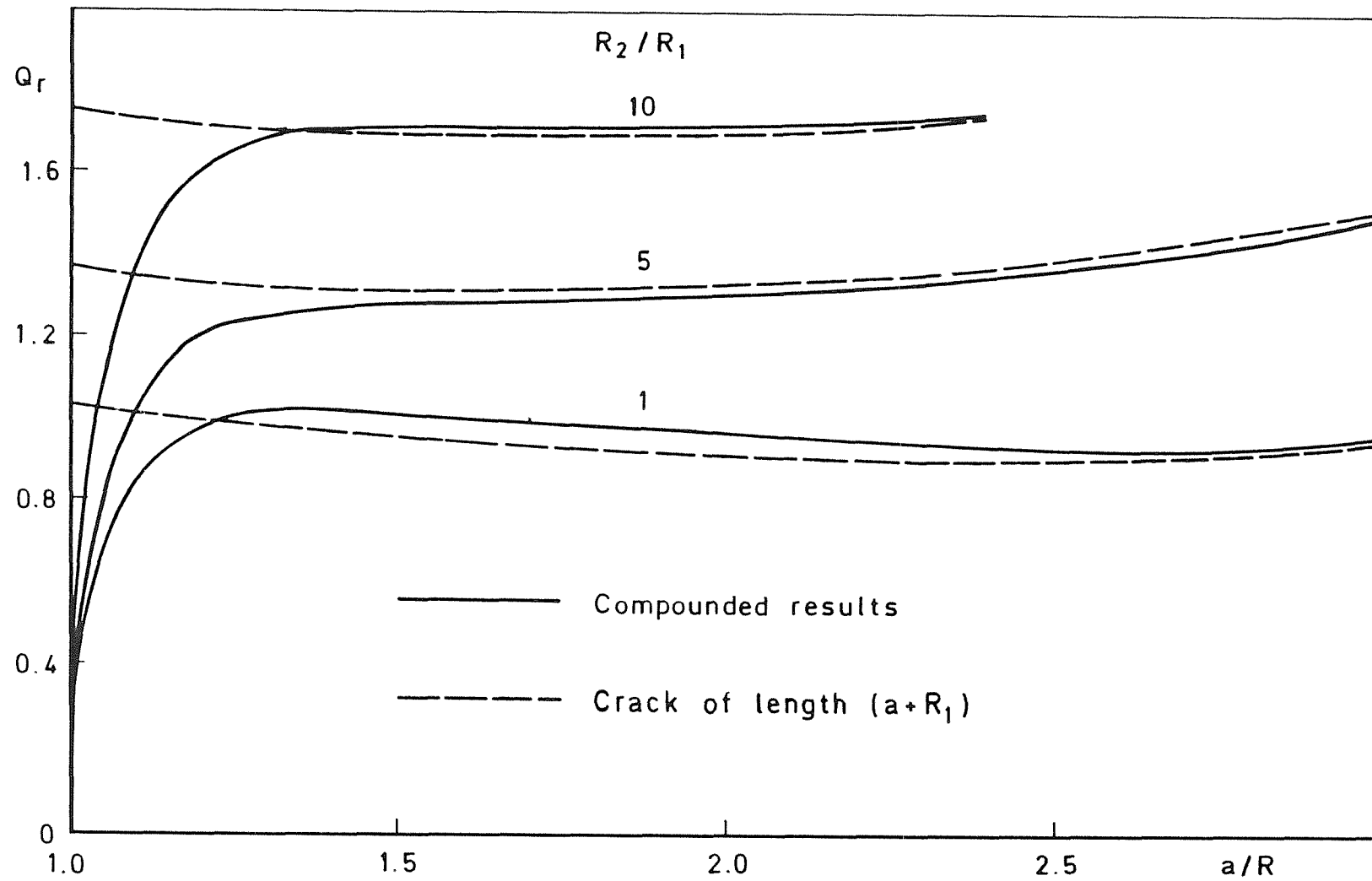


Fig 4.14 Normalized stress intensity factor for a radial crack at the edge of a circular hole near another circular hole

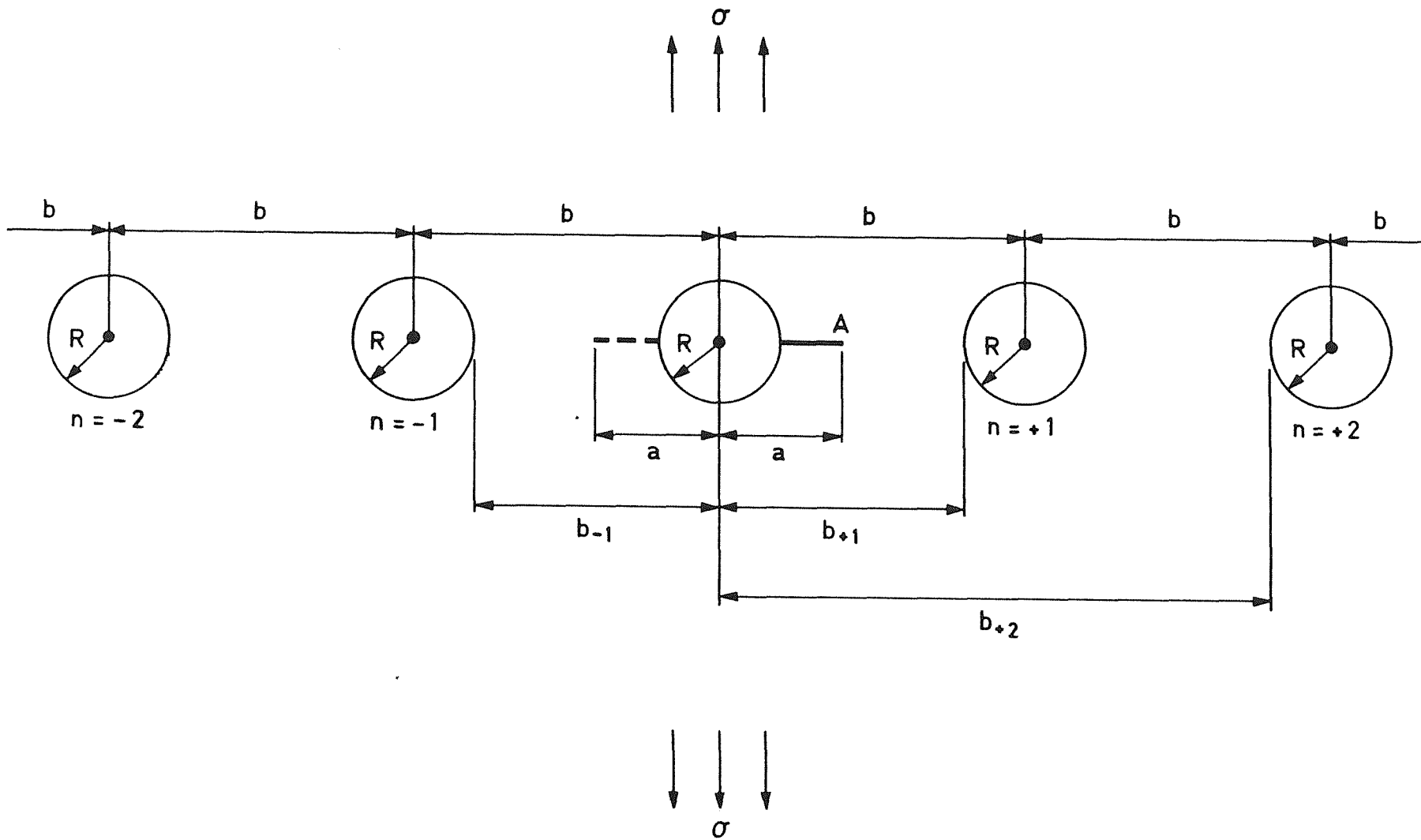
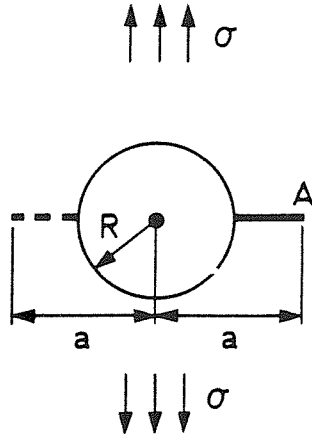
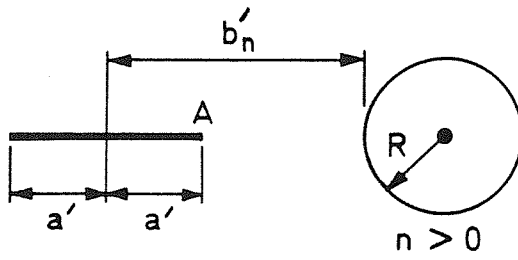


Fig 5.1 One or two radial cracks at the edge of a hole in a row of holes

$$K_0 = Q_0 \bar{K}$$



$$K'_n = Q'_n K_0$$



$$K'_n = Q'_n K_0$$

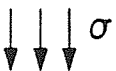
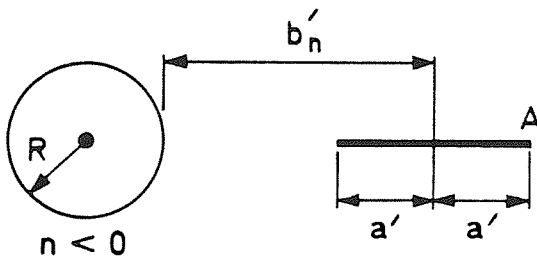


Fig 5.2 Ancillary configurations for one or two radial cracks at the edge of a hole in a row of holes

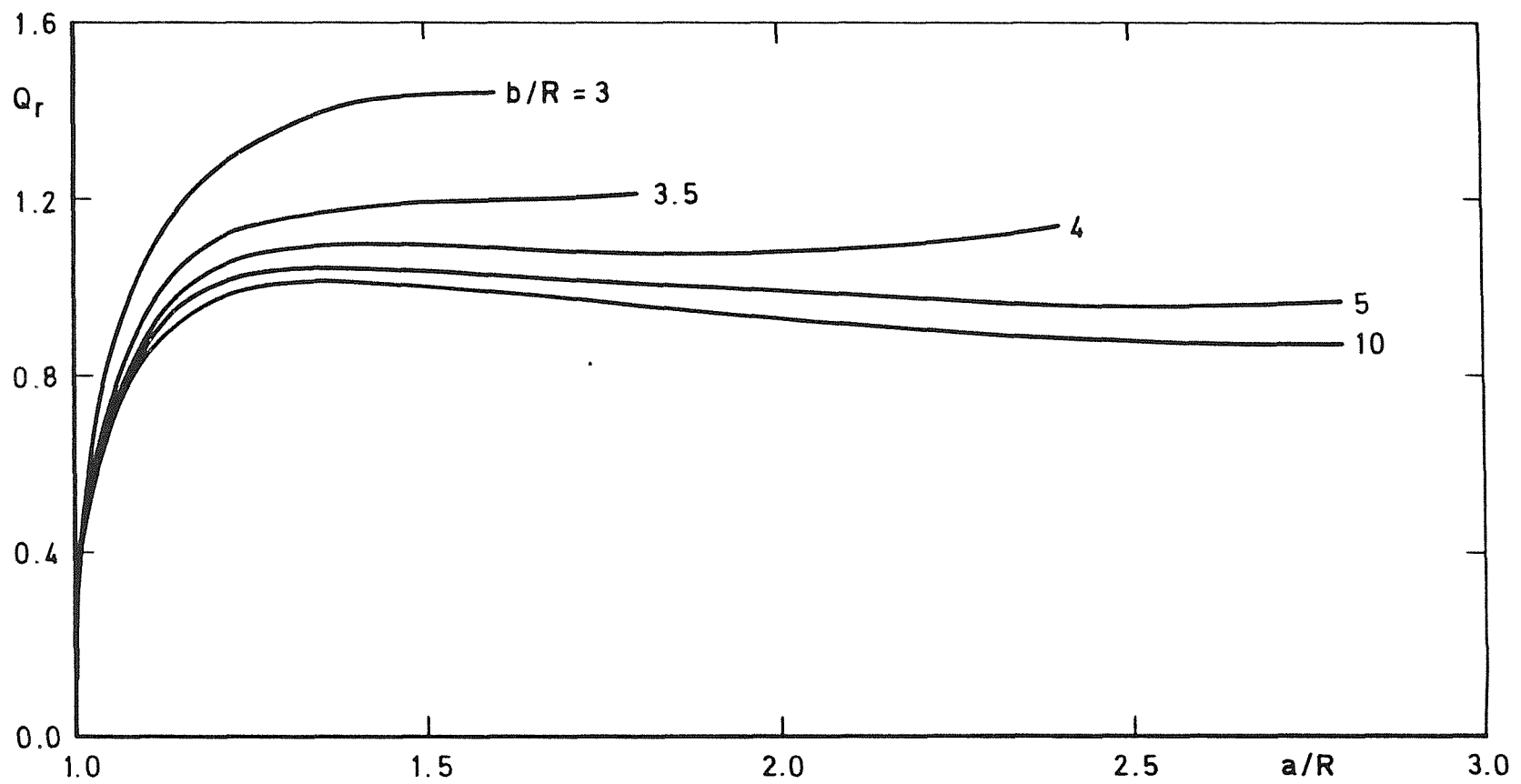


Fig 5.3 Normalized stress intensity factor for one crack at a hole in a row of holes

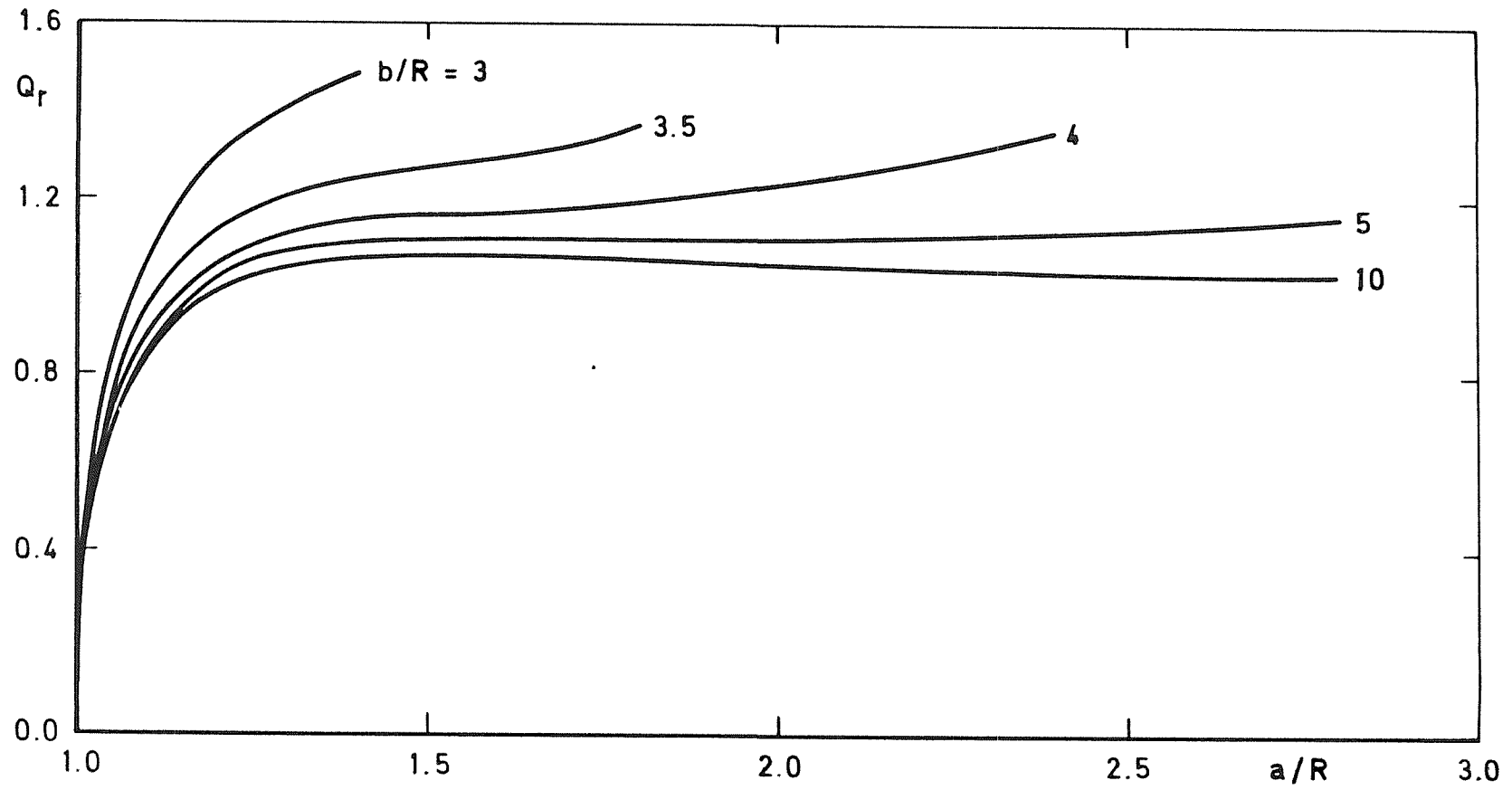


Fig 5.4 Normalized stress intensity factor for two cracks at a hole in a row of holes

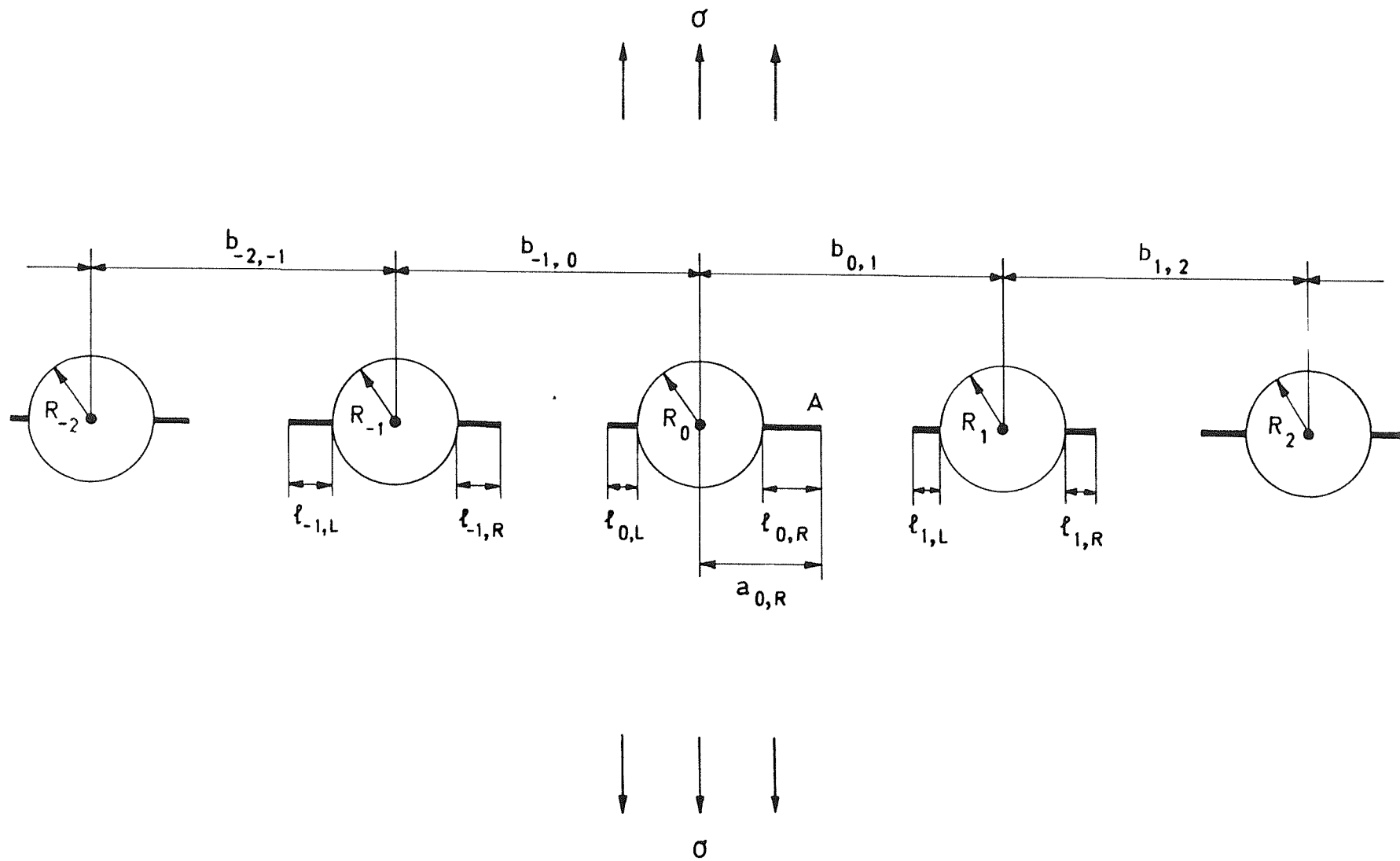


Fig 5.5 Cracks at the edges of holes in a linear array

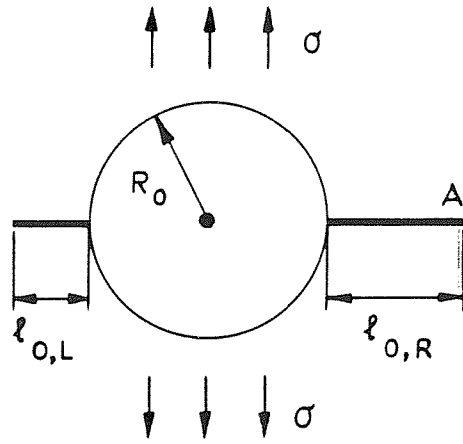


Fig 5.6 Two cracks at the edge of a circular hole:  $n = 0$

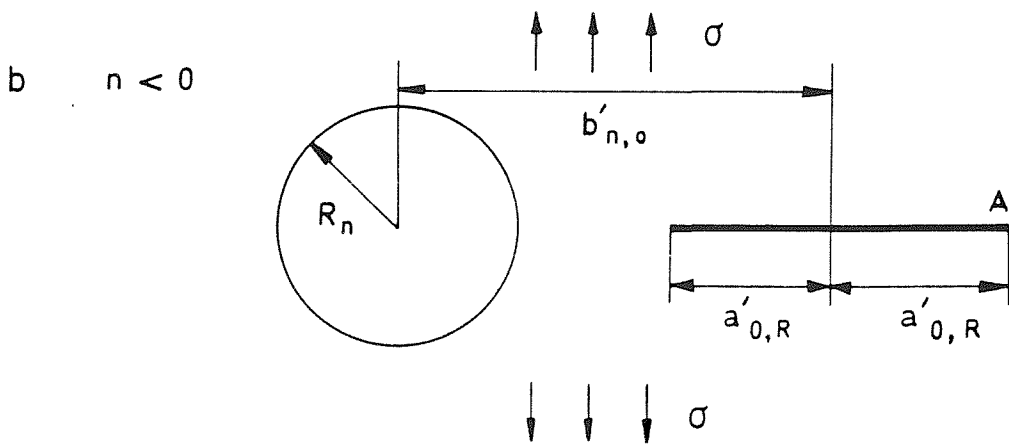
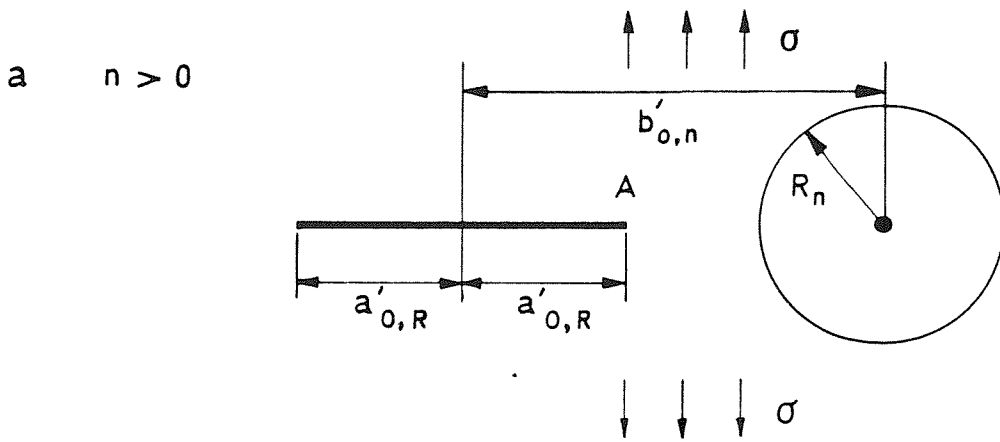


Fig 5.7a&b Crack near a circular hole:  $n \neq 0$

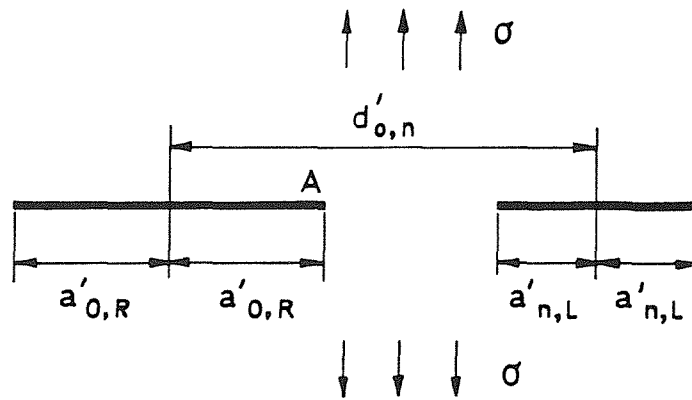
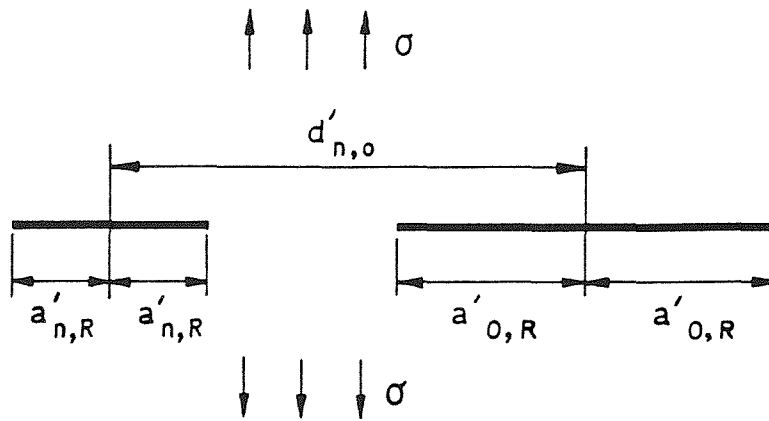
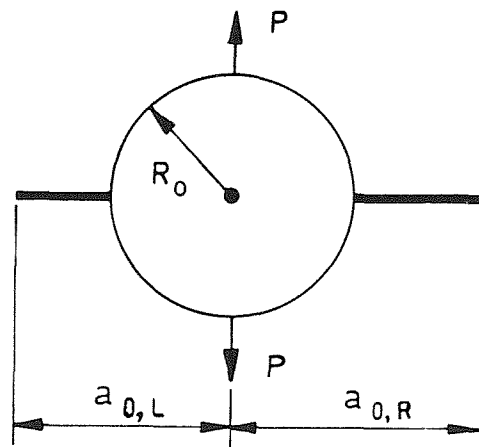
a  $n > 0$ b  $n < 0$ Fig 5.8a&b Two collinear cracks:  $n \neq 0$ 

Fig 5.9 Two cracks at the edge of a circular hole: point loads

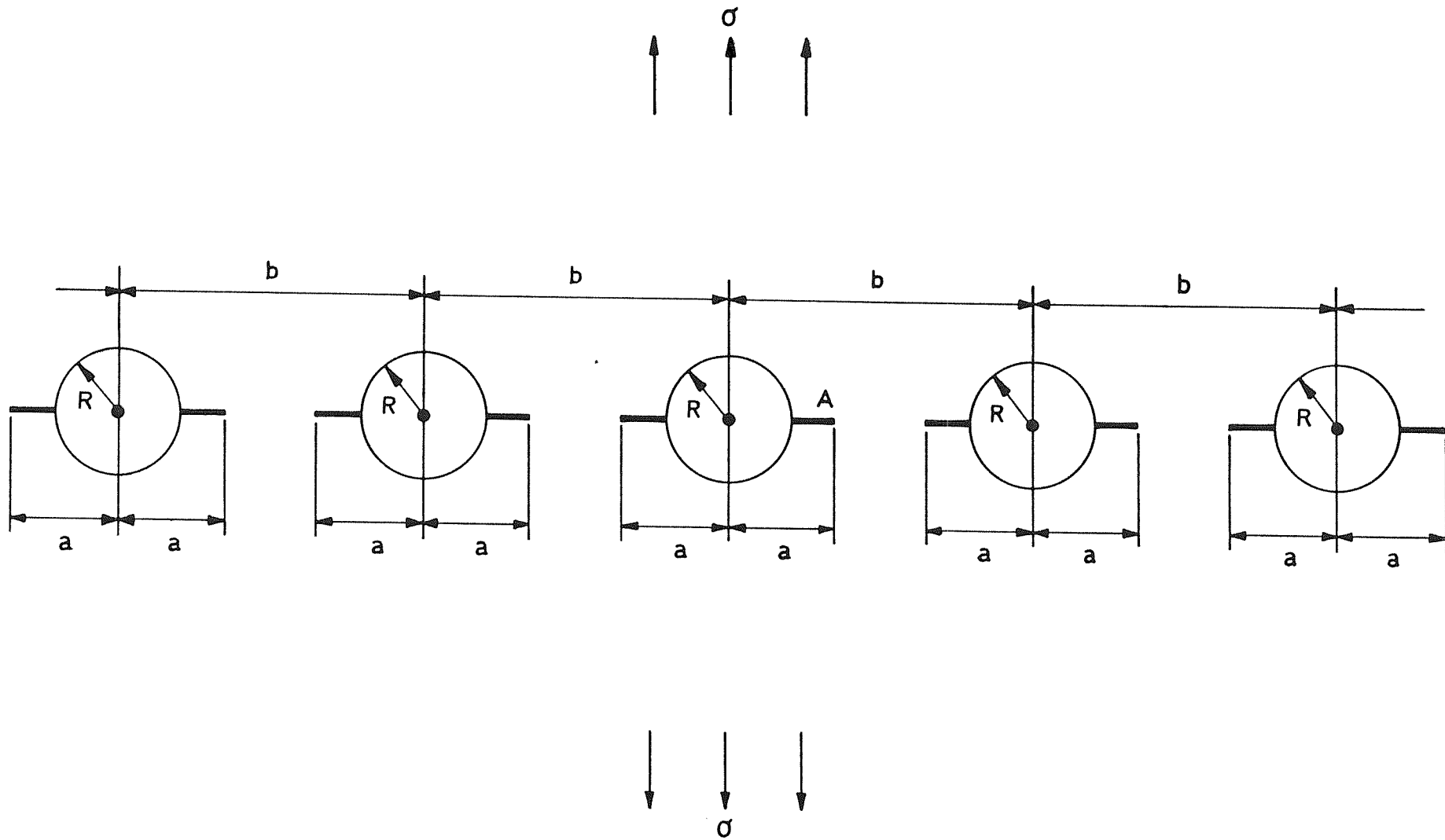


Fig 5.10 Equal-length cracks at the edges of holes in a periodic array

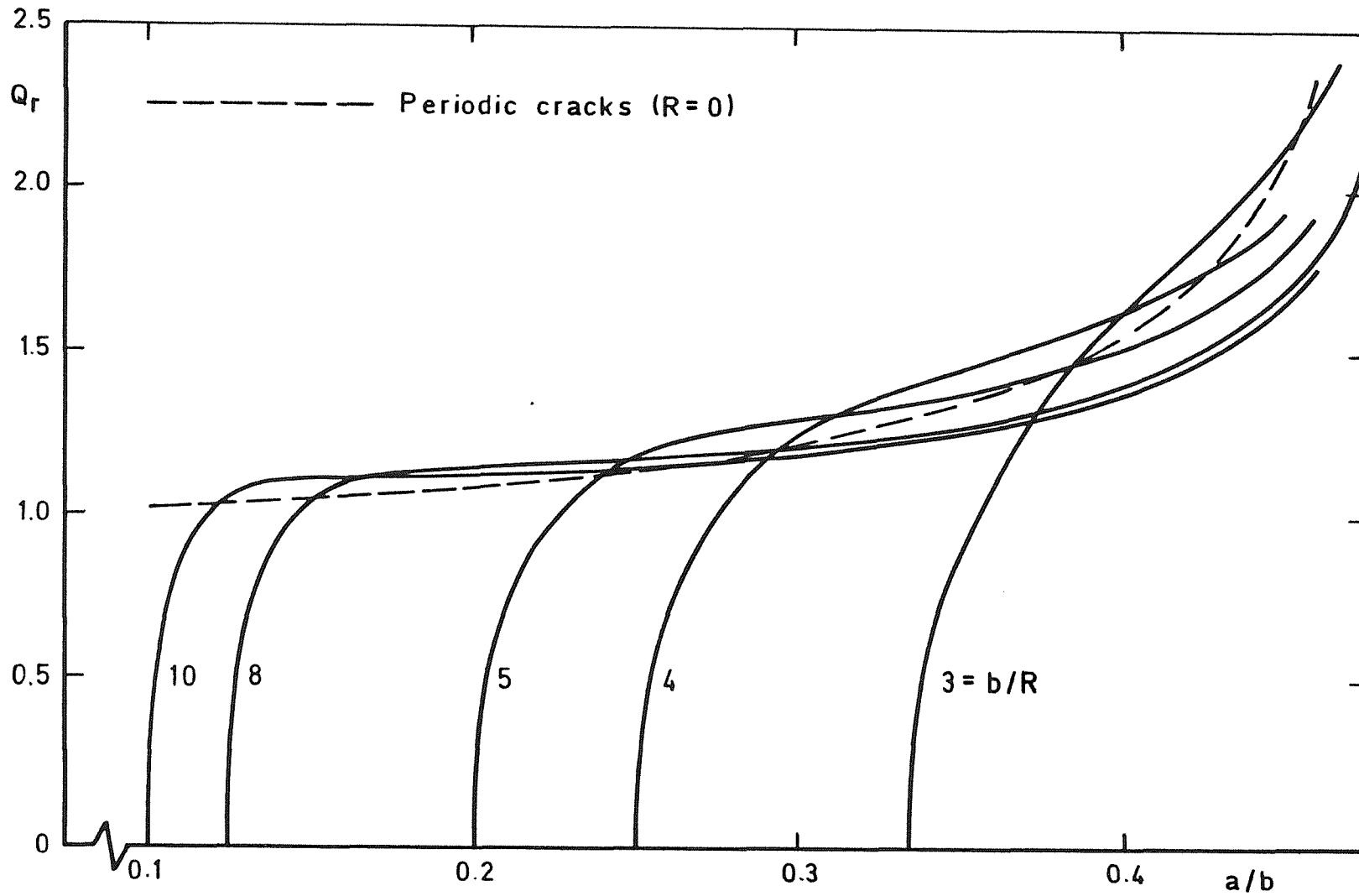


Fig 5.11 Normalized stress intensity factor for equal cracks at a periodic array of holes

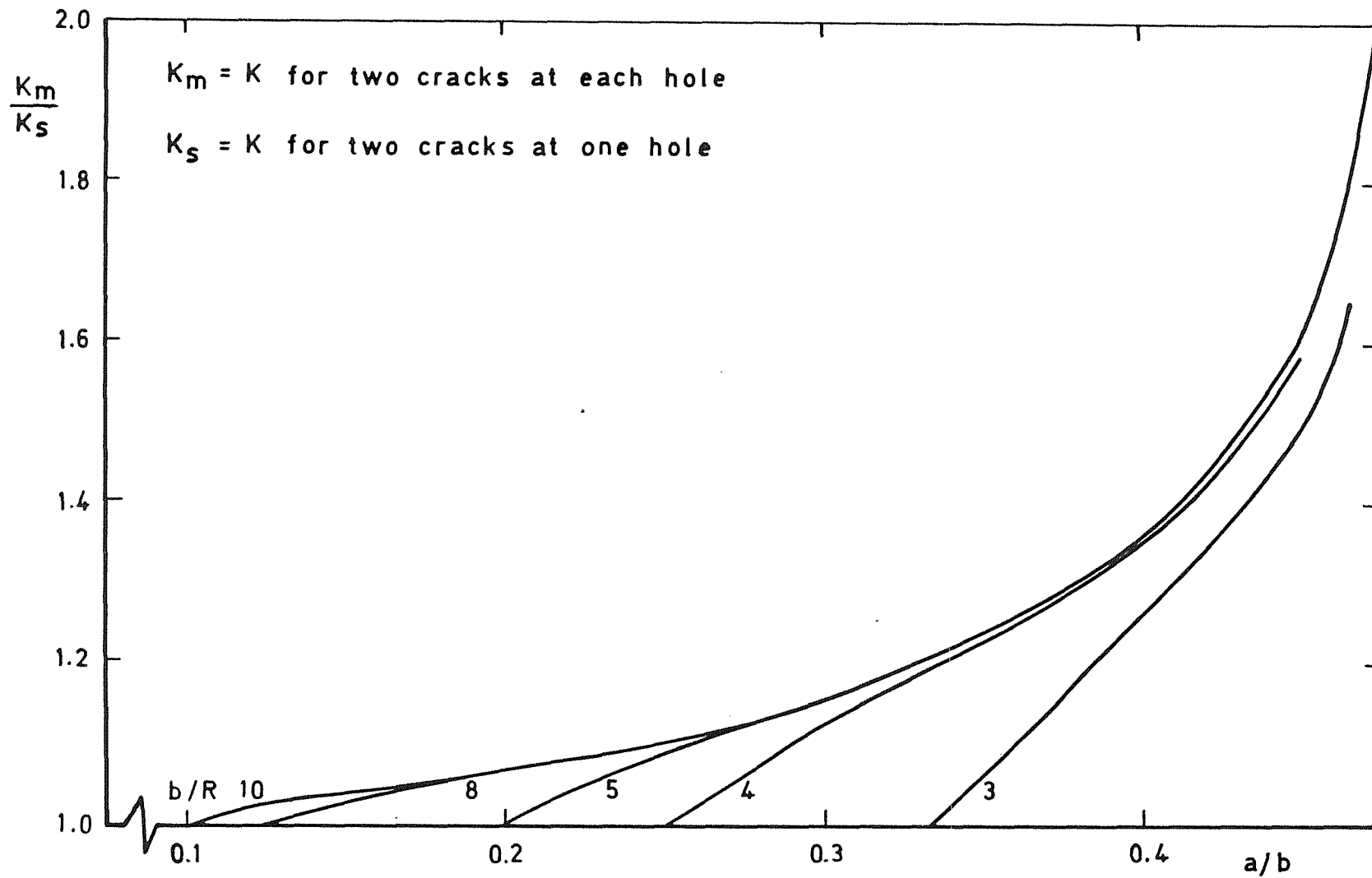


Fig 5.12 Comparison of stress intensity factors for cracks at holes in a periodic array

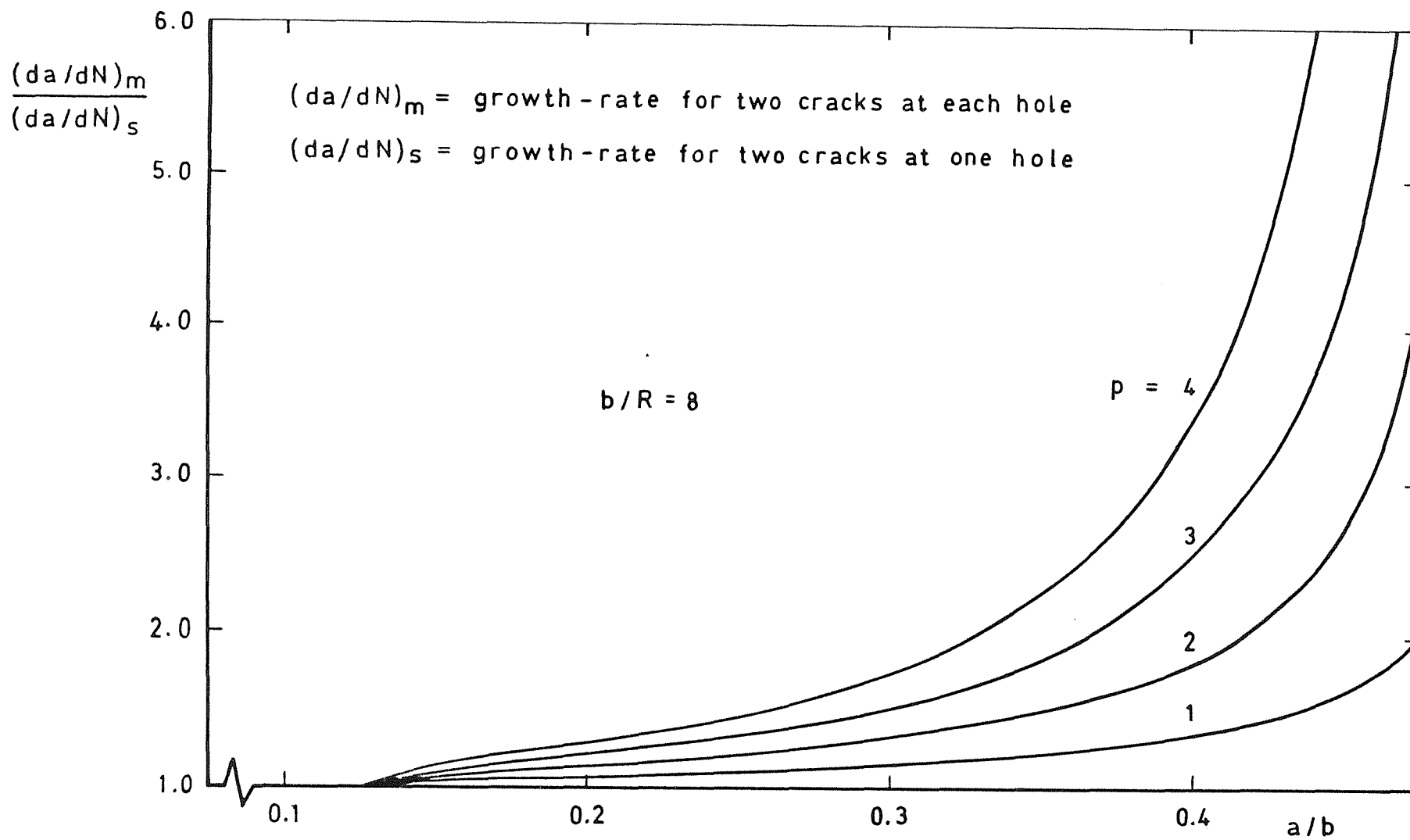
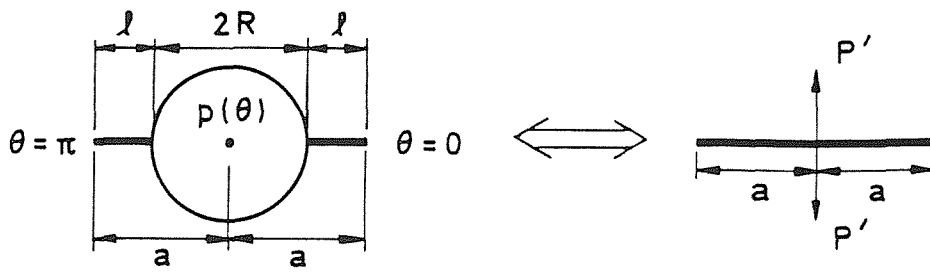


Fig 5.13 Comparison of crack growth-rates for cracks at holes in a periodic array

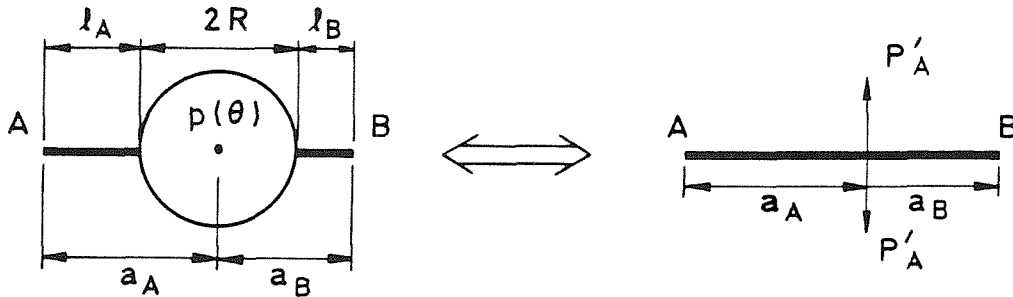


At both tips:  $K = K_0$

$$K = P' / \sqrt{\pi a}$$

for equivalence:  $P' = K_0 \sqrt{\pi a}$

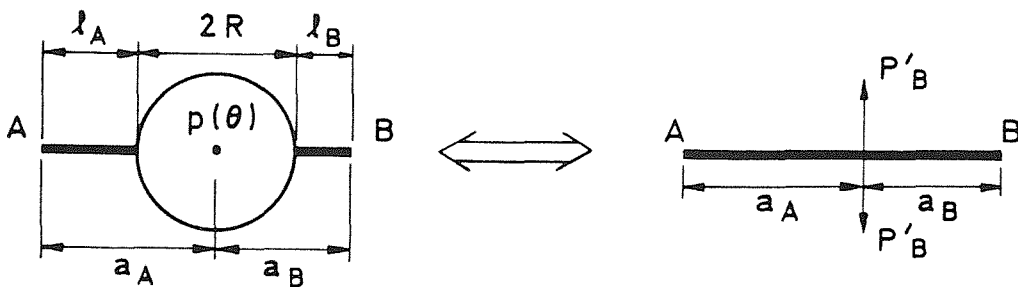
Fig 6.1 The equivalent load for symmetric cracks and symmetric loading



At tip A:  $K = K_{0A}$

$$K = \frac{P'_A}{\sqrt{\pi a}} \sqrt{\frac{a_B}{a_A}}$$

for equivalence:  $P'_A = K_{0A} \sqrt{\pi a} \sqrt{a_A/a_B}$



At tip B:  $K = K_{0B}$

$$K = \frac{P'_B}{\sqrt{\pi a}} \sqrt{\frac{a_A}{a_B}}$$

for equivalence  $P'_B = K_{0B} \sqrt{\pi a} \sqrt{a_B/a_A}$

Fig 6.2 The equivalent loads for asymmetric cracks and symmetric loading

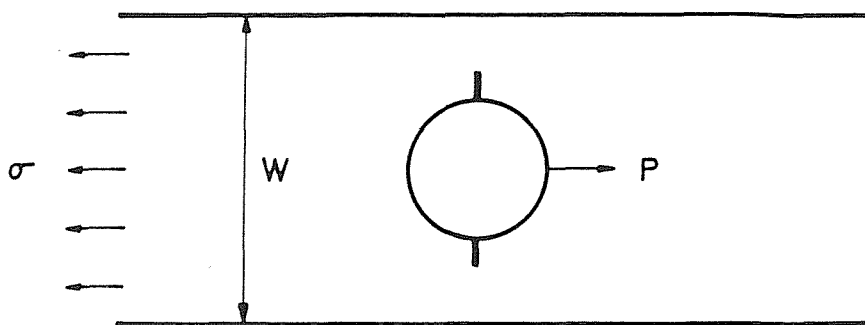


Fig 6.3a Loaded hole in finite-width strip

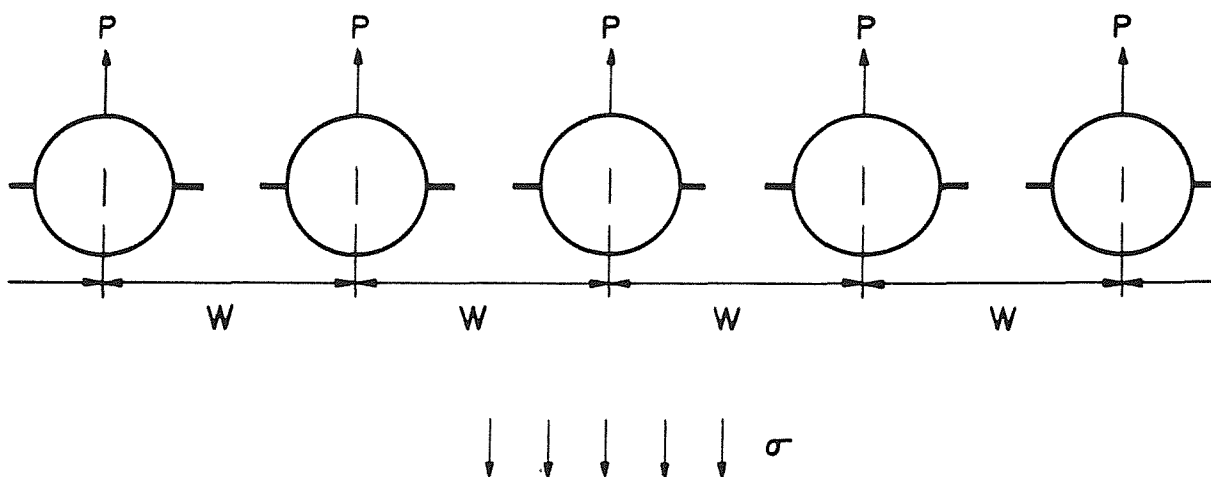
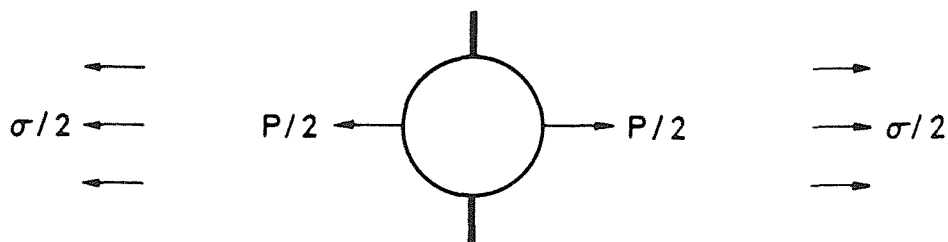


Fig 6.3b Periodic array of loaded holes in infinite sheet

Fig 6.3c Ancillary configuration for  $K_0$

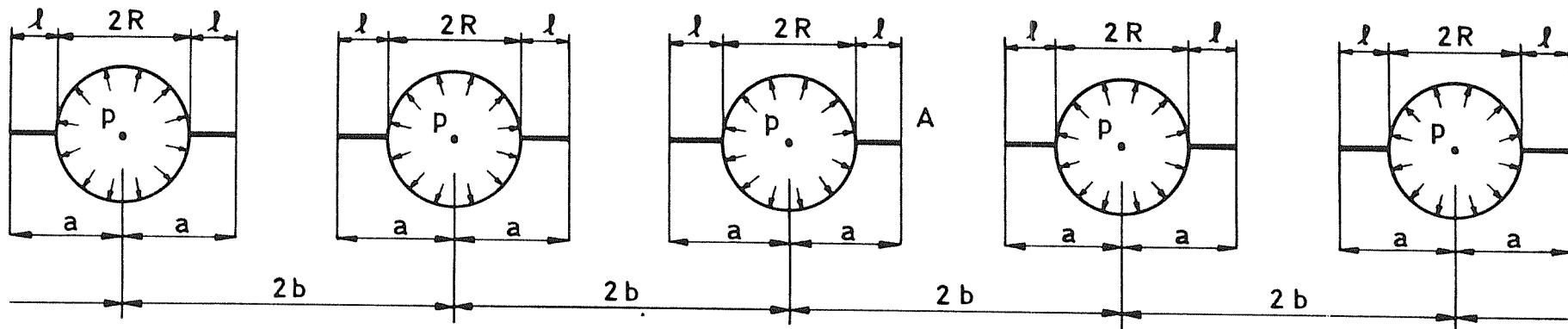


Fig 6.4a Periodic array of pressurized holes with equal-length cracks

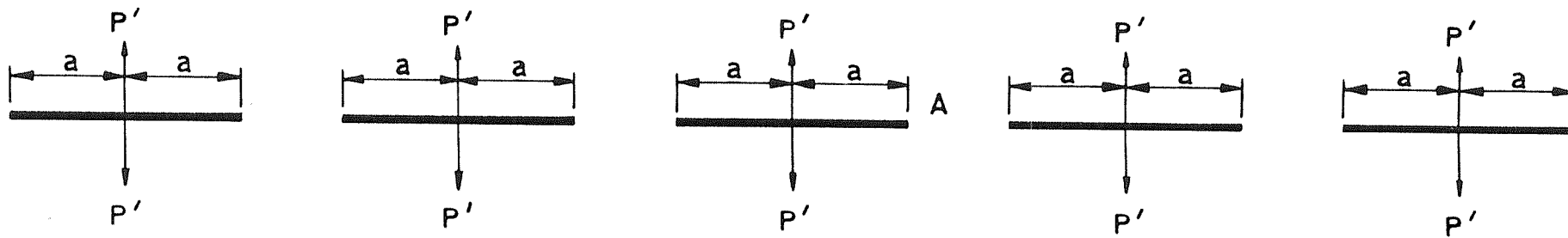


Fig 6.4b Ancillary configuration of equivalent cracks ( $P' = K_0 \sqrt{\pi a}$ )

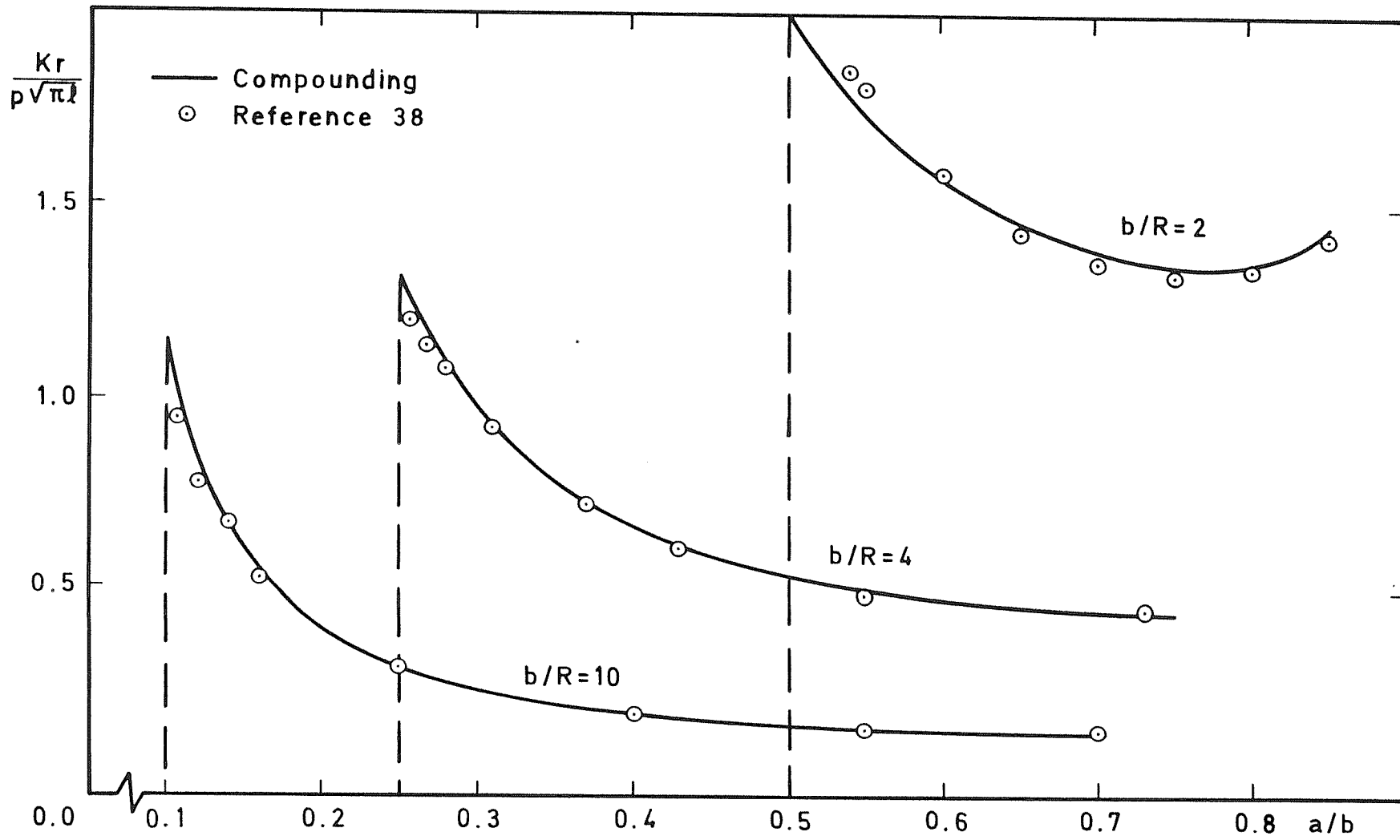


Fig 6.5 Stress intensity factors for cracks at internally pressurized holes

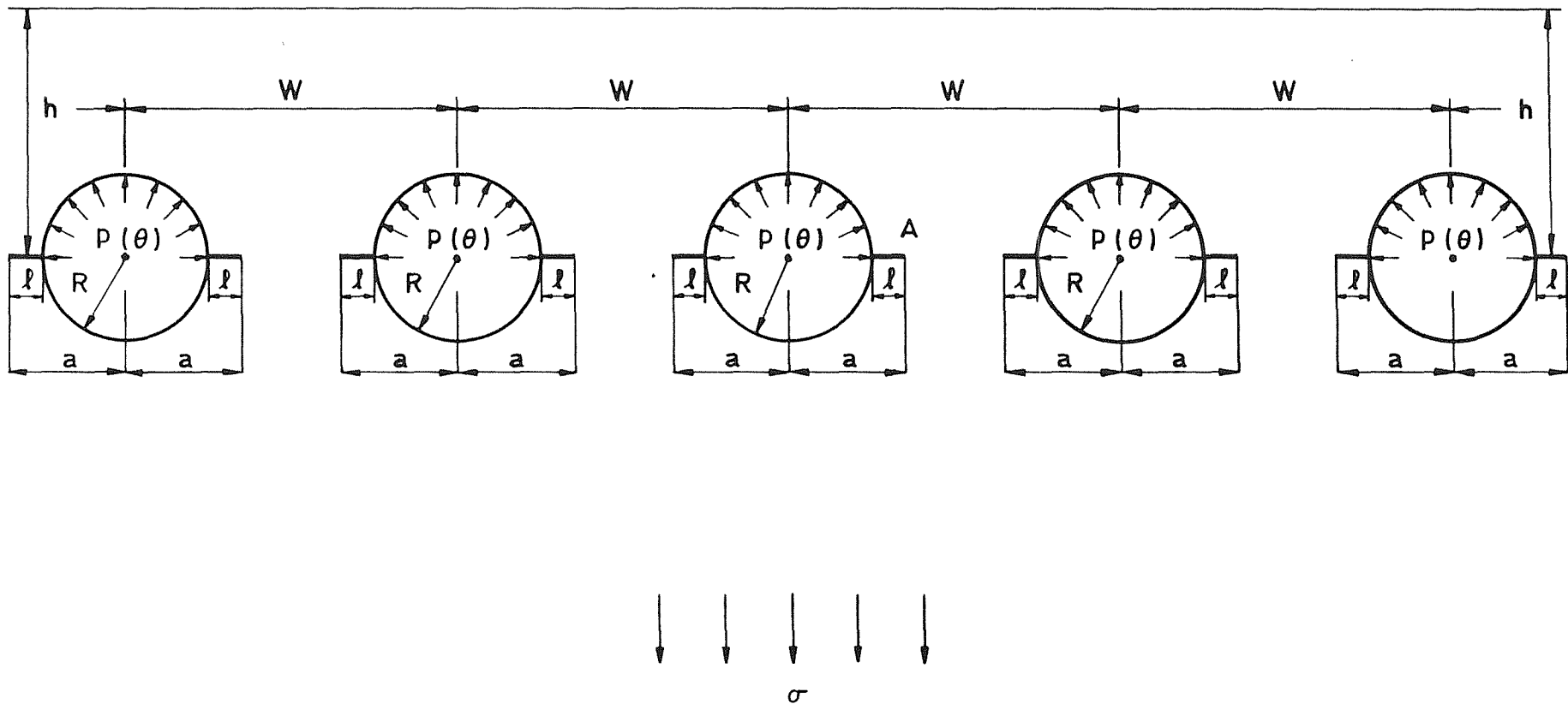


Fig 6.6 Row of loaded holes with cracks near a boundary

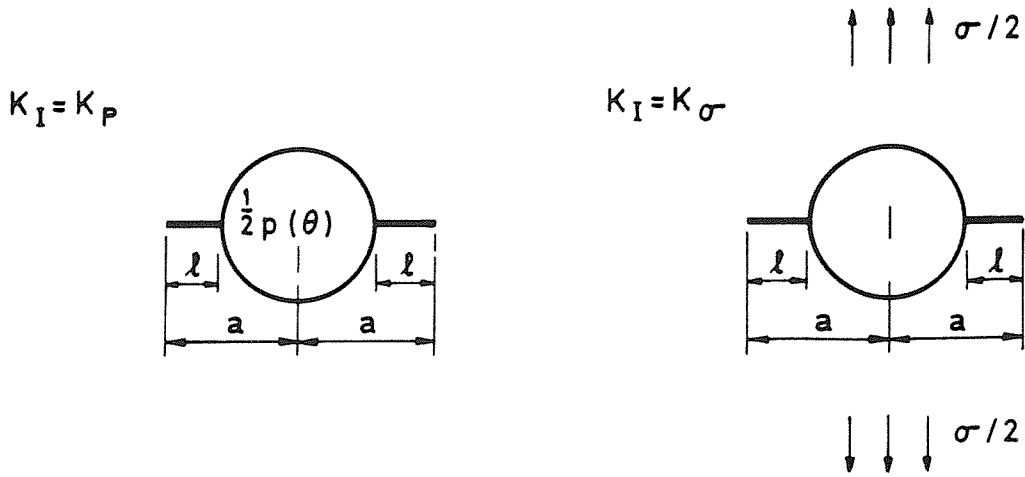


Fig 6.7a Ancillary configurations for  $K_0$

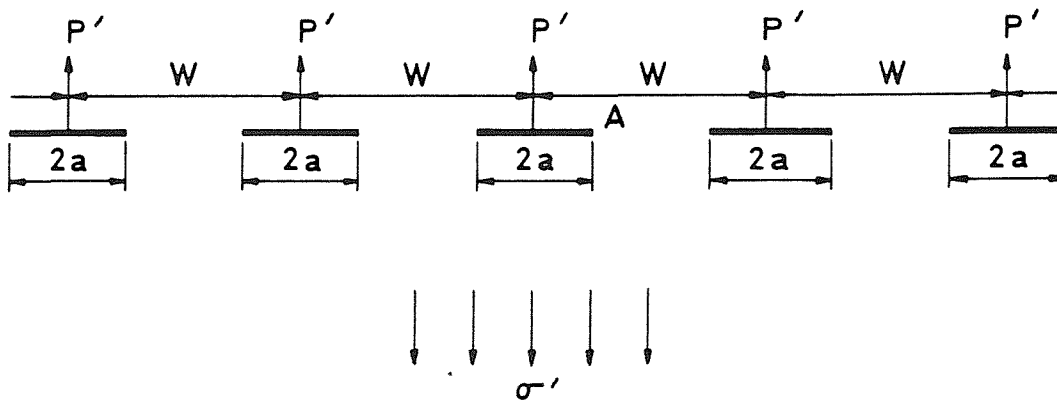


Fig 6.7b Ancillary configuration for  $K_1^1$

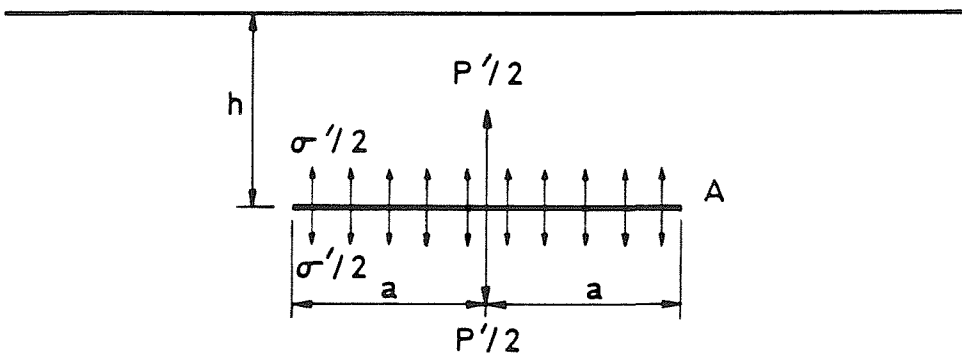


Fig 6.7c Ancillary configuration for  $K_2^1$

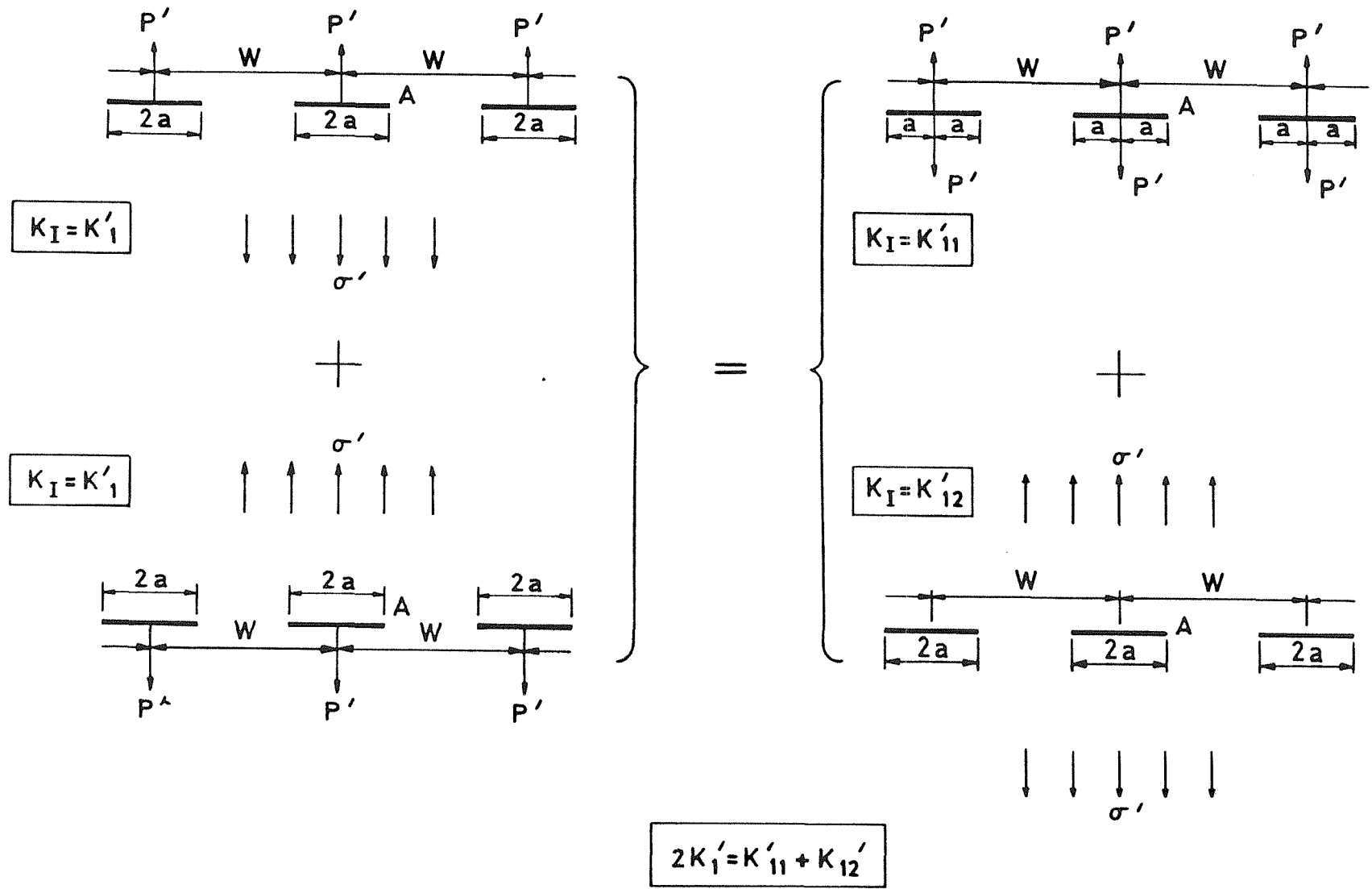
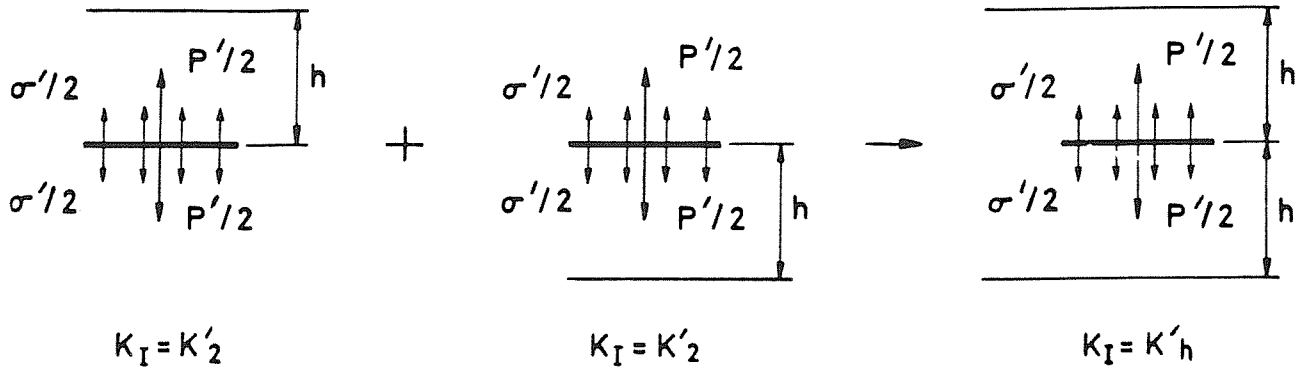
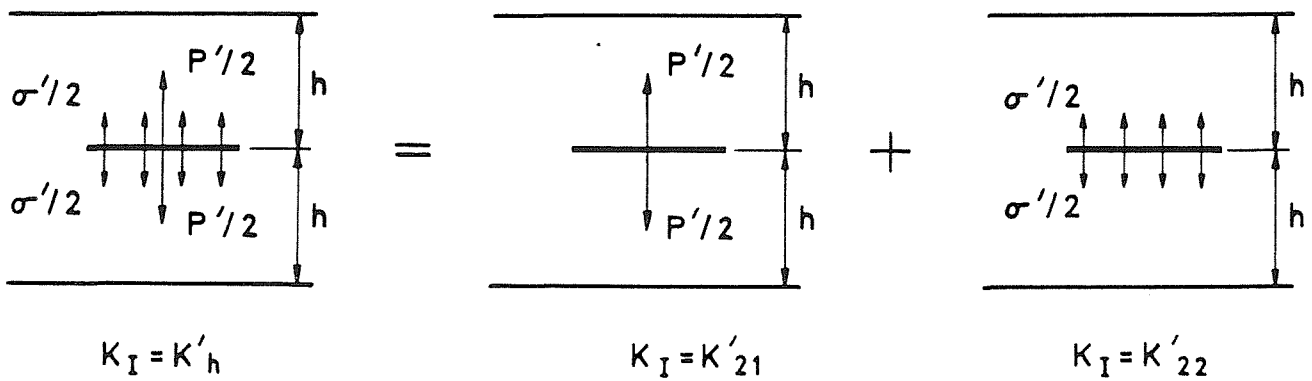


Fig 6.8 Superposition of opening-mode stress intensity factor for  $K_I'$



**Compounding :**       $2K'_2 - K_o = K'_h + K'_e$

Fig 6.9a Compounding opening-mode stress intensity factors for  $K_2^1$



**Superposition:**       $K'_h = K'_{21} + K'_{22}$

Fig 6.9b Superposition of opening-mode stress intensity factors for  $K_h^0$

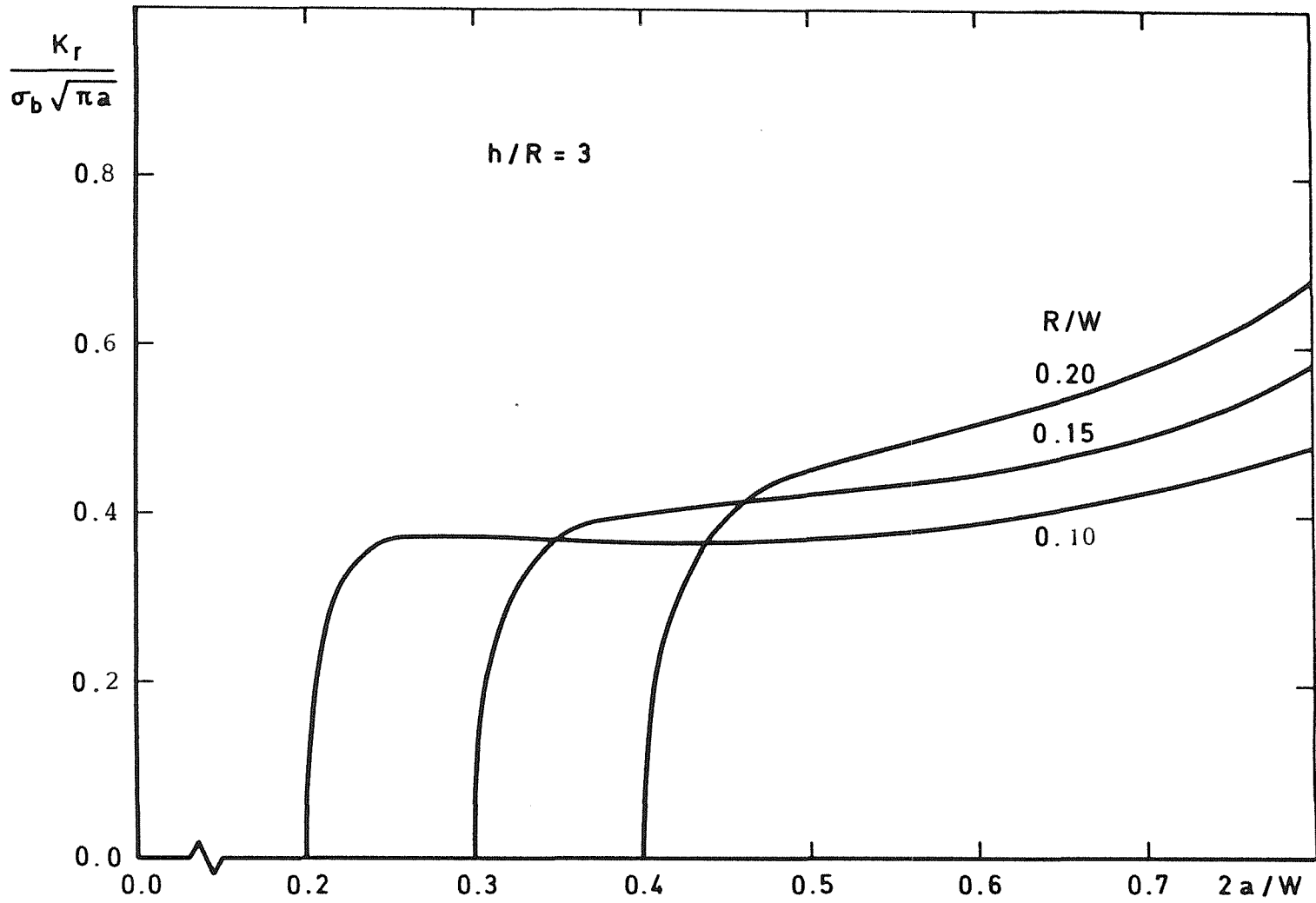


Fig 6.10 Resultant stress intensity factor for cracks at loaded holes near a boundary

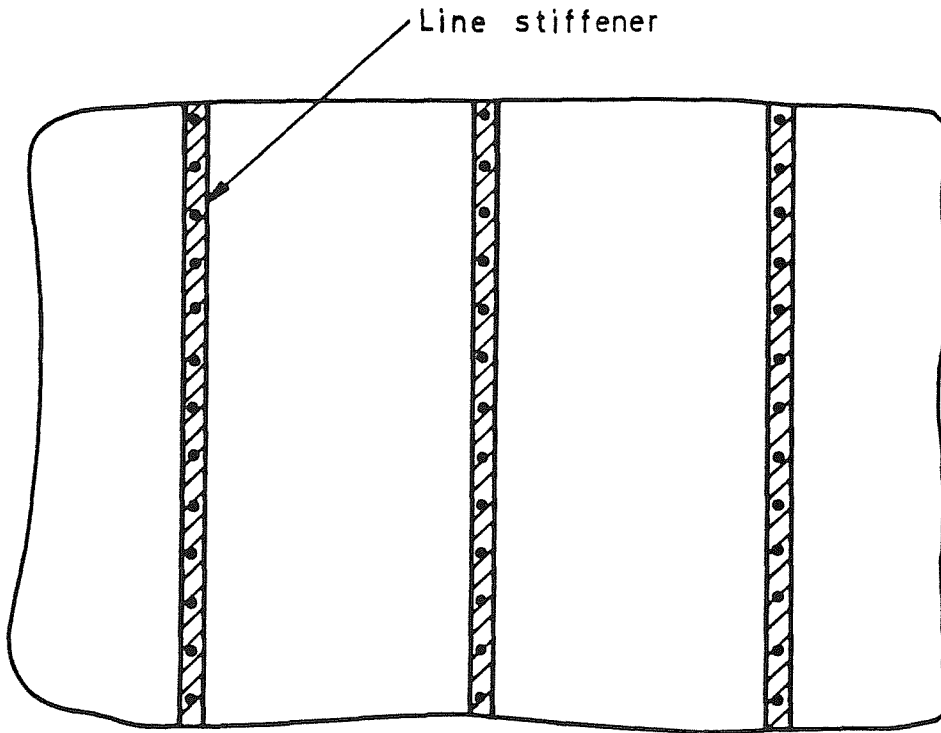


Fig 7.1a Model stiffened sheet

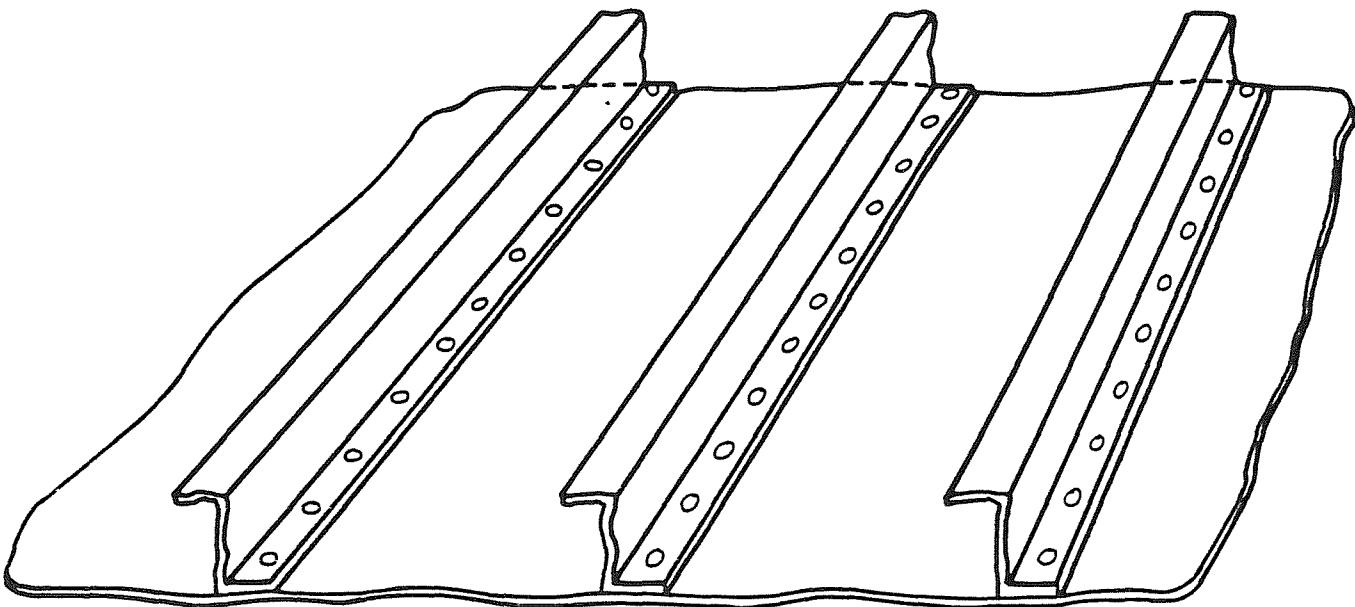


Fig 7.1b A typical stiffened aircraft structure

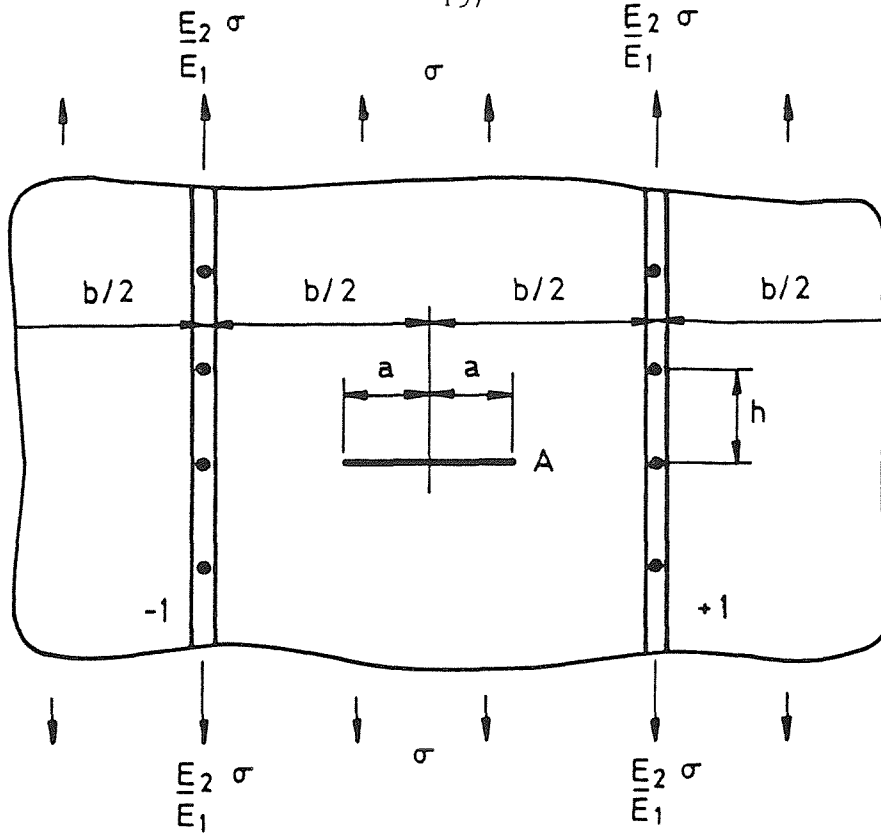


Fig 7.2a Crack located symmetrically between two of the riveted stiffeners in a periodically stiffened sheet

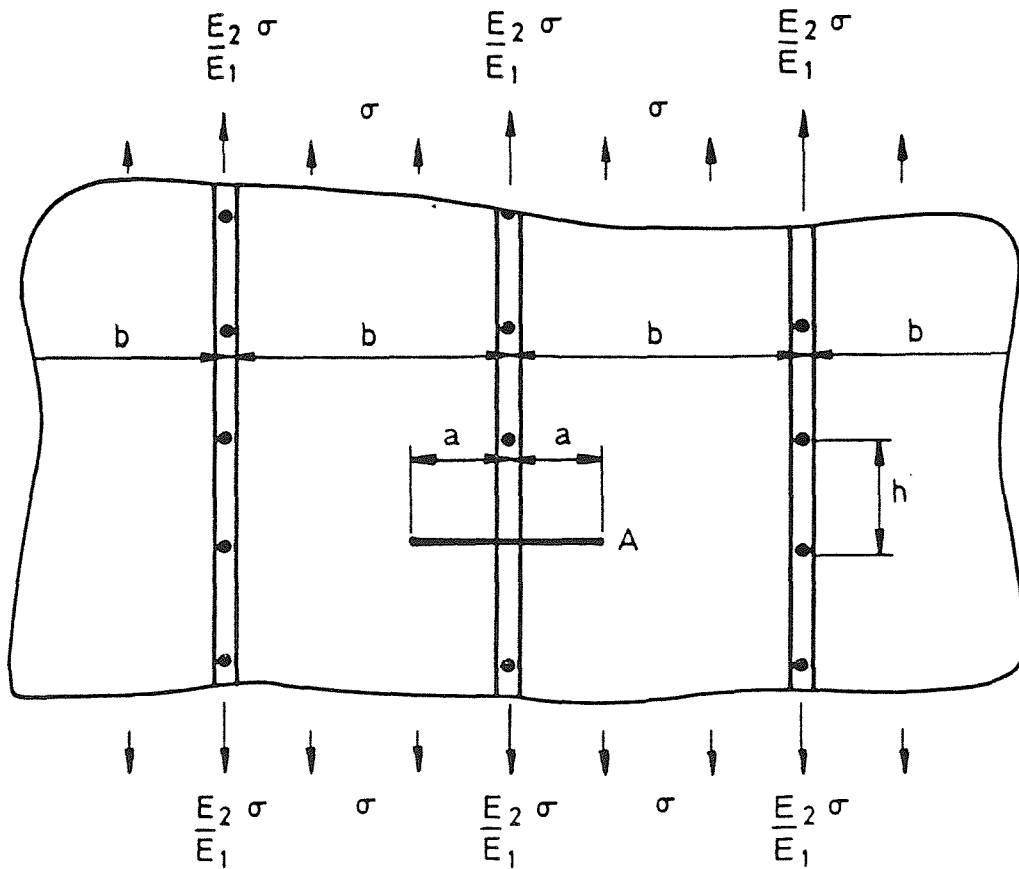


Fig 7.2b Crack located symmetrically about one of the riveted stiffeners in a periodically stiffened sheet

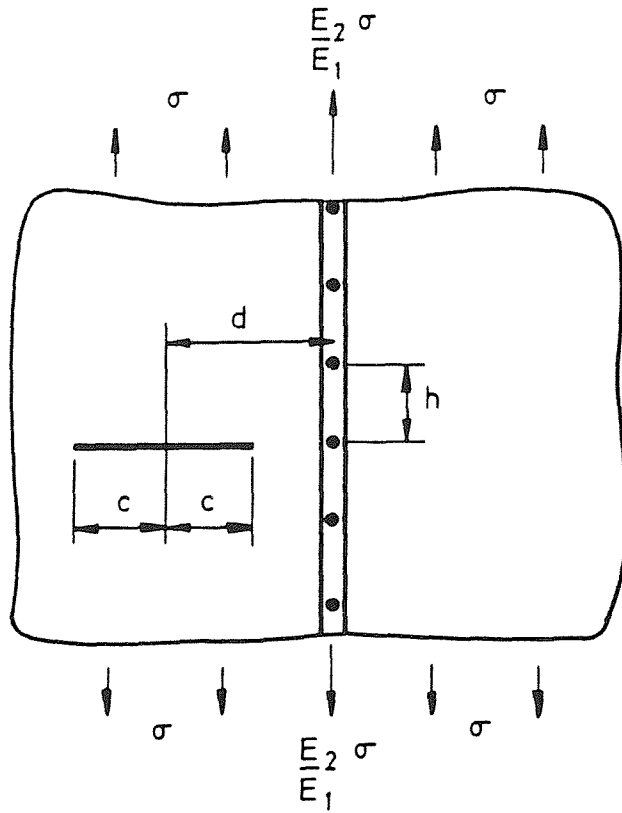


Fig 7.3a Crack near a single riveted stiffener (ancillary configuration for Fig 7.2a&b)

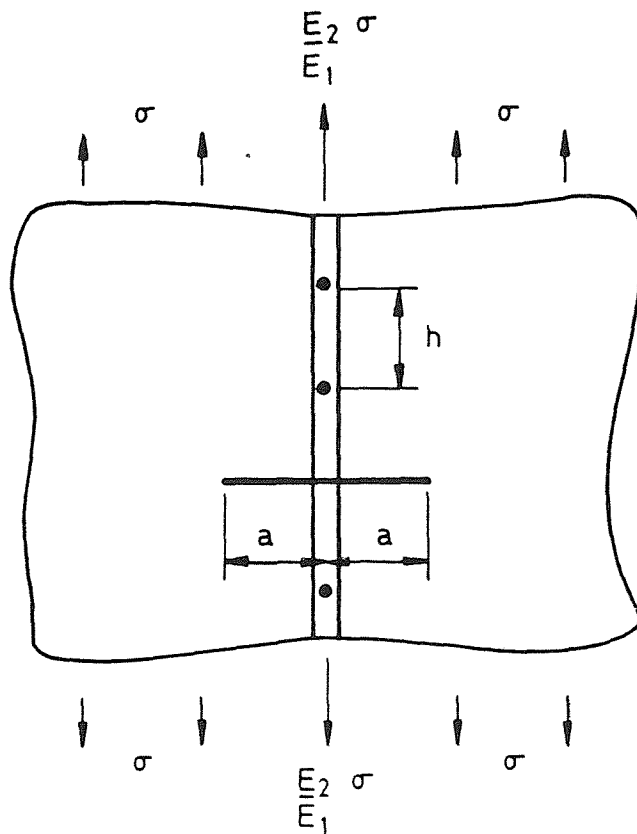


Fig 7.3b Crack located symmetrically about a single riveted stiffener (ancillary configuration for Fig 7.2b)

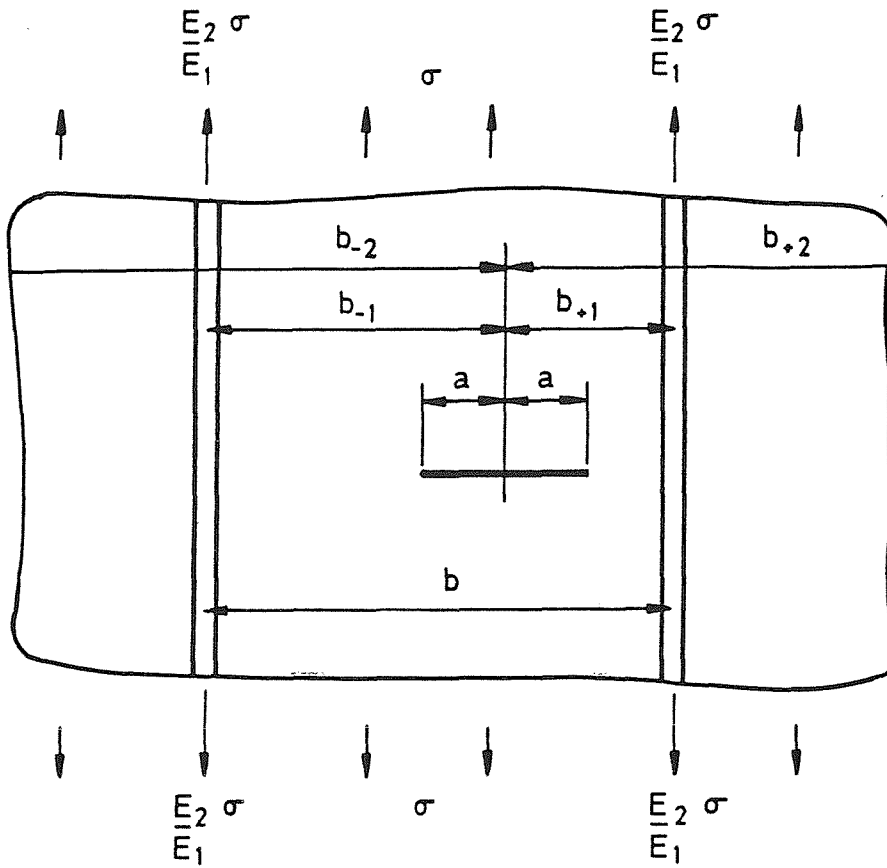


Fig 7.4a Crack located asymmetrically between two of the stiffeners in a periodically stiffened sheet

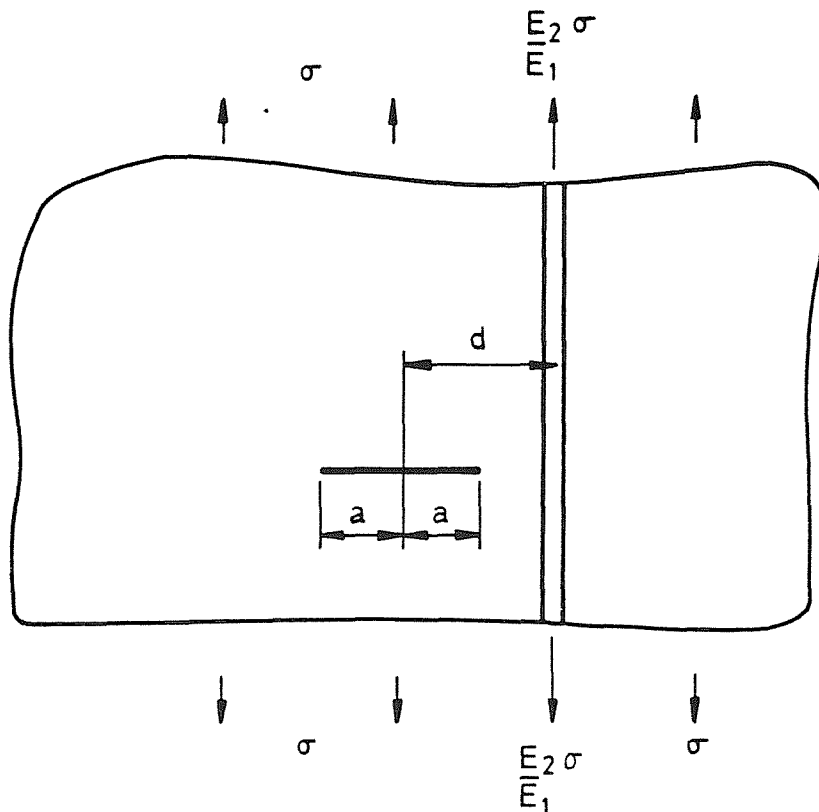


Fig 7.4b Crack near a single stiffener (ancillary configuration for Fig 7.4a)

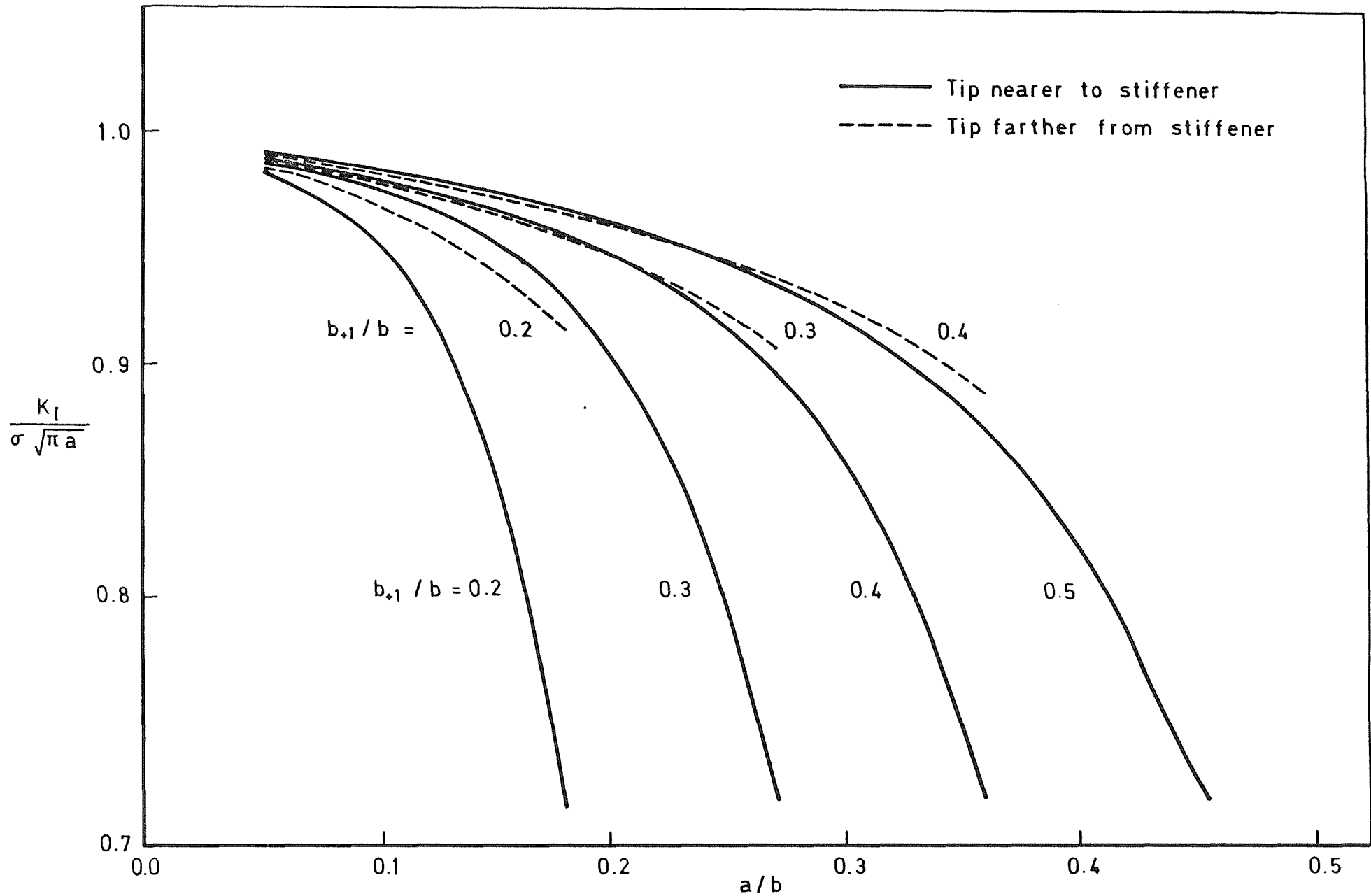


Fig 7.5 Normalized stress intensity factors for a crack located asymmetrically between two of the stiffeners in a periodically stiffened sheet

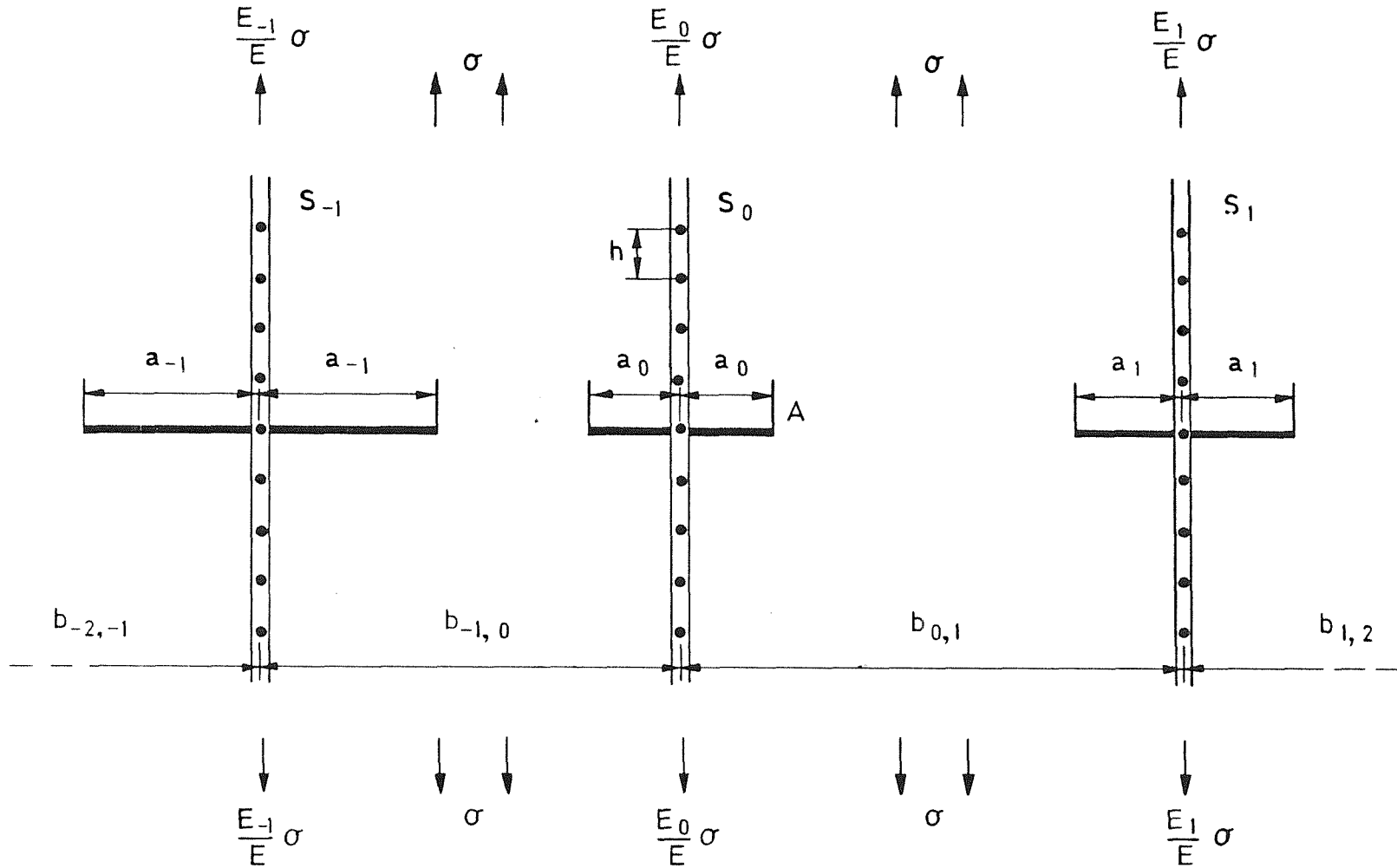
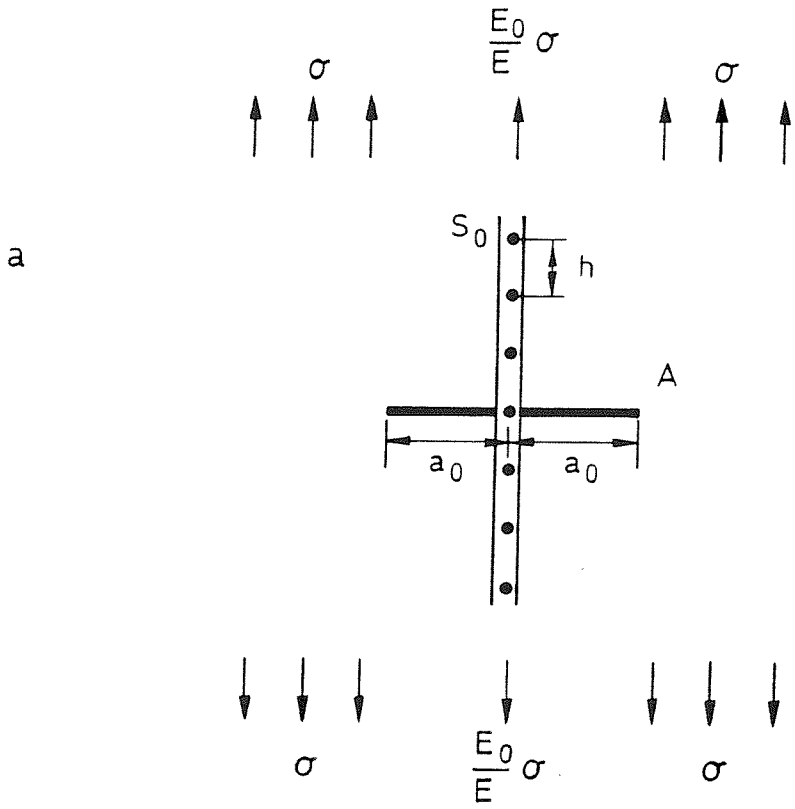
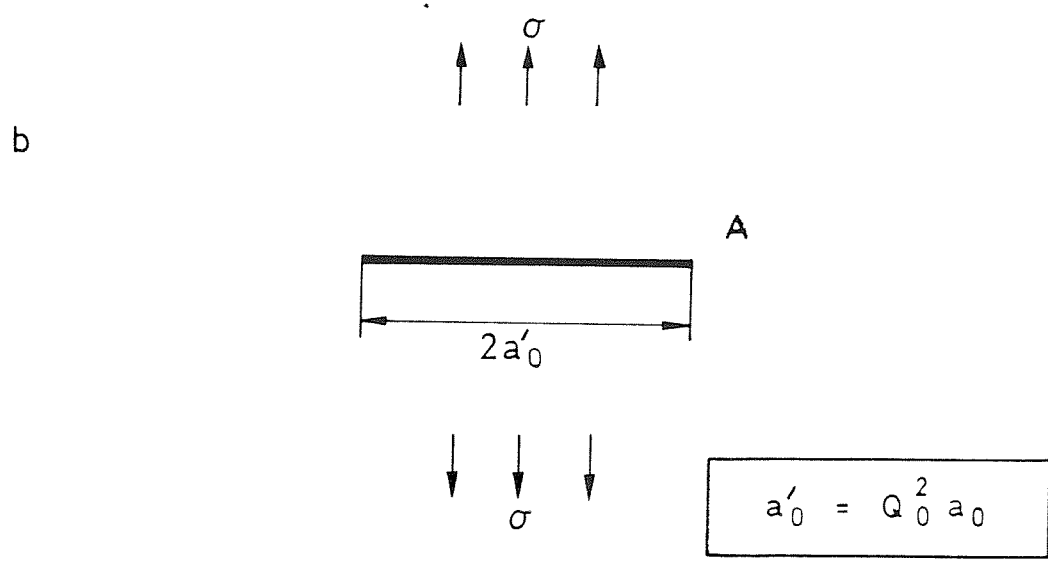


Fig 8.1 Collinear cracks in a stiffened sheet



$$K_0 = Q_0 \sigma \sqrt{\pi a_0}$$



$$a'_0 = Q_0^2 a_0$$

Fig 8.2a Crack centred about a stiffener  $S_0$

Fig 8.2b The equivalent crack

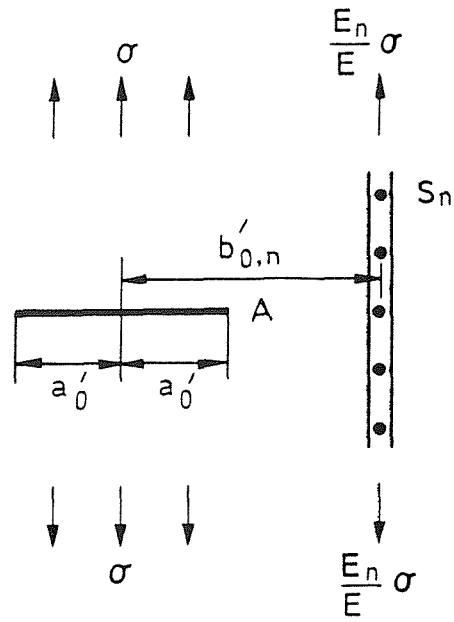
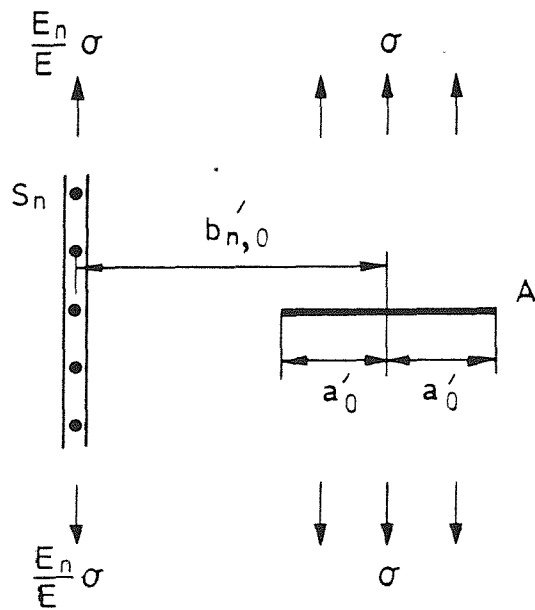
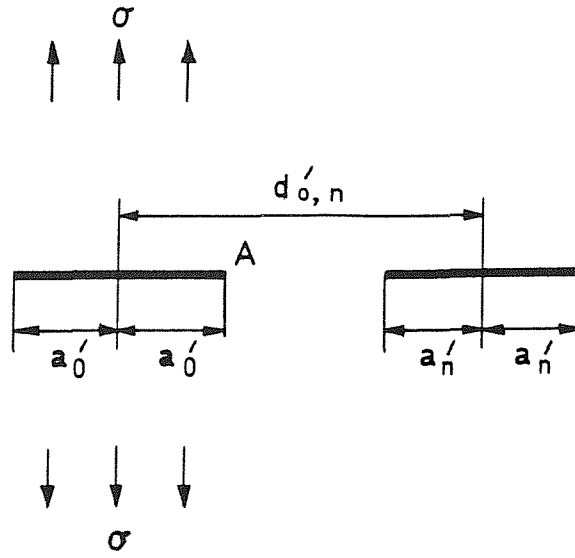
a  $n > 0$ b  $n < 0$ 

Fig 8.3a&amp;b Crack near a stiffener

a  $n > 0$



b  $n < 0$

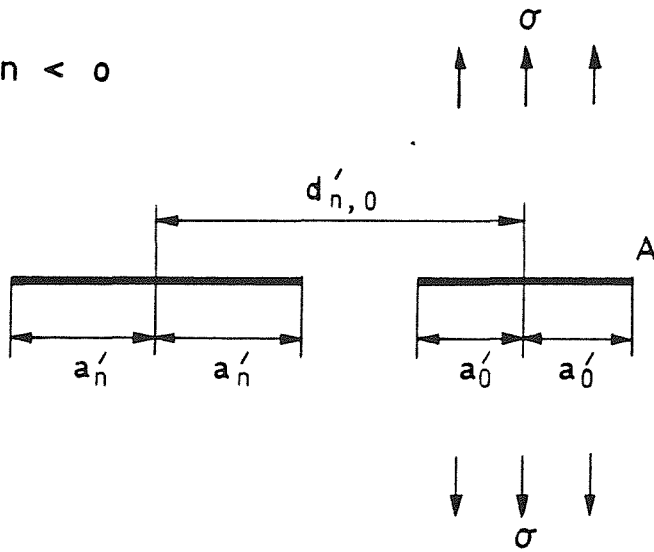


Fig 8.4a&b Crack near another crack

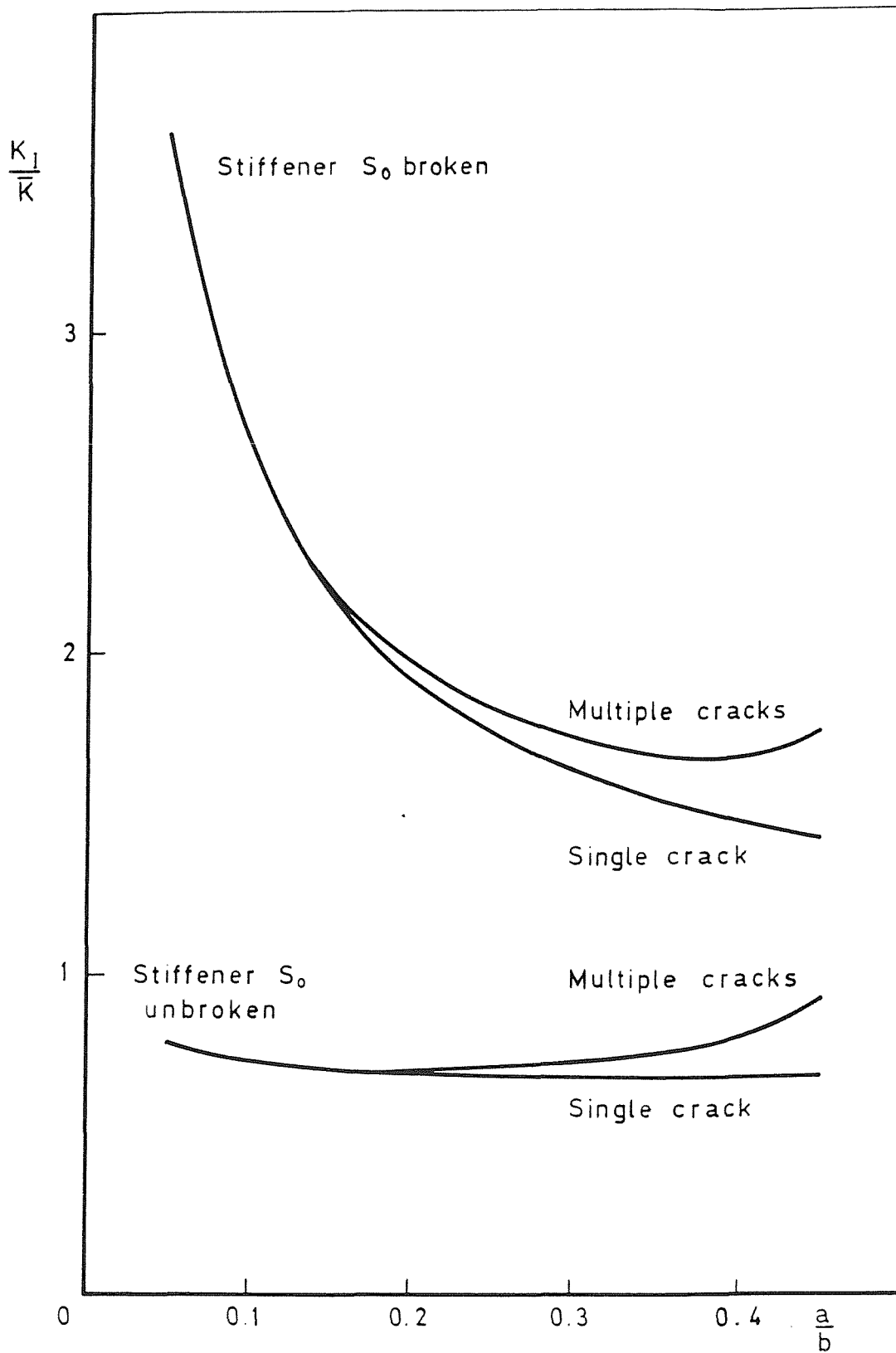


Fig 8.5 Stress intensity factors for single and multiple cracks in a periodically stiffened sheet

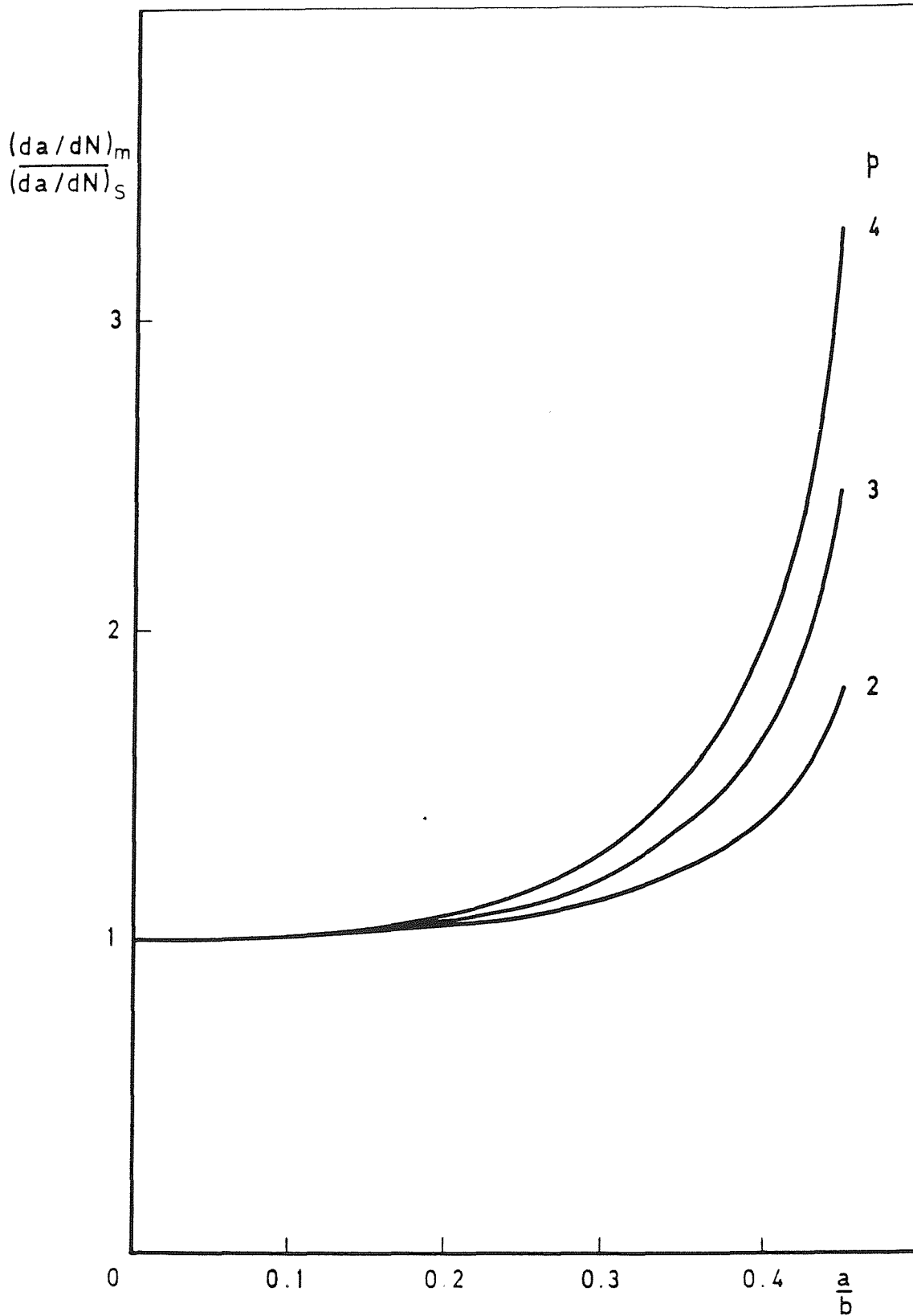


Fig 8.6 Effect of multiple cracks on growth-rates of a crack in a stiffened sheet - central stiffener unbroken

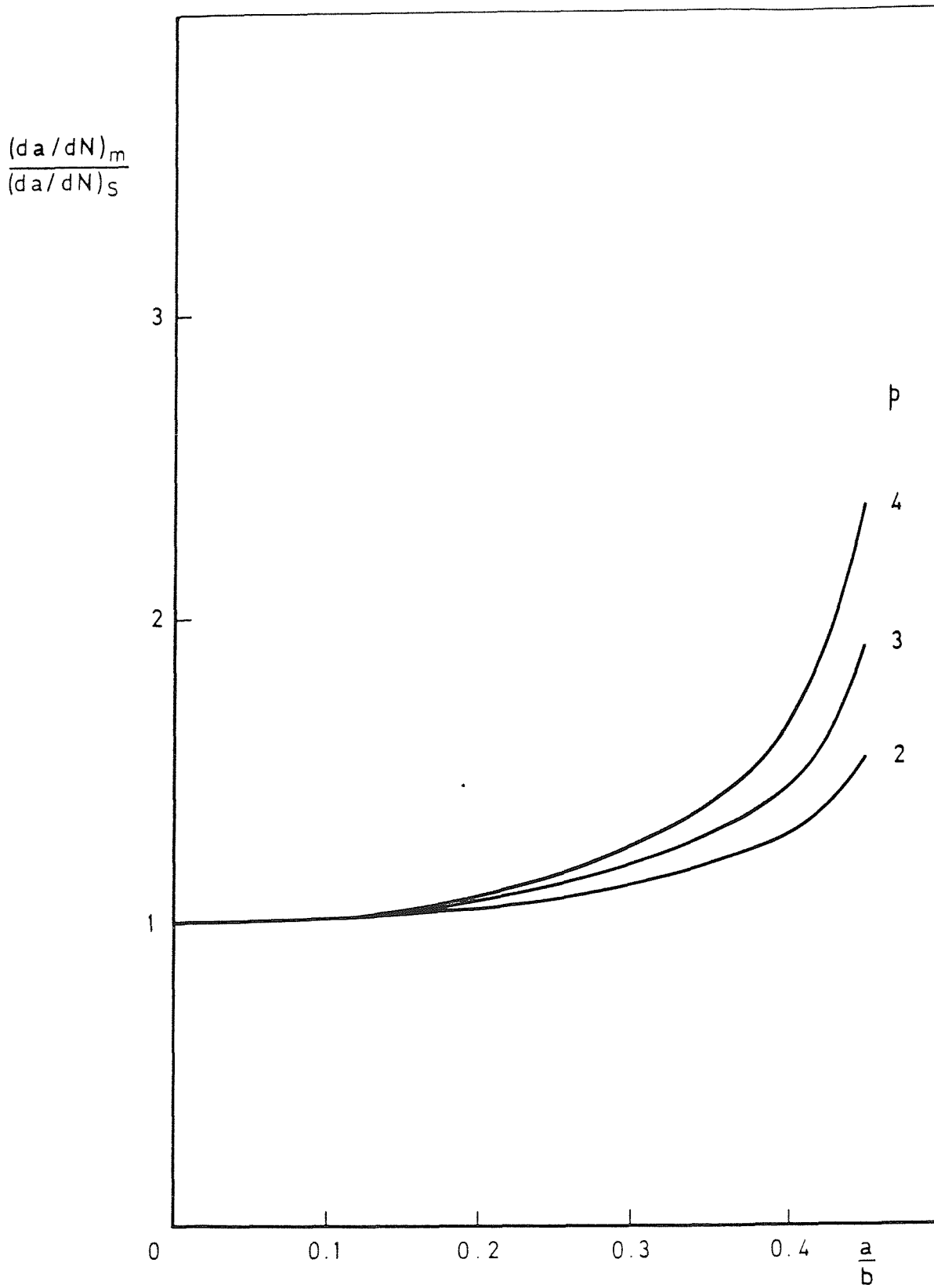


Fig 8.7 Effect of multiple cracks on growth-rates of a crack in a stiffened sheet - central stiffener broken

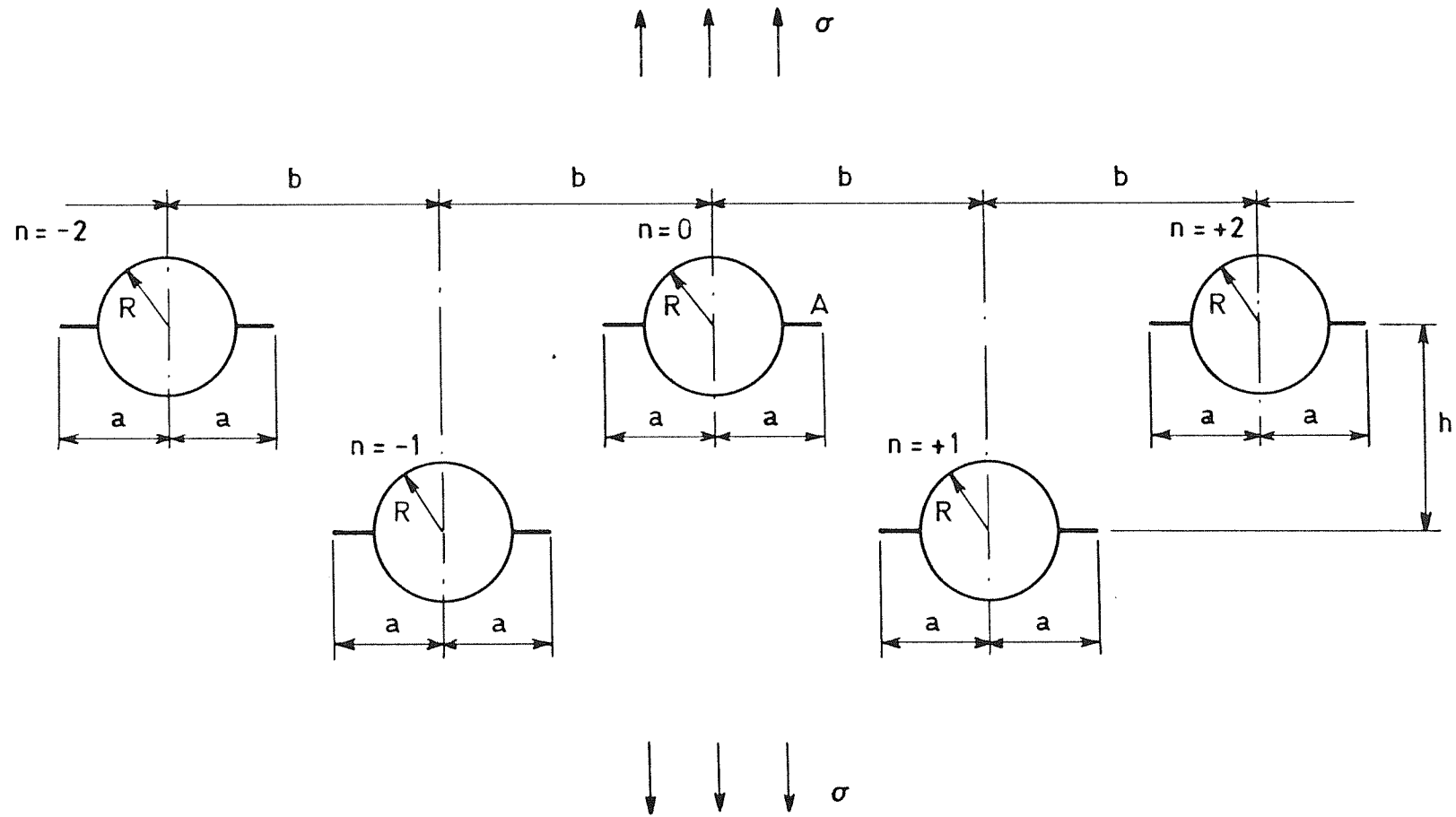
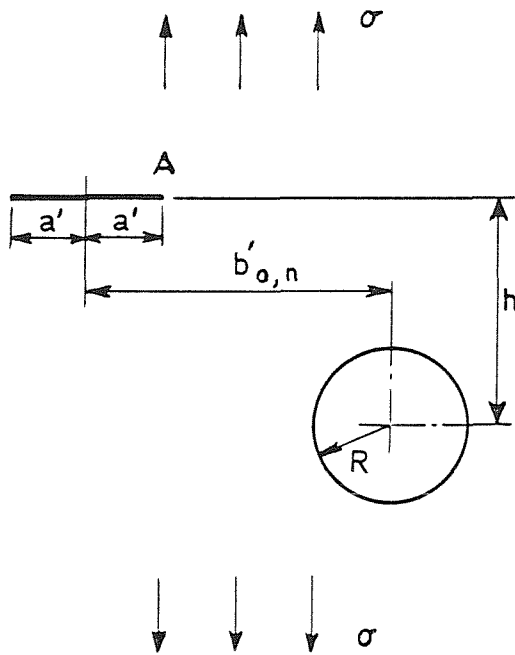
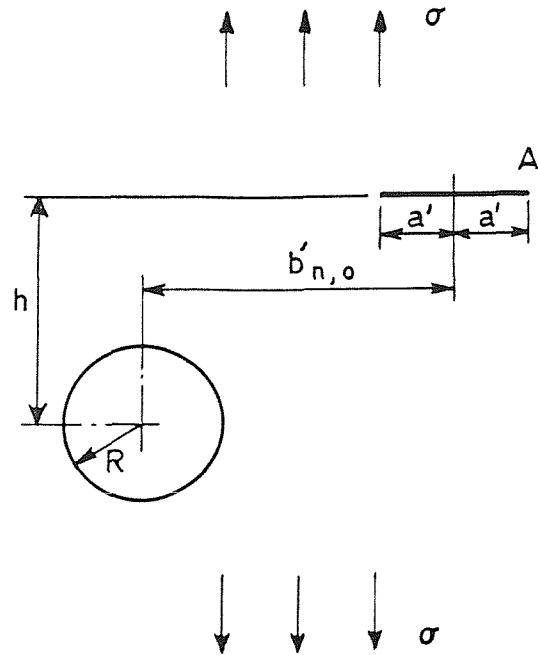
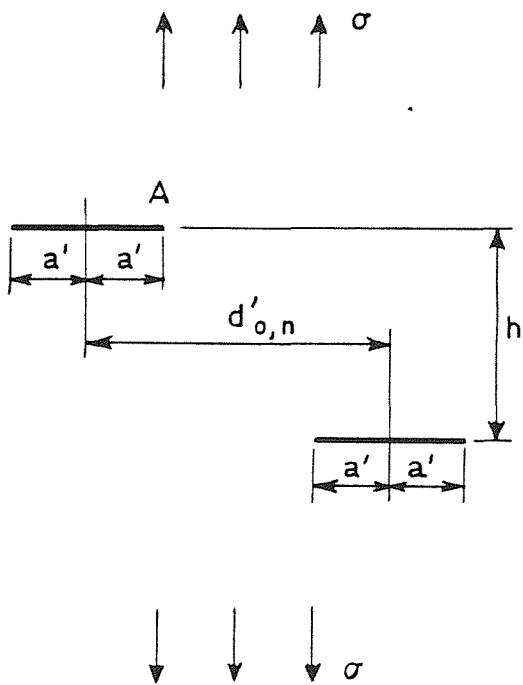
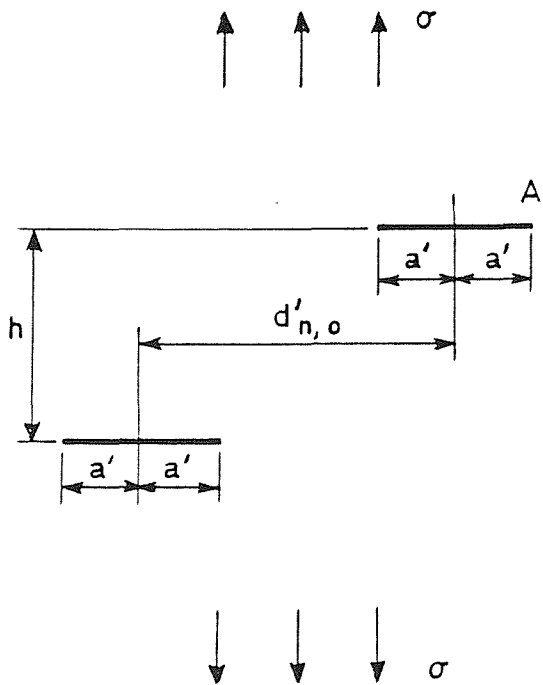
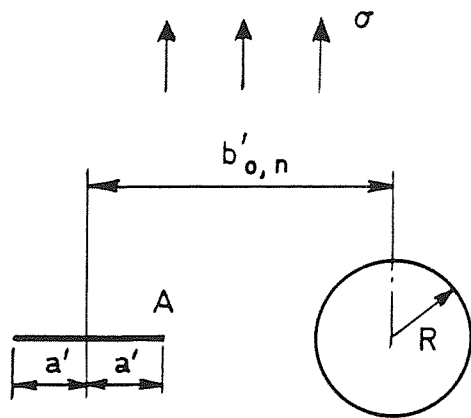
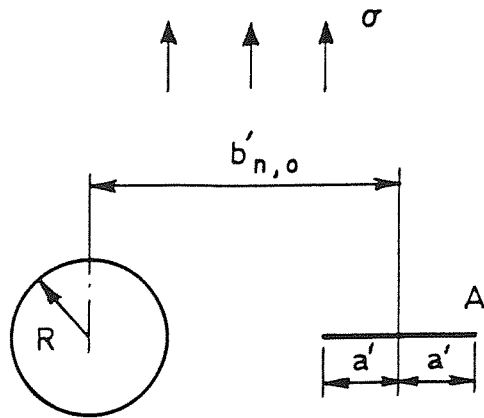
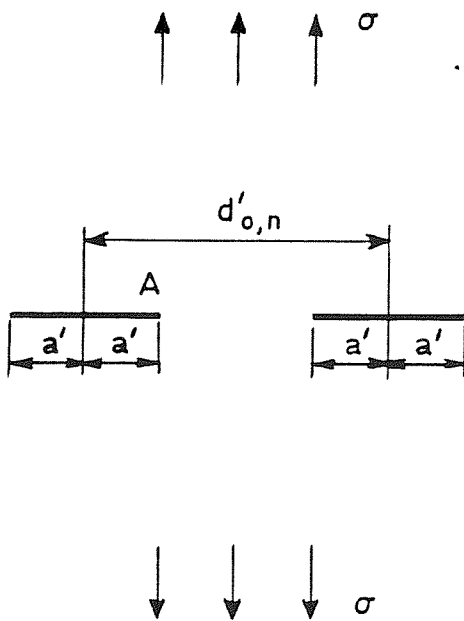
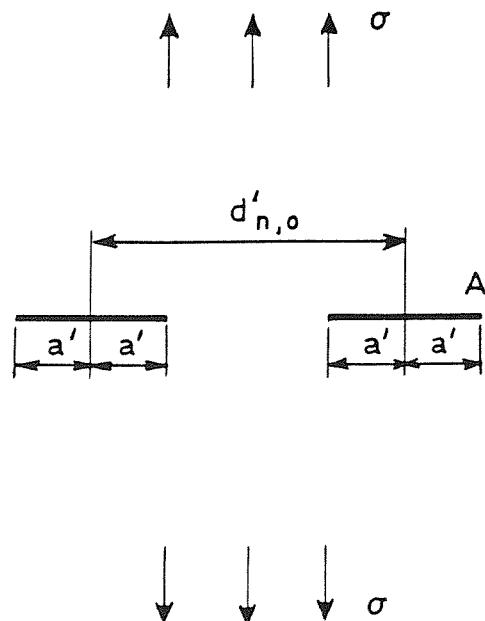


Fig 9.1 Equal cracks at the edges of holes in a double row of holes

a)  $n$ : odd, positiveb)  $n$ : odd, negativec)  $n$ : odd, positived)  $n$ : odd, negativeFig 9.2a-d Ancillary configurations for odd values of  $n$

a)  $n$ : even, positiveb)  $n$ : even, negativec)  $n$ : even, positived)  $n$ : even, negativeFig 9.3a-d Ancillary configurations for even values of  $n$

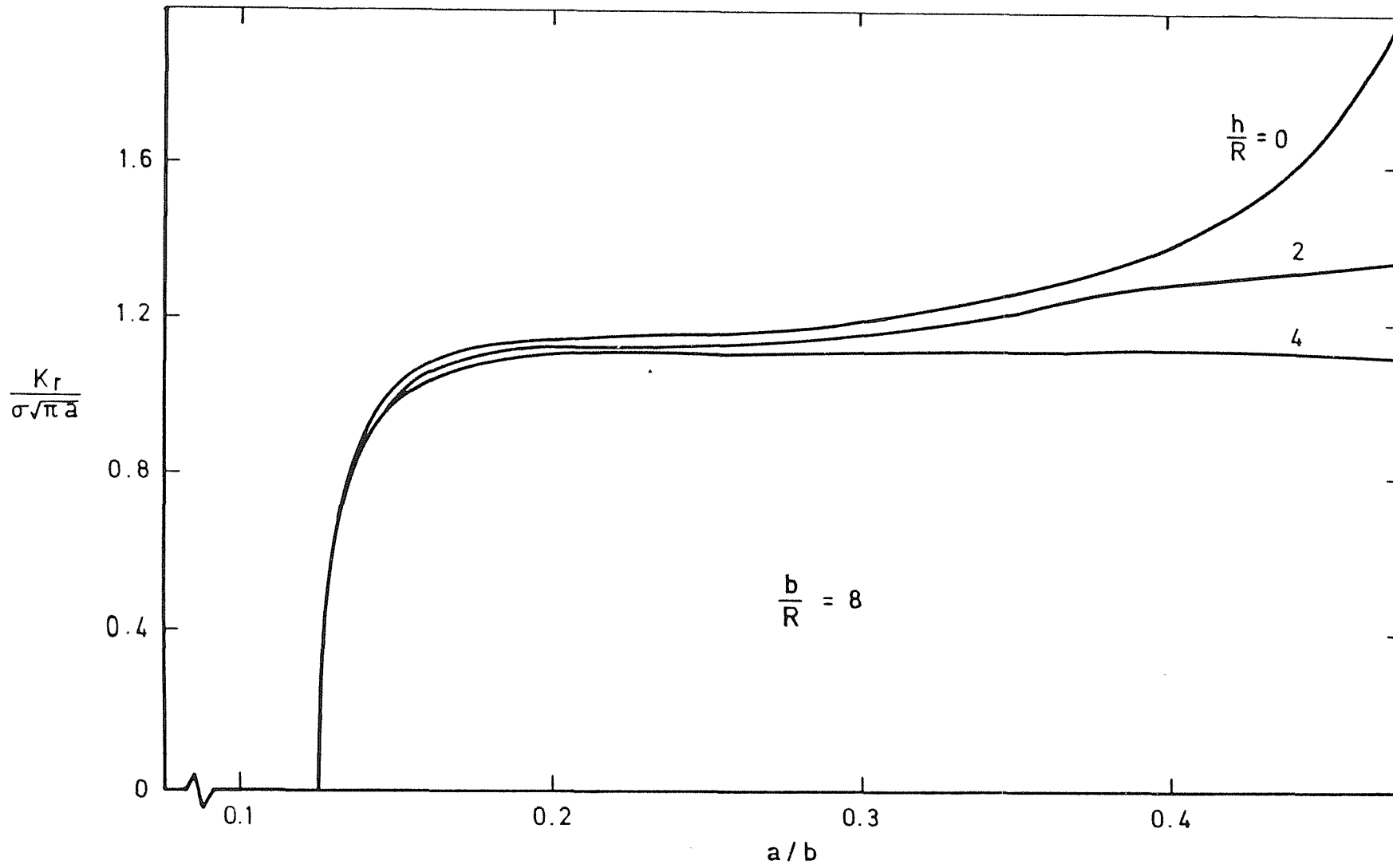


Fig 9.4 Effect of row separation on the resultant stress intensity factors

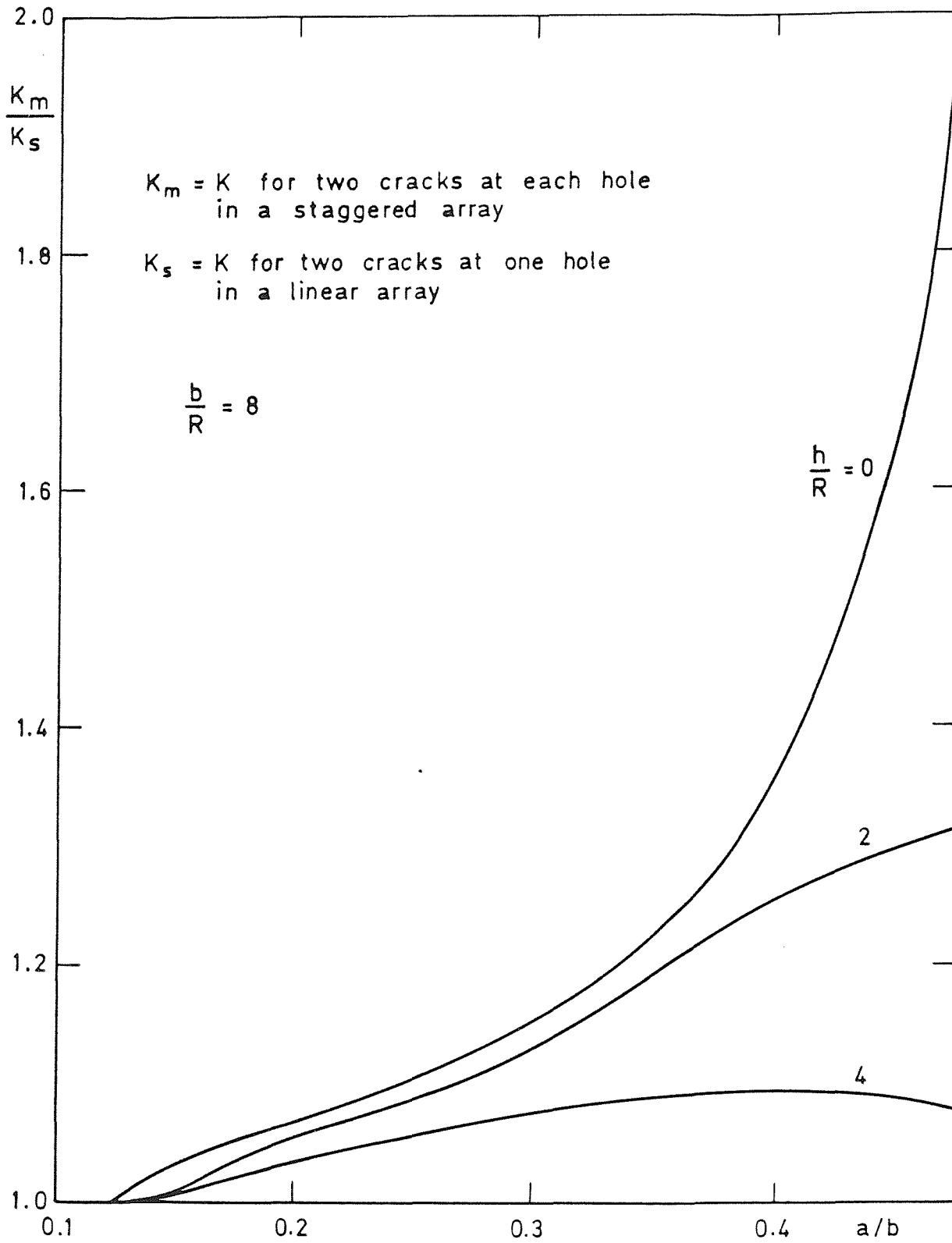


Fig 9.5 Comparison of stress intensity factors for cracks at holes in a single or double row

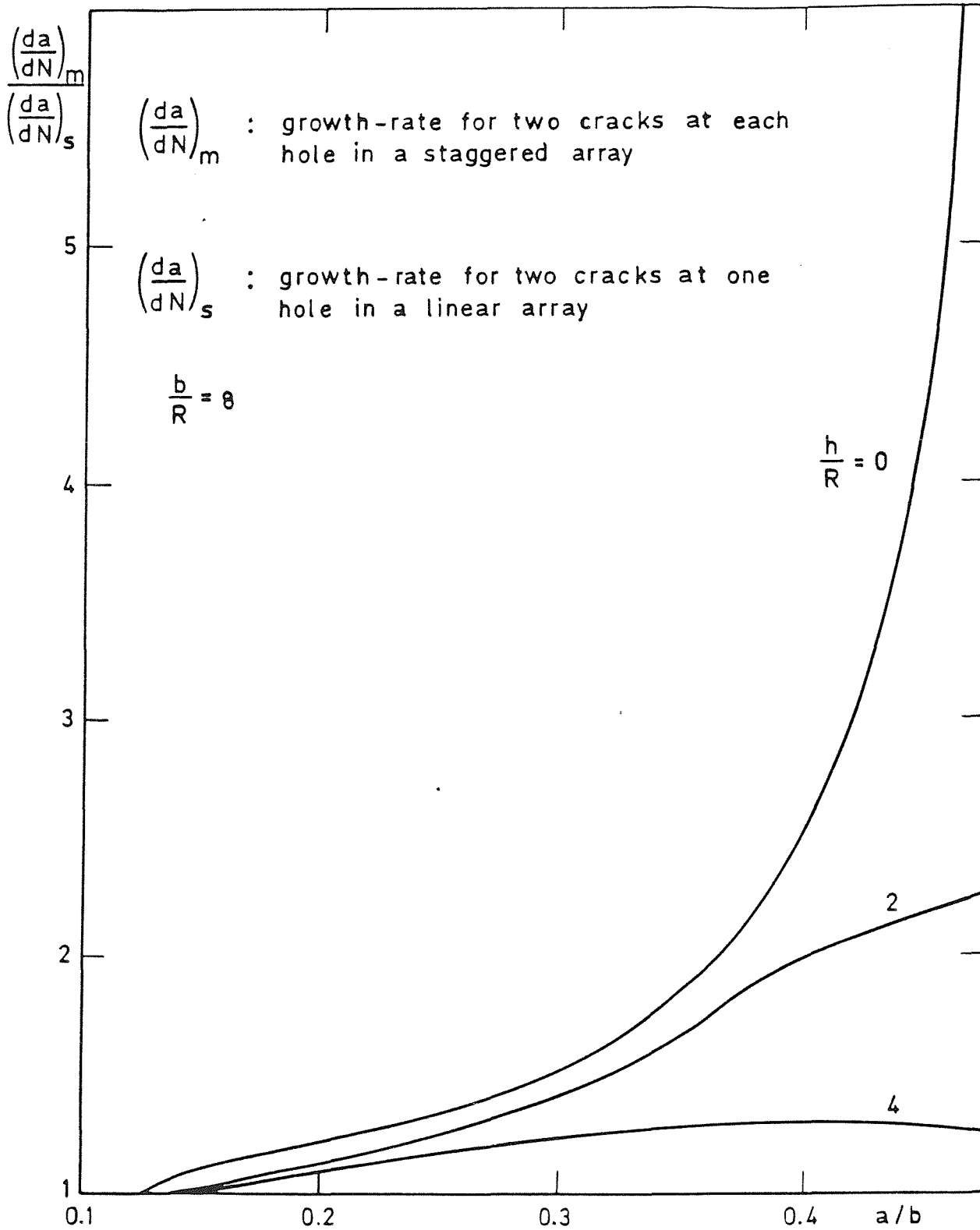


Fig 9.6 Comparison of growth-rates for cracks at holes in a single or double row ( $da/dN \propto (\Delta K)^3$ )

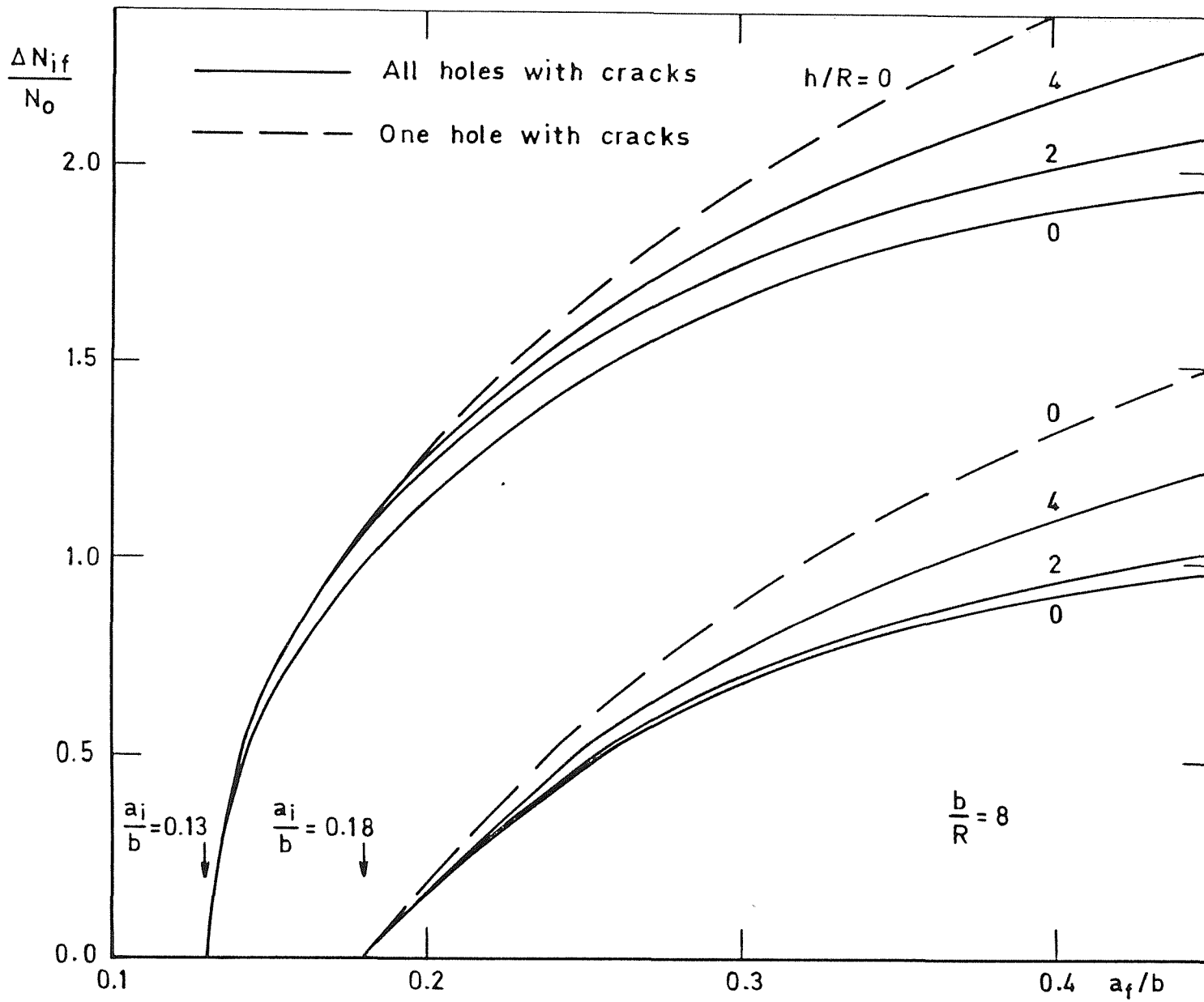


Fig 9.7 Fatigue lifetimes ( $da/dN \propto (\Delta K)^3$ )

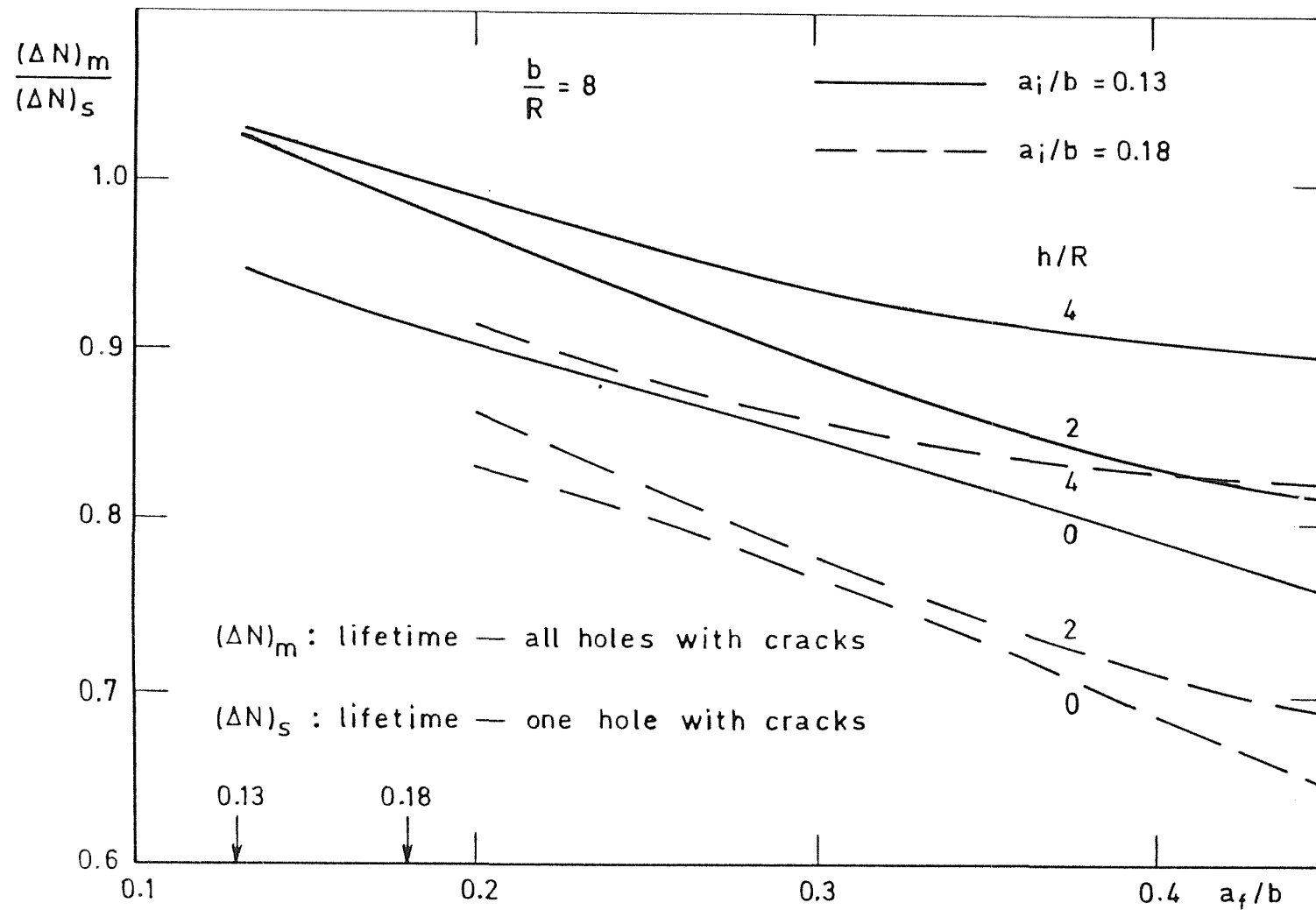


Fig 9.8 Comparison of fatigue lifetimes ( $da/dN \propto (\Delta K)^3$ )